Schriftenreihe der Reiner Lemoine-Stiftung

REINER LEMOINE STIFTUNG

Christian A. Hans

Operation control of islanded microgrids

CHRISTIAN A. HANS

OPERATION CONTROL OF ISLANDED MICROGRIDS

SHAKER VERLAG

OPERATION CONTROL OF ISLANDED MICROGRIDS

vorgelegt von
Dipl.-Ing. Christian A. Hans
(ORCID: 0000-0001-9329-4527)

an der Fakultät IV - Elektrotechnik und Informatik
der Technischen Universität Berlin
zur Erlangung des akademischen Grades
Doktor der Ingenieurwissenschaften (Dr.-Ing.)

GENEHMIGTE DISSERTATION

PROMOTIONSAUSSCHUSS:

Vorsitzender:	Prof. Dr.-Ing. Clemens Gühmann
Gutachter:	Prof. Dr.-Ing. Jörg Raisch
Gutachterin:	Dr. Alessandra Parisio
Gutachter:	Dr. Pantelis Sopasakis

Tag der wissenschaftlichen Aussprache: 15. März 2021

Berlin 2021

Schriftenreihe der Reiner Lemoine-Stiftung

Christian A. Hans

Operation control of islanded microgrids

D 83 (Diss. TU Berlin)

Shaker Verlag
Düren 2021

Bibliographic information published by the Deutsche Nationalbibliothek
The Deutsche Nationalbibliothek lists this publication in the Deutsche Nationalbibliografie; detailed bibliographic data are available in the Internet at http://dnb.d-nb.de.

Zugl.: Berlin, Technische Universität, Diss., 2021

This publication was supported by the Open Access Publication Fund of Technische Universität Berlin.

Printed in Germany.

Print-ISBN 978-3-8440-8233-3
PDF-ISBN 978-3-8440-8300-2
ISSN 2193-7575
https://doi.org/10.2370/9783844083002

Shaker Verlag GmbH • Am Langen Graben 15a • 52353 Düren
Phone: 0049/2421/99011-0 • Telefax: 0049/2421/99011-9
Internet: www.shaker.de • e-mail: info@shaker.de

PREDICTION IS VERY DIFFICULT, ESPECIALLY ABOUT THE FUTURE.

DANISH PROVERB

Abstract

Islanded microgrids (MGs) are small electric power networks that have no connection to a larger grid. They typically comprise storage units, renewable and conventional generators as well as loads. The central question of this work is: How to operate islanded MGs with high renewable share, i.e., how to control the energy of the storage units, and how to maximize infeed from uncertain renewable sources without compromising a safe operation?

To answer this question, different model predictive control (MPC) schemes for the operation of MGs are deduced. These are derived based on a generic model of an islanded MG with high renewable share. The schemes can be distinguished by the way they handle the uncertain load and renewable infeed: (i) certainty equivalence MPC, where a nominal forecast is fully trusted; (ii) minimax MPC, where time-varying forecast intervals are assumed; (iii) risk-neutral stochastic MPC, where a forecast probability distribution is fully trusted; and (iv) risk-averse MPC, where a forecast probability distribution is *not* fully trusted.

All schemes are posed in computationally tractable ways and compared in a numerical case study. The results of this study indicate that (i) certainty equivalence MPC can compromise a safe operation; (ii) minimax MPC leads to a safe operation at the expense of higher costs; (iii) risk-neutral stochastic MPC leads to a safe operation and low costs if the forecast probability distribution is accurate; and (iv) risk-averse MPC provides robustness to misestimated forecasts and unlikely events which leads to a safe operation at low costs.

In conclusion, how uncertain load and renewable infeed are modeled has a significant impact on safety and performance. Overall, risk-averse MPC was identified to be most suitable for the operation of islanded MG as it provides robustness to misestimated forecasts and unlikely events which translates into low costs and a safe operation.

Kurzfassung

Microgrids (MGs) im Inselbetrieb sind kleine elektrische Netze ohne Verbindung zu einem größeren Netz. Sie beinhalten typischerweise Speicher, erneuerbare und konventionelle Einheiten sowie Verbraucher. Die zentrale Frage dieser Arbeit lautet: Wie können MGs mit hohem Anteil erneuerbarer Erzeuger als elektrische Insel betrieben werden, d. h., wie sollte die gespeicherte Energie geregelt werden, und wie kann man erneuerbare Einspeisung maximieren, ohne die Versorgungssicherheit zu gefährden?

Um diese Frage zu beantworten, werden unterschiedliche Ansätze zur modellprädiktiven Regelung (englisch model predictive control, MPC) hergeleitet. Diese basieren auf einem gemeinsamen mathematischen Modell eines MGs. Die Ansätze unterscheiden sich darin, wie unsichere erneuerbare Erzeugung und Last modelliert werden: (i) Sicherheitsäquivalente MPC, bei der die nominelle Vorhersage als sicher angenommen wird; (ii) Robuste MPC, bei der zeitvariante Vorhersageintervalle angenommen werden; (iii) Risikoneutrale stochastische MPC, bei der die Wahrscheinlichkeitsverteilung der Vorhersage als sicher angenommen wird; und (iv) Risikoaverse MPC, bei der die Wahrscheinlichkeitsverteilung der Vorhersage als unsicher angenommen wird.

Alle Ansätze werden so hergeleitet, dass sie mit existierenden Verfahren numerisch gelöst werden können und in einer Simulationsstudie miteinander verglichen. Die Ergebnisse der Studie legen nahe, dass (i) die sicherheitsäquivalente MPC zu verringerter Versorgungssicherheit führt; (ii) die robuste MPC zu einem sicheren Betrieb und erhöhten Kosten führt; (iii) die risikoneutrale stochastische MPC zu einem sicheren Betrieb und niedrigen Kosten führt, wenn die angenommene Wahrscheinlichkeitsverteilung korrekt ist; und (iv) die risikoaverse MPC robust gegenüber fehlerhaften Wahrscheinlichkeitsverteilungen und unwahrscheinlichen Ereignissen ist, was zu einem sicheren Betrieb und niedrigen Kosten führt.

Zusammenfassend lässt sich sagen, dass die Modellierung von unsicherer erneuerbare Erzeugung und Last einen großen Einfluss auf Versorgungssicherheit und Kosten hat. Alles in allem wurde die risikoaverse MPC als tauglicher Ansatz für den Betrieb von MGs im Inselbetrieb identifiziert, da sie robust gegenüber fehlerhaften Vorhersagen und unwahrscheinlichen Vorfällen ist und zu einen sicheren Betrieb mit niedrigen Kosten führt.

Acknowledgements

I want to thank the people who supported me during the last years.

First and foremost, Jörg Raisch. Thank you for your guidance, your support and constructive discussions on many intermediate steps that led to this work. Thank you for providing so much autonomy while being always open for advice. I am very grateful for your trust.

I would also like to thank Pantelis Sopasakis for many discussions in Lucca, Leuven and Belfast. Your patient, uncomplicated and supporting nature makes collaborating with you so enjoyable. Thank you for always having an open ear and a place to crash for a visit.

Moreover, I want to thank Alessandra Parisio for agreeing to be part of doctoral committee. Your work had a big impact on my research and opened perspectives for many things discussed in this thesis. I am very happy that you are on board.

Furthermore, Clemens Gühmann for offering to be the chair of my doctoral committee. Thank you for being such a calm and supporting host in my PhD defense.

This thesis would not have been possible without the ideal and financial support of the Reiner Lemoine Foundation. I am very grateful for the possibility to follow my personal research interest and the freedom to study in Berlin and abroad during the initial phase of my doctoral work. Thank you all, especially, Annegret Jatzkewitz, Clemens Triebel, Anja Lemoine, Busso von Bismarck and Lutz Plöttner.

A big shout out to my colleagues at the Control Systems Group at Technische Universität Berlin. Especially to my office mates Johannes Schiffer, Vladislav Nenchev and Ajay Kumar Sampathirao. Thank you, Johannes and Vlad, for being so welcoming in the first place. In particular, for your friendship and for good chats during coffee breaks and table tennis matches, for many fruitful discussions and great collaborations that led to this thesis. Thank you Ajay for being such a good office mate. I still remember our meetings in the park and us scaring other parents by discussing optimization theory at the playground. I would also like to thank all the other colleagues for fruitful discussions in formal and informal settings, especially, Thomas Schauer, Thomas Seel, Ajay Krishna, Lia Strenge, Steffen Hofmann, Fabio Molinari and Johannes Trunk. Also, a big thanks to all the students who joined our team in the last years, especially, Philipp Zitzlaff, Elin Klages, Pavlo Gaiduk, Adrian Schödl, Alexandre Forel, Joseph Theune and Han Zhou. Furthermore, I want to thank Ulrike Locherer for her help in all the organizational things. Also, thanks to Arne Hertzsch for his support and open mindedness towards new solutions.

I would further like to thank collaborators on topics related to this thesis. Thank you Alberto Bemporad, Lars Grüne, Johannes Schiffer, Carsten Reincke-Collon, Panagiotis (Panos) Patrinos, Pantelis Sopasakis, Philipp Braun, Vladislav Nenchev, Ajay Krishna, Elin Klages, Peter Merk and Thomas Kral.

I also want to thank my former colleagues at Younicos AG. First of all, Carsten Reincke-Collon for his support during my time as a doctoral candidate. You had a great impact on my interest on control-related issues in microgrids. Thank you for your help on a personal, scientific and organizational level. I always appreciate your reflected and pragmatic perspective on things. I would also like to thank Clemens Triebel for his support. I admire your enthusiasm and deep commitment for renewable energies. Erich Bosch for always taking the time for technical and personal conversations. I have learned so much from you and your intrinsic motivation to get to the bottom of things. Peter Merk for helping me to get on board in the first place. You are a great DJ and colleague. Peter as well as Tim Tröndle, Sebastian Klockziem, Thomas Kral and Triin Tamra have not only been colleagues but also friends.

I would also like to thank my parents Michaela Roth, Walter Schackert and Christian Roth for supporting me in all possible ways. You always encouraged me to try new things and believe in what I am doing. Thanks for your love Susanne Hans, Philipp Roth and Pascal Roth; Max and Elfriede Hans as well as Dieter Kühn for being proud and curious grandparents; Hille Piezunka for lending a hand whenever possible; Henning Piezunka for his advice and great sense of humor; and Angela Schrauber for supporting us in always turbulent times. A big thanks to my friends for reminding me of all the things outside university: Martin Stuckenbröker, Martin von der Ohe, Jan Dähne, Moritz Vialon, Daniel Adam, Mary Kuhnt, Andreas Bach, Ilka Schoeneberger, Mathias Schoeneberger, Nina Botsch and Ilkay Oksuz.

Last but definitely not least, I would like to thank Anne Piezunka for being with me in all these years. Thank you for the discussions and the conspiratorial walks in the park, for being always so supportive, open and curious. I could not imagine a better partner in crime than you!

Contents

1 Introduction

Consider an existing setup of an islanded[1] electric power grid with a high share of renewable infeed that serves a village. The grid includes storage units, renewable energy sources and conventional generators that provide power to different loads. How to operate such a grid, i.e., how to decide:

[1] Note that islanded grids are not connected to a larger electrical network.

- When to charge or discharge storage units and at which rate?
- What is a "good" way to deal with infeed from uncertain renewable energy sources?
- When to enable or disable the different conventional generators and how much power to draw from them?

This work circles around these questions. More precisely, it proposes different operation control strategies for islanded microgrids that answer these questions based on historic load and weather data as well as the current state of charge of storage units. The proposed strategies can be distinguished by the way they model the uncertain load and available renewable power. The different control schemes are posed in computationally tractable ways and compared in a case study.

This chapter is structured as follows. First, the motivation is continued in more detail in Section 1.1. Then, the contributions of this work are discussed in Section 1.2. In Section 1.3, related publications are reviewed. Finally, publications by the author are presented in Section 1.4 and a brief outline is given in Section 1.5.

1.1 Motivation

Why a high share of renewable energy sources? Electricity is one of the major energy carriers in the world [4]. It powers commercial, industrial and residential loads, such as, public transportation, industrial processes, information and communication technology, as well as home appliances, light, heating, and many more.

In conventional power systems, electric energy is typically generated using fossil-fueled, nuclear and hydro power plants [127]. Here, steam or water powered turbines [74], in smaller grids also diesel engines, provide mechanical power to generators that convert it into electric power. The operation of most of these so-called conventional generators is associated with waste and safety concerns as well as political issues in the case of nuclear power plants and undesired greenhouse gas emissions[2] in the case of fossil-fueled power plants [6].

[2] The desire for a reduction of greenhouse gas emissions is manifested, e.g., in the Kyoto Protocol [259] and the Paris Agreement [260].

One way to reduce greenhouse gas emissions is by a reduction of electric energy consumption, e.g., via more efficient electric appliances [198]. This, however, can only hamper the worldwide rise in electric power demand as the number of households with access to electric energy keeps increasing [108]. Therefore, a reduction of greenhouse gas emissions by means of a substitution of conventional generators by renewable energy sources (RES) [188], such as photovoltaic power plants or wind turbines, is even more important.

Why islanded microgrids? Access to electricity correlates with an increased education index [111] and better public health as well as decreased poverty and environmental degradation [249]. Worldwide, the number of people without access to electricity decreased since 1990. Still, 840 million people remained without access to electricity in 2017. Of all these people, 87 % live in rural areas [108]. For many of these areas, islanded microgrids (MGs) represent an important alternative to costly power grid extension. As the transport costs for fossil fuels are usually high in these areas [270], RES are often more cost-efficient than conventional generators. Therefore, islanded MGs with high share of RES play an essential role in strategies to increase the electrification rate.

In the context of large-scale power systems with increasing share of RES, MGs also play an important role. Many renewable generators are small-scaled and geographically dispersed over the electric power grid [116]. Consequently, with an increasing share of RES, the structure of electric power systems changes from grids with a small number of large-scale units to a grids with a large number of small-scale units [95]. The increasing number of units in the grid makes their operation very complex [194]. One way to cope with this complexity is by partitioning the overall grid into coupled MGs [61, 134]. The units in an MG, i.e., storage, renewable and conventional generators, are then operated such that the MG appears as a "single controllable system" [132] to the outside world.

MGs can be operated connected to or isolated from the transmission network [115, 187, 209], e.g., in presence of fault events. In grid-connected operation, an MG can act as a source providing energy to others or as a load. By emphasizing a local power balance within each MG, the power flow over transmission lines can be reduced [56, 133]. In islanded operation, no power exchange with others is possible. Here, an equilibrium of partly uncertain generation, demand and storage needs to be ensured at all times using only the units in the MG [175], which renders this operation particularly challenging. Mastering islanded operation therefore provides important insights for the operation of grid-connected MGs.

Why operation control? Operation control is responsible to provide setpoints of desired power to the units [171]. By enabling conventional generators and providing power setpoints to all units on a timescale of minutes, the energy contained in the storage units is controlled. Finding suitable setpoints, by means of a controller that solves an optimal control problem for given historic data and stored energy, a safe and reliable operation can be ensured. Furthermore, operation control plays an important role in the commercial success of an MG. Providing power setpoints that minimize the operation cost of an MG is crucial for an economically meaningful operation. Moreover, the operation strategy has a high impact on the renewable share of a given MG topology. Using suitable control approaches (i.e., "only" software) the renewable share of a grid can be increased without adding new renewable units.

1.2 Contributions

In what follows, the main contributions of this thesis are posed. First, an overview is provided. Then, the contributions of the different chapters are presented in more detail.

1.2.1 Overview

Throughout this thesis, different control schemes are derived and compared to each other. In this context, the main contributions can be divided into the following parts.

Model of islanded MG. A generic control-oriented model of an MGs in islanded operation is derived in this thesis. It includes grid-forming storage units[3] and conventional generators that can be enabled or disabled. Their use allows to disable conventional generators, e.g., in times of high renewable infeed, as their grid-forming capabilities are not required for the operation of the MG. Moreover, proportional power sharing between grid-forming storage units and conventional generators is included in order to model the effects of the underlying control layers. A possible limitation of renewable infeed, e.g., if all storage units are fully charged, is also part of the model. Finally, the power transmitted via the power lines is taken into account using a linear power flow model.

[3] Storage units can be operated in grid-feeding or grid-forming mode. For the operation in grid-feeding mode, where a desired power or current is provided, an existing voltage is required. Grid-forming units, on the contrary, provide a desired voltage with a certain amplitude and frequency and do not require an existing voltage for their operation.

Forecasts of load, wind and PV power. Time-series based autoregressive integrated moving average forecast models for load demand and available power of RES are derived in this thesis. These are required to compute the optimal control trajectories in the different control approaches. The obtained forecasts are compared to benchmark approaches from literature and shown to provide an increased forecast accuracy for the data sets considered in this thesis. Furthermore, the forecasts of available renewable power are shown to often be non-Gaussian which motivates the use of control approaches that do not require normally distributed uncertainties. Based on this observation, different representations of the forecasts are derived. This includes a mean value forecast and robust forecast intervals. Moreover, scenario trees, which can be seen as compact representations of discrete forecast probability distributions, are considered.

Model predictive operation control approaches. To find a suitable controller for the operation of islanded MGs, various model predictive control (MPC) approaches are derived. All of them are formulated in computationally tractable ways such that they can be solved by off-the-shelf software and used to control arbitrary islanded MGs with known topologies. The controllers are all based on a common model of an MG and a common cost function. They can, however, be distinguished by the way they model the uncertain forecast of load and available renewable power. In detail, the approaches are as follows. (i) Certainty equivalence MPC, where the mean value forecast is assumed to be certain. This approach represents the state-of-the-art. (ii) Minimax MPC that considers a forecast in the form of time-varying robust intervals. In this approach, the worst-case cost is minimized, considering bounded uncertain load and renewable infeed. (iii) Risk-neutral stochastic MPC where the uncertain forecast is modeled as a scenario tree, i.e., a discrete time-varying probability distribution. Here, the expected cost over the probability distribution is minimized assuming that the forecast probability distribution is certain. (iv) Risk-averse MPC that allows to consider uncertain probabilities in the forecast scenario tree. This approach can provide robustness to bad forecasts and unlikely events with high impact on the operation cost.

Illustrative simulations. In various examples and simulations, the properties of the MG model and the different control approaches are illustrated. This includes open-loop simulations considering a simple MG that acts as a running example. These simulations illustrate the different representations of the uncertain variables and the resulting decisions of the MPC schemes. Moreover, small examples are included to provide some intuition for the MG model, the forecasts and the MPC approaches.

In a comprehensive simulation case study, all controllers are compared to each other. Here, closed-loop simulations are performed over a simulation horizon of one week for a simple MG and an extended MG that includes two storage units, two conventional and two renewable generators. Additionally, a sensitivity analysis is performed. This analysis includes 6 000 closed-loop simulations over a simulation horizon of three days that illustrate the robustness of the approaches to misestimated forecast probability distributions.

1.2.2 Chapters

The main part of this thesis comprises 11 chapters and comprehensive conclusions. Key contributions of these chapters are as follows.

Chapter 2: Problem statement. Here, the challenges addressed in this thesis are outlined. First, a general introduction to microgrids is provided and hierarchical control of MGs is discussed. Then, requirements for the operation control of islanded MGs are posed. These arise, e.g., from the local power balance that is required at all times in islanded operation or the high share of RES.

Chapter 3: Preliminaries. In this chapter, basics from different domains are provided. This includes an introduction of mathematical operators and sets used in this thesis and MPC fundamentals. Additionally, reformulations from optimization theory that are required to pose the MPC problems in computationally tractable ways are examined. In the end of the chapter, basics regarding the models of transformers and transmission lines are provided. These include the nonlinear AC power flow equations and the derivation of the DC power flow approximations for AC power systems.

Chapter 4: Microgrid model. As a basis for the formulation of different MPC problems, the model of an islanded MG is derived. This is done in a way that enables models with an arbitrary finite number of storage units, renewable and conventional generators as well as loads and an arbitrary transmission network.

The model includes the DC power flow approximations [74, 77, 165, 200] for AC grids that allow to consider power limits of the transmission lines. Moreover, motivated by [231, 232] the storage power plants are modeled as grid-forming units. This allows to control MGs with very high share of RES that are capable of running without conventional generators. Furthermore, the dynamics of the storage units are modeled such that the uncertain load and renewable infeed affects the state of charge. Additionally, motivated by [104, 172, 180], grid-forming conventional generators are modeled such that they can be enabled or disabled. Proportional power sharing of all enabled grid-forming units is also considered to approximately model the lower control layers. Finally, unlike most other approaches (e.g., [110, 141, 180]), the model includes a possible limitation of renewable infeed, e.g., if the storage units are fully charged. This enables a control of MGs with very high share of RES.

Chapter 5: Model predictive control formulation. A generic MPC problem for the operation of islanded MGs is provided. Therefore, a cost function is formulated. It includes costs incurred by utilization of conventional generators and curtailment of renewable infeed as well as costs associated with the state of charge. Using the cost function and the MG model from Chapter 4, a prescient MPC problem is formulated as a mixed-integer quadratic program (MIQP) that can be solved by available software.

Chapter 6: Forecast. Many real-world MPC approaches for the operation of MGs require a forecast of load and available renewable infeed. Motivated by the desire for cost-efficient ways to predict these uncertain inputs [256], time-series based forecast models that only require historic data, i.e., measurements of load, wind speed and irradiance, are employed. For the forecasts, the widely adopted seasonal autoregressive integrated moving average models are employed. Suitable forecast models are identified by means of a hyperparameter search that includes more than 6 000 model configurations. The forecasts are combined with simple models of photovoltaic (PV) power plants and wind turbines in order to obtain predictions of available renewable power and load.

Chapter 7: Certainty equivalence MPC. Using the MG model from Chapter 4, the cost function from Chapter 5 and the forecast from Chapter 6, a certainty equivalence MPC problem is formulated. Motivated by [172, 180], the formulation relies on the assumption that the mean value of the forecast of load and available renewable power is certain. This widely used MPC approach represents the state-of-the-art and serves as a simple reference. The MPC problem is formulated as an MIQP that can be solved by available software.

Chapter 8: Minimax MPC. Based on the model from Chapter 4 and the cost from Chapter 5, a minimax MPC problem is formulated. Motivated by [104, 128], the approach considers a forecast of load and available renewable infeed in the form of time-varying intervals which are obtained using the forecast models from Chapter 6. Considering such intervals, the worst-case cost of all possible realization is minimized. This allows for robustness to uncertain load and renewable infeed at the expense of more conservative control actions than the certainty equivalence approach. The minimax MPC problem is formulated as a mixed-integer quadratically-constrained program (MIQCP) which can be solved by available software.

Chapter 9: Scenario trees. Using the forecast models from Chapter 6, scenario trees are derived. These are compact representations of forecast probability distributions that can be used to formulate stochastic MPC problems. The contributions of this chapter are twofold. The first part is based on [91, 93] and provides a formulation of the MG model from Chapter 4 considering a prediction in the form of a scenario tree. The second part focuses on the generation of scenario trees using a variant of forward tree construction that follows [169]. The resulting scenario tree provides the basis for the scenario-based approaches in Chapters 10 and 11.

Chapter 10: Risk-neutral stochastic MPC. The controller derived in this chapters considers a forecast in the form of a scenario tree (see Chapter 9). Motivated by [22, 103, 158, 178], the approach minimizes the expected value of the cost from Chapter 5 subject to constraints that follow the model from Chapter 4. Considering various forecast scenarios, robustness to uncertain load and renewable infeed can be provided. As the expected cost is minimized, the approach is less conservative than minimax MPC, where no probabilistic information is employed. The resulting MPC problem is formulated as an MIQP that can be solved by available software.

Chapter 11: Risk-averse MPC. Similar to risk-neutral stochastic MPC, this approach is based on the model from Chapter 4, the cost function from Chapter 5 and forecast scenario trees from Chapter 9. Various forecast scenarios are considered to provide robustness to uncertain renewable infeed and load. Additionally, motivated by [48, 118], uncertainty in the probabilities of the scenario tree can be considered. In detail, the approach allows to specify how much a probability distribution can be trusted by tuning the risk that the controller takes. This allows to continuously interpolate between risk-neutral stochastic MPC, where the probability distribution is fully trusted, and worst-case MPC, where the probabilities are not trusted at all. By choosing an acceptable risk, robustness to misestimated forecast probability distributions and so-called high-effect low-probability events can be provided which translates into low costs and a safe operation. In a similar fashion as in [247], the risk-averse MPC problem is reformulated using an epigraph relaxation. This results in an MIQCP which can be solved by available software.

Chapter 12: Case study. The properties of the different control approaches are illustrated in a simulation case study. Here, closed-loop simulations are performed for all model predictive controllers from the preceding chapters. The simulations are carried out with real forecast models and real weather data for two different MG models and a simulation horizon of one week. The first MG model includes a storage unit, a conventional generator, a wind turbine and a load. The second MG is motivated by [123] and includes two storage units, two conventional generators, one wind turbine, one PV power plant, and one load. For both models, closed-loop simulations are employed to compare the controllers with respect to (i) operating cost, (ii) constraint satisfaction, and (iii) robustness to misestimated forecast probability distributions and extreme events. Furthermore, a sensitivity analysis is performed with the simple MG. This analysis investigates robustness of the different schemes to inaccurate forecasts with systematic errors.

Chapter 13: Conclusion. The main results of the thesis are summarized and general conclusions are drawn. Moreover, possible future research directions are briefly outlined.

1.3 Related work

There exist various publications that are concerned with operation control of MGs. These can be distinguished by the way they treat uncertain load and renewable infeed. Well known formulations are (i) certainty equivalence, where a nominal forecast is assumed to be certain, (ii) worst-case, where a forecast in the form of robust intervals is considered, (iii) risk-neutral stochastic, where a forecast probability distribution is fully trusted, and (iv) risk-averse, where ambiguity in the forecast probability distribution is considered.

1.3.1 Certainty equivalence approaches

Many publications related to operation control of MGs rely on the assumption that the forecast of the uncertain input is certain. In what follows, first approaches for the grid-connected operation are reviewed. Then, control schemes for islanded grids are examined. Finally, limitations of the approaches are discussed.

Numerous approaches focus on the operation of grid-connected MGs. A central MG controller that is operated in a hierarchical control structure is presented in [256]. Here, an economic optimization that includes demand-side bidding and a forecast of RES is performed. In [54], the operation of interconnected MGs, modeled as a multi-agent system, is discussed. For a network of interconnected MGs that comprises microturbines, various loads and so-called prosumers that are formed of residential loads, small-scaled PV generators and storage units, an energy management and operational planning approach is presented in [112]. Furthermore, in [129] an MPC-based energy management approach that considers a deterministic forecast is discussed. Similar residential prosumer households are considered in [273]. Here, different approaches to control the households such that their aggregate power is flattened are presented. A distributed algorithm for a similar application is presented in [35]. In [36], an alternative algorithm is introduced that employs the alternating direction method of multipliers. Assuming interconnected MGs with storage units and controllable loads, in [37] a distributed model predictive operation control approach is presented. Based on the energy hub framework [70, 71], a nonlinear MPC algorithm is proposed in [9]. Furthermore, a two-stage approach that combines scheduling and predictive control for a similar application is introduced in [8].

Other certainty equivalent approaches consider both, islanded and grid-connected operation. In [177, 180, 181], mixed-integer MPC formulations for the operation of a single MG are presented. The formulations include storage dynamics with power conversion losses, limits of power consumed or provided by the potentially connected grid as well as conventional generators that can be enabled or disabled. In [110], a two-stage operation control approach is presented that comprises a schedule and a dispatch layer. Furthermore, a day ahead schedule for MGs that employs genetic algorithms is presented in [45].

Some certainty equivalent operation control approaches were exclusively developed for the operation of islanded MGs. In [16], an energy management approach is presented to dispatch generators by adapting power setpoints and droop gains of the units. Additionally, in [141] a method to schedule islanded MGs is introduced. Moreover, in [175] a controller based on a rolling horizon strategy is derived. In [101], an energy management problem for deterministic forecasts of load and renewable generation is formulated. Furthermore, in [155, 172] and in the author's work [89], MPC approaches for the operation of islanded MGs are presented.

Even though the presented approaches are promising, most of them are limited in at least one of the following regards. (i) They do not include a possible limitation of infeed from RES [16, 35, 101, 110, 129, 141, 155, 177, 180, 181, 256, 273]. (ii) The dynamics of the storage units are not modeled [16, 256]. (iii) It is not considered that conventional generators can be switched on and off [8, 9, 16, 112, 129]. (iv) The power flow over a transmission network is not explicitly modeled [16, 35, 37, 101, 112, 129, 141, 155, 175, 177, 180, 181, 256, 273]. (v) They are designed for the operation of grid-connected

MGs and therefore not directly applicable to islanded MGs [8, 9, 35–37, 54, 112, 129, 256, 273]. Furthermore, only in [16, 89] power sharing of grid-forming units is explicitly discussed. An additional drawback of all certainty equivalence approaches is the assumption of a perfect forecast. In settings with high renewable infeed of wind turbines and PV power plants, this assumption often does not hold. In practice, this leads to "unserved energy" [175] or violations of power or energy limits [89] and motivates approaches that model uncertainty in the forecast of load and available infeed from renewable sources, e.g., robust worst-case control schemes.

1.3.2 Worst-case approaches

There exist various publications related to the operation control of MGs, where uncertainties in the form of robust intervals are assumed. In what follows, first approaches associated with the grid-connected operation are reviewed. Then, operation control schemes for islanded grids are examined. Finally, the limitations of these approaches are discussed.

There exist many approaches for the operation of grid-connected MGs. In [279], a scheduling approach that considers uncertain infeed from RES is presented. For the operation of MGs, MPC approaches that consider uncertain renewable infeed and load are introduced in [128, 129] . Assuming uncertain wind turbine parameters, an MPC scheme for energy management is presented in [199]. Moreover, in [44] a multi-objective fuzzy logic expert system for energy management applications is discussed. This system can handle uncertainties related to forecasts. A robust power management system that considers uncertain available infeed from PV power plants and wind turbines is introduced in [104]. There also exist robust schemes for the energy hub framework from [70, 71], e.g., the scheduling approach presented in [179] which considers uncertain unit parameters.

For the operation of islanded MGs, the author's publications [89, 90] include two robust approaches. In [89], a minimax MPC scheme that considers uncertain forecasts of load and available renewable infeed is presented. This scheme was extended in [90] to an approximate closed-loop minimax MPC which is less conservative than the approach in [89].

Even though the presented approaches are promising, most of them are limited in at least one of the following aspects. (i) They do not include a possible limitation of infeed from RES [44, 128, 129]. (ii) Grid-forming storage units are not considered [104, 199]. (iii) Power sharing of grid-forming units is not modeled [44, 128, 129, 199, 279]. (iv) It is not considered that conventional generators can be switched on and off [44, 128, 129, 179, 199, 279]. (v) The power flow over a transmission network is not explicitly modeled [44, 104, 128, 129, 199, 279]. (vi) They are designed for the operation of grid-connected MGs and therefore not directly usable in islanded MGs [44, 128, 129, 179, 199, 279]. An additional drawback of robust approaches is that often the worst-case cost is minimized. In settings with high renewable infeed from wind turbines and PV power plants, this can lead to overly conservative operation regimes as discussed, e.g., in [90, 91]. This motivates the use of approaches where more complex forecasts of load and available renewable infeed are considered, e.g., risk-neutral stochastic control schemes.

1.3.3 Risk-neutral stochastic approaches

There exist numerous publications on operation control of MGs which include more complex probability distributions than, for example, certainty equivalence MPC. The presented schemes can be separated into those that consider random processes in the form of continuous probability distributions and those that consider discrete probability distributions.

Continuous probability distributions. There are several approaches for the operation of grid-connected MGs that consider continuous probability distributions. In [119–121], a wind power forecast with non-Gaussian probability distribution is assumed. In [83], an MPC scheme for a DC MG is presented. The proposed scheme assumes forecasts of load and PV infeed that follow a Gaussian probability distribution. Here, chance constraints on the power exchanged with the utility grid are imposed while minimizing the expected cost associated with this power. An approach that includes a schedule and a stochastic MPC is presented in [202]. Here, uncertain load and PV generation are considered.

Even though the presented approaches are promising, most of them are limited in at least one of the following regards. (i) They do not include a possible limitation of infeed from RES [83, 119, 121, 202]. (ii) Grid-forming storage units are not considered by any approach. (iii) None of the schemes models power sharing of grid-forming units explicitly. (iv) It is not considered that conventional generators can be switched on and off [83, 119–121]. (v) The power flow over a transmission network is not explicitly included in any of the control schemes. (vi) All approaches are designed for the operation of grid-connected MGs and therefore not directly applicable to islanded MGs.

Discrete probability distributions. There are several approaches that consider discrete probability distributions, e.g., independent forecast scenarios or so-called scenario trees. In what follows, first approaches associated with the grid-connected operation are reviewed. Then, operation control schemes for islanded grids are examined. Finally, the limitations of the approaches are discussed.

There exist some approaches for the operation of grid-connected MGs. In [253], a scenario-based two-stage approach is presented. The scheme aims to minimize the expected power losses and costs. Another two-stage approach that comprises an optimal schedule and an MPC is presented in [190]. Here, forecasts of uncertain weather and load in the form of a scenario tree are considered. Moreover, in [161] a scenario-based operation management that considers uncertain load, renewable infeed and market price is introduced.

Some approaches consider both, grid-connected and islanded operation. In [178], a two-stage approach that employs a scenario tree is presented. This approach is extended in [182] and used to control a lab-scale grid-connected MG.

There also exist a small number of approaches for the operation of islanded MGs. In [154], a scenario-based strategy for the operation of droop-controlled MGs is introduced. Here, a heuristic optimization approach is employed to minimize the expected cost. Furthermore, in [103] a sampling-based stochastic MPC scheme is presented assuming uncertain wind power and load. The certainty equivalence scheme from [101] is extended in [100] by using discrete forecast scenarios. In the author's work [91], a risk-neutral stochastic MPC scheme is presented. This scheme considers uncertain forecasts of load and renewable infeed in the form of a scenario tree and minimizes the expected MG operation costs.

Even though the presented approaches are promising, most of them are limited in at least one of the following regards. (i) They do not include a possible limitation of infeed from RES [100, 103, 154, 178, 182, 190, 253]. (ii) Grid-forming storage units are not considered [103, 178, 182, 190, 253]. (iii) Power sharing of grid-forming units is not explicitly modeled [103, 161, 178, 182, 190, 253]. (iv) It is not considered that conventional generators can be switched on and off [103, 154, 253]. (v) The power flow over a transmission network is not explicitly modeled [100, 161, 178, 182, 190, 253]. (vi) They are designed for the operation of grid-connected MGs and therefore not directly applicable to islanded MGs [161, 190]. An additional drawback of aforementioned approaches is that they require exact forecast probability distributions. In practical settings, this might not always be the case[4] [93]. This motivates the use of approaches that can provide robustness to misestimated forecast probability distributions, such as, risk-averse control schemes.

[4] Inexact forecast probability distributions can emerge, for example, from oversimplified forecast models or approximation errors in the construction of scenario trees.

1.3.4 *Risk-averse approaches*

Risk-averse optimization approaches have been popular in stochastic finance and actuarial mathematics for some time [191, 241]. Their key idea is to model inexact knowledge about the probability distribution, i.e., ambiguity, in an optimization problem. This permits resilience against bad forecast models and high-effect low-probability events.

Approaches that provide robustness to uncertain probability distributions are also becoming more popular in the power systems domain. In [274, 281, 282], risk-averse distributionally robust approaches for the unit commitment problem are presented. Furthermore, in [69, 160, 269] risk-averse scheduling strategies that employ the average value-at-risk (AVaR) are derived. For optimal trading of power from wind turbines, in [32, 162] two approaches that make use of the AVaR are introduced. There also exist several risk-averse approaches for optimal power flow, e.g., [147, 207, 208, 254, 278, 280].

The average value-at-risk is also known as conditional value-at-risk.

There is a small number of publications that propose risk-averse approaches in the MG context. In [166], a risk-averse stochastic programming approach for the design process of an MG is presented. Furthermore, in [118] a risk-averse MPC approach is used for the energy management of storage units in an MG. Drawbacks of the presented approach are that it only considers renewable infeed as uncontrollable negative power demand and that it does not include conventional generators. Furthermore, it is designed for the operation of grid-connected MGs and therefore not directly usable for islanded MGs. In the author's work [93], a risk-averse operation control approach for islanded MGs is presented. The approach can be used for the operation of grids with very high share of RES by considering grid-forming storage units and conventional generators that can be disabled. Furthermore, the power flow over the transmission lines as well as power sharing between grid-forming units is modeled. By employing the AVaR, the derived controller can provide robustness to misestimated forecast probability distributions and high-effect low-probability events.

1.4 Publications

Most results presented in this work are based on existing publications. To all of the them, the author of this thesis has made substantial contributions. The publications in reverse chronological order are as follows.

- C. A. Hans, P. Sopasakis, J. Raisch, C. Reincke-Collon, and P. Patrinos. Risk-averse model predictive operation control of islanded microgrids. *IEEE Transactions on Control Systems Technology*, 28(6):2136–2151, 2020.
- C. A. Hans and E. Klages. Very short term time-series forecasting of solar irradiance without exogenous inputs. In *6th International Conference on Time Series and Forecasting*, pages 1007–1018, 2019.
- C. A. Hans, P. Braun, J. Raisch, L. Grüne, and C. Reincke-Collon. Hierarchical distributed model predictive control of interconnected microgrids. *IEEE Transactions on Sustainable Energy*, 10(1):407–416, 2019.

- C. A. Hans, P. Sopasakis, A. Bemporad, J. Raisch, and C. Reincke-Collon. Scenario-based model predictive operation control of islanded microgrids. In *54th IEEE Conference on Decision and Control*, pages 3272–3277, 2015.
- C. A. Hans, V. Nenchev, J. Raisch, and C. Reincke-Collon. Approximate closed-loop minimax model predictive operation control of microgrids. In *European Control Conference*, pages 241–246, 2015.
- C. A. Hans, V. Nenchev, J. Raisch, and C. Reincke-Collon. Minimax model predictive operation control of microgrids. In *19th IFAC World Congress*, pages 10287–10292, 2014.

Moreover, the author of this thesis contributed to publications [102, 122, 123, 168, 223, 229, 232, 284]. They are not a direct part of the thesis, even though many of them address control issues in MGs.

1.5 Outline

The remainder of this thesis is structured as follows. In Chapter 2, control of MGs is discussed and detailed requirements for the operation control of islanded MGs are posed. Then, in Chapter 3 preliminaries on notation and basics on MPC, optimization theory as well as power systems are provided. The model of an islanded MG is introduced in Chapter 4. For this model, a cost function is presented and employed in a prescient MPC formulation in Chapter 5. In Chapter 6, forecasts of load demand and available renewable infeed of wind turbines and PV power plants are discussed. These forecasts are then employed in a certainty equivalence MPC formulation in Chapter 7. Subsequently, a robust minimax MPC formulation is derived in Chapter 8. In Chapter 9, forecast scenario trees are introduced. These are then used to formulate a risk-neutral stochastic MPC problem in Chapter 10 and a risk-averse MPC problem in Chapter 11. In Chapter 12, the different control approaches are compared in various numerical case studies. Chapter 13 concludes the thesis with a summary and future research directions.

2 Problem statement

The goal of this chapter is to identify central challenges in operation control of MGs. These provide an important basis for the design and evaluation of different MPC schemes throughout in this work.

This chapter is structured as follows. In Section 2.1, an introduction to MGs is provided. Then, in Section 2.2 control of MGs with high renewable share is discussed. Finally, in Section 2.3 requirements for operation control of islanded MGs are posed.

2.1 Microgrid concept

Worldwide, the share of RES continuously increased in recent years [205]. From this increase, two major challenges in the electric power sector arise.

The first challenge stems from the change in the power systems' structure. Conventional power systems are typically composed of a small number of large-scale generators. RES in contrast are often small-scaled and geographically dispersed over a wide area [275]. Consequently, as more conventional generators are replaced by renewable ones, the structure of power systems changes from grids with a small number of large-scale conventional units to grids with a large number of small-scale renewable units.

The second challenge arises from the intermittent nature of many renewable generators [113, 275]. In conventional power systems, the operation is typically focused on generation units where the power can be changed in a deterministic manner

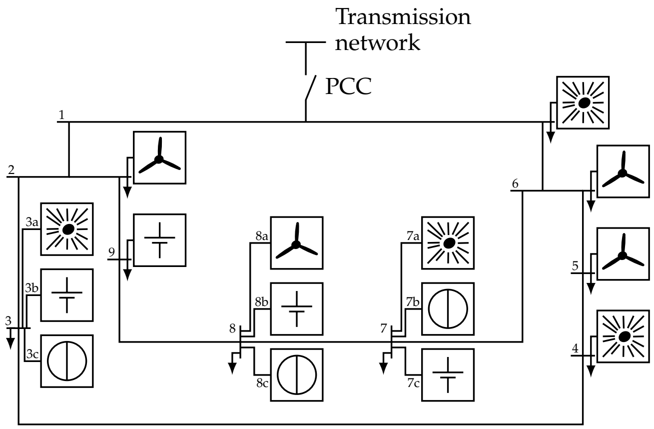

Figure 2.1: Example of an MG. Note that the MG can be connected to or isolated from the transmission network via the point of common coupling (PCC). Example based on [216].

within given operating bounds. In power systems with high share of RES, power generation can be non-deterministic due to intermittent infeed of wind turbines or PV power plants. As long as the share of RES is small, they can be simply treated as negative loads. With increasing renewable share, the renewable sources need to be explicitly considered in operation schemes of electric power systems.

Thus, existing strategies cannot be directly applied to future power systems with high share of RES. This motivates approaches tailored for decentralized and intermittent generation. The microgrid concept [94, 95, 131] represents such an approach for future power systems. It aims to partition the overall network into smaller MG cells that are operated by local control systems. This permits each MG to act as "a single controllable system" [132, 173] to the outside world. By forming MGs that appear as monolithic parts, the complexity of control layers that coordinate a certain part of the grid can be reduced. Furthermore, fluctuations of RES and load can be compensated locally by matching generation and consumption inside each MG as far as possible. This allows to reduce uncertainty in the operation of the overall grid, e.g., regarding power transfer over the power lines that connect the MGs.

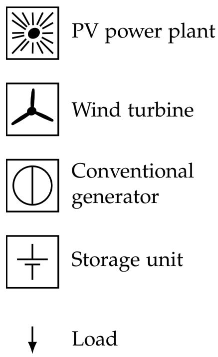

As illustrated in Figure 2.1, MGs are typically composed of storage units, renewable and conventional generators [81, 114, 132]. These units are interconnected by transmission lines and operated to provide power to the loads. MGs can be operated in grid-connected or island mode [62, 95, 131, 132].

An MG in grid-connected mode is electrically coupled with a larger grid via the point of common coupling (PCC). In case of failures, it can be disconnected from the transmission network and operated as an islanded MG [135, 187]. Small power systems that do not have a connection to a transmission network due to their geographical location, e.g., islands or rural areas, also fall into the class of islanded MGs. In islanded operation, all fluctuations of renewable generation and load must be covered locally by adapting the power of the remaining units. Maintaining this local power equilibrium renders the operation of islanded MGs particularly challenging.

2.2 *Hierarchical control of MGs*

Based on requirements on different timescales and to facilitate the transition from conventional power systems, hierarchical control approaches have been advocated for MGs [27, 62, 80, 82]. Motivated by conventional power systems[1], the lower control layers are often denoted as primary and secondary control. The control layer that comprises scheduling [7, 174, 242] and tertiary control [149, 235] is often referred to as operation control or energy management.[2]

[1] More information on control of conventional power systems can be found, for example, in [149, 235].

[2] In some publications this layer is also referred to as tertiary control. To emphasize that it comprises schedule and tertiary control, in this thesis it is referred to it as operation control.

2.2.1 *Primary control*

The lowest control layer that typically acts on a timescale of milliseconds to seconds is widely referred to as primary control. The goal of this layer is to maintain frequency and voltage stability [27, 210, 225]. Furthermore, it aims to ensure that a change in power, e.g., caused by uncertain renewable infeed or load, is covered by the grid-forming units in a desired proportional manner such that an equilibrium of generation, consumption and storage power is maintained [227]. This so-called power sharing [197] is often provided by inverter-interfaced storage units and conventional generators [210].

To ensure a safe and reliable operation, primary control is frequently implemented in a decentralized manner using, e.g., droop control [187, 232]. Thus, typically this control layer only relies on the physical coupling of the units via the electrical lines and does not require explicit communication. This, however, typically leads to steady state deviations in frequency and voltage amplitudes [123]. Secondary control can be employed to compensate these deviations.

2.2.2 *Secondary control*

The control layer above primary control is widely referred to as secondary control and typically acts on a timescale of minutes. It aims to compensate steady state frequency deviations and keep voltage amplitudes in a desired range. Furthermore, it can be used to ensure reactive power sharing [125, 228, 230] as well as accurate active power sharing in presence of primary control schemes with inaccurate clocks [123, 124, 126]. In literature, one can find both, secondary control approaches that rely on communication with a central entity [152, 159] and distributed secondary control schemes that only require peer-to-peer communication between the units [28, 237, 243, 244].

Using a hierarchical control approach composed of primary and secondary control, a stable operation where frequency and voltages remain in desired ranges can be achieved. Moreover, active and reactive power sharing can be ensured. However, it is very challenging to optimize the operation of complex MGs using only primary and secondary control. Therefore, a supervisory operation control layer is often used to ensure a safe and economically meaningful operation.

2.2.3 *Operation control*

The layer above secondary control is often referred to as operation control or energy management. It typically acts on a timescale of minutes to fractions of hours and optimizes the MG operation by providing power setpoints to the lower control layers. These setpoints can be found by solving optimization problems that include a cost function as well as a set of constraints that represent the MG's behavior [116]. The solutions of the optimal control problems usually depend on the state of charge as well as forecasts of available renewable power and load. With increasing share of RES, it becomes hard to accurately predict these values and obtain a meaningful operation schedule over an entire day. Therefore, it appears beneficial to combine the functionalities of schedule

[7, 174, 242] and tertiary control [149, 235] to form a single optimal operation control layer.

A widely adopted approach in this context is model predictive control. In MPC, the system behavior is predicted into the future using forecasts of renewable infeed and load as well as measurements of the state of charge. By minimizing a cost function subject to constrains, that represent, e.g., the dynamics of the system or energy and power limits, optimal power setpoints for the units can be obtained.[3]

[3] There exist various operation control approaches for grid-connected and islanded MGs. For a comprehensive overview, the reader is kindly referred to Section 1.3.

2.3 *Requirements for operation control of islanded microgrids*

One big challenge arises from the fact that RES are typically located relatively close to each other in islanded MGs. This reduces the effects of smoothing by geographical dispersion of RES [117, 151]. Consequently, more fluctuations than in conventional power systems can be found in islanded MGs.

Another important challenge originates from the local power balance. In grid-connected operation, the fluctuations of loads and RES can be covered outside the MG, e.g., by large-scale power plants or other grid-connected MGs. Unfortunately, in island mode this is not possible. Here, all fluctuations of load and weather-dependent RES need to be covered by the units in the MG [187]. This renders islanded operation of MGs with high renewable share particularly challenging.

It is useful to employ storage units that participate in primary control to deal with the fluctuations in islanded MGs. These allow to reduce frequency variations and enable an operation without conventional generators in some time instants. Moreover, renewable sources must be controlled, e.g., by allowing to limit their infeed. Additionally, operation control schemes must be robust to uncertain renewable infeed and inaccurate forecasts. From these general considerations, the following requirements for the operation control of islanded MGs with high share of RES can be deduced.

Remark 2.3.1. The requirements in this section were posed having an islanded AC MG with primary and secondary control layers as described in Section 2.2 in mind. However, they also apply for MGs with other control approaches on the lower layers as long as they consider proportional power sharing of grid-forming units and allow a limitation of RES.

2.3.1 *Renewable generators*

One big challenge that comes with many RES is that their infeed depends on uncertain weather conditions [86]. Consequently, a significant number of RES has uncertain infeed. Operation strategies for MGs with high share of RES therefore need to deal with this uncertainty [252].

In the design of islanded MGs with a desired renewable share, there is a trade-off between storage size and the amount of installed RES. Here, one extreme case is to install storage units with a large capacity that allow to store all renewable generation. Unfortunately, this comes with a high financial invest for the storage units. It is also possible to choose a smaller storage capacity and install more RES. This, however, requires a curtailment of RES [276], e.g., if all storage units are fully charged. Consequently, operation control must take a possible limitation of RES into account.

Moreover, the nature of the financial investment in renewable and conventional generators differs significantly. Many conventional generators come with a small capital cost per expected annual infeed and higher running costs per provided energy that is often driven by fuel costs [261]. RES, such as, wind turbines and PV power plants, on the contrary have a high capital cost and almost no power-dependent operation costs [261]. Therefore, in operation control of existing MGs, it is desired to substitute conventional by renewable generation as much as possible.

If MG topology and weather conditions allow, it is even desired to disable conventional generators and operate the grid only with renewable and storage units. For MGs to work without conventional generators providing voltage and frequency, it is therefore required that storage units are able to operate in grid-forming mode as discussed in the next section.

2.3.2 *Storage units*

Storage units are often connected to the grid via inverters. These can be operated in grid-feeding or grid-forming mode, depending on the implementation of the lower control layers [231]. In grid-feeding mode, the units connect to an existing grid and provide or consume a desired active and reactive power or current. In grid-forming mode, the units provide a desired voltage with a certain amplitude and frequency [268]. In islanded MGs, it is desirable to operate them in grid-forming mode for the following reasons.

In MGs with high renewable share, there are time instants where renewable infeed fully covers the load. In such conditions, it is desirable to disable all conventional generators[4]. Unfortunately, renewable generators, such as, PV power plants or wind turbines, are usually operated in grid-feeding mode, i.e., they require a grid with a given voltage and frequency that they can connect to [17]. This voltage and frequency can be provided by storage units with grid-forming inverters.

[4] Note that conventional generators are typically operated as grid-forming units.

The power of the grid-forming units changes with intermittent renewable infeed and load to maintain a local power equilibrium. In grids without storage units that react to frequency deviations, these fluctuations need to be covered by grid-forming conventional generators which can drive them to operating conditions with lower fuel efficiencies. Furthermore, the change in renewable infeed can lead to violations of their power limits if the setpoints are not chosen accordingly. Grid-feeding storage units can cover some of the fluctuations such that the conventional generators can be operated closer to their desired operating conditions. The lower control layers can even be designed such that storage units cover most fluctuations (see, e.g., [246]), which allows to keep conventional generators even closer to their desired operating conditions.

As observed in [164], a transient operation does not per se lead to an increase in fuel consumption.

Another important challenge is that uncertain load and renewable infeed affect the power and energy of grid-forming storage units. Depending on load and renewable infeed, the storage power can be lower or higher than the power setpoint provided by the operation control layer. This difference between power setpoint and power can be significant in grids with high renewable share. Therefore, it is required to model the effects of uncertain infeed and load on the power and energy of grid-forming storage units to ensure that their physical constraints are satisfied.

2.3.3 *Conventional generators*

In the context of islanded MGs with high renewable share, grid-forming conventional generators are often used as backup generators in times of low renewable infeed and empty storage units. Moreover, they can be used if the load is very high and cannot be solely covered by the other units.

One challenge associated with conventional units is that, similar to grid-forming storage units, uncertain load and renewable infeed drive their power away from their power setpoints. Therefore, it is required to consider the effects of uncertain load and renewable infeed on their power to ensure that they remain within given bounds [116].

Moreover, in MGs that include storage units, conventional generators are often disabled during periods of high renewable infeed or available stored energy. The decision whether they are enabled or disabled has to be taken by the operation control keeping in mind their running costs and the cost associated with enabling or disabling them [180].

2.3.4 *Power sharing*

In presence of uncertain load and renewable infeed, an equilibrium of generation, consumption and storage power needs to be maintained. This is typically ensured by adapting the power provided or consumed by the grid-forming units [187]. Among these units, it is desired to compensate the fluctuations that drive them away from their power setpoints in a proportional manner, e.g., according to their rated power. There are different ways to achieve a desired proportional power sharing, for example, droop control [227].

The major challenge that comes with power sharing is that the operation control needs to model how much a change in load or renewable power affects the power output of the grid-forming units to ensured that all units remain within their operational limits and that the cost associated with the units' power is minimal. This is particularly challenging in settings where grid-forming conventional units are enabled and disabled as this affects power sharing (see Examples 4.8.1 and 4.8.2).

2.3.5 *Power flow over transmission lines*

In islanded operation, MGs are not connected to a bigger transmission network. However, the units within the MG are connected to each other by power lines. In setups where the units are not in one place feeding into a single bus as in [180], the transmission lines of the grid need to be considered. More precisely, the power flow over the transmission lines needs to be taken into account in order to prevent a violation of power limits [172].

2.3.6 *Robustness to uncertain load and renewable generation*

In MGs without RES, forecasts of the uncertain input often follow a normal distribution [30, Section 2.8]. With increasing share of RES, this is no longer the case as the forecast probability distributions can significantly change with weather conditions, e.g., because of the nonlinear relation between wind speed and available renewable power of wind turbines [195]. Additionally, the power of renewable units can be limited which can additionally modify forecast probability distributions. Therefore, it is required to employ control schemes that do *not* require the uncertain input to be Gaussian.

The forecast accuracy of available renewable power can be much lower than the accuracy of load forecasts (see Chapter 6). This effect plays an important role in grids with high share of uncertain RES, where the installed renewable power exceeds the rated load demand. Therefore, the operation control layer must provide power setpoints that ensure a safe MG operation in the sense that the units and transmission lines remain within their given operating limits, in presence of uncertainties. Moreover, the power setpoints should be provided in a way that enables an economic operation of the grid by maximizing renewable and minimizing conventional generation in settings where load and renewable infeed are not exactly known.

2.3.7 *Robustness to inaccurate forecast models and extreme events*

Islanded MGs can be small-scaled in terms of rated load power. Consequently, the project volume of the deployment of such an MG can be quite small. Therefore, it is desired to use cost-efficient forecast models [256], that do not require exhaustive training or many observations and can be easily identified. Such simple models can come with a decreased forecast accuracy. Moreover, it can happen that forecast models very roughly approximate the underlying probability distribution. Therefore, robustness of the operation control to misestimated forecast probability distributions is important.

Some events in the operation of MG can have a high effect on the cost if they occur, but have a small probability of occurring. Such high-effect low-probability events usually play a minor role in operation control schemes due to their low probabilities. However, it is desired to operate MGs in ways that are averse to this risk, i.e., that ensure that such events do not lead excessive costs.

2.4 *Summary*

In this chapter a problem statement targeted towards the operation control of islanded MGs was given. First, the MG concept was introduced and hierarchical control of MGs was discussed. Then, requirements for the operation control of MGs with high share of RES were posed.

Based on this problem statement, in Chapter 4, the model of an islanded MG is derived. Moreover, in Chapters 5, 7, 8, 10 and 11 different control approaches are deduced and assessed regarding their compliance with the control challenges posed in this chapter. Furthermore, in Chapter 6 different time-series based forecast models are identified. However, first, some preliminaries are posed in the next chapter.

3 Preliminaries

In the previous chapter, the MG concept was introduced and important challenges in MG operation control were posed. Before formulating an MG model in Chapter 4, we discuss some basics from different domains in order to keep the successive chapters more compact and prevent repetitions.

This chapter is structured as follows. In Section 3.1, some basics on notation are given. Then, in Section 3.2 basic principles of model predictive control are discussed. In Section 3.3, some reformulations from optimization theory are introduced. Finally, in Section 3.4 basics regarding the power flow over the transmission network are provided.

3.1 Notation

Sets. Throughout this work, blackboard bold letters denote sets. The sets of real numbers, negative real numbers and positive real numbers are denoted by $\mathbb{R}$, $\mathbb{R}_{<0}$ and $\mathbb{R}_{>0}$, respectively. Moreover, the set of nonpositive real numbers is $\mathbb{R}_{\leq 0}$ and the set of nonnegative real numbers is $\mathbb{R}_{\geq 0}$. The set of natural numbers is $\mathbb{N}$ and the set of nonnegative integers is $\mathbb{N}_0$. The set of nonnegative integers in the closed interval $[a, b] \subset \mathbb{N}_0$ is $\mathbb{N}_{[a,b]} = \{x | x \in \mathbb{N}_0 \wedge a \leq x \leq b\}$. Furthermore, the set of Boolean numbers is $\mathbb{B} = \{0, 1\}$ and the set of complex numbers is $\mathbb{C}$. The complex number $x \in \mathbb{C}$ is given by $x = \hat{x}\mathrm{e}^{\imath\phi}$, where $\hat{x} = |x|$ is the modulus of x, ϕ is the argument of x, e is Euler's number and $\imath$ is the imaginary unit. Alternatively, every complex number can be described by $x = \Re(x) + \imath\Im(x) = |x|(\cos(\phi) + \imath \sin(\phi))$.

Here, $\Re(x) = |x|\cos(\phi)$ is the real part and $\Im(x) = |x|\sin(\phi)$ the imaginary part of x. The complex conjugate of $x \in \mathbb{C}$ is $x^* = \Re(x) - \imath\Im(x)$. The cardinality of a countable set $\mathbb{I}$ is denoted by $|\mathbb{I}|$. The set $\{a_0, a_1, \ldots, a_N\}$ of cardinality $N+1$, $N \in \mathbb{N}$ is referred to as $\{a_i\}_{i=0}^{N}$. Likewise, the set including the elements a_i for all $i \in \mathbb{I} \subset \mathbb{N}_0$ is referred to as $\{a_i\}_{i\in\mathbb{I}}$.

Vectors. A vector of size N where all entries are 1 is denoted by 1_N and a vector of same size where all entries are 0 by 0_N. Similarly, an $N \times M$ matrix where all entries are 1 is denoted by $1_{N\times M}$ and a matrix of the same size where all entries are 0 by $0_{N\times M}$. The $N \times N$ identity matrix is denoted by I_N. Consider a scalar $b \in \mathbb{R}$ and a vector $a = [a_1 \ \cdots \ a_N]^\top \in \mathbb{R}^N$. For a compact notation, $a + b$ is used instead of $a + 1_N b$. Likewise, $a - b$ is shorthand for $a - 1_N b$. The matrix with diagonal entries $a_1, \ldots, a_N$ and zeros else is denoted by $\mathrm{diag}(a)$. The Euclidean norm of a is $\|a\|_2 = \sqrt{\sum_{i=1}^N a_i^2}$. The vector with elements $a_1, \ldots, a_N$ is denoted by $[a_i]_{i=1}^N = [a_1 \ \ldots \ a_N]^\top$. Consider the set $\mathbb{V} = \{v_1, v_2, \ldots, v_N\} \subset \mathbb{N}_0$ with elements $v_i < v_j$ for $i < j$, $i \in \mathbb{N}_{[1,N]}$, $j \in \mathbb{N}_{[1,N]}$. Then, the vector $[a_{v_1} \ a_{v_2} \ \ldots \ a_{v_N}]^\top$ can be equally expressed as $[a_i]_{i\in\mathbb{V}}$. The sum over all a_i for $i = v_1, v_2, \ldots, v_N$ is denoted by $\sum_{i\in\mathbb{V}} a_i$.

Basic operators. Consider the vectors $a \in \mathbb{R}^N$ and $b \in \mathbb{R}^N$. The relationship $a > b$ is understood in an element-wise sense, i.e., $a > b$ is identical to $a_i > b_i$ for all $i \in \mathbb{N}_{[1,N]}$. The same holds for $a < b$, $a = b$, $a \geq b$ and $a \leq b$. In a similar fashion, $\max(a, b)$ provides the element-wise maximum and $\min(a, b)$ the element-wise minimum of the vectors. Consider $a \in \mathbb{R}^N$ and $b \in \mathbb{R}$. The relation $a > b$ is shorthand for $a > 1_N b$. The same holds for $a < b$, $a = b$, $a \geq b$ and $a \leq b$ as well as $\max(a, b)$ and $\min(a, b)$. When used with one single vector as input, $\max(a)$ returns the largest element of a and $\min(a)$ the smallest element of a. Consider the nonempty set $\mathbb{X} \subseteq \mathbb{R}^N$ and a function $f : \mathbb{X} \to \mathbb{R}$ that exhibits a minimum over $\mathbb{X}$. Then, the minimum value of f over $\mathbb{X}$ is denoted by $\min_{x\in\mathbb{X}} f(x)$ and the maximum value of f over $\mathbb{X}$ by $\max_{x\in\mathbb{X}} f(x)$. The domain $\mathbb{X}^\star \subseteq \mathbb{X}$ for which the function attains the minimum value is denoted by $\mathbb{X}^\star = \arg\min_{x\in\mathbb{X}} f(x)$.

Box plots. Box plots [257] are used to visualize probability distributions in some parts of this thesis. The variant of box plots considered is shown in Figure 3.1. Here, the dot in the middle indicates the median, i.e., the middle value that separates the lower from the upper half of the distribution. The lower end of the white area, q_1, marks the first quartile, i.e., the 25th percentile and the upper end, q_3, marks the third quartile, i.e., the 75th percentile. Thus, the white area around the median contains the middle 50 % of the values. The difference $q_3 - q_1$ is often referred to as interquantile range. The lower whisker, i.e., the lower end of the lower line, marks the smallest value that is greater than $q_1 - 1.5(q_3 - q_1)$. The upper whisker marks the largest value that is smaller than $q_3 + 1.5(q_3 - q_1)$. The outliers, i.e., the values that are below or above the whiskers, are marked by circles.

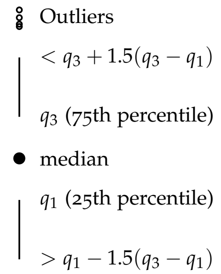

Figure 3.1: Example of a box plot. Illustration motivated by [88].

3.2 *Model predictive control*

Model predictive control is an optimal control based approach that is widely adopted in industry [31, 68, 163, 201]. The goal of MPC is to find a control input $v(k) \in \mathbb{R}^{N_\text{v}}$, $N_\text{v} \in \mathbb{N}$ at time instant $k \in \mathbb{N}_0$ by minimizing the cost function of an optimal control problem [3, 79, 150, 156, 203, 204] over a finite prediction horizon $J \in \mathbb{N}$. Therefore, state and auxiliary variables are predicted into the future. Typically, these variables are affected not only by the control input but also by uncertain inputs (see Figure 3.2). These can be accounted for by using forecasts in MPC problem formulations.

The decision variables of an MPC problem formulated at time $k \in \mathbb{N}_0$ are the inputs $v(k+j|k) \in \mathbb{R}^{N_\text{v}}$ at prediction steps $j = 0, \dots, J-1$ which are collected in $\boldsymbol{v} = [v(k+j|k)]_{j=0}^{J-1}$

The variable $a(k+j|k)$ refers to a prediction performed at time instant k for prediction step j, i.e., for future time instant $k+j$.

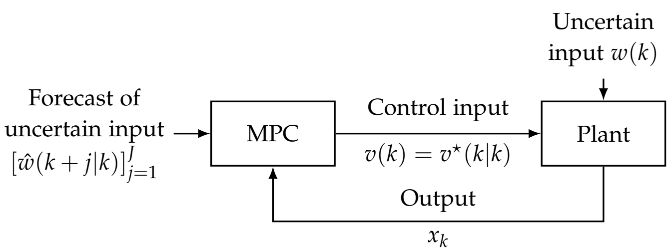

Figure 3.2: Block diagram of model predictive controller (MPC) and controlled plant.

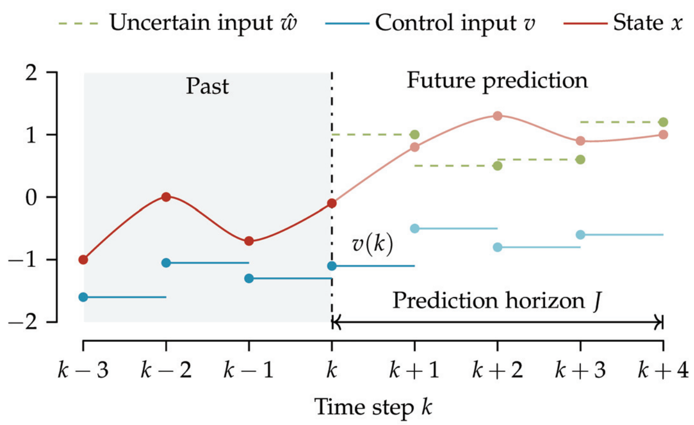

Figure 3.3: Example trajectories of MPC approach with prediction horizon $J = 4$. The first value of the predicted optimal input $v^\star(k|k), \dots, v^\star(k+3|k)$ is applied to the system, i.e., $v(k) = v^\star(k|k)$. Based on [68].

and the states[1] $x(k+j+1|k) \in \mathbb{R}^{N_\mathrm{s}}$, $N_\mathrm{s} \in \mathbb{N}$, which are collected in $\boldsymbol{x} = [x(k+j|k)]_{j=1}^{J}$. Moreover, a forecast of the uncertain input $\hat{w}(k+j+1|k) \in \mathbb{R}^{N_\mathrm{w}}$, $N_\mathrm{w} \in \mathbb{N}$ is employed. An MPC problem can be formulated using the stage cost function ℓ_j, the discrete time state transition function f_x and the state inequality constraints function $\tilde{f}_x$ as well as the functions $\tilde{f}_{vw}$ and f_{vw} that represent inequality and equality constraints related to the uncertain input and the control input. With these functions, the MPC problem reads as follows.

[1] Note that the plant model which includes the discrete time dynamics enters the optimization problem in the form of the constraints (3.1). Therefore, inputs *and* states are considered as decision variables throughout this work.

Problem 1 (Model predictive control)**.** Solve the optimization problem

$$\min_{\boldsymbol{v},\boldsymbol{x}} \sum_{j=0}^{J-1} \ell_j\big(v(k+j|k), \hat{w}(k+j+1|k), x(k+j+1|k)\big)$$

subject to

$$x(k+j+1|k) = f_x(x(k+j|k), v(k+j|k), \hat{w}(k+j+1|k)), \tag{3.1a}$$

$$0 \leq \tilde{f}_x(x(k+j+1|k)), \tag{3.1b}$$

$$0 \leq \tilde{f}_{vw}(v(k+j|k), \hat{w}(k+j+1|k)), \tag{3.1c}$$

$$0 = f_{vw}(v(k+j|k), \hat{w}(k+j+1|k)). \tag{3.1d}$$

$\forall j = 0, \dots, J-1$,
with given[2] initial state $x(k|k) = x_k$.

[2] In this example, full state measurement is assumed, i.e., the output of the plant is the state x_k at time instant k.

In Problem 1, the cost function is minimized over the prediction horizon subject to constraints (3.1). The resulting predicted optimal input trajectory $v^\star(k|k), \ldots, v^\star(k+J-1|k)$ is obtained by solving Problem 1 with given initial state x_k. This trajectory for a given forecast of the uncertain input and state as well as past control inputs and states is shown in Figure 3.3.

Remark 3.2.1. Note that throughout the thesis, in MPC problem formulations, the time instant of the predicted uncertain input is associated with the predicted state that result from it. For example, the uncertain $\hat{w}(k+j+1|k)$ directly influences the state $x(k+j+1|k)$ via (3.1a).

From the predicted optimal input trajectory, $v(k) = v^\star(k|k)$ is applied to the plant. After a certain time, typically the sampling time T_s, has passed, a new measurement x_{k+1} is obtained and Problem 1 is solved again at time instant $k+1$. This scheme is repeated in a receding horizon manner (see [18, 23, 204]) as illustrated in Algorithm 1. By using the updated state measurement x_k as initial value every time the MPC problem is solved, we include feedback in the system.

1: At time k: Measure state x_k and obtain forecast $[\hat{w}(k+j|k)]_{j=1}^{J}$.
2: Solve Problem 1.
3: Apply control input $v(k) = v^\star(k|k)$.
4: At the next time instant: increment $k = k+1$ and **go to** 1.

Algorithm 1: Model predictive control.

3.3 *Optimization theory*

In this section, some preliminaries from optimization theory are discussed. These include auxiliary results required to reformulate different MPC problems in computationally tractable ways. Furthermore, the so-called "Big-M" reformulations of two operators are posed.

3.3.1 *Auxiliary results*

In what follows two lemmata that are required to formulate the optimal control problems in Chapters 8 and 11 in computationally tractable ways are introduced. First, a lemma that was published in the author's work [93, Lemma 1.1] is repeated.

Lemma 3.3.1. Let $\emptyset \neq \mathbb{X} \subseteq \mathbb{R}^{N_\mathrm{x}}$ and $\emptyset \neq \mathbb{Y} \subseteq \mathbb{R}^{N_\mathrm{y}}$ as well as $f : \mathbb{X} \times \mathbb{Y} \to \mathbb{R}$ and $\beta \in \mathbb{R}$. Consider that for every $x \in \mathbb{X}$, $f(x, y)$ attains a minimum over $\mathbb{Y}$, i.e., $\min_{y \in \mathbb{Y}} f(x, y)$ exists. Then, the optimization problem

$$\min_{x \in \mathbb{X},\, v \in \mathbb{R}^{N_\mathrm{v}}} \ell(x, v) \quad \text{subject to} \quad \min_{y \in \mathbb{Y}} f(x, y) \leq \beta,$$

with cost function $\ell : \mathbb{R}^{N_\mathrm{x}} \times \mathbb{R}^{N_\mathrm{v}} \to \mathbb{R}$ is equivalent to

$$\min_{\substack{x \in \mathbb{X},\, v \in \mathbb{R}^{N_\mathrm{v}}, \\ y \in \mathbb{Y}}} \ell(x, v) \quad \text{subject to} \quad f(x, y) \leq \beta$$

in the sense that both problems share the same optimal cost and sets of optimal values.

Proof. As the two problems have the same cost function, it suffices to show that they have the same constraint sets. Therefore, we define the sets

$$\begin{aligned} \mathbb{S} &= \left\{x \in \mathbb{R}^n \mid \min_{y \in \mathbb{Y}} f(x, y) \leq \beta\right\} \quad \text{and} \\ \mathbb{S}' &= \{x \in \mathbb{R}^n \mid \exists y \in \mathbb{Y} \text{ such that } f(x, y) \leq \beta\}. \end{aligned}$$

Take $x \in \mathbb{S}$, i.e., $\min_{y \in \mathbb{Y}} f(x, y) \leq \beta$. Since the minimum exists, there is a $y^\star \in \mathbb{Y}$ such that $f(x, y^\star) \leq \beta$. Hence, $x \in \mathbb{S}'$ and consequently $\mathbb{S} \subseteq \mathbb{S}'$.

Take $x \in \mathbb{S}'$, i.e., there is a $y_0 \in \mathbb{Y}$ such that $f(x, y_0) \leq \beta$. Then, $x \in \mathbb{S}$ because $\min_{y \in \mathbb{Y}} f(x, y) \leq f(x, y_0) \leq \beta$, and consequently $\mathbb{S}' \subseteq \mathbb{S}$. This proves that $\mathbb{S}' = \mathbb{S}$. $\square$

The next lemma is motivated by [34, 52, 138, 139]. It provides an epigraph formulation of the max operator (see Figure 3.4) which is later required in Sections 8.3 and 11.1. For more information on epigraphs, the reader is kindly referred to [26, 34, 211, 215].

Lemma 3.3.2. Consider two functions $\ell_1 : \mathbb{R}^{N_\mathrm{x}} \to \mathbb{R}$ and $\ell_2 : \mathbb{R}^{N_\mathrm{x}} \to \mathbb{R}$. For every $x \in \mathbb{X} \subseteq \mathbb{R}^{N_\mathrm{x}}$, $\mathbb{X} \neq \emptyset$ the maximum of $\ell_1(x)$ and $\ell_2(x)$ is

$$\max(\ell_1(x), \ell_2(x)) = \min_{\substack{\beta \in \mathbb{R} \\ \ell_1(x) \leq \beta \\ \ell_2(x) \leq \beta}} \beta. \tag{3.2}$$

Proof. Consider a function $\ell : \mathbb{R}^{N_\mathrm{x}} \to \mathbb{R}$ and the auxiliary variable $\beta \in \mathbb{R}$. Then, for given $x \in \mathbb{X}$, it holds that

$$\ell(x) = \min_{\substack{\beta \in \mathbb{R} \\ \ell(x) \leq \beta}} \beta. \tag{3.3}$$

For $\ell(x) = \max(\ell_1(x), \ell_2(x))$, this becomes

$$\max(\ell_1(x), \ell_2(x)) = \min_{\substack{\beta \in \mathbb{R} \\ \max(\ell_1(x), \ell_2(x)) \leq \beta}} \beta. \tag{3.4}$$

The result of $\ell(x) = \max(\ell_1(x), \ell_2(x))$ is either $\ell_1(x)$ or $\ell_2(x)$. Hence, we know that either $\ell_2(x) \leq \ell_1(x) \leq \beta$ or $\ell_1(x) \leq \ell_2(x) \leq \beta$ holds. Replacing $\max(\ell_1(x), \ell_2(x)) \leq \beta$ by $\ell_1(x) \leq \beta$ and $\ell_2(x) \leq \beta$, therefore leads to a minimization where the largest value, $\ell_1(x)$ or $\ell_2(x)$, provides the lower bound for β while the other inequality automatically holds. Therefore, (3.4) is equivalent to the right-hand side of (3.2). This completes the proof. □

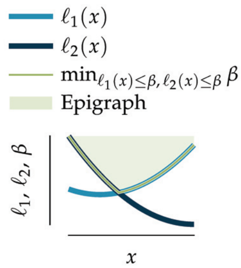

Figure 3.4: Example of epigraph formulation of max operator. Note that the epigraph of $\max(\ell_1(x), \ell_2(x))$ is the set

$$\{(x, \beta) \in \mathbb{X} \times \mathbb{R} \mid \ell_1(x) \geq \beta, \ell_2(x) \geq \beta\}$$

Remark 3.3.3. Lemma 3.3.2 can be extended to find the maximum over $N_\mathrm{I} \in \mathbb{N}$ functions. With $\ell_i : \mathbb{R}^{N_\mathrm{x}} \to \mathbb{R}$, $i \in \mathbb{N}_{[1, N_\mathrm{I}]}$, this is

$$\max_{i \in \mathbb{N}_{[1, N_\mathrm{I}]}} \ell_i(x). \tag{3.5}$$

Using an epigraph reformulation with auxiliary variable $\beta \in \mathbb{R}$, this can be equally stated as

$$\min_{\substack{\beta \in \mathbb{R} \\ \ell_i(x) \leq \beta \\ i \in \mathbb{N}_{[1, N_\mathrm{I}]}}} \beta. \tag{3.6}$$

Remark 3.3.4. Note that the epigraph formulation is especially useful in cases where the maximum of a finite number of functions is minimized, e.g.,

$$\min_{x \in \mathbb{X}} \max(\ell_1(x), \ell_2(x)). \tag{3.7}$$

Here, the epigraph formulation (3.3.2) yields

$$\min_{x \in \mathbb{X}} \min_{\substack{\ell_1(x) \leq \beta \\ \ell_2(x) \leq \beta}} \beta \tag{3.8}$$

which is equivalent to

$$\min_{\substack{x \in \mathbb{X} \\ \ell_1(x) \leq \beta \\ \ell_2(x) \leq \beta}} \beta. \tag{3.9}$$

3.3.2 Big-M reformulation

In Chapter 4, the model of an MG is derived in the form of linear inequalities that are employed to formulate different MPC problems. Unfortunately, the physical behavior of the MGs includes two nonlinear operators, namely, the min operator and a multiplication between a real-valued and a Boolean decision variable. Here, the so-called "Big-M reformulation", also known as "Big-M method", can be used to transform the nonlinear operators into a set of linear inequalities [14, 18, 41, 42, 263, 271, 272].

The following lemma concerns a multiplication of Boolean and real-valued decision variables. It stems from [18].

Lemma 3.3.5 (Big-M reformulation of multiplication)**.** Consider the relation

$$y = x\delta \tag{3.10}$$

with bounded variables $y \in \mathbb{R}$, $x \in [x^{\min}, x^{\max}] \subset \mathbb{R}$ and Boolean $\delta \in \mathbb{B}$. Equation (3.10) can be equally stated as

$$y = \begin{cases} 0, & \text{if } \delta = 0, \\ x, & \text{if } \delta = 1. \end{cases} \tag{3.11}$$

Using $\mathrm{m} \in \mathbb{R}$ with $\mathrm{m} < x^{\min}$ and $\mathrm{M} \in \mathbb{R}$ with $\mathrm{M} > x^{\max}$, (3.11) can be transformed into the set of linear inequalities

Note that m and M can be easily derived offline as illustrated, e.g., in Section 4.8.

$$\mathrm{m}\delta \le y \le \mathrm{M}\delta, \tag{3.12a}$$

$$x - \mathrm{M}(1-\delta) \le y \le x - \mathrm{m}(1-\delta). \tag{3.12b}$$

Proof. For $\delta = 0$, (3.12) becomes

$$0 \le y \le 0, \tag{3.13a}$$

$$x - \mathrm{M} \le y \le x - \mathrm{m}. \tag{3.13b}$$

This makes (3.13a) into the equality constraint $y = 0$. Inserting this into (3.13b) yields

$$x - \mathrm{M} \le 0 \le x - \mathrm{m}, \tag{3.14a}$$

$$\iff \mathrm{m} \le x \le \mathrm{M}. \tag{3.14b}$$

As m and M were chosen such that $[x^{\min}, x^{\max}] \subset [\mathrm{m}, \mathrm{M}]$, (3.14b) does not imply any restriction on x. Note that for

$\delta = 0$, $x = y$ contradicts (3.13a) except for $y = x = 0$ which also holds for $\delta = 0$.

For $\delta = 1$, (3.12) becomes

$$m \leq y \leq M, \tag{3.15a}$$

$$x \leq y \leq x. \tag{3.15b}$$

This makes (3.15b) into the equality constraint $y = x$. As $y = x$ and $x \in [x^{\min}, x^{\max}] \subset [m, M]$, (3.15a) represents no additional restriction on y. Note that for $\delta = 1$, $y = 0$ contradicts (3.15b) except for $y = x = 0$ which also holds for $\delta = 1$. □

In the derivation of the control-oriented MG model in Chapter 4, the min operator is used in a context where the result is not necessarily minimized. Therefore, it is not useful to replace it in a similar fashion as in Section 3.3.1 by relatively simple reformulations. It is rather required to use additional decision variables in order to express the min operator by a set of linear inequalities as in Lemma 3.3.5. Note that the following lemma closely follows the reformulations in [18].

Lemma 3.3.6 (Big-M reformulation of minimum operator)**.** Consider the minimum operator

$$y = \min(x_1, x_2) \tag{3.16}$$

with real-valued bounded $y \in \mathbb{R}$, $x_1 \in [x_1^{\min}, x_1^{\max}] \subset \mathbb{R}$ and $x_2 \in [x_2^{\min}, x_2^{\max}] \subset \mathbb{R}$. This operator can be equally represented by the set of linear inequalities

$$x_1 - M\delta \leq y \leq x_1, \tag{3.17a}$$

$$x_2 + m(1 - \delta) \leq y \leq x_2, \tag{3.17b}$$

with parameters $m < x_1^{\min} - x_2^{\max}$ and $M > x_1^{\max} - x_2^{\min}$ as well as the additional Boolean variable $\delta \in \mathbb{B}$.

Note that m and M can be easily derived offline as illustrated, e.g., in Section 4.5.

Proof. As δ is a Boolean variable, two exclusive cases emerge from (3.17): $\delta = 0$ and $\delta = 1$.

For $\delta = 0$, (3.17) becomes

$$x_1 \leq y \leq x_1, \tag{3.18a}$$

$$x_2 + m \leq y \leq x_2. \tag{3.18b}$$

Inserting $y = x_1$ from (3.18a) into (3.18b) yields

$$x_2 + \mathrm{m} \leq x_1 \leq x_2. \tag{3.19}$$

As the parameter m is chosen such that $\mathrm{m} < x_1^{\min} - x_2^{\max}$, we know that $x_2 + \mathrm{m} < x_2 + x_1^{\min} - x_2^{\max} \leq x_1^{\min} \leq x_1$. Therefore, the inequality at the left-hand side in (3.19) always holds. The inequality at the right-hand side, however, only allows for $x_1 \leq x_2$. The case where $x_1 > x_2$ does not lead to a feasible set of inequalities for $\delta = 0$ as it contradicts (3.19). As $y = \min(x_1, x_2) = x_1$ for $x_1 \leq x_2$, the minimum value is provided in this case.

For $\delta = 1$, (3.17) becomes

$$x_1 - \mathrm{M} \leq y \leq x_1, \tag{3.20a}$$
$$x_2 \leq y \leq x_2. \tag{3.20b}$$

Inserting $y = x_2$ from (3.20b) into (3.20a) yields

$$x_1 - \mathrm{M} \leq x_2 \leq x_1. \tag{3.21}$$

As the parameter M is chosen such that $\mathrm{M} > x_1^{\max} - x_2^{\min}$, we know that $x_1 - \mathrm{M} < x_1 - (x_1^{\max} - x_2^{\min}) \leq x_2^{\min} \leq x_2$. Therefore, the inequality at the left-hand side in (3.21) always holds. The inequality at the right-hand side, however, only allows for $x_2 \leq x_1$. The case where $x_2 > x_1$ does not lead to a feasible set of inequalities for $\delta = 1$ as it contradicts (3.21). As $y = \min(x_1, x_2) = x_2$ for $x_2 \leq x_1$, the minimum value is provided in this case.

Note that (3.19) and (3.21) both include the edge case $x_1 = x_2$. As then $\min(x_1, x_2) = x_1 = x_2$, this does not cause any problems. □

3.4 *Power transmission*

As stated in Section 2.3.5, power flow over the transmission network needs to be considered in operation control of MGs. Therefore, in what follows different power flow models are discussed. First, some assumptions are made.

Assumption 3.4.1 (Balanced, symmetric grid at steady state). In the analysis of power flows, we assume balanced and symmetric three-phase grids. Thus, the admittances of all phases

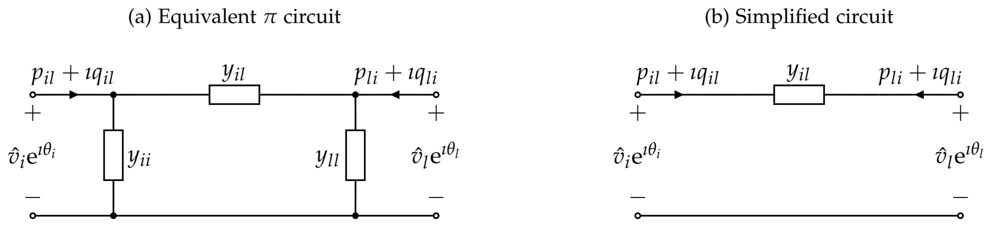

Figure 3.5: Equivalent electrical circuits of transmission line at steady state.

as well as currents and voltages are identical, except for a phase shift of $\pm 2\pi/3$. Consequently, the three-phase system can be equivalently represented by its single-phase equivalent circuit [74, 77, 127].

Assumption 3.4.2 (Dynamics of electric components)**.** The dynamics of the transmission lines are assumed to have much smaller time constants than dynamics of the units in the grid. Therefore, the transmission system is assumed to be at steady state, i.e., the admittances are assumed to be constant [127].

Remark 3.4.3 (Per-unit notation)**.** The numerical values used throughout this thesis are in per-unit (pu) [74, 77, 127]. This allows for a more generic modeling and more general examples where the actual power ratings of the units play a minor role. However, this thesis is written with islanded MGs in the lower MW range in mind. The base quantities of the per-unit system are defined such that all ideal transformers can be removed from the model of the transmission network. More about this common elimination can be found, e.g., in [74].

3.4.1 *Passive electrical components used for transmission*

In the MGs considered in this work, the different units and loads are connected by AC transmission lines and transformers. In what follows, simplified models for both are derived.

Transmission lines. The equivalent π circuit of a transmission line connecting points $i \in \mathbb{N}$ and $l \in \mathbb{N}$ is shown in Figure 3.5(a) which closely follows [5, 74, 77, 127]. It comprises the two shunt admittances $y_{ii} \in \mathbb{C}$, $y_{ll} \in \mathbb{C}$ and a series admittance $y_{il} \in \mathbb{C}$. For overhead transmission lines that are shorter than 80 km, the shunt admittances can be neglected [74, 77, 127]. This results in the simplified circuit of a trans-

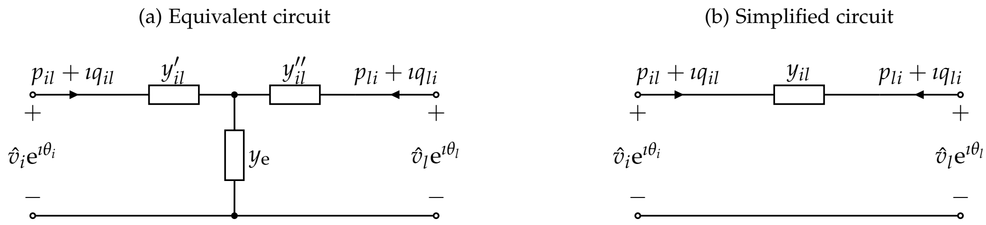

Figure 3.6: Equivalent electrical circuits of transformer at steady state.

mission line shown in Figure 3.5(b) that only comprises the series admittance y_{il}. As MGs are usually composed of units and loads that are geographically close to each other (see Section 2.1), the following assumption can be made.

Assumption 3.4.4 (Simplified transmission lines)**.** In the context of MGs, short transmission lines can be assumed. Thus, the shunt admittances can be neglected and transmission lines can be represented solely by their series admittance.

Transformers. The equivalent circuit of a transformer connecting points $i \in \mathbb{N}$ and $l \in \mathbb{N}$ is shown in Figure 3.6(a) which closely follows [74, 77, 127]. It comprises the series admittances $y'_{il} \in \mathbb{C}$ and $y''_{il} \in \mathbb{C}$ as well as the shunt admittance $y_{\mathrm{e}} \in \mathbb{C}$. Following Remark 3.4.3, the base voltages of the per-unit system are chosen such that the ideal transformers can be eliminated. The current running through admittance y_{e} is usually small compared to the currents running through the series admittances and therefore often neglected [74, 77]. This results in the simplified circuit of a transformer shown in Figure 3.6(b) that only consists of series admittance $y_{il} = \frac{y'_{il}y''_{il}}{y'_{il}+y''_{il}}$. As the excitation current of the transformer is of minor importance in the operation control of MGs, the following assumption is formulated.

Assumption 3.4.5 (Simplified transformer model)**.** In the context of operation control of islanded MGs, the shunt admittance of transformers can be neglected. Thus transformers can be represented solely by their series admittance.

Using these simplified circuits, we can easily compute the series admittance between two nodes in the electric network by combining the admittances of all lines and transformers connecting them. The resulting admittance can be used to determine the power flowing between the nodes as illustrated in the next section.

3.4.2 *AC power flow*

Assume a network composed of $N_\mathrm{b} \in \mathbb{N}$ nodes. Following Assumptions 3.4.4 and 3.4.5, every passive electrical component in the network can be expressed by its series admittance. Consequently the overall series admittance y_{il} between nodes $i \in \mathbb{N}_{[1,N_\mathrm{b}]}$ and $l \in \mathbb{N}_{[1,N_\mathrm{b}]}$ can be easily derived by combining all series admittances between these nodes. For simplicity the connection between i and l is referred to as transmission line, even though it can comprise a finite number of transmission lines and transformers. Using the admittances of the transmission lines, the AC power flow equations can be formulated as follows.

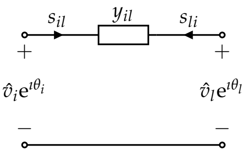

Figure 3.7: Power flow between two nodes of transmission network.

Consider the complex voltages $\hat{v}_i \mathrm{e}^{\imath\theta_i}$ and $\hat{v}_l \mathrm{e}^{\imath\theta_l}$ with amplitudes $\hat{v}_i \in \mathbb{R}_{\geq 0}$ and $\hat{v}_l \in \mathbb{R}_{\geq 0}$ as well as phase angles $\theta_i \in [0, 2\pi)$ and $\theta_l \in [0, 2\pi)$. These nodes are connected by series admittance y_{il} as shown in Figure 3.7. The current flowing from node i to node l is

$$c_{il} = (\hat{v}_i \mathrm{e}^{\imath\theta_i} - \hat{v}_l \mathrm{e}^{\imath\theta_l}) y_{il}. \tag{3.22}$$

Using the complex conjugate of this current, the apparent power flowing into the line at node i is [74]

$$\begin{aligned} s_{il} &= \hat{v}_i \mathrm{e}^{\imath\theta_i} c_{il}^*, && \text{(3.23a)} \\ &= \hat{v}_i \mathrm{e}^{\imath\theta_i} (\hat{v}_i \mathrm{e}^{-\imath\theta_i} - \hat{v}_l \mathrm{e}^{-\imath\theta_l}) y_{il}^*. && \text{(3.23b)} \end{aligned}$$

With $\theta_{il} = \theta_i - \theta_l$ and $\hat{v}_i \hat{v}_l \mathrm{e}^{\imath\theta_{il}} = \hat{v}_i \hat{v}_l (\cos(\theta_{il}) + \imath \sin(\theta_{il}))$, this can be equivalently stated as

$$s_{il} = \big(\hat{v}_i^2 - \hat{v}_i \hat{v}_l (\cos(\theta_{il}) + \imath \sin(\theta_{il}))\big) y_{il}^*. \tag{3.24}$$

Separating admittance y_{il} into conductance $g_{il} = \Re(y_{il}) \in \mathbb{R}_{\geq 0}$ and susceptance $b_{il} = \Im(y_{il}) \in \mathbb{R}$, we can equivalently state (3.24) as

$$\begin{aligned} s_{il} = {} & \hat{v}_i^2 g_{il} - \hat{v}_i \hat{v}_l \big(g_{il} \cos(\theta_{il}) + b_{il} \sin(\theta_{il})\big) \\ & + \imath \big(- \hat{v}_i^2 b_{il} - \hat{v}_i \hat{v}_l \big(g_{il} \sin(\theta_{il}) + b_{il} \cos(\theta_{il})\big)\big). \end{aligned} \tag{3.25}$$

Finally, we can decompose the apparent power s_{il} into active power

$$p_{il} = \Re(s_{il}) = \hat{v}_i \big(\hat{v}_i g_{il} - \hat{v}_l \big(g_{il} \cos(\theta_{il}) + b_{il} \sin(\theta_{il})\big)\big) \tag{3.26a}$$

and reactive power

$$q_{il} = \Im(s_{il}) = \hat{v}_i\big(- \hat{v}_i b_{il} - \hat{v}_l\big(g_{il}\sin(\theta_{il}) - b_{il}\cos(\theta_{il})\big)\big). \tag{3.26b}$$

Each pair of nodes $\{i, l\}$ in the electric network is associated with an admittance $y_{il} = y_{li}$ that is zero if no direct connection between the nodes exists and nonzero if a direct connection exists. Using Kirchhoff's law, we know that for each node in the network, the injected active and reactive power, $p_{\mathrm{g},i}$ and $q_{\mathrm{g},i}$, equals the sum of power flowing into all connected transmission lines. Using (3.26), the power flowing out of the node i is [49, 63, 74, 77, 127, 232]

$$p_{\mathrm{g},i} = \hat{v}_i \sum_{\substack{l=1\\ l\neq i}}^{N_\mathrm{b}} \left(\hat{v}_i g_{il} - \hat{v}_l\left(g_{il}\cos(\theta_{il}) + b_{il}\sin(\theta_{il})\right)\right), \tag{3.27a}$$

$$q_{\mathrm{g},i} = \hat{v}_i \sum_{\substack{l=1\\ l\neq i}}^{N_\mathrm{b}} \left(-\hat{v}_i b_{il} - \hat{v}_l\left(g_{il}\sin(\theta_{il}) - b_{il}\cos(\theta_{il})\right)\right). \tag{3.27b}$$

With the AC power flow model given by (3.26) and (3.27), the power of every transmission line and every node in the grid can be determined. This model is now used to derive the simplified DC power flow equations for AC grids.

3.4.3 DC power flow

In what follows, the simplified DC power flow approximations for AC grids are derived. Despite the name, the approximations are used to calculate the power flow of an AC grid. One big advantage of these approximations is that they provide a linear relation between the power injected at the nodes and the power flowing over the lines. This makes them especially suitable for convex optimization problems.

For a general overview over different power flow models that can be employed in an optimization context, the reader is kindly referred to [5, 64, 65]. Different convex optimal power flow formulations can be also found in [144–146].

Assumption 3.4.6 (Constant and equal voltages)**.** The base quantities of the per-unit system (see Remark 3.4.3) are assumed to be chosen such that the voltage amplitudes at all nodes $i \in \mathbb{N}_{[1,N_\mathrm{b}]}$ are $\hat{v}_i = 1\,\mathrm{pu}$ [49, 63, 74, 77, 127, 200].

Assumption 3.4.7 (Small angle differences)**.** The phase angle differences between the nodes are assumed to be small. Thus, $\cos\theta_{il} \approx 1$ and $\sin(\theta_{il}) \approx \theta_{il} = \theta_i - \theta_l$ [49, 63, 74, 77, 127, 200].

Using Assumptions 3.4.6 and 3.4.7, (3.26) becomes

$$p_{il} = -b_{il}\theta_{il}, \tag{3.28a}$$

$$q_{il} = -g_{il}\theta_{il}. \tag{3.28b}$$

These equations can be further simplified by using the following common assumption.

Assumption 3.4.8 (Inductive grid)**.** The connections between the nodes in the grid are dominantly inductive, i.e., the conductance g_{il} is smaller that the absolute value of the susceptance $|b_{il}|$. Therefore, g_{il} can be neglected, i.e., $g_{il} = 0$ [49, 63, 74, 77, 200]. For MGs that provide power to small villages or cities, this does not represent a major drawback as most transmission lines are operated at a medium voltage level with units and loads typically connected via transformers. These transformers are almost always dominantly inductive.[3] The same does *not* hold for the short transmission lines which can be often found in MGs. However, as the connections between the units and the loads represent a combination of short lines and inductive transformers, the overall admittance between the nodes of the grid can be considered dominantly inductive.

A thorough analysis of the error introduced by the DC power flow approximations for AC grids, which rely on the on the assumption of inductive connections between the nodes, can be found in [200]. Using a power grid with 30 nodes, the authors show that "even for very low X/R ratios" of $X/R = 2$, the "5 % error margin is virtually never exceeded". Consequently, for geographically close nodes in the grid that are connected by short lines and transformers, the overall admittance can be assumed to be dominantly inductive and the DC power flow approximations can be employed.

[3] Following [109, Figure 30], the X/R ratio (which is equivalent to a $|b|/g$ ratio for admittance $y = g + \imath b$) is typically above 5, even for small-scale transformers.

Remark 3.4.9 (Alternative power flow models)**.** Note that the controllers deduced in this thesis work with most linear power flow models such as a linearized AC power flow or a linearized version of the DistFlow equations [15, 73] for radial distribution networks (see, e.g., [245]). Using more general network models can allow to drop Assumption 3.4.8 and thereby model a wider range of MG topologies. As long as alternative linearized power flow models can be expressed by affine equality and inequality constraints, most[4] controllers presented in this thesis can still be employed. However, for simplicity, in the remainder of this thesis the linearized DC power flow equations for AC grid were used.

[4] The minimax MPC approach in Chapter 8 might need to be modified in order to include the maximum and minimum power flow values in the constraints.

Using Assumption 3.4.8, i.e., $g_{il} = 0$, the reactive power in (3.28b) becomes $q_{il} = 0$. Consequently, the apparent power is equal to the active power. The power injected at node i can be determined in a similar fashion from (3.27), i.e.,

$$p_{\mathrm{g},i} = \sum_{\substack{l=1 \\ l\neq i}}^{N_\mathrm{b}} -b_{il}\theta_{il}. \tag{3.29}$$

For simplicity we define the admittance used in DC power flow as $y_{il} = -b_{il}$. Then (3.28a) and (3.29) become

$$p_{il} = y_{il}\theta_{il}, \tag{3.30a}$$

$$p_{\mathrm{g},i} = \sum_{\substack{l=1 \\ l\neq i}}^{N_\mathrm{b}} y_{il}\theta_{il}. \tag{3.30b}$$

Using these equations, we can now form a DC power flow model for the entire network.

3.4.4 *Representation of transmission network as graph*

To formulate (3.30) for each node, it is convenient to model the transmission network as a weighted undirected connected graph. This graph is a triple $\mathcal{G} = (\mathbb{V}, \mathbb{E}, \tilde{y})$ where $\mathbb{V} = \mathbb{N}_{[1,N_\mathrm{b}]}$ is the set of nodes, i.e., the set of buses in the grid, and $\mathbb{E} = \{\breve{e}_1, \dots, \breve{e}_{N_\mathrm{e}}\} \subseteq [\mathbb{V}]^2$ is the set of edges, i.e., the set of transmission lines in the grid, with cardinality $|\mathbb{E}| = N_\mathrm{e} \in \mathbb{N}$. Here, $[\mathbb{V}]^2$ refers to the set of all subsets of $\mathbb{V}$ with two elements. Every edge $\breve{e}_n = \{i, l\} \in \mathbb{E}$, $n \in \mathbb{N}_{[1,N_\mathrm{e}]}$, is associated with the weight $y_n = y_{il}$ which corresponds to the admittance between nodes $i \in \mathbb{V}$ and $l \in \mathbb{V}$. The weighting function $\tilde{y} : \mathbb{E} \to \mathbb{R}_{\geq 0}$ provides this admittance for a given edge, i.e., $\tilde{y}(\breve{e}_n) = \tilde{y}(\{i, l\}) = y_{il} = y_n$.

Because of (3.30a) and assumed inductive lines with $y_{il} = y_{li}$, it holds that $p_{il} = -p_{li}$. Hence, it is sufficient to include either p_{il} or p_{li} in the DC power flow model. To include the power of each line only once, we deduce a directed graph from $\mathcal{G}$ by choosing an arbitrary direction for each edge $\check{e}_n \in \mathbb{E}$. The entries of the edge-node incidence matrix $F \in \mathbb{R}^{N_\mathrm{b} \times N_\mathrm{e}}$ associated with the directed graph are [29, 77]

$$F_{in} = \begin{cases} -1, & \text{if node } i \text{ is the sink of edge } \check{e}_n, \\ 1, & \text{if node } i \text{ is the source of edge } \check{e}_n, \text{ and} \\ 0, & \text{otherwise.} \end{cases}$$

Using F, the line admittances $y_n = \tilde{y}(\check{e}_n)$ and the vector of phase angles $\theta = [\theta_1 \ \cdots \ \theta_{N_\mathrm{b}}]^\top$, the power of all transmission lines $p_\mathrm{e} = [p_{\mathrm{e},1} \ \cdots \ p_{\mathrm{e},N_\mathrm{e}}]^\top$ is given by

$$p_\mathrm{e} = \mathrm{diag}([y_1 \ \cdots \ y_{N_\mathrm{e}}])F^\top \theta. \tag{3.31a}$$

The power provided or consumed by all nodes is collected in $p_\mathrm{g} = [p_{\mathrm{g},1} \ \cdots \ p_{\mathrm{g},N_\mathrm{b}}]^\top$. It can be calculated with the weighted Laplacian $\mathcal{L} = F\,\mathrm{diag}([y_1 \ \cdots \ y_{N_\mathrm{e}}])F^\top$ [89, 92] via

$$p_\mathrm{g} = \mathcal{L}\theta. \tag{3.31b}$$

As discussed in [53, 75], the Laplacian is independent of the orientation of the underlying graph. Therefore, the weighted Laplacian is also independent of the orientation captured by F.

Remark 3.4.10. Each node in the transmission network represents one bus in the electric grid. To each bus, multiple units or loads can be connected. There can also be buses with no unit and no load connected. Such buses typically serve to connect a number of transmission lines with each other.

Remark 3.4.11. By replacing all weights y_o by the corresponding line admittances y_{il}, one can see that (3.31b) has the form

$$\begin{bmatrix} p_{\mathrm{g},1} \\ p_{\mathrm{g},2} \\ \vdots \\ p_{\mathrm{g},N_\mathrm{b}} \end{bmatrix} = \begin{bmatrix} \sum_{l=2}^{N_\mathrm{b}} y_{1l} & \cdots & -y_{1N_\mathrm{b}} \\ -y_{21} & \cdots & -y_{2N_\mathrm{b}} \\ \vdots & \ddots & \vdots \\ -y_{N_\mathrm{b}1} & \cdots & \sum_{j=1}^{N_\mathrm{b}-1} y_{N_\mathrm{b}l} \end{bmatrix} \begin{bmatrix} \theta_1 \\ \theta_2 \\ \vdots \\ \theta_{N_\mathrm{b}} \end{bmatrix}. \tag{3.32}$$

This makes (3.31b) into an equivalent representation of (3.30b).

3.5 *Summary*

In this chapter, basics from different domains were discussed. This includes an introduction on notation and box plots as well as MPC. Also, preliminary results from optimization theory that allow to formulate the MPC problems in computationally tractable ways were recalled. Finally, AC and DC power flow models were derived. Using these basics, the model of an islanded MG as well as different control approaches are obtained in the next chapters.

4 Microgrid model

In Chapter 2, the MG concept was introduced and central challenges in islanded operation were posed. Based on these challenges, the model of an MG that includes the behavior of the underlying control layers is derived in this chapter. This model provides the basis for the formulation of various operation controllers in the subsequent chapters.

The main contribution of this chapter is the derivation of a generic control-oriented MG model in the form of affine equality and inequality constraints. This model includes an arbitrary finite number of storage units, conventional and renewable generators as well as loads and an arbitrary transmission network. It exhibits the following important features.

1. Opposed to many other approaches [16, 44, 110, 180, 253, 256], a possible limitation of infeed from RES is considered. This enables the control of MGs where the power provided by renewable sources can fully serve the load and charge the storage units. In such setups, a limitation of RES is important if available renewable power exceeds the load and the storage units *cannot* be charged any further.

2. In a similar fashion as in [104, 172, 180], the presented model includes conventional generators that can be disabled. This allows to consider islanded MGs with high share of RES, where in presence of sufficient renewable infeed or stored energy, conventional units are disabled.

3. Grid-forming storage units are considered. These enable an operation where all conventional generators are disabled. This mode of operation is important in MGs with high

renewable share where conventional generators are partly substituted by a combination of storage and renewable units. To the knowledge of the author, grid-forming storage units are only considered in [100, 101] and in the authors' work [89–91, 93] which provides the basis for this chapter.

4. Motivated by [110, 112, 179, 180, 253, 279], the dynamics of the storage units are modeled. They include the effects of uncertain load and renewable generation on the state of charge of the storage units.

5. In contrast to many other approaches, proportional power sharing between the grid-forming units is considered. This allows to model how variations in load and renewable infeed affect the power of storage and enabled conventional units. Hereby, it is possible to ensure constraint satisfaction in presence of uncertainties. To the knowledge of the author, proportional power sharing is only included in [16, 154] and in the author's publications [89–91, 93].

6. Unlike many existing approaches [16, 112, 175, 253, 256, 279], power flow over the transmission lines that connect the units and loads is explicitly modeled. The transmitted power is calculated based on the power of the units and loads via the DC power flow approximations for AC grids [74, 77, 165, 200]. This allows to explicitly consider the limits of the transmission lines.

The majority of the model presented in this chapter was introduced in the authors' work [89] and refined in [90, 91, 93]. In what follows, first a general introduction on the model is given in Section 4.1. Then, some assumptions are posed in Section 4.2. Consecutively, the different parts of an MG are introduced, starting with the loads in Section 4.3. Conventional generators are introduced in Section 4.4, renewable generators in Section 4.5, and storage units in Section 4.6. A model of the transmission network is derived in Section 4.7 and power sharing of grid-forming units is discussed in Section 4.8. Finally, in Section 4.9, the overall model of an islanded MG is stated.

4.1 Introduction

The control-oriented model of an islanded MG includes $N_\mathrm{e} \in \mathbb{N}$ transmission lines, $N_\mathrm{t} \in \mathbb{N}$ conventional generators, $N_\mathrm{s} \in \mathbb{N}$ storage units, $N_\mathrm{r} \in \mathbb{N}$ RES and $N_\mathrm{d} \in \mathbb{N}$ loads. Thus, it is composed of $N_\mathrm{u} = N_\mathrm{t} + N_\mathrm{s} + N_\mathrm{r}$ units. At time instant $k \in \mathbb{N}_0$, the model is formed using the affine constraints

$$x(k+1) = Ax(k) + \tilde{B}z(k), \quad \text{with} \quad x(0) = x_0, \tag{4.1a}$$

$$h_1 \leq H_1\, x(k+1), \tag{4.1b}$$

$$h_2 \leq H_2 \begin{bmatrix} v(k)^\top & z(k)^\top & w(k)^\top \end{bmatrix}^\top, \tag{4.1c}$$

$$g = G \begin{bmatrix} v(k)^\top & z(k)^\top & w(k)^\top \end{bmatrix}^\top. \tag{4.1d}$$

Here, $x(k) \in \mathbb{R}^{N_\mathrm{s}}$ represents the state vector with initial value $x_0 \in \mathbb{R}^{N_\mathrm{s}}$. This vector is composed of entries $x_i(k)$ that represent the stored energy of unit $i \in \mathbb{N}_{[1,N_\mathrm{s}]}$. Furthermore, $v(k) = [u(k)^\top \; \delta_\mathrm{t}(k)^\top]^\top$ is the vector of control inputs, composed of real-valued inputs $u(k) \in \mathbb{R}^{N_\mathrm{u}}$ and Boolean inputs $\delta_\mathrm{t}(k) \in \mathbb{B}^{N_\mathrm{t}}$. Moreover, $w(k) \in \mathbb{R}^{N_\mathrm{w}}$, $N_\mathrm{w} \in \mathbb{N}$ is the uncertain external input and $z(k) \in \mathbb{R}^{N_\mathrm{z}}$, $N_\mathrm{z} \in \mathbb{N}$ a vector of auxiliary variables. The matrices of the discrete time dynamics are $A \in \mathbb{R}^{N_\mathrm{s} \times N_\mathrm{s}}$ and $\tilde{B} \in \mathbb{R}^{N_\mathrm{s} \times N_\mathrm{z}}$. The matrices H_1, H_2, G and the vectors h_1, h_2, g are all real-valued and of appropriate dimensions. These matrices and vectors are used to formulate state inequality constraints (4.1b) as well as power-related inequality constraints (4.1c) and equality constraints (4.1d).

In detail, the real-valued control inputs are the units' power setpoints $u(k) = [u_\mathrm{t}(k)^\top \; u_\mathrm{s}(k)^\top \; u_\mathrm{r}(k)^\top]^\top$. Here, $u_\mathrm{t}(k) \in \mathbb{R}^{N_\mathrm{t}}_{\geq 0}$ is associated with the conventional generators, $u_\mathrm{s}(k) \in \mathbb{R}^{N_\mathrm{s}}$ with the storage units and $u_\mathrm{r}(k) \in \mathbb{R}^{N_\mathrm{r}}_{\geq 0}$ with the renewable generators. For storage and conventional generators, $u_\mathrm{s}(k)$ and $u_\mathrm{t}(k)$ represent desired power values. For RES, $u_\mathrm{r}(k)$ represents an upper limit on the weather-dependent renewable infeed. Thus, $u_\mathrm{r}(k)$ is the maximum allowed infeed. Additionally, each conventional generator $i \in \mathbb{N}_{[1,N_\mathrm{t}]}$ has a Boolean control input $\delta_{\mathrm{t},i} \in \mathbb{B}$. This input indicates whether generator i is enabled ($\delta_{\mathrm{t},i} = 1$) or disabled ($\delta_{\mathrm{t},i} = 0$). The Boolean variables of all conventional generators are collected in the vector $\delta_\mathrm{t}(k)$.

The uncertain external input is $w(k) = [w_\mathrm{r}(k)^\top \; w_\mathrm{d}(k)^\top]^\top$. Here, $w_\mathrm{r}(k) \in \mathbb{R}^{N_\mathrm{r}}_{\geq 0}$ is the available infeed under weather conditions of all renewable units and $w_\mathrm{d}(k) \in \mathbb{R}^{N_\mathrm{d}}$ the load.

Due to time-varying load and renewable generation and a physically dictated local balance of generation, storage and load, the power of unit $i \in \mathbb{N}_{[1,N_\mathrm{u}]}$, $p_i(k) \in \mathbb{R}$, can differ from the power setpoint $u_i(k)$. Therefore, the power of the units $p(k) = [p_\mathrm{t}(k)^\top \; p_\mathrm{s}(k)^\top \; p_\mathrm{r}(k)^\top]^\top$, which is part of the auxiliary vector $z(k)$, needs to be explicitly modeled. The vector $p(k)$ includes the power of the conventional generators, $p_\mathrm{t}(k) \in \mathbb{R}^{N_\mathrm{t}}_{\geq 0}$, storage units, $p_\mathrm{s}(k) \in \mathbb{R}^{N_\mathrm{s}}$ and renewable generators, $p_\mathrm{r}(k) \in \mathbb{R}^{N_\mathrm{r}}_{\geq 0}$. Additionally, the power of the loads, $p_\mathrm{d}(k) \in \mathbb{R}^{N_\mathrm{d}}$, and the power transmitted over N_e transmission lines, $p_\mathrm{e}(k) \in \mathbb{R}^{N_\mathrm{e}}$, are modeled. However, these variables do not need to be included in $z(k)$ as discussed Section 4.7.

The reader is kindly referred to Remark 4.9.2 as well as Examples 8.2.1 and 9.2.2 for detailed discussions on the difference between power and power setpoint.

Remark 4.1.1 (Running example)**.** Throughout this work, the running example Figure 4.1 is used to illustrate basic principles in the operation of islanded MGs. It is based on the MG used in the case studies of [89–91, 93] and comprises a wind turbine that represents the class of renewable units, a storage unit, a conventional generator and a load. The units and the load are connected by a network of four transmission lines. Thus, all basic components discussed in this chapter are included. For an easy understanding, the running example is kept very simple and only represents a tiny fraction of potential islanded MG topologies.

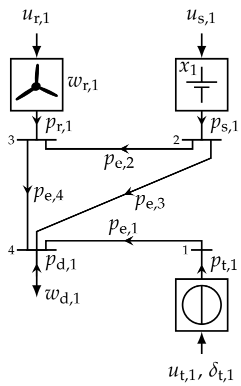

Figure 4.1: MG used as a running example. The MG includes the basic components introduced in this chapter, i.e., a conventional, a storage and a renewable unit as well as transmission lines and a load. Motivated by [93].

4.2 *Assumptions*

Assumption 4.2.1 (Lower control layers)**.** It is assumed that the control layers below operation management, i.e., primary and secondary control (see Section 2.2), are designed such that the voltages and the frequencies remain in a desired safe operating area.

Assumption 4.2.2 (Steady state model of lower control layers)**.** The lower control layers are assumed to be designed such that the units can run for several minutes in a stable way without the need to update the power setpoints provided by the operation control layer. As the lower control layers (see Section 2.2) are acting on a much faster timescale, the steady state equations for all units can be considered. Hence, the only remaining dynamics are those associated with the energy of the storage units. Considering storage units that can require hours for a full charging cycle, running the operation control on a timescale of several minutes is sufficient.

Assumption 4.2.3 (Loads). In the context of this thesis it is assumed that all loads can be modeled as constant power loads. Moreover, the loads are assumed to be uncontrollable.

Assumption 4.2.4 (Grid-forming units). As discussed in Sections 2.3.2 and 2.3.3, all storage units and conventional generators are assumed to be operated in grid-forming mode.

Assumption 4.2.5 (Power sharing of grid-forming units). The lower control layers provide a predefined proportional active power sharing among all enabled grid-forming units (see Section 2.3.4). Thus, the enabled grid-forming units share fluctuations of loads and RES in a known proportional manner. This behavior can be achieved using, for example, droop control [226, 227, 229, 232, 243] on the primary control layer.

Assumption 4.2.6 (Conventional generators). The time that conventional generators require to start or shut down is assumed to be small compared to the sampling time of operation control. Therefore, it is assumed that they are immediately able to provide power to the MG after being enabled. Considering units with a rated power in the range of hundreds of kW to some MW that require less than 1 min for startup or shutdown, this does not represent a major limitation assuming sampling times in the range of minutes (see Assumption 4.2.2). Moreover, the dynamics of the conventional generators are assumed to be fast such that climb rates, etc., do not need to be modeled.

Assumption 4.2.7 (Storage units). It is assumed that the state, i.e., the energy of all storage units, is available to the operation control layer. Moreover, the effects of storage losses, e.g., self-discharge or conversion losses, are assumed to be negligible compared to the uncertainty introduced by renewable generators and loads.

Assumption 4.2.8 (Transmission lines). For the combination of transmission lines and transformers considered in the grid model, the line resistance and the reactive power flow are assumed to be negligible.[1] Furthermore, the phase angle differences in the MG are assumed to be small and the voltage

[1] In presence of line resistances that cannot be neglected, alternative power flow models, such as the linearized DistFlow equations (see, e.g., [245]) could be used. Please refer to Remark 3.4.9 for a more detailed discussion on this topic.

amplitudes constant. Thus, the simplified DC power flow approximations [200] for AC grids (see Section 3.4.3) can be used. For the MGs considered in this work, the uncertainty introduced by RES and loads is assumed to be much larger than the error associated with these simplifications.

4.3 Load

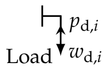

All uncontrollable loads, e.g., households, industrial consumers and uncontrolled RES, are collected in the vector $w_{\mathrm{d}}(k) \in \mathbb{R}^{N_{\mathrm{d}}}$ and modeled as an uncertain external input. Note that $w_{\mathrm{d},i}(k) \in \mathbb{R}$, $i \in \mathbb{N}_{[1,N_{\mathrm{d}}]}$ can also be a combination of both, load and uncontrolled renewable infeed, e.g., in the case of houses with installed rooftop PV units. However, for readability, $w_{\mathrm{d},i}(k) \in \mathbb{R}$ is simply referred to as load, even though it may comprise many things. The load $w_{\mathrm{d}}(k)$ is defined negative for consumption and positive for generation. To comply with the power definition of the units in Sections 4.4 to 4.6, the load power provided to the grid is

$$p_{\mathrm{d}}(k) = w_{\mathrm{d}}(k). \tag{4.2}$$

Remark 4.3.1 (Controllable loads)**.** In this work, controllable loads are not considered (see Assumption 4.2.3). Compared to MGs with controllable loads, those with uncontrollable loads are often harder to operate as the load demand always has to be met. It is still worth noting that controllable loads can increase the degrees of freedom and therefore help to achieve certain goals in the operation of MGs. If desired to include controllable loads in the framework presented in this thesis, they could be modeled using a real-valued control input $u_{\mathrm{d}}(k) \in \mathbb{R}^{N_{\mathrm{d}}}$ that reduce the load, i.e.,

$$p_{\mathrm{d}}(k) = w_{\mathrm{d}}(k) + u_{\mathrm{d}}(k). \tag{4.3}$$

To only allow a certain reduction, the control input could be bounded by $p_{\mathrm{d}}^{\mathrm{min}} \in \mathbb{R}^{N_{\mathrm{d}}}$ and $p_{\mathrm{d}}^{\mathrm{max}} \in \mathbb{R}^{N_{\mathrm{d}}}$, i.e.,

$$p_{\mathrm{d}}^{\mathrm{min}} \leq u_{\mathrm{d}}(k) \leq p_{\mathrm{d}}^{\mathrm{min}}. \tag{4.4}$$

Alternatively, some loads could be considered switchable. Such loads could be modeled using a Boolean control input $\delta_{\mathrm{d}}(k) \in \mathbb{B}^{N_{\mathrm{d}}}$, i.e.,

$$p_{\mathrm{d}}(k) = \mathrm{diag}(\delta_{\mathrm{d}}(k)) w_{\mathrm{d}}(k). \tag{4.5}$$

Naturally, (4.4) and (4.5) could also be combined into

$$p_{\mathrm{d}}(k) = \mathrm{diag}(\delta_{\mathrm{d}}(k))w_{\mathrm{d}}(k) + u_{\mathrm{d}}(k). \tag{4.6}$$

However, many operators of islanded MGs wish to run their grid without the need to reduce the security of supply by making some loads controllable. Therefore, controllable loads were not considered in this work.

4.4 *Conventional generators*

As discussed in Section 2.3.3, it is desirable to switch conventional generators off if they are temporarily dispensable in the operation of an MG. Therefore, each conventional generator $i \in \mathbb{N}_{[1,N_{\mathrm{t}}]}$ is equipped with a Boolean input $\delta_{\mathrm{t},i}(k)$. If $\delta_{\mathrm{t},i}(k) = 0$, then unit i is disabled and power as well as power setpoint need to be zero. If unit i is enabled and $\delta_{\mathrm{t},i}(k) = 1$, then power and setpoint are between $p_{\mathrm{t},i}^{\min} \in \mathbb{R}_{\geq 0}$ and $p_{\mathrm{t},i}^{\max} \in \mathbb{R}_{\geq 0}$. This can be modeled for all conventional generators by

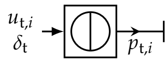

Conventional generator

$$\mathrm{diag}(p_{\mathrm{t}}^{\min})\delta_{\mathrm{t}}(k) \leq p_{\mathrm{t}}(k) \leq \mathrm{diag}(p_{\mathrm{t}}^{\max})\delta_{\mathrm{t}}(k), \tag{4.7a}$$
$$\mathrm{diag}(p_{\mathrm{t}}^{\min})\delta_{\mathrm{t}}(k) \leq u_{\mathrm{t}}(k) \leq \mathrm{diag}(p_{\mathrm{t}}^{\max})\delta_{\mathrm{t}}(k), \tag{4.7b}$$

with $p_{\mathrm{t}}^{\min} \in \mathbb{R}_{\geq 0}^{N_{\mathrm{t}}}$ and $p_{\mathrm{t}}^{\max} \in \mathbb{R}_{\geq 0}^{N_{\mathrm{t}}}$.

Remark 4.4.1. For conventional generator $i \in \mathbb{N}_{[1,N_{\mathrm{t}}]}$, (4.7) becomes

$$p_{\mathrm{t},i}^{\min}\delta_{\mathrm{t},i} \leq p_{\mathrm{t},i} \leq p_{\mathrm{t},i}^{\max}\delta_{\mathrm{t},i}, \tag{4.8a}$$
$$p_{\mathrm{t},i}^{\min}\delta_{\mathrm{t},i} \leq u_{\mathrm{t},i} \leq p_{\mathrm{t},i}^{\max}\delta_{\mathrm{t},i}. \tag{4.8b}$$

Thus, if unit i is disabled, then $\delta_{\mathrm{t},i} = 0$ and

$$0 \leq p_{\mathrm{t},i} \leq 0, \tag{4.9a}$$
$$0 \leq u_{\mathrm{t},i} \leq 0, \tag{4.9b}$$

i.e., power and power setpoint are forced to zero. If the unit is enabled and $\delta_{\mathrm{t},i} = 1$, then (4.8) becomes

$$p_{\mathrm{t},i}^{\min} \leq p_{\mathrm{t},i} \leq p_{\mathrm{t},i}^{\max}, \tag{4.10a}$$
$$p_{\mathrm{t},i}^{\min} \leq u_{\mathrm{t},i} \leq p_{\mathrm{t},i}^{\max}. \tag{4.10b}$$

i.e., power and setpoint are within the bounds of the unit.

4.5 *Renewable generators*

Assumption 4.5.1 (Always enabled renewable units)**.** The renewable units are assumed to be always enabled. As it is desired to use as much power as possible from RES and as their run time cost is very low, this assumption usually does not significantly increase the operating costs. If required, this assumption can be easily abandoned by including a Boolean input and modifying (4.11) to resemble the power and set-point limits of the conventional generators in (4.7).

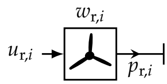

Wind turbine

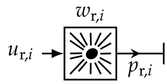

PV power plant

The power and the setpoint are limited by the rated power of the renewable units. This limitation can be included by

$$p_{\mathrm{r}}^{\min} \leq p_{\mathrm{r}}(k) \leq p_{\mathrm{r}}^{\max}, \tag{4.11a}$$
$$p_{\mathrm{r}}^{\min} \leq u_{\mathrm{r}}(k) \leq p_{\mathrm{r}}^{\max}, \tag{4.11b}$$

with $p_{\mathrm{r}}^{\min} \in \mathbb{R}_{\geq 0}^{N_{\mathrm{r}}}$ and $p_{\mathrm{r}}^{\max} \in \mathbb{R}_{\geq 0}^{N_{\mathrm{r}}}$.

As discussed in Section 2.3.1, a high share of RES is considered. Therefore, it can be required to limit the renewable infeed in the operation of the grid. This limitation can be performed via the power setpoint $u_{\mathrm{r},i}(k) \in \mathbb{R}_{\geq 0}$ of each renewable unit $i \in \mathbb{N}_{[1,N_{\mathrm{r}}]}$, which represents an upper limit on the power infeed $p_{\mathrm{r},i}(k) \in \mathbb{R}_{\geq 0}$. With the available infeed under weather conditions $w_{\mathrm{r},i}(k) \in \mathbb{R}_{\geq 0}$, the limitation can be modeled by

$$p_{\mathrm{r}}(k) = \min(u_{\mathrm{r}}(k), w_{\mathrm{r}}(k)). \tag{4.12}$$

Unfortunately, it is not sufficient to represent (4.12) solely by $p_{\mathrm{r}}(k) \leq u_{\mathrm{r}}(k)$ and $p_{\mathrm{r}}(k) \leq w_{\mathrm{r}}(k)$ as this allows for values of $p_{\mathrm{r}}(k)$ that are smaller than $u_{\mathrm{r}}(k)$ and $w_{\mathrm{r}}(k)$ but not equal to either one of them. Consequently, the element-wise min operator needs to be employed.

Following Lemma 3.3.6 and [14, 18, 42, 263], the min operator in (4.12) can be transformed into a set of affine inequalities. Therefore, a vector of auxiliary free variables $\delta_{\mathrm{r}}(k) \in \mathbb{B}^{N_{\mathrm{r}}}$ is introduced. Moreover, the constants $\mathrm{m_r} \in \mathbb{R}^{N_{\mathrm{r}}}$ and $\mathrm{M_r} \in \mathbb{R}^{N_{\mathrm{r}}}$ with $\mathrm{m_r} < p_{\mathrm{r}}^{\min} - p_{\mathrm{r}}^{\max}$ and $\mathrm{M_r} > p_{\mathrm{r}}^{\max} - p_{\mathrm{r}}^{\min}$ are chosen accordingly.[2] As they only depend on the known parameters $p_{\mathrm{r}}^{\min}$ and $p_{\mathrm{r}}^{\max}$, $\mathrm{m_r}$ and $\mathrm{M_r}$ can be derived offline.

[2] For the derivation of $\mathrm{m_r}$ and $\mathrm{M_r}$, we assume, without loss of generality, that the available power of the renewable units is bounded by the units' operational limits, i.e., that $p_{\mathrm{r}}^{\min} \leq w_{\mathrm{r}}(k) \leq p_{\mathrm{r}}^{\max}$.

Finally, (4.12) can be reformulated as (see Lemma 3.3.6)

$$u_{\mathrm{r}}(k) - \mathrm{diag}(\mathrm{M}_{\mathrm{r}})\delta_{\mathrm{r}}(k) \leq p_{\mathrm{r}}(k) \leq u_{\mathrm{r}}(k), \tag{4.13a}$$
$$w_{\mathrm{r}}(k) + \mathrm{diag}(\mathrm{m}_{\mathrm{r}})(1_{N_{\mathrm{r}}} - \delta_{\mathrm{r}}(k)) \leq p_{\mathrm{r}}(k) \leq w_{\mathrm{r}}(k). \tag{4.13b}$$

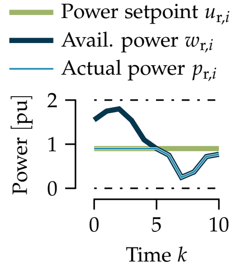

Figure 4.2: Limitation of renewable infeed using the power setpoint. The power limits in the example are $p_{\mathrm{r}}^{\min} = 0$ and $p_{\mathrm{r}}^{\max} = 2$.

Example 4.5.2. For renewable unit $i \in \mathbb{N}_{[1,N_{\mathrm{r}}]}$, a possible limitation is illustrated in Figure 4.2. In the example, the power setpoint $u_{\mathrm{r},i}(k)$ is constant over the entire time horizon. For $k \leq 5$, the available renewable infeed under weather conditions $w_{\mathrm{r},i}(k)$ lies above $u_{\mathrm{r},i}(k)$. Therefore, the provided renewable infeed is $p_{\mathrm{r},i}(k) = u_{\mathrm{r},i}(k)$. For $k > 5$, $w_{\mathrm{r},i}(k)$ is below the power setpoint $u_{\mathrm{r},i}(k)$. Therefore, power from the RES is not limited by $u_{\mathrm{r},i}(k)$ and $p_{\mathrm{r},i}(k) = w_{\mathrm{r},i}(k)$.

Remark 4.5.3 (Uncontrolled RES)**.** The modeling framework presented in this thesis allows to consider uncontrolled RES, e.g., PV rooftop installations, small hydroelectric power stations or wind turbines without an operation control input. As posed in Section 4.3, these units can be simply modeled as negative loads. The separation into loads and RES performed in this thesis aims to clarify which uncertain inputs can be limited and which cannot. However, it is only performed in favor of a clear terminology and not supposed to restrict the modeling to certain types of MGs.

4.6 *Storage units*

Motivated by Section 2.3.2, grid-forming storage units [231] are considered. Their model is discussed in what follows.

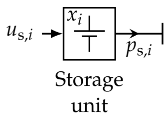

4.6.1 *Power*

Assumption 4.6.1 (Always enabled storage units)**.** It is assumed that the storage units are always enabled which is useful for two reasons. (i) A proper selection of droop gains for conventional and storage units can lead to an operation where the storage units cover most of the fluctuations which can help to reduce fuel consumption. (ii) There is always a chance that the renewable infeed is higher than expected such that storage units can be charged. If desired, the assumption of always enabled storage units can be easily abandoned by including a Boolean input and modifying the constraints to resemble the power and setpoint limits of the conventional units in (4.7).

The power and the power setpoints of the storage units are limited by the nominal power of the units. This is captured by

$$p_{\mathrm{s}}^{\min} \leq p_{\mathrm{s}}(k) \leq p_{\mathrm{s}}^{\min}, \tag{4.14a}$$

$$p_{\mathrm{s}}^{\min} \leq u_{\mathrm{s}}(k) \leq p_{\mathrm{s}}^{\min}, \tag{4.14b}$$

with $p_{\mathrm{s}}^{\min} \in \mathbb{R}_{\leq 0}^{N_{\mathrm{s}}}$ and $p_{\mathrm{s}}^{\max} \in \mathbb{R}_{\geq 0}^{N_{\mathrm{s}}}$.

4.6.2 *Energy*

Motivated by [43, 103], the dynamics of the storage units are modeled by the discrete time state model

$$x(k+1) = Ax(k) + Bp_{\mathrm{s}}(k), \quad \text{with } x(0) = x_0 \tag{4.15a}$$

and $A = I_{N_{\mathrm{s}}}$, $B = -\mathrm{T_s}\, I_{N_{\mathrm{s}}}$. Here, $\mathrm{T_s} \in \mathbb{R}_{>0}$ is the discrete sampling time and $x_0 \in \mathbb{R}_{\geq 0}^{N_{\mathrm{s}}}$ the initial state. Because of a finite storage capacity, $x(k)$ is bounded by $x^{\min} \in \mathbb{R}_{\geq 0}^{N_{\mathrm{s}}}$ and $x^{\max} \in \mathbb{R}_{\geq 0}^{N_{\mathrm{s}}}$, i.e.,

$$x^{\min} \leq x(k) \leq x^{\max}. \tag{4.15b}$$

Note that storage unit $i \in \mathbb{N}_{[1,N_{\mathrm{s}}]}$ is

- charged if $p_{\mathrm{s},i} < 0$ and
- discharged if $p_{\mathrm{s},i} > 0$.

Remark 4.6.2 (Storage efficiency)**.** Self-discharge of batteries can be modeled in (4.15a) by choosing the diagonal entries of A smaller than 1. Alternatively, a constant $x_{\mathrm{sd}} \in \mathbb{R}_{\geq 0}^{N_{\mathrm{s}}}$ can be employed to model a constant discharge via no-load losses. This would result in the modified dynamics

$$x(k+1) = Ax(k) + Bp_{\mathrm{s}}(k) - x_{\mathrm{sd}}. \tag{4.16}$$

Remark 4.6.3 (Complexity of storage model)**.** It is possible to use more complex storage models, e.g., based on the mixed integer formulation in [180]. In our modeling framework, the storage model from [180] would take the form

$$x(k+1) = Ax(k) + Bp_{\mathrm{s}}(k) - x_{\mathrm{sd}}, \tag{4.17a}$$

where $x_{\mathrm{sd}} \in \mathbb{R}_{\geq 0}^{N_{\mathrm{s}}}$ represents self-discharge, e.g., via no-load losses. Moreover, $B = \operatorname{diag}([b_1 \ \cdots \ b_{N_{\mathrm{s}}}]) \in \mathbb{R}_{\leq 0}^{N_{\mathrm{s}} \times N_{\mathrm{s}}}$ with

$$b_i = \begin{cases} -\mathrm{T_s}\eta_i^{\mathrm{c}}, & \text{if } p_{\mathrm{s},i} < 0 \text{ (charge)}, \\ -\mathrm{T_s}/\eta_i^{\mathrm{d}}, & \text{if } p_{\mathrm{s},i} \geq 0 \text{ (discharge)}, \end{cases} \tag{4.17b}$$

for all $i \in \mathbb{N}_{[1,N_\mathrm{s}]}$ and $\eta_i^\mathrm{c}, \eta_i^\mathrm{d} \in (0,1]$. As indicated in [180], (4.17) can be reformulated into a set of affine inequalities using additional real-valued and Boolean decision variables.

The simple storage model (4.15a) considered in this thesis can be derived from (4.17) by setting $\eta_i^\mathrm{c} = \eta_i^\mathrm{d} = 1$ and $x_\mathrm{sd} = 0_{N_\mathrm{s}}$. Compared to the model from [180], it does not require additional decision variables and therefore helps to keep the computational complexity of potential optimization problems manageable.

Remark 4.6.4 (Thermal storage)**.** It is possible to model $N_\mathrm{h} \in \mathbb{N}$ storage heaters using a modified version of (4.15a). This, however, requires to limit the electric power $p_\mathrm{s}(k)$ to negative values in order to only allow for electric charging of thermal storage units, i.e.,

$$p_\mathrm{s}^\mathrm{min} \leq p_\mathrm{s}(k) \leq 0. \tag{4.18a}$$

with $p_\mathrm{s}^\mathrm{min} \in \mathbb{R}_{\leq 0}^{N_\mathrm{h}}$. Adding a term to model the uncertain heat demand, $w_\mathrm{h}(k) \in \mathbb{R}_{\geq 0}^{N_\mathrm{h}}$, the dynamics take the form

$$x_\mathrm{h}(k+1) = A_\mathrm{h} x_\mathrm{h}(k) + B_\mathrm{s} p_\mathrm{s}(k) + B_\mathrm{h} w_\mathrm{h}(k), \tag{4.18b}$$

where $A_\mathrm{h} = \mathrm{diag}([a_1 \ \cdots \ a_{N_\mathrm{h}}]) \in [0,1]^{N_\mathrm{h} \times N_\mathrm{h}}$ models self-discharge, $B_\mathrm{s} = \mathrm{diag}([b_{\mathrm{s},1} \ \cdots \ b_{\mathrm{s},N_\mathrm{h}}]) \in \mathbb{R}_{\leq 0}^{N_\mathrm{h} \times N_\mathrm{h}}$ the electric charging efficiency and $B_\mathrm{h} = \mathrm{diag}([b_{\mathrm{h},1} \ \cdots \ b_{\mathrm{h},N_\mathrm{h}}]) \in \mathbb{R}_{\leq 0}^{N_\mathrm{h} \times N_\mathrm{h}}$ the heat discharge efficiency. Naturally, the storage capacity is finite and the stored thermal energy limited by $x_\mathrm{h}^\mathrm{min} \in \mathbb{R}_{\geq 0}^{N_\mathrm{s}}$ and $x_\mathrm{h}^\mathrm{max} \in \mathbb{R}_{\geq 0}^{N_\mathrm{h}}$, i.e.,

$$x_\mathrm{h}^\mathrm{min} \leq x_\mathrm{h}(k) \leq x_\mathrm{h}^\mathrm{max}. \tag{4.18c}$$

4.7 *Transmission network*

Assumption 4.7.1 (Connectedness of network graph)**.** It is assumed that the graph $\mathcal{G} = (\mathbb{V}, \mathbb{E}, \tilde{y})$ that represents the transmission network is connected. In the context of this work, this means that there exists an electric path between any two buses in the network.

As stated in Section 2.3.5, it is important to model power flow over the electric grid to keep the transmitted power within given limits. In this work, this is done by means of the

DC power flow approximations (see Section 3.4.3). To use the least number of decision variables, (3.31) is reformulated to determine the power flowing over the lines, $p_{\mathrm{e}}(k) \in \mathbb{R}^{N_{\mathrm{e}}}$, directly from the power of the buses[3], $p_{\mathrm{g}}(k) \in \mathbb{N}_{[1,N_{\mathrm{g}}]}$, without introducing additional decision variables.

[3] Recall from Remark 3.4.10 that each bus in the network, i.e., each node of the graph $\mathcal{G}$, can have multiple units or loads connected to it.

Recall from Section 3.4.4 that

$$p_{\mathrm{e}}(k) = \operatorname{diag}([y_1 \ \cdots \ y_{N_{\mathrm{e}}}])F^\top \theta(k), \tag{4.19a}$$
$$p_{\mathrm{g}}(k) = \mathcal{L}\theta(k), \tag{4.19b}$$

with $\mathcal{L} = F \operatorname{diag}([y_1 \ \cdots \ y_{N_{\mathrm{e}}}])F^\top$. As a connected electric network graph $\mathcal{G}$ is assumed, the Laplacian $\mathcal{L}$ is symmetric and has rank $N_{\mathrm{g}} - 1$ [75, 92]. To calculate the line power $p_{\mathrm{e}}(k)$ from the power injected into the network $p_{\mathrm{g}}(k)$, the transformation

$$\begin{bmatrix} \tilde{\theta}(k) \\ \theta_{N_{\mathrm{g}}}(k) \end{bmatrix} = \begin{bmatrix} \theta_1(k) - \theta_{N_{\mathrm{g}}}(k) \\ \vdots \\ \theta_{N_{\mathrm{g}}-1}(k) - \theta_{N_{\mathrm{g}}}(k) \\ \theta_{N_{\mathrm{g}}}(k) \end{bmatrix} = \underbrace{\begin{bmatrix} I_{N_{\mathrm{g}}-1} & -1_{N_{\mathrm{g}}-1} \\ 0_{N_{\mathrm{g}}-1}^\top & 1 \end{bmatrix}}_{T} \theta(k) \tag{4.20}$$

is employed. Using $\tilde{p}_{\mathrm{g}}(k) = [p_{\mathrm{g},1}(k) \ \cdots \ p_{\mathrm{g},N_{\mathrm{g}}-1}(k)]^\top$ and combining (4.19b) and (4.20) yields

$$\begin{bmatrix} \tilde{p}_{\mathrm{g}}(k) \\ p_{\mathrm{g},N_{\mathrm{g}}}(k) \end{bmatrix} = \mathcal{L}T^{-1} \begin{bmatrix} \tilde{\theta}(k) \\ \theta_{N_{\mathrm{g}}}(k) \end{bmatrix} \tag{4.21a}$$
$$= \begin{bmatrix} \tilde{\mathcal{L}} & 0_{N_{\mathrm{g}}-1} \\ b^\top & 0 \end{bmatrix} \begin{bmatrix} \tilde{\theta}(k) \\ \theta_{N_{\mathrm{g}}}(k) \end{bmatrix} \tag{4.21b}$$

where $\tilde{\mathcal{L}} \in \mathbb{R}^{(N_{\mathrm{g}}-1)\times(N_{\mathrm{g}}-1)}$ is the upper left block of $\mathcal{L}$ and $b^\top$ contains the first $N_{\mathrm{g}} - 1$ entries of the last row of $\mathcal{L}$, i.e.,

$$\mathcal{L} = \left[\begin{array}{c|c} \tilde{\mathcal{L}} & * \\ \hline b^\top & * \end{array}\right].$$

Using $\tilde{T} = [I_{N_{\mathrm{g}}-1} \ 0_{N_{\mathrm{g}}-1}]$, $\tilde{\mathcal{L}} = \tilde{T}\mathcal{L}\tilde{T}^\top$ and $b^\top = [0_{N_{\mathrm{g}}-1}^\top \ 1]\mathcal{L}\tilde{T}^\top$ can be deduced. As $\tilde{\mathcal{L}}$ is invertible [227], the phase angle differences $\tilde{\theta}(k)$ can determined via

$$\tilde{\theta}(k) = \tilde{\mathcal{L}}^{-1}\tilde{p}_{\mathrm{g}}(k). \tag{4.22}$$

Moreover, using (4.20) the phase angles can be reconstructed from the injected power at the nodes $\tilde{p}_{\mathrm{g}}(k)$ and the phase angle $\theta_{N_\mathrm{g}}(k)$ as

$$\theta(k) = T^{-1}\begin{bmatrix}\tilde{\theta}(k)\\ \theta_{N_\mathrm{g}}(k)\end{bmatrix} \tag{4.23a}$$

$$= T^{-1}\begin{bmatrix}\tilde{\mathcal{L}}^{-1}\tilde{p}_\mathrm{g}(k)\\ \theta_{N_\mathrm{g}}(k)\end{bmatrix}. \tag{4.23b}$$

Inserting this into (4.19a) yields

$$p_\mathrm{e}(k) = \mathrm{diag}([y_1 \ \cdots \ y_{N_\mathrm{e}}])F^\top T^{-1}\begin{bmatrix}\tilde{\mathcal{L}}^{-1}\tilde{p}_\mathrm{g}(k)\\ \theta_{N_\mathrm{g}}(k)\end{bmatrix}. \tag{4.24a}$$

From (4.21) also originates the equation

$$p_{\mathrm{g},N_\mathrm{g}}(k) = b^\top\tilde{\theta}(k).$$

which with (4.22) becomes

$$p_{\mathrm{g},N_\mathrm{g}}(k) = b^\top\tilde{\mathcal{L}}^{-1}\tilde{p}_\mathrm{g}(k). \tag{4.24b}$$

Remark 4.7.2. Note that $b^\top\tilde{\mathcal{L}}^{-1} = -1_{N_\mathrm{g}-1}^\top$ holds.[4] Therefore, (4.24b) represents the power equilibrium of all nodes, i.e.,

$$1_{N_\mathrm{g}}^\top p_\mathrm{g}(k) = 0.$$

Due to the structure of $F^\top$ and T^{-1}, the choice of $\theta_{N_\mathrm{g}}(k)$ does not affect the transmitted power in (4.24a). Therefore, it can be arbitrary chosen as $\theta_{N_\mathrm{g}}(k) = 0$ such that (4.24a) becomes

$$p_\mathrm{e}(k) = \mathrm{diag}([y_1 \ \cdots \ y_{N_\mathrm{e}}])F^\top T^{-1}\begin{bmatrix}\tilde{\mathcal{L}}^{-1}\tilde{p}_\mathrm{g}(k)\\ 0\end{bmatrix}, \tag{4.25a}$$

$$= \mathrm{diag}([y_1 \ \cdots \ y_{N_\mathrm{e}}])F^\top T^{-1}\begin{bmatrix}\tilde{\mathcal{L}}^{-1}\tilde{T}p_\mathrm{g}(k)\\ 0\end{bmatrix}, \tag{4.25b}$$

$$= \mathrm{diag}([y_1 \ \cdots \ y_{N_\mathrm{e}}])F^\top T^{-1}\tilde{T}^\top\tilde{\mathcal{L}}^{-1}\tilde{T}p_\mathrm{g}(k). \tag{4.25c}$$

Thus, with $\tilde{F} = \mathrm{diag}([y_1 \ \cdots \ y_{N_\mathrm{e}}])F^\top T^{-1}\tilde{T}^\top\tilde{\mathcal{L}}^{-1}\tilde{T}$, (4.24a) becomes

$$p_\mathrm{e}(k) = \tilde{F}p_\mathrm{g}(k). \tag{4.26}$$

To connect the units and loads to the different buses in the network, the matrix $U \in \mathbb{B}^{N_\mathrm{g}\times(N_\mathrm{u}+N_\mathrm{d})}$ is introduced.

[4] $\mathcal{L}$ and $\tilde{\mathcal{L}}$ are symmetric. Moreover, it holds that $\mathcal{L}1_{N_\mathrm{g}} = 0_{N_\mathrm{g}}$ [75]. Therefore,

$$\begin{aligned}0_{N_\mathrm{g}} &= \mathcal{L}1_{N_\mathrm{g}},\\ &= \mathcal{L}^\top 1_{N_\mathrm{g}},\\ &= \begin{bmatrix}\tilde{\mathcal{L}}^\top & b\\ * & *\end{bmatrix}1_{N_\mathrm{g}},\\ &= \begin{bmatrix}\tilde{\mathcal{L}}^\top 1_{(N_\mathrm{g}-1)} + b\\ *\end{bmatrix}.\end{aligned}$$

Hence, $b^\top\tilde{\mathcal{L}}^{-1} = -1_{(N_\mathrm{g}-1)}^\top$. An alternative derivation of this relation can be found in [92, Section III.B].

Note that the number of nodes N_g, i.e., the number of buses in the network, is not necessarily identical to the number of units and loads $N_u + N_d$. Therefore, U is not always a square matrix. Using $\tilde{p}(k) = \left[p_t(k)^\top \; p_s(k)^\top \; p_r(k)^\top \; p_d(k)^\top\right]^\top$, it can be defined element-wise for $i \in \mathbb{N}_{[1,N_g]}$ and $j \in \mathbb{N}_{[1,N_u+N_d]}$ as

$$U_{ij} = \begin{cases} 1, & \text{if the unit or load associated with entry } \tilde{p}_j \text{ is connected to bus } i, \\ 0, & \text{otherwise.} \end{cases}$$

Thus, the power that flows into the grid at every bus is

$$p_g(k) = U\left[p_t(k)^\top \quad p_s(k)^\top \quad p_r(k)^\top \quad p_d(k)^\top\right]^\top.$$

Finally, using $\tilde{F}$ and U, the power of the transmission lines can be determined from the power of the units and loads as

$$\begin{aligned} & p_e(k) = \tilde{F}U\left[p_t(k)^\top \quad p_s(k)^\top \quad p_r(k)^\top \quad p_d(k)^\top\right]^\top, \\ \iff \; & p_e(k) = \tilde{F}U\left[p_t(k)^\top \quad p_s(k)^\top \quad p_r(k)^\top \quad w_d(k)^\top\right]^\top. \end{aligned} \tag{4.27}$$

With (4.27), the limits on the transmission lines can be finally formulated. The power flow over the lines is limited by $p_e^{\min} \in \mathbb{R}^{N_e}$ and $p_e^{\max} \in \mathbb{R}^{N_e}$. Using (4.27), the line limits can be expressed by

$$p_e^{\min} \leq \tilde{F}U\left[p_t(k)^\top \quad p_s(k)^\top \quad p_r(k)^\top \quad w_d(k)^\top\right]^\top \leq p_e^{\max}. \tag{4.28a}$$

Furthermore, (4.24b) which, as stated in Remark 4.7.2, is equivalent to $1_{N_g}^\top p_g(k) = 0$ must hold. As every unit is connected to exactly one bus, each column of U contains precisely one 1-entry and $N_g - 1$ entries that are 0. Therefore, $1_{N_g}^\top U = 1_{(N_u+N_d)}^\top$ and $1_{N_g}^\top p_g(k) = 0$ is equivalent to

$$0 = 1_{(N_u+N_d)}^\top \left[p_t(k)^\top \quad p_s(k)^\top \quad p_r(k)^\top \quad w_d(k)^\top\right]^\top. \tag{4.28b}$$

Example 4.7.3. The transmission network from the running example is shown in Figure 4.3. For this topology, the edges are collected in $\mathbb{E} = \{\{1,4\},\{2,3\},\{2,4\},\{3,4\}\}$, where $\{1,4\} = \check{e}_1$, $\{2,3\} = \check{e}_2$, $\{2,4\} = \check{e}_3$ and $\{3,4\} = \check{e}_4$. All nodes are elements of $\mathbb{I} = \{1,2,3,4\}$. Hence, the edge-node incidence matrix is

$$F = \begin{bmatrix} 1 & 0 & 0 & 0 \\ 0 & 1 & 1 & 0 \\ 0 & -1 & 0 & 1 \\ -1 & 0 & -1 & -1 \end{bmatrix}. \tag{4.29}$$

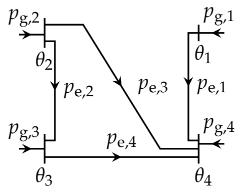

Figure 4.3: Transmission network of running example.

With the line susceptances $y_1, \dots, y_4$, the power flowing over the transmission lines can be calculated via (4.19a) as

$$\begin{bmatrix} p_{e,1}(k) \\ p_{e,2}(k) \\ p_{e,3}(k) \\ p_{e,4}(k) \end{bmatrix} = \begin{bmatrix} y_1 & 0 & 0 & -y_1 \\ 0 & y_2 & -y_2 & 0 \\ 0 & y_3 & 0 & -y_3 \\ 0 & 0 & y_4 & -y_4 \end{bmatrix} \begin{bmatrix} \theta_1(k) \\ \theta_2(k) \\ \theta_3(k) \\ \theta_4(k) \end{bmatrix}. \tag{4.30}$$

Bus power and phase angles are linked via (4.19b), i.e.,

$$\begin{bmatrix} p_{g,1}(k) \\ p_{g,2}(k) \\ p_{g,3}(k) \\ p_{g,4}(k) \end{bmatrix} = \underbrace{\begin{bmatrix} y_1 & 0 & 0 & -y_1 \\ 0 & y_2 + y_3 & -y_2 & -y_3 \\ 0 & -y_2 & y_2 + y_4 & -y_4 \\ -y_1 & -y_3 & -y_4 & y_1 + y_3 + y_4 \end{bmatrix}}_{\mathcal{L}} \begin{bmatrix} \theta_1(k) \\ \theta_2(k) \\ \theta_3(k) \\ \theta_4(k) \end{bmatrix}. \tag{4.31}$$

Using $\tilde{T} = [I_3 \quad 0_3]$ and $T = \begin{bmatrix} I_3 & -1_3 \\ 0_3^\top & 1 \end{bmatrix}$ results in

$$\tilde{\mathcal{L}} = \begin{bmatrix} y_1 & 0 & 0 \\ 0 & y_2 + y_3 & -y_2 \\ 0 & -y_2 & y_2 + y_4 \end{bmatrix}.$$

Consequently,

$$\begin{aligned} \tilde{F} &= \operatorname{diag}([y_1 \quad \cdots \quad y_4]) F^\top T^{-1} \tilde{T}^\top \tilde{\mathcal{L}}^{-1} \tilde{T} \\ &= \frac{1}{\breve{y}^2} \begin{bmatrix} \breve{y}^2 & 0 & 0 & 0 \\ 0 & y_2 y_4 & -y_2 y_3 & 0 \\ 0 & y_3 (y_2 + y_4) & y_2 y_3 & 0 \\ 0 & y_2 y_4 & y_4 (y_2 + y_3) & 0 \end{bmatrix} \end{aligned} \tag{4.32}$$

with $\breve{y}^2 = y_2 y_3 + y_2 y_4 + y_3 y_4$. Assuming the same impedance for all transmission lines, i.e., $y_1 = y_2 = y_3 = y_4$, yields

$$\tilde{F} = \begin{bmatrix} 1 & 0 & 0 & 0 \\ 0 & 1/3 & -1/3 & 0 \\ 0 & 2/3 & 1/3 & 0 \\ 0 & 1/3 & 2/3 & 0 \end{bmatrix}. \tag{4.33}$$

The matrix that connects the power of the units and loads to the power of the buses for the example in Figure 4.1 is

$$U = \begin{bmatrix} 1 & 0 & 0 & 0 \\ 0 & 1 & 0 & 0 \\ 0 & 0 & 1 & 0 \\ 0 & 0 & 0 & 1 \end{bmatrix}. \tag{4.34}$$

Note that only in a limited number of cases U is a diagonal matrix. For more complex networks, e.g., the Cigre Benchmark model in Figure 2.1 or the extended MG in Figure 12.11, it has a less trivial structure.

4.8 Power sharing of grid-forming units

In islanded operation, an equilibrium of generation, consumption and storage power has to be ensured at all times in presence of uncertain load and renewable infeed (see Section 2.3). Therefore, the lower control layers of MGs are often designed such that the grid-forming units change their power depending on the uncertain load and renewable infeed. As discussed in Assumption 4.2.5, we consider proportional active power sharing between the grid-forming conventional generators and storage units [123, 226, 227, 232, 243]. This leads to an operation where all grid-forming units share the variations of uncertain loads and RES in proportional manner.

Proportional active power sharing between the enabled units $i \in \mathbb{N}_{[1,N_\mathrm{t}+N_\mathrm{s}]}$ and $j \in \mathbb{N}_{[1,N_\mathrm{t}+N_\mathrm{s}]}$, $i \neq j$ with $\chi_i \in \mathbb{R}_{>0}$ and $\chi_j \in \mathbb{R}_{>0}$ can be described by[5]

$$\frac{p_i(k) - u_i(k)}{\chi_i} = \frac{p_j(k) - u_j(k)}{\chi_j}. \tag{4.35}$$

Disabled conventional generators with $\delta_{\mathrm{t},i}(k) = u_{\mathrm{t},i}(k) = 0$ and $p_{\mathrm{t},i}(k) = 0$ cannot participate in power sharing. To model this relation, the auxiliary variable $\mu(k) \in \mathbb{R}$ is used. With $\mu(k)$, power sharing for the storage units can be modeled by

$$\frac{p_{\mathrm{s},i}(k) - u_{\mathrm{s},i}(k)}{\chi_{\mathrm{s},i}} = \mu(k) \tag{4.36a}$$

[5] The parameter χ_i can be chosen, for example, based on the nominal power of units. Its choice is, however, part of the low layer control design. Therefore, we assume that it cannot be modified by operation control. More information on the choice of droop gains which is closely related to the choice of χ_i can be found, for example, in [16].

for all $i \in \mathbb{N}_{[1,N_\mathrm{s}]}$ with $\chi_{\mathrm{s},i} \in \mathbb{R}_{>0}$. Power sharing of all conventional generators can be equally modeled by

$$\frac{p_{\mathrm{t},i}(k) - u_{\mathrm{t},i}(k)}{\chi_{\mathrm{t},i}} = \begin{cases} \mu(k), & \text{if } \delta_{\mathrm{t},i}(k) = 1, \\ 0, & \text{if } \delta_{\mathrm{t},i}(k) = 0, \end{cases}$$

$$\iff \frac{p_{\mathrm{t},i}(k) - u_{\mathrm{t},i}(k)}{\chi_{\mathrm{t},i}} = \mu(k)\delta_{\mathrm{t},i}(k). \tag{4.36b}$$

for all $i \in \mathbb{N}_{[1,N_\mathrm{t}]}$ with $\chi_{\mathrm{t},i} \in \mathbb{R}_{>0}$. In vector notation, (4.36) can be equally expressed by

$$K_\mathrm{s}(p_\mathrm{s}(k) - u_\mathrm{s}(k)) = \mu(k)1_{N_\mathrm{s}} \text{ and} \tag{4.37a}$$

$$K_\mathrm{t}(p_\mathrm{t}(k) - u_\mathrm{t}(k)) = \mu(k)\delta_\mathrm{t}(k), \tag{4.37b}$$

with $K_\mathrm{t} = \mathrm{diag}\left(\frac{1}{\chi_{\mathrm{t},1}}, \dots, \frac{1}{\chi_{\mathrm{t},N_\mathrm{t}}}\right)$ and $K_\mathrm{s} = \mathrm{diag}\left(\frac{1}{\chi_{\mathrm{s},1}}, \dots, \frac{1}{\chi_{\mathrm{s},N_\mathrm{s}}}\right)$.

Unfortunately, the multiplication $\mu(k)\delta_\mathrm{t}(k)$ is nonlinear. Therefore, (4.37b) cannot be directly used in formulations of MIQPs or MIQCPs which can be solved by off-the-shelf software. Luckily, we can equivalently express (4.37b) by a set of affine constraints as indicated in [14, 18, 42, 263] and described in Lemma 3.3.5. For this reformulation, the constant parameters $\mathrm{m}_\mathrm{t} \in \mathbb{R}_{\leq 0}$ and $\mathrm{M}_\mathrm{t} \in \mathbb{R}_{\geq 0}$ are introduced. These must be chosen such that m_t is less than the minimum value that $\mu(k)$ can take and M_t is greater than the maximum value that $\mu(k)$ can take. As $\mu(k)$ is a function of power and setpoints, the maximum and minimum values can be derived by combining the limits of power and power setpoints. For all storage units, the greatest value that $K_\mathrm{s}(p_\mathrm{s}(k) - u_\mathrm{s}(k)) = \mu(k)1_{N_\mathrm{s}}$ can take is

$$\mu_\mathrm{s}^{\max} = \max\left(K_\mathrm{s}(p_\mathrm{s}^{\max} - p_\mathrm{s}^{\min})\right). \tag{4.38a}$$

The smallest value of $\mu(k)$ caused by the storage units is

$$\mu_\mathrm{s}^{\min} = \min\left(K_\mathrm{s}(p_\mathrm{s}^{\min} - p_\mathrm{s}^{\max})\right). \tag{4.38b}$$

For the conventional generators, the limits can be determined in a similar manner as

$$\mu_\mathrm{t}^{\max} = \max\left(K_\mathrm{t}(p_\mathrm{t}^{\max} - p_\mathrm{t}^{\min})\right), \tag{4.38c}$$

$$\mu_\mathrm{t}^{\min} = \min\left(K_\mathrm{t}(p_\mathrm{t}^{\min} - p_\mathrm{t}^{\max})\right). \tag{4.38d}$$

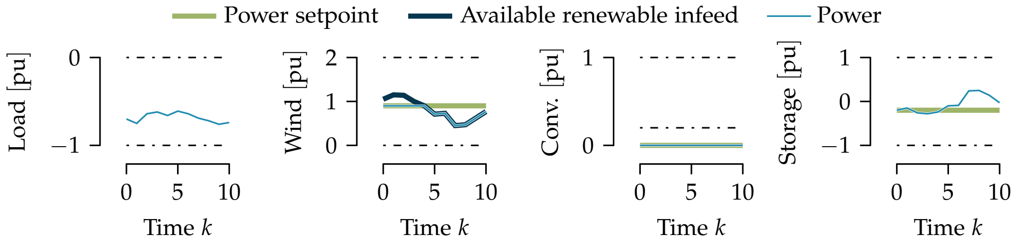

Figure 4.4: Power sharing with disabled conventional generator.

Combining these values, we know that $\mu(k)$ is always between $\mathrm{m_t}$ and $\mathrm{M_t}$, given by

$$\mathrm{M_t} > \max\left(\mu_\mathrm{s}^{\max}, \mu_\mathrm{t}^{\max}\right), \tag{4.38e}$$

$$\mathrm{m_t} < \min\left(\mu_\mathrm{s}^{\min}, \mu_\mathrm{t}^{\min}\right). \tag{4.38f}$$

Using $\mathrm{m_t}$ and $\mathrm{M_t}$, (4.37b) can be reformulated as[6]

$$K_\mathrm{t}(p_\mathrm{t}(k) - u_\mathrm{t}(k)) \leq \mathrm{M_t}\delta_\mathrm{t}(k), \tag{4.39a}$$

$$K_\mathrm{t}(p_\mathrm{t}(k) - u_\mathrm{t}(k)) \geq \mathrm{m_t}\delta_\mathrm{t}(k), \tag{4.39b}$$

$$K_\mathrm{t}(p_\mathrm{t}(k) - u_\mathrm{t}(k)) \leq 1_{N_\mathrm{t}}\mu(k) - \mathrm{m_t}(1_{N_\mathrm{t}} - \delta_\mathrm{t}(k)), \tag{4.39c}$$

$$K_\mathrm{t}(p_\mathrm{t}(k) - u_\mathrm{t}(k)) \geq 1_{N_\mathrm{t}}\mu(k) - \mathrm{M_t}(1_{N_\mathrm{t}} - \delta_\mathrm{t}(k)). \tag{4.39d}$$

[6] A detailed discussion of this reformulation can be found in Lemma 3.3.5.

Example 4.8.1 (Power sharing with disabled conventional generator)**.** Consider the running example from Figure 4.1. If the conventional generator is disabled, i.e., $p_\mathrm{t}(k) = 0$, then the power balance equation (4.28b) becomes

$$p_\mathrm{s}(k) + p_\mathrm{r}(k) + w_\mathrm{d}(k) = 0. \tag{4.40a}$$

Using (4.12), the power provided by the storage unit is

$$p_\mathrm{s}(k) = -\min(u_\mathrm{r}(k), w_\mathrm{r}(k)) - w_\mathrm{d}(k), \tag{4.40b}$$

i.e., the storage unit covers all fluctuations of uncertain renewable infeed and load. This can be clearly observed in Figure 4.4, where the excess power of the RES that is not consumed by the loads is used to charge the storage unit. Note that in this operation mode, the storage power only depends on renewable infeed $p_\mathrm{r}(k) = \min(u_\mathrm{r}(k), w_\mathrm{r}(k))$ and load $p_\mathrm{d}(k) = w_\mathrm{d}(k)$, i.e., it is independent of the setpoint $u_\mathrm{s}(k)$.

Example 4.8.2 (Power sharing with enabled conventional generator)**.** Consider the running example from Figure 4.1.

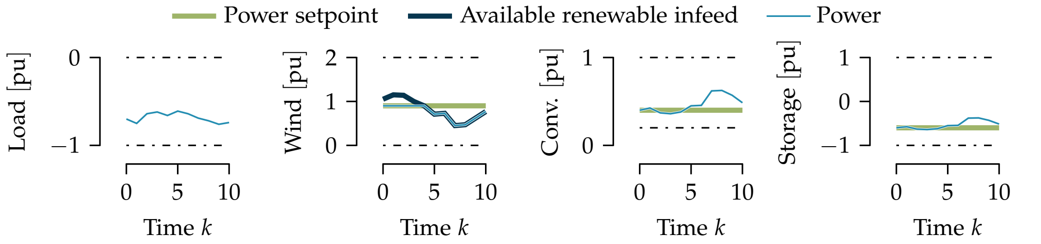

Figure 4.5: Power sharing with enabled conventional generator and power sharing factors $\chi_s = \chi_t = 1$.

If conventional generator and storage unit are enabled, then the power of the units becomes harder to determine than in the previous example as both units share the variations of renewable infeed and load. In this example, (4.35), yields

$$\frac{p_s(k) - u_s(k)}{\chi_s} = \frac{p_t(k) - u_t(k)}{\chi_t} \tag{4.41a}$$

$$\iff \quad p_t(k) = \frac{\chi_t}{\chi_s}\big(p_s(k) - u_s(k)\big) + u_t(k). \tag{4.41b}$$

Combining this equation with the power balance (4.28b), i.e., $p_t(k) + p_s(k) + p_r(k) + w_d(k) = 0$, results in

$$\frac{\chi_t}{\chi_s}\big(p_s(k) - u_s(k)\big) + u_t(k) + p_s(k) + p_r(k) + w_d(k) = 0. \tag{4.42}$$

Thus, the power provided or consumed by the storage unit is

$$p_s(k) = \frac{\chi_t u_s(k) - \chi_s u_t(k)}{\chi_s + \chi_t} - \frac{\chi_s}{\chi_s + \chi_t}\big(p_r(k) + w_d(k)\big), \tag{4.43a}$$

$$= \frac{\chi_t u_s(k) - \chi_s u_t(k)}{\chi_s + \chi_t} - \frac{\chi_s}{\chi_s + \chi_t}\big(\min(u_r(k), w_r(k)) + w_d(k)\big). \tag{4.43b}$$

One can see that the storage power in (4.43b) is composed of two parts. The first part depends on the power setpoints $u_s(k)$ and $u_t(k)$.[7] The second part changes with $w_r(k)$ and $w_d(k)$. Compared to (4.40b), the effects of the uncertain input, $w_r(k)$ and $w_d(k)$, on the storage power $p_s(k)$ decreased by a factor of $1 - \frac{\chi_s}{\chi_s+\chi_t} = \frac{\chi_t}{\chi_s+\chi_t}$. The reason for this is that the fluctuations caused by RES and load are now distributed among both grid-forming units. This is also notable when comparing the storage power in Figures 4.4 and 4.5. Here, it can be seen that in Figure 4.4 the deviation of the actual storage power from the setpoint is much higher than in Figure 4.5.

[7] Note that the storage power now depends on the setpoints of the storage *and* the conventional unit.

In conclusion, operating multiple grid-forming units in parallel for the same uncertain input allows to choose power setpoints that lie closer to the power limits because less overhead for fluctuations needs to be reserved. With an increasing number of grid-forming units, the fluctuations that each unit covers decrease and less conservative power setpoints can be selected.

Remark 4.8.3 (Constant power conventional or storage units)**.** There are setups, where it is desired to operate conventional generators or storage units as constant power sources. In such an operation, their power equals their power setpoint, i.e., $p_{\mathrm{t},i} = u_{\mathrm{t},i}$, $i \in \mathbb{N}_{[1,N_\mathrm{t}]}$ or $p_{\mathrm{s},i} = u_{\mathrm{s},i}$, $i \in \mathbb{N}_{[1,N_\mathrm{s}]}$. In our framework this case can be approximately included by choosing sufficiently small values χ_i for the corresponding units, such that they participate very little in power sharing. If this solution is found to be insufficient, the presented MG model could be easily extended by excluding the corresponding unit from the power sharing equations and adding the hard constraint $p_{\mathrm{t},i} = u_{\mathrm{t},i}$, $i \in \mathbb{N}_{[1,N_\mathrm{t}]}$ or $p_{\mathrm{s},i} = u_{\mathrm{s},i}$, $i \in \mathbb{N}_{[1,N_\mathrm{s}]}$.

4.9 Overall model

In what follows, the model of an islanded MG deduced in the past sections is summarized. First, the detailed model is presented in Section 4.9.1. Then, a compact version is posed in Section 4.9.2.

4.9.1 Detailed model

Using the equations of the different parts, the overall model of an islanded MG can be formulated as follows. The limits on power and setpoint originate from (4.7), (4.11) and (4.14). They are

$$\begin{bmatrix} \mathrm{diag}(p_\mathrm{t}^{\min})\delta_\mathrm{t}(k) \\ p_\mathrm{s}^{\min} \\ p_\mathrm{r}^{\min} \end{bmatrix} \leq u(k) \leq \begin{bmatrix} \mathrm{diag}(p_\mathrm{t}^{\max})\delta_\mathrm{t}(k) \\ p_\mathrm{s}^{\max} \\ p_\mathrm{r}^{\max} \end{bmatrix} \tag{4.44a}$$

and

$$\begin{bmatrix} \mathrm{diag}(p_\mathrm{t}^{\min})\delta_\mathrm{t}(k) \\ p_\mathrm{s}^{\min} \\ p_\mathrm{r}^{\min} \end{bmatrix} \leq p(k) \leq \begin{bmatrix} \mathrm{diag}(p_\mathrm{t}^{\max})\delta_\mathrm{t}(k) \\ p_\mathrm{s}^{\max} \\ p_\mathrm{r}^{\max} \end{bmatrix}. \tag{4.44b}$$

Following (4.15), the dynamics of the storage unit are

$$x(k+1) = Ax(k) + Bp_{\mathrm{s}}(k), \quad \text{with } x(0) = x_0 \tag{4.44c}$$

and limits

$$x^{\min} \leq x(k+1) \leq x^{\max}. \tag{4.44d}$$

The renewable infeed, which is a function of setpoint and weather-dependent available infeed, can be described by (4.13) as

$$u_{\mathrm{r}}(k) - \mathrm{diag}(\mathrm{M}_{\mathrm{r}})\delta_{\mathrm{r}}(k) \leq p_{\mathrm{r}}(k) \leq u_{\mathrm{r}}(k), \tag{4.44e}$$

$$w_{\mathrm{r}}(k) + \mathrm{diag}(\mathrm{m}_{\mathrm{r}})(1_{N_{\mathrm{r}}} - \delta_{\mathrm{r}}(k)) \leq p_{\mathrm{r}}(k) \leq w_{\mathrm{r}}(k). \tag{4.44f}$$

Power sharing of the grid-forming units is given by (4.37) which, using (4.39), can be transformed into

$$K_{\mathrm{s}}(p_{\mathrm{s}}(k) - u_{\mathrm{s}}(k)) = \mu(k)1_{N_{\mathrm{s}}}, \tag{4.44g}$$

$$K_{\mathrm{t}}(p_{\mathrm{t}}(k) - u_{\mathrm{t}}(k)) \leq \mathrm{M}_{\mathrm{t}}\delta_{\mathrm{t}}(k), \tag{4.44h}$$

$$K_{\mathrm{t}}(p_{\mathrm{t}}(k) - u_{\mathrm{t}}(k)) \geq \mathrm{m}_{\mathrm{t}}\delta_{\mathrm{t}}(k), \tag{4.44i}$$

$$K_{\mathrm{t}}(p_{\mathrm{t}}(k) - u_{\mathrm{t}}(k)) \leq 1_{N_{\mathrm{t}}}\mu(k) - \mathrm{m}_{\mathrm{t}}(1_{N_{\mathrm{t}}} - \delta_{\mathrm{t}}(k)), \tag{4.44j}$$

$$K_{\mathrm{t}}(p_{\mathrm{t}}(k) - u_{\mathrm{t}}(k)) \geq 1_{N_{\mathrm{t}}}\mu(k) - \mathrm{M}_{\mathrm{t}}(1_{N_{\mathrm{t}}} - \delta_{\mathrm{t}}(k)). \tag{4.44k}$$

Finally, the power limit of the lines is modeled by (4.28a), i.e.,

$$p_{\mathrm{e}}^{\min} \leq \tilde{F}U\begin{bmatrix} p_{\mathrm{t}}(k)^\top & p_{\mathrm{s}}(k)^\top & p_{\mathrm{r}}(k)^\top & w_{\mathrm{d}}(k)^\top \end{bmatrix}^\top \leq p_{\mathrm{e}}^{\max} \tag{4.44l}$$

and the power equilibrium by (4.28b), i.e.,

$$0 = 1_{(N_{\mathrm{u}}+N_{\mathrm{d}})}^\top \begin{bmatrix} p_{\mathrm{t}}(k)^\top & p_{\mathrm{s}}(k)^\top & p_{\mathrm{r}}(k)^\top & w_{\mathrm{d}}(k)^\top \end{bmatrix}^\top. \tag{4.44m}$$

Remark 4.9.1 (Feasible values of power and setpoints)**.** Note that (4.44l) represents a constraint on the power of the units which can, in general, be more restrictive than the unit power limits (4.44b). Through the relation of power and power setpoints, (4.44l) can also lead to constraints on the setpoints which can be more restrictive than (4.44a).

4.9.2 Compact model

In the following chapters, a more compact version of (4.44) is desirable. Using the control input $v(k) = [u(k)^\top \; \delta_{\mathrm{t}}(k)^\top]^\top$ and the auxiliary vector $z(k) = [p(k)^\top\ \delta_\mathrm{r}(k)^\top\ \mu(k)]^\top$, (4.44) can be written in a way that resembles (4.1) as

$$
\begin{aligned}
x(k+1) &= Ax(k) + \tilde{B}z(k), \quad \text{with} \quad x(0) = x_0, && \text{(4.45a)}\\
h_1 &\leq H_1\, x(k+1), && \text{(4.45b)}\\
h_2 &\leq H_2 \left[v(k)^\top \quad z(k)^\top \quad w(k)^\top\right]^\top, && \text{(4.45c)}\\
g &= G \left[v(k)^\top \quad z(k)^\top \quad w(k)^\top\right]^\top. && \text{(4.45d)}
\end{aligned}
$$

Here, the dynamics are formed with state matrix $A = I_{N_\mathrm{s}}$ and input matrix $\tilde{B} = [0_{N_\mathrm{s}\times N_\mathrm{t}}\ B\ 0_{N_\mathrm{s}\times(2N_\mathrm{r}+1)}]$. Furthermore, $h_1 = [(x^{\min})^\top\ (-x^{\max})^\top]^\top$ and $H_1 = [I_{N_\mathrm{s}}\ \ -I_{N_\mathrm{s}}]^\top$. Matrix H_2 and vector h_2 are such that (4.45c) includes inequalities (4.7), (4.11), (4.13), (4.14), (4.28a) and (4.39). To formulate H_2, it is convenient to decompose $\tilde{F}U$ into submatrices $\tilde{f}_\mathrm{t} \in \mathbb{R}^{N_\mathrm{e}\times N_\mathrm{t}}$, $\tilde{f}_\mathrm{s} \in \mathbb{R}^{N_\mathrm{e}\times N_\mathrm{s}}$, $\tilde{f}_\mathrm{r} \in \mathbb{R}^{N_\mathrm{e}\times N_\mathrm{r}}$, and $\tilde{f}_\mathrm{d} \in \mathbb{R}^{N_\mathrm{e}\times N_\mathrm{d}}$ such that $\tilde{F}U = [\tilde{f}_\mathrm{t} \quad \tilde{f}_\mathrm{s} \quad \tilde{f}_\mathrm{r} \quad \tilde{f}_\mathrm{d}]$. In detail, H_2 and h_2 are given by[8]

[8] For compactness, the size of zero matrices and identity matrices was omitted.

$$
\left[\begin{array}{c|c} h_2 & H_2 \end{array}\right] =
$$

$$
\left[\begin{array}{c|cccc|ccccc|cc}
0_{N_\mathrm{t}} & I & 0 & 0 & -\operatorname{diag}(p_\mathrm{t}^{\min}) & 0 & 0 & 0 & 0 & 0 & 0 & 0\\
p_\mathrm{s}^{\min} & 0 & I & 0 & 0 & 0 & 0 & 0 & 0 & 0 & 0 & 0\\
p_\mathrm{r}^{\min} & 0 & 0 & I & 0 & 0 & 0 & 0 & 0 & 0 & 0 & 0\\
\hline
0_{N_\mathrm{t}} & -I & 0 & 0 & \operatorname{diag}(p_\mathrm{t}^{\max}) & 0 & 0 & 0 & 0 & 0 & 0 & 0\\
-p_\mathrm{s}^{\max} & 0 & -I & 0 & 0 & 0 & 0 & 0 & 0 & 0 & 0 & 0\\
-p_\mathrm{r}^{\max} & 0 & 0 & -I & 0 & 0 & 0 & 0 & 0 & 0 & 0 & 0\\
\hline
0_{N_\mathrm{t}} & 0 & 0 & 0 & -\operatorname{diag}(p_\mathrm{t}^{\min}) & I & 0 & 0 & 0 & 0 & 0 & 0\\
p_\mathrm{s}^{\min} & 0 & 0 & 0 & 0 & 0 & I & 0 & 0 & 0 & 0 & 0\\
p_\mathrm{r}^{\min} & 0 & 0 & 0 & 0 & 0 & 0 & I & 0 & 0 & 0 & 0\\
\hline
0_{N_\mathrm{t}} & 0 & 0 & 0 & \operatorname{diag}(p_\mathrm{t}^{\max}) & -I & 0 & 0 & 0 & 0 & 0 & 0\\
-p_\mathrm{s}^{\max} & 0 & 0 & 0 & 0 & 0 & -I & 0 & 0 & 0 & 0 & 0\\
-p_\mathrm{r}^{\max} & 0 & 0 & 0 & 0 & 0 & 0 & -I & 0 & 0 & 0 & 0\\
\hline
0_{N_\mathrm{r}} & 0 & 0 & -I & 0 & 0 & 0 & I & \operatorname{diag}(\mathrm{M}_\mathrm{r}) & 0 & 0 & 0\\
0_{N_\mathrm{r}} & 0 & 0 & I & 0 & 0 & 0 & -I & 0 & 0 & 0 & 0\\
\mathrm{m}_\mathrm{r} & 0 & 0 & 0 & 0 & 0 & 0 & I & \operatorname{diag}(\mathrm{m}_\mathrm{r}) & 0 & -I & 0\\
0_{N_\mathrm{r}} & 0 & 0 & 0 & 0 & 0 & 0 & -I & 0 & 0 & I & 0\\
\hline
0_{N_\mathrm{t}} & K_\mathrm{t} & 0 & 0 & \mathrm{M}_\mathrm{t} I & -K_\mathrm{t} & 0 & 0 & 0 & 0 & 0 & 0\\
0_{N_\mathrm{t}} & -K_\mathrm{t} & 0 & 0 & -\mathrm{m}_\mathrm{t} I & K_\mathrm{t} & 0 & 0 & 0 & 0 & 0 & 0\\
\mathrm{m}_\mathrm{t} 1_{N_\mathrm{t}} & K_\mathrm{t} & 0 & 0 & \mathrm{m}_\mathrm{t} I & -K_\mathrm{t} & 0 & 0 & 0 & 1_{N_\mathrm{t}} & 0 & 0\\
-\mathrm{M}_\mathrm{t} 1_{N_\mathrm{t}} & -K_\mathrm{t} & 0 & 0 & -\mathrm{M}_\mathrm{t} I & K_\mathrm{t} & 0 & 0 & 0 & -1_{N_\mathrm{t}} & 0 & 0\\
\hline
p_\mathrm{e}^{\min} & 0 & 0 & 0 & 0 & \tilde{f}_\mathrm{t} & \tilde{f}_\mathrm{s} & \tilde{f}_\mathrm{r} & 0 & 0 & 0 & \tilde{f}_\mathrm{d}\\
-p_\mathrm{e}^{\max} & 0 & 0 & 0 & 0 & -\tilde{f}_\mathrm{t} & -\tilde{f}_\mathrm{s} & -\tilde{f}_\mathrm{r} & 0 & 0 & 0 & -\tilde{f}_\mathrm{d}
\end{array}\right].
$$

Moreover, matrix G and vector g are such that (4.45d) includes (4.28b) and (4.37a), i.e.,

$$
\left[\begin{array}{c|c} g & G \end{array}\right] =
$$
$$
\left[\begin{array}{c|cccc:ccccc:cc}
0_{N_\mathrm{s}} & 0 & -K_\mathrm{s} & 0 & 0 & 0 & K_\mathrm{s} & 0 & 0 & -1_{N_\mathrm{s}} & 0 & 0 \\ \hdashline
0 & 0 & 0 & 0 & 0 & 1_{N_\mathrm{t}}^\top & 1_{N_\mathrm{s}}^\top & 1_{N_\mathrm{r}}^\top & 0 & 0 & 0 & 1_{N_\mathrm{d}}^\top
\end{array}\right].
$$

Note that the relation of variables in (4.45) follows Figure 4.6. Thus, the variables that are assumed during the time interval between k and $k+1$ are $v(k)$, $z(k)$ and $w(k)$. Moreover, the power of the storage units, which is part of the auxiliary vector $z(k)$, and the state at time $x(k)$ affect the stored energy at time $k+1$.

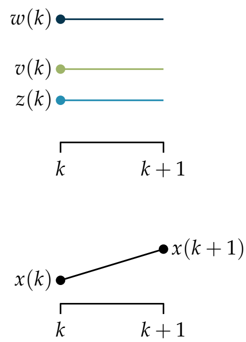

Figure 4.6: Temporal relation of variables in compact model.

Remark 4.9.2 (Power and power setpoint)**.** Looking at the formulations presented in this chapter, it might appear like one could reduce most of the *power* variables and formulate the model only in terms of *power setpoints*. This seems beneficial, as it leads to MPC formulations with a smaller number of decision variables.

One major reason against this reduction lies in the minimax and the scenario-based MPC formulations in Chapters 8, 10 and 11. In these approaches, each optimal power setpoints is associated with multiple uncertain inputs. This, in the end, leads to multiple power values which are associated with one power setpoint. Therefore, it is fundamental to distinguish between power and power setpoints in these approaches.

The reader is kindly referred to Examples 8.2.1 and 9.2.2 for more detailed discussions on the distinction between power and setpoint.

In the prescient and the certainty equivalence MPC formulations in Chapters 5 and 7, a reduction of some power variables would be possible and could lead to lower computing times of the numerical solvers. However, the solve times of aforementioned approaches are already quite low compared to the other approaches (see Chapter 12). Therefore, the distinction between power and power setpoint was kept in Chapters 5 and 7 in order to pose MPC problems that resemble each other.

4.10 Summary

In this chapter, the model of an islanded MG with very high share of RES was derived. It comprises RES, storage and conventional units as well as transmission lines and loads.

In detail, the model includes renewable sources that can be limited. This is an important property in grids with very high share of RES as it enables MG configurations with a rated renewable power that exceeds the nominal load. In such configurations, it is necessary to limit renewable infeed, e.g., if all storage units are fully charged. Moreover, grid-forming storage units were considered. These enable an operation where all conventional generators are disabled. Furthermore, power sharing of grid-forming units is modeled. This allows to take the effects of fluctuating renewable generators and loads on the power of storage and conventional units into account. Finally, a DC power flow model that allows to approximately account for limits of transformers or power lines has been derived.

The overall model deduced in this chapter can now be employed to formulate different MPC problems in Chapters 7, 8, 10 and 11. However, first the cost function and a prescient MPC formulation are presented in Chapter 5.

5
Model predictive control formulation

Previously, the model of an islanded MG was derived. Based on this model, a prescient MPC problem that assumes perfect knowledge of the uncertain input is formulated in this chapter. This formulation serves as a basis for real-world MPC approaches that employ real forecasts of the uncertain input.

The contributions of this chapter are as follows. A cost function is formulated that includes the costs of the different units: (i) operating and switching costs of conventional generators, (ii) costs incurred by a limitation of renewable infeed, and (iii) costs associated with the power and the state of charge of storage units. Using this cost and the model of and islanded MG from Chapter 4, a prescient MPC problem is formulated as an MIQP. This problem can be solved efficiently by off-the-shelf solvers to obtain optimal power setpoints for a given MG.

The remainder of this chapter is based on [89–91, 93] and structured as follows. First, the relation of model variables assumed for the prescient MPC is discussed in Section 5.1. Then, a cost function which is composed of an economic part and a part that is related to the state of charge is introduced in Section 5.2. Using this cost function, a prescient MPC problem is formulated in Section 5.3.

5.1 Model variables

To formulate all MPC problems in a consistent way that complies with Problem 1, it is convenient to change how the variables are associated with the different time instants. Based on

(4.45), the updated control-oriented model reads

$$x(k+1) = Ax(k) + \tilde{B}z(k+1), \quad \text{with} \quad x(0) = x_0, \tag{5.1a}$$
$$h_1 \leq H_1\, x(k+1), \tag{5.1b}$$
$$h_2 \leq H_2 \left[v(k)^\top \quad z(k+1)^\top \quad w(k+1)^\top\right]^\top, \tag{5.1c}$$
$$g = G \left[v(k)^\top \quad z(k+1)^\top \quad w(k+1)^\top\right]^\top. \tag{5.1d}$$

The main difference between this model and (4.45) is that the uncertain input $w(k+1)$ and the auxiliary vector $z(k+1)$ are now associated with the time instant of the state $x(k+1)$ that they directly affect.[1] More precisely, in (4.45) the uncertainty associated with the time interval between k and $k+1$ is $w(k)$. In (5.1), the uncertainty uncertainty associated with the time interval between k and $k+1$ is $w(k+1)$. Note that this change only affects how the variables are associated with the different time instants. The relation of the variables in the time interval between k and $k+1$ remains unchanged.

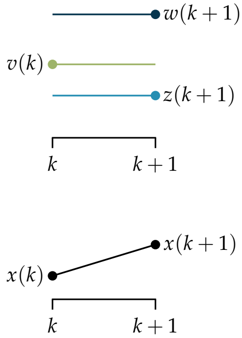

Figure 5.1: Temporal relation of variables in control-oriented model.

[1] Associating the uncertain input and the auxiliary variables with the next time instant will allow us to formulate all MPC problems in a consistent way.

In Figure 5.1, the changed relation of variables in the control-oriented model is illustrated. Here, the uncertain input preset between time instants k and $k+1$ is $w(k+1)$ and the control input during this period is $v(k)$. The vector of auxiliary variables $z(k+1)$ changes with the control input $v(k)$ and the uncertain input $w(k+1)$.[2] Similarly, the state $x(k+1)$ is a function of the previous state $x(k)$ and the auxiliary vector $z(k+1)$, i.e., $x(k+1) = f_x(x(k), z(k+1))$.[3]

[2] Note that $z(k+1)$, $v(k)$ and $w(k+1)$ are linked via constraints (5.1c) and (5.1d).

[3] Note that f_x can be easily derived from (5.1a).

5.2 *Cost function*

The cost function for time instant $k \in \mathbb{N}_0$ is composed of two parts. The first part, $\ell_o(v(k-1), v(k), z(k+1))$, is motivated economically. The second part, $\ell_x(x(k+1))$, is a cost associated with a desired region of operation of the state of charge. Thus, the cost function at time instant k, i.e., the stage cost, is

$$\ell(v(k-1), v(k), z(k+1), x(k+1)) = \\ \ell_o(v(k-1), v(k), z(k+1)) + \ell_x(x(k+1)). \tag{5.2}$$

Remark 5.2.1 (Time instants in cost function)**.** The reason why the cost at the current time instant depends on the past control input $v(k-1)$, the current control actions $v(k)$ and auxiliary variables $z(k+1)$ as well as on the future state

$x(k+1)$ is as follows. The cost at time instant k is influenced by the control input $v(k)$. The cost associated with this control decision, depends on the on/off condition of the conventional generators at time instant $k-1$. This leads to the dependence of the cost on the last control input $v(k-1)$. Furthermore, the decision taken at k in the form of $v(k)$ has an effect on the future state $x(k+1)$. Therefore, ℓ_x is a function of $x(k+1)$. Moreover, the auxiliary variable $z(k+1)$ changes with $v(k)$ and $w(k+1)$ (see Section 5.1). Therefore, ℓ_{o} is a function of $v(k)$ and $z(k+1)$.

5.2.1 *Economically motivated costs*

The economically motivated parts of (5.2) can be divided into (i) costs incurred by curtailing infeed of renewable units $\ell_{\mathrm{r}}(z(k+1))$, (ii) fuel costs of conventional generators $\ell_{\mathrm{t}}^{\mathrm{rt}}(v(k), z(k+1))$, (iii) switching costs of conventional generators $\ell_{\mathrm{t}}^{\mathrm{sw}}(v(k-1), v(k))$, and (iv) costs associated with the power of the storage units $\ell_{\mathrm{s}}(z(k+1))$. Thus, the economically motivated stage costs are

$$\begin{aligned}\ell_{\mathrm{o}}(v(k-1), v(k), z(k+1)) &= \ell_{\mathrm{r}}(v(k), z(k+1)) + \\ &\ell_{\mathrm{t}}^{\mathrm{rt}}(v(k), z(k+1)) + \ell_{\mathrm{t}}^{\mathrm{sw}}(v(k-1), v(k)) + \ell_{\mathrm{s}}(z(k+1)).\end{aligned} \tag{5.3}$$

Renewable units. As stated in Section 2.3.1, RES, such as, PV power plants or wind turbines, usually come with a very high initial invest and small operation costs once they are installed [252, 261]. Therefore, the owners of RES want to keep the units' infeed as high as possible. Limiting a renewable unit can be seen as a loss in money as the weather-dependent available infeed is not sold to customers. The desire to maximize renewable infeed can be included in the cost function by a penalty for using less than the maximal power $p_{\mathrm{r}}^{\max}$, i.e.,

$$\begin{aligned}\ell_{\mathrm{r}}(v(k), z(k+1)) &= c_{\mathrm{r}}'^{\top} u_{\mathrm{r}}(k) + \\ &(p_{\mathrm{r}}^{\max} - p_{\mathrm{r}}(k+1))^{\top} \operatorname{diag}(c_{\mathrm{r}}'')(p_{\mathrm{r}}^{\max} - p_{\mathrm{r}}(k+1)),\end{aligned} \tag{5.4}$$

with $c_{\mathrm{r}}' \in \mathbb{R}_{>0}^{N_{\mathrm{r}}}$, $c_{\mathrm{r}}'' \in \mathbb{R}_{>0}^{N_{\mathrm{r}}}$. The small cost associated with the power setpoints $u_{\mathrm{r}}(k)$ was included to ensure that the entries of $u_{\mathrm{r}}(k)$ are only as high as really needed. In practice, this typically leads to power setpoints that are less than or equal to the largest available power forecasts. This is important in the closed loop, as it prevents unexpectedly high renewable infeed if the available infeed exceeds the largest forecast. Note that the elements of c'_r are chosen much smaller than the elements of c''_r such that the effect of this term is negligible compared to the power-related term.

Conventional generators. Motivated by [265, 266, 277], the costs for the conventional generators was modeled by the mixed-integer quadratic function

$$\ell_\mathrm{t}^\mathrm{rt}(v(k), z(k+1)) = c_\mathrm{t}^\top \delta_\mathrm{t} + \\ c_\mathrm{t}'^\top p_\mathrm{t}(k+1) + p_\mathrm{t}(k+1)^\top \operatorname{diag}(c''_\mathrm{t}) p_\mathrm{t}(k+1), \quad (5.5)$$

with weights $c_\mathrm{t} \in \mathbb{R}_{>0}^{N_\mathrm{t}}$, $c'_\mathrm{t} \in \mathbb{R}_{>0}^{N_\mathrm{t}}$ and $c''_\mathrm{t} \in \mathbb{R}_{>0}^{N_\mathrm{t}}$. In Figure 5.2, this function with parameters from [265] is shown.

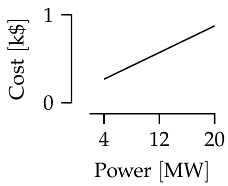

Figure 5.2: Operation cost of conventional generator as function of power. In this example, the parameters from unit 6 in [265, Table 1(a)] were used, i.e., $c_\mathrm{t} = 117.755\,\mathrm{k\$}$, $c'_\mathrm{t} = 37.5510\,\mathrm{k\$/MW}$, and $c''_\mathrm{t} = 0.01199\,\mathrm{k\$/MW^2}$. Note that the minimum power of unit 6 is 4 MW.

Enabling or disabling a conventional generator causes costs [40]. Therefore, as stated in Section 2.3.3, it is desirable to enable or disable these units as little as possible. The switching cost occurs if a conventional generator (i) was disabled at time instant $k-1$ and is enabled at time instant k, or (ii) was enabled at time instant $k-1$ and is disabled at time instant k. With the weight $c_\mathrm{t}^\mathrm{sw} \in \mathbb{R}_{>0}^{N_\mathrm{t}}$, this can be modeled by

$$\ell_\mathrm{t}^\mathrm{sw}(v(k-1), v(k)) = \\ (\delta_\mathrm{t}(k) - \delta_\mathrm{t}(k-1))^\top \operatorname{diag}(c_\mathrm{t}^\mathrm{sw})(\delta_\mathrm{t}(k) - \delta_\mathrm{t}(k-1)). \quad (5.6)$$

Storage units. Storing energy usually causes conversion losses.[4] To represent the costs associated with these losses, the term

$$\ell_\mathrm{s}(z(k+1)) = p_\mathrm{s}(k+1)^\top \operatorname{diag}(c''_\mathrm{s}) p_\mathrm{s}(k+1), \quad (5.7)$$

with $c''_\mathrm{s} \in \mathbb{R}_{>0}^{N_\mathrm{s}}$ is included in the cost function. In Figure 5.3, the cost is illustrated for a single storage unit.

[4] See, e.g., [67, 224], for more details on losses in electrochemical storage units.

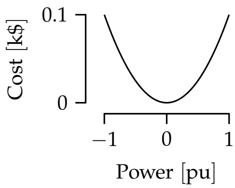

Figure 5.3: Power-related cost of storage unit for $c_\mathrm{s} = 0.1\,\mathrm{k\$/pu}$.

5.2.2 *Energy-related costs*

The aging of electrochemical storage units is influenced by the state of charge [2, 39, 264]. Therefore, it is often desired to keep $x(k+1)$ in the interval $[\tilde{x}^\mathrm{min}, \tilde{x}^\mathrm{max}]$, with $\tilde{x}^\mathrm{min} \in \mathbb{R}_{\geq 0}^{N_\mathrm{s}}$,

$\tilde{x}^{\max} \in \mathbb{R}^{N_s}_{\geq 0}$ and $\tilde{x}^{\min} \leq \tilde{x}^{\max}$. Motivated by [93], this is done by formulating the energy-related costs as

$$\ell_x(x(k+1)) = c_x^\top (\max(\tilde{x}^{\min} - x(k+1), 0_{N_s}) + \max(x(k+1) - \tilde{x}^{\max}, 0_{N_s})). \quad (5.8)$$

with $c_x \in \mathbb{R}^{N_s}_{>0}$. For a single storage unit, the cost ℓ_x as a function of the stored energy x_1 is shown in Figure 5.4.

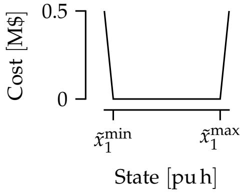

Figure 5.4: Cost associated with state of charge for $c_x = 1\,$M$/pu h. Note that the function returns zero as long as the state is in the interval $[\tilde{x}_1^{\min}, \tilde{x}_1^{\max}]$.

Remark 5.2.2 (Reformulation of energy-related costs)**.** Using the additional decision variables $\sigma(k+1) \in \mathbb{R}^{N_s}$, the max functions in (5.8) can be transformed into

$$\ell_x(x(k+1)) = \min_{\substack{\tilde{x}^{\min} - x(k+1) \leq \sigma(k+1) \\ x(k+1) - \tilde{x}^{\max} \leq \sigma(k+1) \\ 0 \leq \sigma(k+1)}} c_x^\top \sigma(k+1) \quad (5.9)$$

in a similar fashion as in Lemma 3.3.2. Note that the min operator represents the minimum of $c_x^\top \sigma(k+1)$ subject to the constraints that are written below. As the cost $\ell_x(x(k+1))$ is minimized, it is sufficient to add $c_x^\top \sigma(k+1)$ to the cost function and $\tilde{x}^{\min} - x(k+1) \leq \sigma(k)$, $x(k+1) - \tilde{x}^{\max} \leq \sigma(k+1)$ as well as $0 \leq \sigma(k+1)$ to the constraints.

5.3 *Problem formulation*

Using the cost function, we can now pose a prescient MPC problem that resembles Problem 1. As shown in Figure 5.5, in the context of operation control of islanded MG, $w(k)$ comprises the uncertain available renewable generation and the uncertain load. Furthermore, the output of the microgrid is the stored energy $x(k)$ and the last applied input v_{k-1} which is required for the switching cost (5.6).

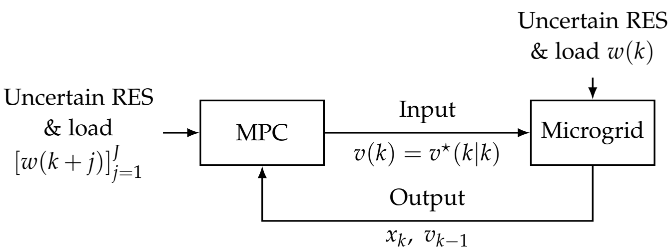

Figure 5.5: Prescient MPC scheme used for the optimal operation of islanded MGs at time instant k.

Based on the MG model (5.1) and the cost function (5.2) an MPC problem can be formulated as an MIQP which includes real-valued and Boolean decision variables, a quadratic cost function and linear constraints. With the decision variables $\boldsymbol{v} = [v(k+j|k)]_{j=0}^{J-1}$, $\boldsymbol{x} = [x(k+j|k)]_{j=1}^{J}$, $\boldsymbol{z} = [z(k+j|k)]_{j=1}^{J}$ and a discount factor $\gamma \in (0, 1]$ that is used to emphasize decisions in the near future, the MPC problem reads as follows.

Problem 2 (Prescient MPC of islanded MGs)**.** Solve the optimization problem

$$\min_{\boldsymbol{v},\boldsymbol{x},\boldsymbol{z}} \sum_{j=0}^{J-1} \ell\big(v(k+j-1|k), v(k+j|k), z(k+j+1|k), x(k+j+1|k)\big)\gamma^{j+1}$$

subject to

$$\begin{aligned} x(k+j+1|k) &= Ax(k+j|k) + \tilde{B}z(k+j+1|k), \\ h_1 &\leq H_1\, x(k+j+1|k), \\ h_2 &\leq H_2 \begin{bmatrix} v(k+j|k)^\top & z(k+j+1|k)^\top & w(k+j+1)^\top \end{bmatrix}^\top, \\ g &= G \begin{bmatrix} v(k+j|k)^\top & z(k+j+1|k)^\top & w(k+j+1)^\top \end{bmatrix}^\top, \end{aligned}$$

$\forall j = 0, \ldots, J-1$,
with given initial conditions $x(k|k) = x_k$ and $v(k-1) = v_{k-1}$.

The problem of this MPC formulation is that in deterministic real-world applications the uncertain input $[w(k+j)]_{j=1}^{J}$ is not exactly known and can only be forecast. As we consider islanded MGs with very high share of renewable sources, the uncertainty that these units introduce plays an important role. It is therefore crucial for a safe and reliable operation to find suitable models of the uncertain load and renewable generation. In what follows, we deduce different predictive controllers and forecasts that model the uncertain input in different ways. The goal is to find a control scheme that is as close as possible to the prescient MPC with perfect knowledge about future renewable infeed and load. Note that the hypothetical perfect knowledge can be modeled in simulations by assuming that $w(k+j)$ is known for $j = 1, \ldots, J$ which results in a prescient MPC formulation [91, 93, 206, 267].

Remark 5.3.1. The prescient MPC strategy associated with Problem 2 is only used as a reference to represent the best

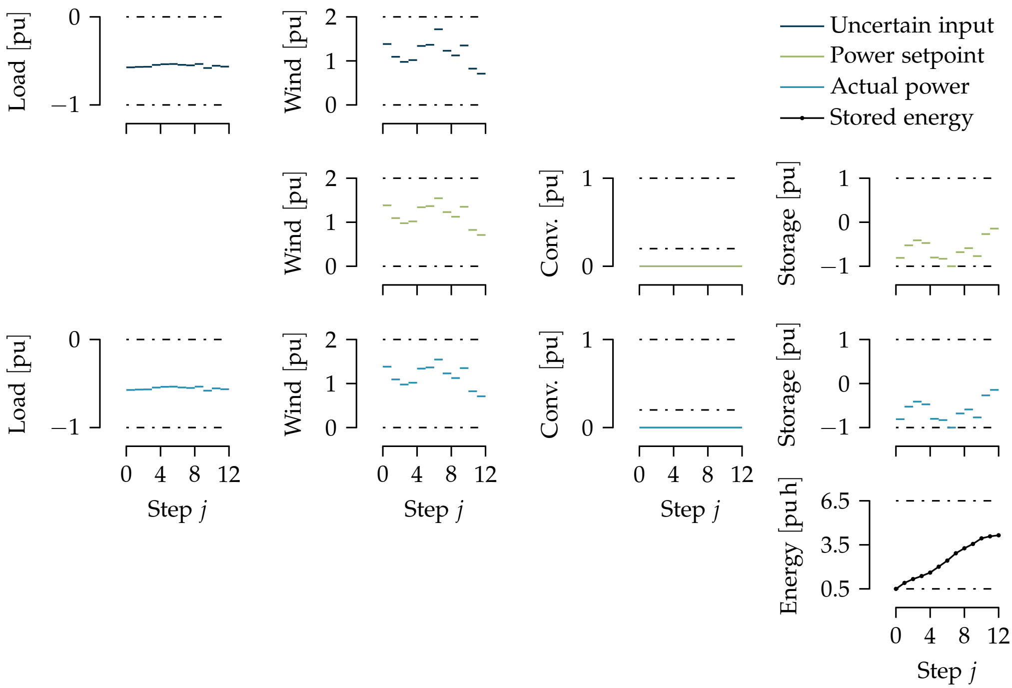

Figure 5.6: Open-loop trajectories of prescient MPC.

disturbance model possible, i.e., a perfect forecast. It could never be used in a real-world setup as the future available renewable infeed and load are uncertain and therefore never perfectly known. The goal in the design of real-world control strategies is to obtain an operation regime that is as close as possible to the one that results from Problem 2. It must be noted, that Problem 2 only represents a best case of MPC approaches with prediction horizon J. Using a longer prediction horizon can to lead to even better closed-loop results.

5.4 *Example*

In Figure 5.6, the uncertain input, power, setpoints and stored energy are shown. As MG model, the running example from Figure 4.1 was used.[5] The values were derived by solving Problem 2 with initial conditions $x^{(0)} = 0.5\,\text{pu}\,\text{h}$ and $\delta_t^{(0_-)} = 0$. The uncertain input was assumed to be perfectly known.

[5] The unit parameters and the weights of the cost function can be found in Tables 12.1 and 12.2.

Load and available renewable infeed are shown in the first row of the plot. It can be observed that the load varies a little. The available renewable power of the wind turbine shows higher variation than the load. The renewable infeed is such that the load can be fully provided over the entire prediction horizon. Therefore, the conventional generator remains disabled. The infeed of the renewable unit is only limited in one time instant in order to prevent overpower of the storage unit.

In the example, the excess energy of the renewable unit is used to charge the battery. In Figure 5.6 this is indicated by negative storage power values in the third row. Furthermore, the stored energy in the fourth row continuously increases from 0.5 pu h to 4.15 pu h.

5.5 *Summary*

In the chapter, the stage cost and an MPC formulation for the operation of islanded MG were discussed. More precisely, a prescient MPC scheme that serves as a reference by assuming perfect knowledge about future renewable infeed and load was derived.

In Chapters 7, 8, 10 and 11, different real-world MPC formulations that are based on Problem 2 are presented. They all vary in the way they model the uncertain available renewable infeed and load. Before presenting the first real-world MPC formulation, suitable forecast models for the available infeed of wind turbines and PV generators as well as load are deduced in the next chapter.

6
Forecast

In the previous chapter, a prescient MPC problem for islanded MGs with uncertain load and available renewable infeed was formulated. To deduce real-world MPC schemes, forecasts of the uncertain inputs are required. Such forecasts are derived in this chapter.

In what follows, time-series based forecasts without exogenous inputs, i.e., using only past observations of load, wind speed and irradiance, are employed to predict future load and available renewable power. The use of forecasts without exogenous inputs is motivated by the fact that MG projects often come with a small financial project volume. As stated in Section 2.3.7, it is therefore desired to employ approaches that are cost-efficient [256]. Because of their simplicity, time-series based forecasts meet this desire. In this thesis, the widely used autoregressive integrated moving average (ARIMA) models are employed.[1] Suitable models are identified in a systematic search that includes more than 6 000 model candidates.

[1] ARIMA models can be found in many domains, such as, forecasting of water demand [220], electric load [47] or wind speed [176].

The remainder of this chapter is partly based [88, 91] and structured as follows. First, preliminaries on forecasting, e.g., simple benchmark methods and multi-step ahead forecasts, are provided in Section 6.1. Then, seasonal and non-seasonal ARIMA forecasts are introduced and a strategy to find suitable models is discussed in Section 6.2. Finally, forecast models for load and available infeed of PV power plants and wind turbines are identified in Sections 6.3 to 6.5.

6.1 Preliminaries

In this section, basics on time-series forecasting required throughout this chapter are introduced. First, simple benchmark forecasting methods are posed. Then, multi-step ahead forecasts and the prediction root mean squared error are addressed. Finally, the generation of a collection of forecasts is discussed.

6.1.1 Simple benchmark methods

Consider a given time-series of measurements of the form $w_i(0), w_i(1), \ldots, w_i(K)$ with finite $K \in \mathbb{N}_0$, $i \in \mathbb{N}_{[1,N_\mathrm{r}+N_\mathrm{d}]}$ and $w_i(k) \in \mathbb{R}$ for all time instants $k \in \mathbb{N}_{[0,K]}$. In the context of time-series based forecasting, some simple prediction methods are often used as references. In what follows, two of them are discussed: persistence and seasonal persistence forecast.

Recall from Chapter 4 that N_r is the number of renewable units and N_d is the number of loads in an MGs.

Persistence forecast. Here, the forecast $\hat{w}_i(k+j|k)$ performed at time k for each prediction step $j \in \mathbb{N}_{[1,J]}$ within prediction horizon $J \in \mathbb{N}$ equals the last observation [106], i.e.,

$$\hat{w}_i(k+j|k) = w_i(k). \tag{6.1}$$

This is illustrated in Figure 6.1 for the load of an MG. Persistence forecasts represent one of the least complex forecasts possible by assuming that everything will remain as it is. More complex forecast methods that require more computations always have to be at least as good as the persistence forecast to justify the increased effort.

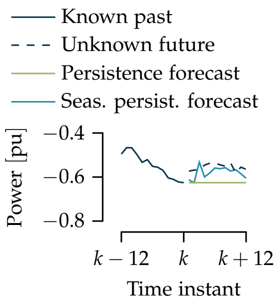

Figure 6.1: Persistence and seasonal persistence forecasts of load with seasonality of one week and a sampling time of 30 min.

Seasonal persistence forecast. Another very simple method is the seasonal persistence forecast [106]. Here, the forecast equals the measured value that lies one season, e.g., one year or one week[2], in the past. Broadly speaking, for a seasonality of one week, the forecast value on Monday at 12 pm is the value of last Monday at 12 pm. Let us denote the seasonal period by $N_\mathrm{p} \in \mathbb{N}$. Then, the forecast at prediction time instant j with $j \leq N_\mathrm{p}$ is

$$\hat{w}_i(k+j|k) = w_i(k+j-N_\mathrm{p}). \tag{6.2}$$

In Figure 6.1 a seasonal persistence forecast of load with a seasonality of one week is shown.

[2] The seasonal persistence forecast with a seasonality of one week represents a "same-time-same-day-last-week" approach.

6.1.2 Multi-step ahead forecasts

Each forecast can be seen as a function $f_w : \mathbb{R}^{K+1} \to \mathbb{R}$ of $K+1$ past observations, i.e.,

$$\hat{w}_i(k+1|k) = f_w\big(w_i(k), w_i(k-1), \ldots, w_i(k-K)\big), \tag{6.3}$$

with $k \geq K$. For multi-step ahead forecasts, a recursive strategy that employs previous predictions can be used [33, 59, 87, 255], i.e.,

$$\hat{w}_i(k+1|k) = f_w\big(w_i(k), w_i(k-1), \ldots, w_i(k-K)\big), \tag{6.4a}$$
$$\hat{w}_i(k+2|k) = f_w\big(\hat{w}_i(k+1|k), w_i(k), \ldots, w_i(k-K+1)\big), \tag{6.4b}$$
$$\hat{w}_i(k+3|k) = f_w\big(\hat{w}_i(k+2|k), \hat{w}_i(k+1|k), \ldots, w_i(k-K+2)\big), \tag{6.4c}$$
$$\vdots$$

6.1.3 Prediction root mean square error

Consider a test data set that was not used for the training of a forecast model. Using sample $w_i(k+j)$ from this set, the error of forecast $\hat{w}_i(k+j|k)$ performed at time k for instant $k+j$ is

$$e_i(k+j|k) = w_i(k+j) - \hat{w}_i(k+j|k). \tag{6.5}$$

Using $e_i(k+j|k)$, the prediction root mean squared error for a prediction performed at time k over prediction horizon J is

$$\mathrm{PRMSE}_J(k) = \sqrt{\frac{1}{J}\sum_{j=1}^{J}(e_i(k+j|k))^2}. \tag{6.6}$$

PRMSE_J is a random variable which can be accessed via its samples, i.e., via the elements of the set $\{\mathrm{PRMSE}_J(k)\}_{k=K_1}^{K_2}$, where $K_1 \in \mathbb{N}_0$, $K_2 \in \mathbb{N}$ with $K_1 < K_2$ are the limits of the test data. As a measure of the multi-step ahead prediction ability, the quantiles of the empirical distribution of PRMSE_J can be visualized using, for example, box plots or histograms.

6.1.4 Generation of a collection of forecasts

For some approaches, e.g., stochastic MPC, the forecast probability distribution is required. In this thesis, these are obtained in a similar fashion as in [196] via Monte Carlo sampling.

Here, a collection of $N_\Omega \in \mathbb{N}$ independent and equiprobable forecast scenarios, i.e., a scenario fan [97], is generated employing random errors $e_i^l(j) \in \mathbb{R}$, $l \in \mathbb{N}_{[1,N_\Omega]}$. A scenario $\hat{w}_i^l(k+1|k), \dots, \hat{w}_i^l(k+J|k)$ can be generated by considering appropriate[3] additive random errors [87, 255], i.e.,

$$\hat{w}_i^l(k+j|k) = f_w(\cdots) + e_i^l(j). \tag{6.7}$$

[3] In this thesis, it is assumed that the random errors follow the probability distribution of the errors from the training of the forecast models.

Using (6.4) the multi-step ahead forecast of scenario l is

$$\hat{w}_i^l(k+1|k) = f_w\big(w_i(k), \dots, w_i(k-K)\big) + e_i^l(1), \tag{6.8a}$$

$$\hat{w}_i^l(k+2|k) = f_w\big(\hat{w}_i^l(k+1|k), \dots, w_i(k-K+1)\big) + e_i^l(2), \tag{6.8b}$$

$$\hat{w}_i^l(k+3|k) = f_w\big(\hat{w}_i^l(k+2|k), \dots, w_i(k-K+2)\big) + e_i^l(3), \tag{6.8c}$$

$$\vdots$$

Via (6.8), the error propagates from one prediction stage to the subsequent ones, i.e., the error $e_i^l(j)$ influences the forecasts at time instants $k+j+1$ to $k+j+J$.

A collection of load forecasts is shown in Figure 6.2. Each scenario was generated using the persistence method from Section 6.1.1 and adding appropriate random errors $e_i^l(1), e_i^l(2), \dots$ from the training of the model, i.e.,

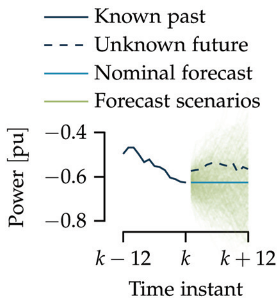

Figure 6.2: Collection of 500 independent load forecast scenarios based on the persistence forecast with a sampling time of 30 min.

$$\hat{w}_i^l(k+1|k) = w_i(k) + e_i^l(1), \tag{6.9a}$$

$$\begin{aligned}\hat{w}_i^l(k+2|k) &= \hat{w}_i^l(k+1|k) + e_i^l(2) \\ &= w(k) + e_i^l(1) + e_i^l(2),\end{aligned} \tag{6.9b}$$

$$\begin{aligned}\hat{w}_i^l(k+3|k) &= \hat{w}_i^l(k+2|k) + e_i^l(3) \\ &= w(k) + e_i^l(1) + e_i^l(2) + e_i^l(3),\end{aligned} \tag{6.9c}$$

$$\vdots$$

Remark 6.1.1. In this thesis, the use of collections of forecast scenarios is motivated by non-Gaussian probability distributions of available renewable power. To determine the available power of a wind turbine, for example, first a collection of wind *speed* forecast scenarios is derived, assuming a Gaussian forecast error distribution. The resulting scenarios are then transformed into available wind *power* using the nonlinear model of a wind turbine. Because of this nonlinear transformation from wind speed to power, the resulting probability distribution for power is typically non-Gaussian.

A detailed discussion on the Gaussian nature of wind speed forecast residuals and the non-Gaussian nature of the associated wind power forecast can be found in [130].

6.2 ARIMA forecasting

ARIMA models are widely adoped for time-series forecasting. Before discussing non-seasonal and seasonal ARIMA models, the backshift operator is introduced.

6.2.1 Backshift operator

To refer to past values of a time-series $w_i(0), w_i(1), \dots, w_i(K)$, the backshift operator B with $\mathrm{B}\, w_i(k) = w_i(k-1)$ is used. Note that $\mathrm{B}^j = \mathrm{B}\,\mathrm{B}^{(j-1)}$ for $j \in \mathbb{N}_{[2,k]}$. Consequently, we have that $\mathrm{B}^j\, w(k) = w(k-j)$.

6.2.2 ARIMA

Autoregressive integrated moving average (ARIMA) models can be described by [33, 106]

$$f_{\mathrm{AR}}(\mathrm{B}) f_{\mathrm{I}}(\mathrm{B}) w_i(k) = a_{\mathrm{T}} + f_{\mathrm{MA}}(\mathrm{B}) e_i(k). \tag{6.10}$$

Here, $e_i(k) = w_i(k) - \hat{w}_i(k|k-1)$ is the one-step ahead training error, i.e., the error between training data point $w_i(k)$ and the associated one-step forecast $\hat{w}_i(k|k-1)$ performed at time instant $k-1$. The autoregressive part of the model is captured by the polynomial

$$f_{\mathrm{AR}}(\mathrm{B}) = 1 - a_{\mathrm{AR},1}\, \mathrm{B}^1 - \dots - a_{\mathrm{AR},N_{\mathrm{AR}}}\, \mathrm{B}^{N_{\mathrm{AR}}} \tag{6.11a}$$

with parameters $a_{\mathrm{AR},1}, \dots, a_{\mathrm{AR},N_{\mathrm{AR}}} \in \mathbb{R}$ for $N_{\mathrm{AR}} \in \mathbb{N}_0$ and $a_{\mathrm{AR},N_{\mathrm{AR}}} \neq 0$. Furthermore,

$$f_{\mathrm{I}}(\mathrm{B}) = (1 - \mathrm{B})^{N_{\mathrm{I}}} \tag{6.11b}$$

with $N_{\mathrm{I}} \in \mathbb{N}_0$ represents a backward difference and $a_{\mathrm{T}} \in \mathbb{R}$ a trend. The moving average part of the model is captured by

$$f_{\mathrm{MA}}(\mathrm{B}) = 1 + a_{\mathrm{MA},1}\, \mathrm{B}^1 + \dots + a_{\mathrm{MA},N_{\mathrm{MA}}}\, \mathrm{B}^{N_{\mathrm{AR}}} \tag{6.11c}$$

with parameters $a_{\mathrm{MA},1}, \dots, a_{\mathrm{MA},N_{\mathrm{MA}}} \in \mathbb{R}$ for $N_{\mathrm{MA}} \in \mathbb{N}_0$ and $a_{\mathrm{MA},N_{\mathrm{MA}}} \neq 0$. Models of the form (6.10) are referred to as ARIMA$(N_{\mathrm{AR}}, N_{\mathrm{I}}, N_{\mathrm{MA}})$.

By default, ARIMA models do not consider periodic behavior of signals, i.e., seasonality. For time-series that include periodicity, e.g., daily pattern of PV infeed or load, seasonal ARIMA models can lead to an improved forecast accuracy.

6.2.3 Seasonal ARIMA

Seasonal ARIMA models can be described by the equation [33, 106]

$$f_{\mathrm{AR}}(\mathrm{B}) f_{\mathrm{SAR}}(\mathrm{B}) f_{\mathrm{I}}(\mathrm{B}) f_{\mathrm{SI}}(\mathrm{B}) w_i(k) = a_{\mathrm{T}} + f_{\mathrm{MA}}(\mathrm{B}) f_{\mathrm{SMA}}(\mathrm{B}) e_i(k). \tag{6.12}$$

Here, $f_{\mathrm{AR}}(\mathrm{B})$, $f_{\mathrm{I}}(\mathrm{B})$ and $f_{\mathrm{MA}}(\mathrm{B})$ are the polynomials and a_{T} is the trend from the non-seasonal ARIMA models in Section 6.2.2. The seasonal autoregressive part with seasonal period N_{p} is captured by

$$f_{\mathrm{SAR}}(\mathrm{B}) = 1 - a_{\mathrm{SAR},1}\, \mathrm{B}^{N_{\mathrm{p}}1} - \ldots - a_{\mathrm{SAR},N_{\mathrm{SAR}}}\, \mathrm{B}^{N_{\mathrm{p}}N_{\mathrm{SAR}}} \tag{6.13a}$$

with coefficients $a_{\mathrm{SAR},1}, \ldots, a_{\mathrm{SAR},N_{\mathrm{SAR}}} \in \mathbb{R}$ for $N_{\mathrm{SAR}} \in \mathbb{N}_0$ and $a_{\mathrm{SAR},N_{\mathrm{SAR}}} \neq 0$. The seasonal difference is included via

$$f_{\mathrm{SI}}(\mathrm{B}) = (1 - \mathrm{B}^{N_{\mathrm{p}}})^{N_{\mathrm{SI}}}, \tag{6.13b}$$

with $N_{\mathrm{SI}} \in \mathbb{N}_0$. Finally, the seasonal moving average part with $a_{\mathrm{SMA},1}, \ldots, a_{\mathrm{SMA},N_{\mathrm{SMA}}} \in \mathbb{R}$ for $N_{\mathrm{SMA}} \in \mathbb{N}_0$ and $a_{\mathrm{SMA},N_{\mathrm{SMA}}} \neq 0$ is captured by the polynomial

$$f_{\mathrm{SMA}}(\mathrm{B}) = 1 + a_{\mathrm{SMA},1}\, \mathrm{B}^{N_{\mathrm{p}}1} + \ldots + a_{\mathrm{SMA},N_{\mathrm{SMA}}}\, \mathrm{B}^{N_{\mathrm{p}}N_{\mathrm{SMA}}}. \tag{6.13c}$$

In what follows, seasonal ARIMA models of the form (6.12) are referred to as $\mathrm{ARIMA}(N_{\mathrm{AR}}, N_{\mathrm{I}}, N_{\mathrm{MA}})(N_{\mathrm{SAR}}, N_{\mathrm{SI}}, N_{\mathrm{SMA}})_{N_{\mathrm{p}}}$.

6.2.4 Model selection

Note that the models were trained in MATLAB 2015a using the Econometrics toolbox.

For the identification of suitable ARIMA forecast models, a hyperparameter search space is formed by combining different values of N_{AR}, N_{I}, N_{MA}, N_{SAR}, N_{SI}, N_{SMA} and N_{p} in a similar fashion as in [88]. For every model structure in this search space[4], the (seasonal) ARIMA model parameters are derived using maximum likelihood estimation [33, 59, 87] under the assumption that the forecast residuals follow a normal distribution. For the evaluation of the estimated forecast model, the Ljung-Box test [33] is used to check for uncorrelatedness of training residuals. Those models that pass the Ljung-Box test are then compared using the PRMSE.

[4] Consider a hyperparameter search space with $N_{\mathrm{AR}} \in \{0,1\}$, $N_{\mathrm{I}} \in \{1\}$ and $N_{\mathrm{MA}} \in \{3,5\}$. Then the model structures

- $\mathrm{ARIMA}(0,1,3)$,
- $\mathrm{ARIMA}(1,1,3)$,
- $\mathrm{ARIMA}(0,1,5)$, and
- $\mathrm{ARIMA}(1,1,5)$

would be considered.

Remark 6.2.1. The control schemes presented in Chapters 7, 8, 10 and 11 do not rely on linear forecasting models or Gaussian forecast probability distributions. Consequently, alternative nonlinear forecast algorithms, such as, neural networks (see, e.g., [258]) or nearest neighbor regression (see, e.g., [88]) could be easily employed in these control approaches.

6.3 *Load*

For the training of forecast model candidates, one year of instantaneous power values from an islanded MG in the MW range were used. The time-series had a sampling interval of 30 min which resulted in 17 520 training data points. To identify suitable models, similar to [88], a hyperparameter search as described in Section 6.2.4 was performed. Motivated by high autocorrelation for the lags $48, 96, \dots$ (see Figure 6.3), a seasonality of $N_\mathrm{p} = 48$, i.e., 1 d, was selected. Moreover, due to a higher autocorrelation for the lag 336, $N_\mathrm{SAR} = 7$ and $N_\mathrm{SMA} = 7$ were chosen. The remaining model parameter candidates were considered to be $N_\mathrm{AR} \in \{0, \dots, 10\}$, $N_\mathrm{I} \in \{0, \dots, 5\}$, $N_\mathrm{MA} \in \{0, \dots, 10\}$, and $N_\mathrm{SI} = 1$. Combining all model parameter candidates resulted in a hyperparameter search space that included 726 model structures. The training algorithm could not identify suitable parameters for 32 of the model structure candidates. Still, 694 models were successfully trained and tested on an unknown data set of 21 d with a prediction interval of 30 min and a prediction horizon of 12 steps. To assess the forecast performance, the PRMSE_{12} of all models was compared. Here, the $\mathrm{ARIMA}(10, 0, 8)(7, 1, 7)_{48}$ model exhibited the lowest mean PRMSE_{12} (0.037 pu) while passing the Ljung-Box test [33] for uncorrelatedness of residuals (p-value 0.9996).

Using the augmented Dickey–Fuller test [59] with a 5 % significance level, we could not accept the hypothesis that the load forecast training data time-series is stationary.

In Figure 6.4, the seasonal ARIMA model is compared with seasonal persistence models with a seasonality of 1 d and 7 d as well as a non-seasonal persistence model. In the box

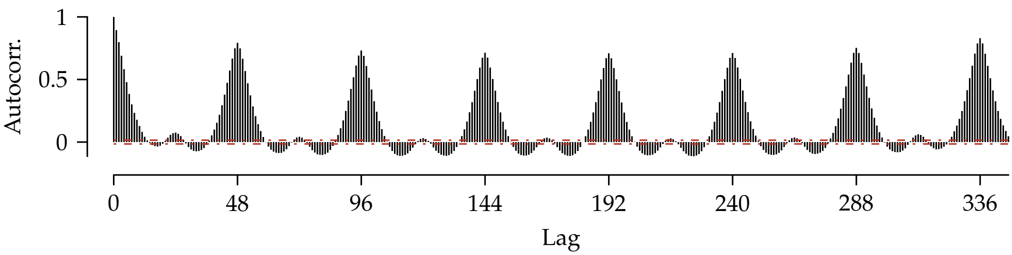

Figure 6.3: Autocorrelation of the load forecast training data.

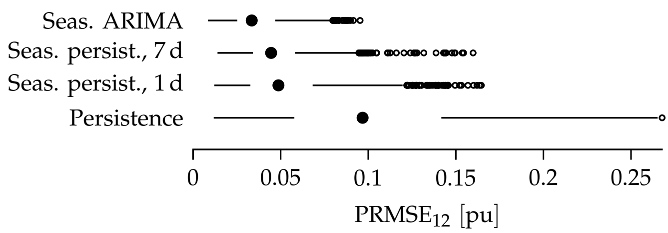

Figure 6.4: PRMSE_{12} of load forecast over 1 008 predictions, i.e., 21 d of test data. The seasonal ARIMA model has the form $\mathrm{ARIMA}(10, 0, 8)(7, 1, 7)_{48}$.

plots[5], the 3rd quartile of PRMSE_{12}, indicated by the right end of the white box, is significantly lower for the seasonal persistence model with a seasonality of 7 d than for the one with a seasonality of 1 d. The 3rd quartile of the persistence model has the highest value of all forecast techniques shown. The seasonal ARIMA model shows the smallest values in all quantiles indicating a decent forecast performance.

[5] An introduction on box plots can be found in Section 3.1.

Technique	Mean [pu]	Std. dev. [pu]
$\mathrm{ARIMA}(10, 0, 8)(7, 1, 7)_{48}$	0.037	0.016
Seasonal persistence, 7 d	0.049	0.022
Seasonal persistence, 1 d	0.055	0.031
Persistence	0.103	0.053

Table 6.1: Mean and standard deviation of PRMSE_{12} for different load forecast models.

Similar conclusions can be drawn from Table 6.1. Here, the $\mathrm{ARIMA}(10, 0, 8)(7, 1, 7)_{48}$ model also outperforms the persistence methods in terms of mean and standard deviation.

In Figure 6.5, one of the forecasts used in the evaluation of the forecast accuracy is shown. Here, the collection of forecast approximately follows a normal distribution. This statement is supported by the Kolmogorov-Smirnov test [153] for a Gaussian distribution which passed the 5 % significance level for all prediction steps and all predictions performed with the test data set.

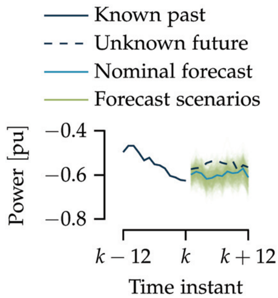

Figure 6.5: Example of load forecast with $\mathrm{ARIMA}(10, 0, 8)(7, 1, 7)_{48}$ model.

6.4 *Wind turbine*

The forecast of available power of wind turbine i is obtained in two steps. First, a time-series forecast of wind speed $\hat{v}_{\mathrm{r},i}$ is performed. Then, the wind speed values are transformed into available wind power $\hat{w}_{r,i}$ using the nonlinear relation

$$\hat{w}_{r,i}(\hat{v}_{r,i}) = \begin{cases} \left(\frac{\hat{v}_{r,i}}{12\,\mathrm{m/s}}\right)^3 p_{r,i}^{\max}, & \text{if } 2.5\,\mathrm{m/s} < \hat{v}_{r,i} \leq 12\,\mathrm{m/s}, \\ p_{r,i}^{\max}, & \text{if } 12\,\mathrm{m/s} \leq \hat{v}_{r,i} \leq 25\,\mathrm{m/s}, \\ p_{r,i}^{\min}, & \text{otherwise.} \end{cases} \quad (6.14)$$

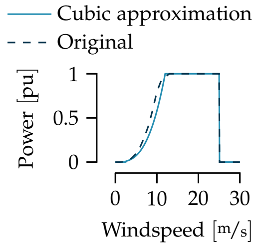

Figure 6.6: Wind speed to wind power curve of Enercon E53 [60] and corresponding cubic approximation for $p_{r,i}^{\min} = 0\,\mathrm{pu}$, $p_{r,i}^{\max} = 1\,\mathrm{pu}$.

As shown in Figure 6.6, the function (6.14) approximates the wind speed to power relation of a real-world wind turbine.

Remark 6.4.1. The focus of this work is to obtain and compare different MPC schemes. Therefore, a generic wind speed to power function (6.14) was chosen. In real-world setups, this function would probably be replaced by the wind speed to power curves of the employed units to obtain more accurate estimates. The same holds for the irradiance to power curve used in Section 6.5.

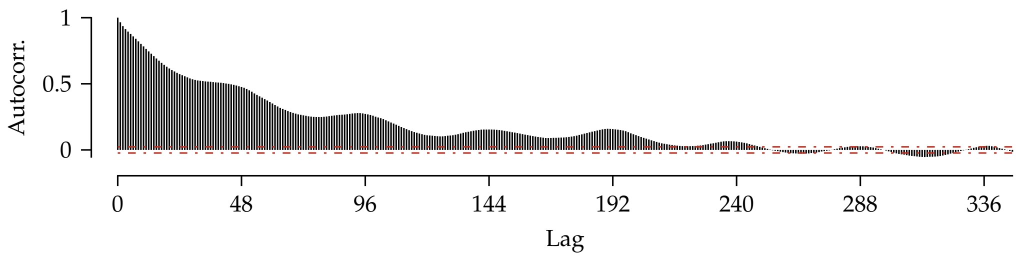

Figure 6.7: Autocorrelation of the wind speed forecast training data.

For the forecast of wind speed, $\hat{v}_{r,i}$, different models were trained using 154 d of wind data from [12] at an interval of 30 min. Thus, 7 392 data points were used. Suitable models were identified via a hyperparameter search as described in Section 6.2.4. No significant seasonality of the wind speed measurements could be observed (see Figure 6.7). Therefore, non-seasonal ARIMA models were considered for the wind speed forecast. The hyperparameter search space created to train and test ARIMA model candidates was derived by combining the model parameters $N_{AR} \in \{0, \dots, 20\}$, $N_I \in \{0, \dots, 5\}$ and $N_{MA} \in \{0, \dots, 20\}$. This resulted in a search space that included 2 646 model structures. The training algorithm could not identify suitable parameters for 141 of the model structure candidates. Still, 2 505 models were successfully trained and tested on a data set of 21 d with a

Using the augmented Dickey–Fuller test [59] with a 5 % significance level, we could not accept the hypothesis that the wind speed forecast training data time-series is stationary.

prediction interval of 30 min and a prediction horizon of 12 steps. To assess the forecast performance, PRMSE_{12} of all models was compared.[6] Here, the ARIMA$(16, 0, 6)$ model exhibited the lowest mean PRMSE_{12} (0.072 pu) while passing the Ljung-Box test [33] for uncorrelatedness of residuals (p-value 0.974).

[6] Note that the PRMSE was calculated for the available wind power $\hat{w}_{r,i}$.

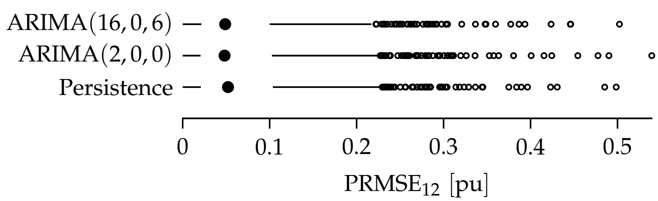

Figure 6.8: PRMSE_{12} of wind power forecast over 1 008 predictions, i.e., 21 d of test data.

In Figure 6.8, the ARIMA$(16, 0, 6)$ model is compared to a persistence forecast and the ARIMA$(0, 0, 2)$ model identified in [176]. It can be noted that the 1st quartile and the median of all approaches are very close to each other. Yet, the 3rd quartile and the right whisker of the ARIMA$(16, 0, 6)$ model are closer to zero than those of the others, indicating that more accurate forecasts can be obtained with it.

Technique	Mean [pu]	Std. dev. [pu]
ARIMA$(16, 0, 6)$	0.072	0.072
ARIMA$(2, 0, 0)$	0.074	0.076
Persistence	0.075	0.075

Table 6.2: Mean and standard deviation of PRMSE_{12} for different wind power forecast models.

Similar conclusions can be drawn from Table 6.2. Here, the ARIMA$(16, 0, 6)$ model also outperforms the other methods in terms of mean value and standard deviation. In general, the difference in forecast quality is not as significant as it is for the load forecast in Section 6.3 and the forecast of available PV power in Section 6.5. This indicates that less complex models are also acceptable for the wind power forecast. Still, as the best model is identified, it is also used in the remainder of this thesis.

In Figure 6.9, one of the forecasts used in the evaluation of the forecast accuracy is shown. For many prediction steps, the forecast scenarios do not follow a normal distribution. This could also be noted applying the Kolmogorov-Smirnov test [153] for a Gaussian distribution which did not pass the 5 %

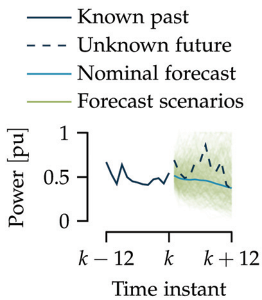

Figure 6.9: Example of wind power forecast with ARIMA$(16, 0, 6)$ model.

significance level for some predictions performed on the test data set. This motivates the use of control approaches that allow for non-Gaussian forecast probability distributions.

6.5 *Photovoltaic power plant*

The forecast of available power $\hat{w}_{\mathrm{r},i}$ of PV power plant i is obtained in two steps. First, a time-series forecast of irradiance $\hat{I}_{\mathrm{r},i}$ is performed. Then, the available power is obtained from irradiance via

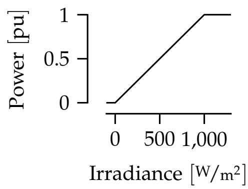

Figure 6.10: Available PV power plant infeed as function of irradiance for $p_{\mathrm{r},i}^{\min} = 0\,\mathrm{pu}$, $p_{\mathrm{r},i}^{\max} = 1\,\mathrm{pu}$.

$$\hat{w}_{\mathrm{r},i}(\hat{I}_{\mathrm{r},i}) = \begin{cases} p_{\mathrm{r},i}^{\min}, & \text{if } \hat{I}_{\mathrm{r},i} < 0\,\mathrm{W/m^2} \\ \hat{I}_{\mathrm{r},i}\,\frac{p_{\mathrm{r},i}^{\max}}{1\,000\,\mathrm{W/m^2}}, & \text{if } 0\,\mathrm{W/m^2} \le \hat{I}_{\mathrm{r},i} \le 1\,000\,\mathrm{W/m^2}, \\ p_{\mathrm{r},i}^{\max}, & \text{if } \hat{I}_{\mathrm{r},i} > 1\,000\,\mathrm{W/m^2}. \end{cases} \tag{6.15}$$

Irradiance values above $1\,000\,\mathrm{W/m^2}$ or below $0\,\mathrm{W/m^2}$ are very unlikely to occur on the earth's surface. The limitation via (6.15) is still required as the Gaussian error distribution used to generate the collection of forecast scenarios (see Section 6.1.4) can lead to irradiance values above or below these limits. To ensure that the available power of every power plant remains within the limits of the unit, (6.15), which is illustrated in Figure 6.10, is employed.

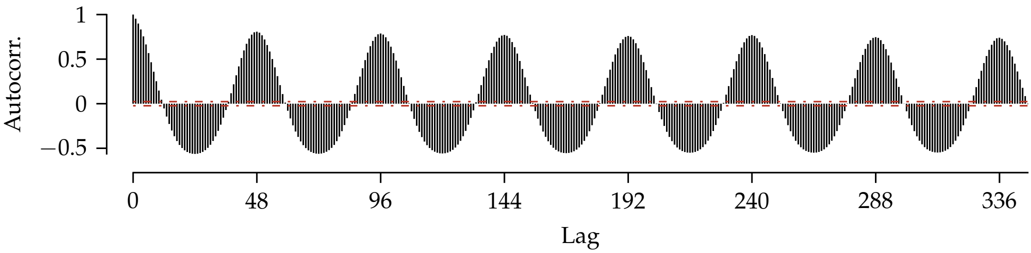

Figure 6.11: Autocorrelation of the irradiance forecast training data.

For the forecast of irradiance $\hat{I}_{\mathrm{r},i}$, different models were trained using 154 d of irradiance data from [12] with an interval of 30 min. Thus, 7 392 data points were used. Suitable models were identified via a hyperparameter search as described in Section 6.2.4. Motivated by high autocorrelation for the lags $48, 96, \ldots$ (see Figure 6.11), a seasonality of $N_{\mathrm{p}} = 48$, i.e., 1 d, was selected. Moreover, the model parameters $N_{\mathrm{AR}} \in \{0, \ldots, 10\}$, $N_{\mathrm{I}} \in \{0, \ldots, 5\}$, $N_{\mathrm{MA}} \in \{0, \ldots, 10\}$,

$N_{\mathrm{SAR}} \in \{1,7\}$, $N_{\mathrm{SMA}} \in \{1,7\}$ and $N_{\mathrm{SI}} = 1$ were considered which resulted in 2 904 seasonal ARIMA model structure candidates. The training algorithm could not identify suitable parameters for 245 of the model structure candidates. Still, 2 659 models were successfully trained and tested on a data set of 21 d with a prediction interval of 30 min and a prediction horizon of 12 steps. To assess the forecast performance, the resulting PRMSE_{12} of all models was compared.[7] Here, the $\mathrm{ARIMA}(6,1,2)(1,1,1)_{48}$ model exhibited the lowest mean PRMSE_{12} (0.065 pu) while passing the Ljung-Box test [33] for uncorrelatedness of residuals (p-value 0.957).

Using the augmented Dickey–Fuller test [59] with a 5 % significance level, we could not accept the hypothesis that the irradiance forecast training data time-series is stationary.

[7] Note that the PRMSE was calculated for the available PV power $\hat{w}_{\mathrm{r},i}$.

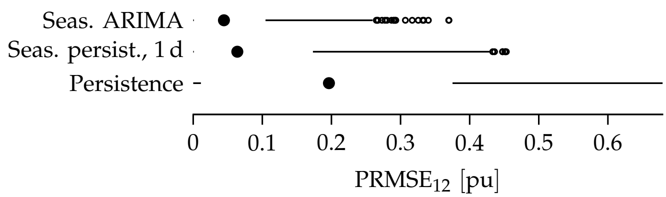

Figure 6.12: PRMSE_{12} of PV power forecast over 1 008 predictions, i.e., 21 d of test data. The seasonal ARIMA model has the form $\mathrm{ARIMA}(6,1,2)(1,1,1)_{48}$.

In Figure 6.12, box plots for the $\mathrm{ARIMA}(6,1,2)(1,1,1)_{48}$, the persistence and the seasonal persistence forecasts are shown. It can be noted that the median and the third quartile of the seasonal ARIMA model are smaller than those of the other methods. Thus, the additional effort of using a seasonal ARIMA model pays off.

Technique	Mean [pu]	Std. dev. [pu]
$\mathrm{ARIMA}(6,1,2)(1,1,1)_{48}$	0.065	0.072
Seasonal persistence, 1 d	0.103	0.113
Persistence	0.217	0.192

Table 6.3: Mean and standard deviation of PRMSE_{12} for different PV infeed forecast models.

Similar conclusions can be drawn when comparing mean and standard deviation of PRMSE_{12} in Table 6.3. Here, the $\mathrm{ARIMA}(6,1,2)(1,1,1)_{48}$ model significantly outperforms the persistence methods in terms of both indicators.

In Figure 6.13, one of the forecasts used in the evaluation of the forecast accuracy is shown. For some prediction steps, the forecast scenarios do not follow a normal distribution. This could also be noted applying the Kolmogorov-Smirnov test [153] for a Gaussian distribution which did not pass the 5 % significance level for some predictions performed on the test

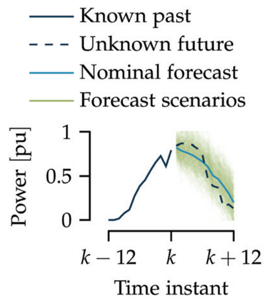

Figure 6.13: Example of PV power forecast with $\mathrm{ARIMA}(10,0,4)$ model.

data set. This motivates the use of control approaches that allow for non-Gaussian forecast probability distributions.

6.6 Summary

In this chapter time-series forecast models for load, wind turbines and PV power plants were derived. Based on a systematic hyperparameter search, suitable ARIMA models were identified. Using these models and simple representations of a PV power plant and a wind turbine, nominal forecasts as well as collections of independent forecast scenarios were derived.

The Kolmogorov-Smirnov test for a Gaussian forecast distribution did not always pass the 5 % significance level for the predictions of available renewable power. Therefore, control approaches that require normally distributed uncertainties appear unsuitable. However, the models derived in this chapter can be used for other MPC formulations that do not rely on such distributions: In Chapter 7 the nominal forecast is employed to formulate a certainty equivalence MPC. Based on the collections of independent forecast scenarios from this chapter, the bounds of robust forecast intervals are employed to formulate a minimax MPC approach in Chapter 8. Moreover, the collections of independent forecast scenarios are used to generate scenario trees in Chapter 9 which serve as a basis for the scenario-based MPC formulations in Chapters 10 and 11.

7 Certainty equivalence MPC

In Chapter 5, a prescient MPC approach for the operation of islanded MG was posed for the hypothetical case where the uncertain input is perfectly known. Unfortunately, in deterministic real-world setups, this is never the case and forecasts of the uncertain input (see Chapter 6) need to be employed. In this chapter such an MPC approach is deduced, assuming that the uncertain input equals the nominal forecast.

The main contribution of this chapters is the derivation of a deterministic certainty equivalence MPC scheme. The formulation is based on the model from Chapter 4 and therefore intended for islanded MGs with high share of RES. Using the cost function from Chapter 5, it is posed as an MIQP which can be solved by available software. Motivated by [172, 180], we assume that the uncertain input follows the nominal forecast. The large number of publications on the operation of MG with certainty equivalence MPC (see Section 1.3.1) indicates that this is a widely adopted assumption. Therefore, the scheme derived in this chapter can be seen as the state-of-the-art for MG operation control.

An overview of certainty equivalence approaches in MG operation control can be found in Section 1.3.1.

This chapter is based on [89] and structured as follows. First, the relation of model variables is discussed in Section 7.1. Then, a certainty equivalence MPC problem is posed in Section 7.2 and used in a simulation example in Section 7.3.

7.1 Model variables

The certainty equivalence approach relies on the assumption that the future is certain [23, 24, 89, 186]. More precisely, it assumes that the nominal forecast is certain. This forecast can be obtained using, e.g., the ARIMA models from Chapter 6.

In Figure 7.1 the forecast of the uncertain input performed at time instant k for the time between j and $j+1$ is represented by the dark blue line next to $\hat{w}(k+j+1|k)$. As discussed in Section 5.1, the uncertain input during this time interval, $\hat{w}(k+j+1|k)$, is associated with the state that it directly affects, $x(k+j+1|k)$. The control input during this period is $v(k+j|k)$ and the auxiliary vector during this period is $z(k+j+1|k)$. As discussed in Chapter 5, the vector of auxiliary variables $z(k+j+1|k)$ changes with the control input $v(k+j|k)$ and the prediction of the uncertain input $\hat{w}(k+j+1|k)$.[1] Similarly, the state $x(k+j+1|k)$ is a function of the previous state $x(k+j|k)$ and $z(k+j+1)$, i.e., $x(k+j+1|k) = f_x(x(k+j|k), z(k+j+1|k))$.[2] With these relations, the following MPC problem can be derived.

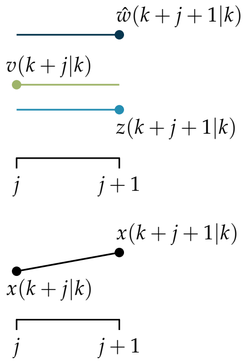

Figure 7.1: Temporal relation of variables in certainty equivalence MPC.

[1] Note that $z(k+j+1|k)$ is linked with $v(k+j|k)$ and $\hat{w}(k+j+1|k)$ through (5.1c) and (5.1d).

[2] Note that f_x can be derived from constraint (5.1a).

7.2 *MPC problem formulation*

The MPC problem combines the overall cost (5.2) with the constraints that represent the islanded MG (5.1). As stated in Section 7.1, the nominal forecasts of load and available renewable infeed, collected in $\hat{w}(k+j+1|k)$, are assumed to be certain over the entire prediction horizon. With this assumption, the following certainty equivalence MPC approach with decision variables $\boldsymbol{v}$, $\boldsymbol{x}$ and $\boldsymbol{z}$ can be formulated.

Recall from Section 5.3 that $\gamma \in (0,1]$ is a discount factor that is used emphasize decisions in the near future. Further recall that the decision variables are $\boldsymbol{v} = [v(k+j|k)]_{j=0}^{J-1}$, $\boldsymbol{x} = [x(k+j|k)]_{j=1}^{J}$ and $\boldsymbol{z} = [z(k+j|k)]_{j=1}^{J}$.

Problem 3 (Certainty equivalence MPC of islanded MGs)**.** Solve the optimization problem

$$\min_{\boldsymbol{v},\boldsymbol{x},\boldsymbol{z}} \sum_{j=0}^{J-1} \ell\big(v(k+j-1|k), v(k+j|k), z(k+j+1|k), x(k+j+1|k)\big)\gamma^{j+1}$$

subject to

$$\begin{aligned} x(k+j+1|k) &= Ax(k+j|k) + \tilde{B}z(k+j+1|k), \\ h_1 &\leq H_1\, x(k+j+1|k), \\ h_2 &\leq H_2 \left[v(k+j|k)^\top \quad z(k+j+1|k)^\top \quad \hat{w}(k+j+1|k)^\top\right]^\top, \\ g &= G \left[v(k+j|k)^\top \quad z(k+j+1|k)^\top \quad \hat{w}(k+j+1|k)^\top\right]^\top, \end{aligned}$$

$\forall j = 0, \dots, J-1$,
with given initial conditions $x(k|k) = x_k$ and $v(k-1|k) = v_{k-1}$.

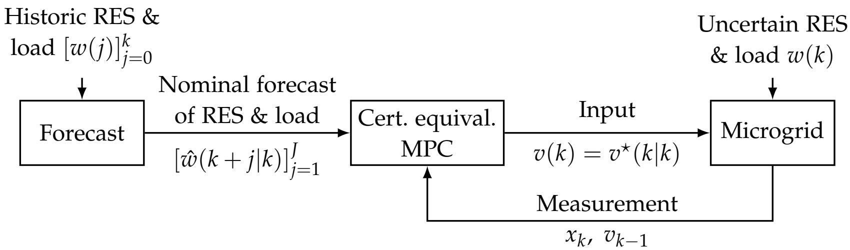

Figure 7.2: Certainty equivalence MPC scheme for operation of islanded MGs at time instant k.

Note that Problem 3 is almost identical to Problem 2. The only difference between the problems is that the future uncertain inputs $w(k+j+1)$ are replaced by the corresponding nominal forecasts $\hat{w}(k+j+1|k)$.

Remark 7.2.1. One major drawback of the certainty equivalent approach is that the assumption of a perfect forecast, in particular for islanded MG with high share of RES, does not hold. In the closed loop, this leads to violations of constraints and to undesired states of charge. This is discussed in more detail in Sections 12.2.2 and 12.3.2. Here, the certainty equivalence approach is shown to be unsuitable for the operation of islanded MG with high renewable share as it does not ensure robustness to uncertain renewable generation and load as desired in Section 2.3.6. Furthermore, the approach does not provide robustness to misestimated forecasts as required in Section 2.3.7.

7.2.1 *MPC scheme*

As illustrated in Figure 7.2, from the resulting optimal control input trajectory, the first predicted value $v^{\star}(k|k)$ is applied to the plant. At the next sampling time instant, Problem 3 is solved repeatedly in a receding horizon fashion (see, e.g., [18, 23, 204] and Section 3.2) using updated initial conditions and updated forecasts of renewable infeed and load. An example solution of Problem 3 is discussed next.

7.3 *Example*

In Figure 7.3, the trajectories of uncertain inputs, power, setpoints and stored energy are shown. They were derived by

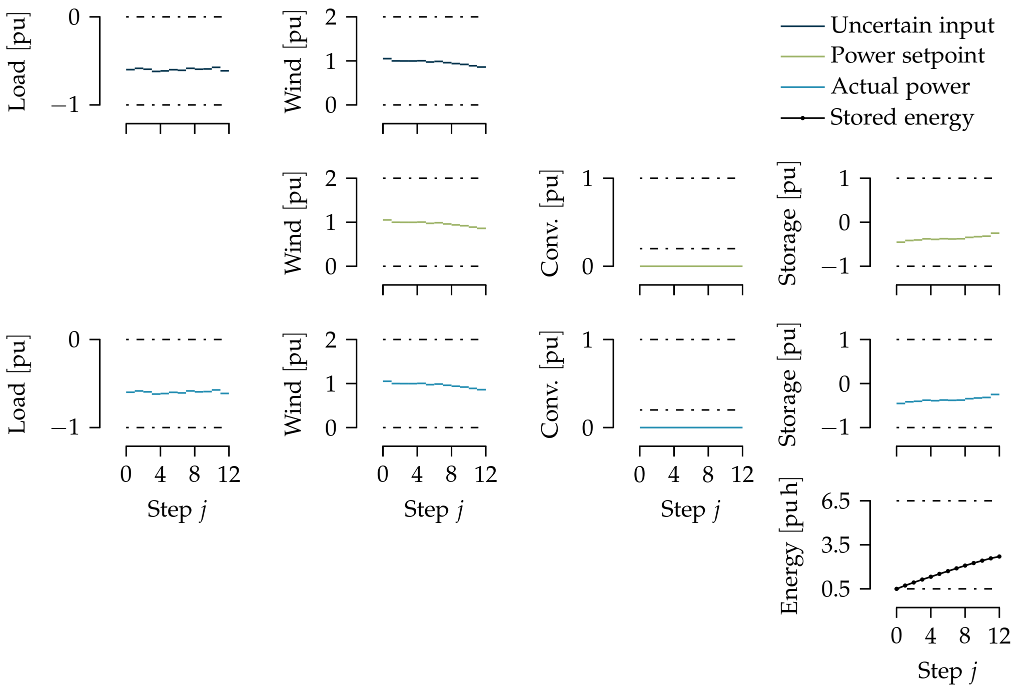

Figure 7.3: Open-loop trajectories of certainty equivalence MPC.

solving Problem 3 for initial conditions $x_k = 0.5\,\text{pu h}$ and $\delta_t(k-1|k) = 0$. The forecasts were obtained using the models identified in Chapter 6 considering a rated wind power of 2 pu. As MG model, the example from Figure 4.1 was used.[3]

In Figure 7.3, the forecasts of load and available renewable infeed are shown shown in the first row of the plot. It can be observed that the load varies a little. The available power of the wind turbine shows a slight trend towards lower power values. The load demand is smaller than the predicted available wind power. Therefore, the load can be fully served by the wind turbine and the conventional generator remains disabled over the entire prediction horizon. The renewable power setpoints is always greater than or equal to the predicted available power. This results in a predicted power for the wind turbine that identical to the available wind power.

The difference in load and renewable power is used to charge the battery. In the Figure 7.3, this can be noted by negative power values of the storage unit and an increase in stored energy from 0.5 pu h to 2.7 pu h.

[3] The unit parameters and the weights of the cost function can be found in Tables 12.1 and 12.2.

7.4 Summary

In this chapter a certainty equivalence MPC approach for islanded MGs was derived. The approach assumes that the uncertain input follows the nominal forecast of load and available renewable infeed. This assumption unfortunately does not hold for islanded MG with high share of renewable infeed. In such grids, load and available renewable power can significantly differ from their nominal forecasts. As in islanded operation all fluctuations need to be covered locally, this can lead to violations of power and energy limits in the closed loop, as illustrated in Chapter 12. To address this, a robust minimax MPC approach that assumes a bounded uncertain input with a forecast in the form of time-varying prediction intervals is derived in the next chapter.

8 Minimax MPC

In the last chapter, a certainty equivalence approach that assumes that the uncertain available renewable infeed and load follow their nominal forecasts was presented. Unfortunately, this approach can lead to constraint violations in the closed loop, as the uncertain input can significantly differ from the nominal forecast in MGs with high share of RES. To overcome this drawback, more complex forecasts, e.g., time-varying prediction intervals, need to be considered.

The main contributions of this chapter are as follows. Motivated by [104, 128], a robust minimax MPC formulation for the operation of islanded MG is derived. This formulation minimizes the worst-case cost assuming a forecast of the uncertain input in the form of time-varying lower and upper bounds [19, 20, 31, 139]. The formulation is based on the model from Chapter 4 and therefore allows to control islanded MGs with high share of RES. Using the cost function from Chapter 5, the MPC problem is formulated as a mixed-integer quadratically-constrained program (MIQCP) that can be solved by available numerical solvers. Unlike other robust formulations [13, 104], the presented MPC problem includes a possible limitation of renewable infeed, storage dynamics and power sharing of grid-forming units. Opposed to the certainty equivalence approach in Chapter 7, it guarantees robustness with respect to the uncertain inputs.

An overview of robust approaches in MG operation control can be found in Section 1.3.2.

The majority of this chapter is based on [89] and structured as follows. First, the derivation of robust forecast intervals from forecast scenarios is discussed in Section 8.1. Moreover, a general minimax MPC problem for the operation of

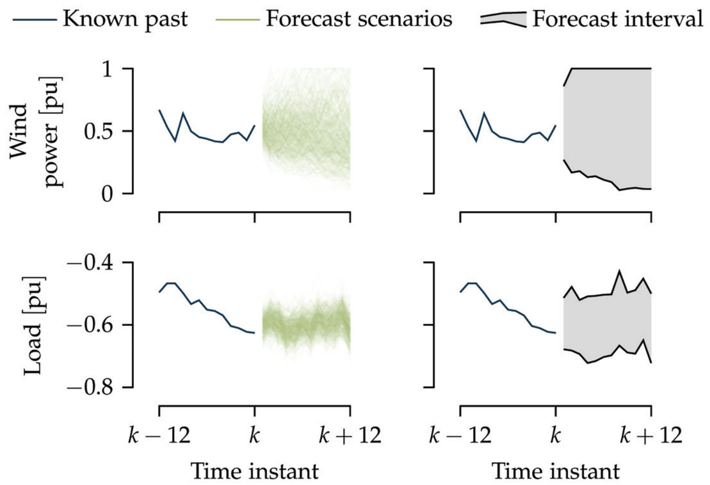

Figure 8.1: Example of robust forecast intervals of available wind power and load. The intervals on the right were derived via the stage-wise maximum and minimum of the collections of independent forecast scenarios on the left.

islanded MGs is posed. As this problem is hard to solve, a tractable alternative is deduced in the subsequent sections. In Section 8.2 the relation of model variables in the alternative minimax MPC approach is discussed. Then, in Section 8.3 the cost function is reformulated. Finally, in Section 8.4 a tractable minimax MPC problem for the operation of islanded MG is posed and used in a simulation example in Section 8.5.

8.1 Introduction

In this section, the derivation of forecasts in the form of lower and upper bounds is illustrated. Moreover, a minimax MPC problem that employs these bounds is posed.

8.1.1 Forecast of uncertain input

The bounds of the robust forecast intervals are derived as follows. Consider N_Ω forecast scenarios (see Section 6.1.4) for each renewable unit and each load.[1] Then, for each renewable unit $i \in \mathbb{N}_{[1,N_\mathrm{r}]}$ the maximum available renewable infeed of all N_Ω forecast scenarios $\hat{w}^l_{\mathrm{r},i}(k+j|k)$, $l \in \mathbb{I} = \mathbb{N}_{[1,N_\Omega]}$, at prediction time instant $k+j$ and time instant k is

$$\overline{w}_{\mathrm{r},i}(k+j|k) = \max_{l\in\mathbb{I}} \hat{w}^l_{\mathrm{r},i}(k+j|k) \tag{8.1a}$$

[1] Naturally, this approach would also work if we would assume different numbers of forecast scenarios for each load and each renewable unit.

and the minumum at the same prediction time instant is

$$\underline{w}_{\mathrm{r},i}(k+j|k) = \min_{l \in \mathbb{I}} \hat{w}^l_{\mathrm{r},i}(k+j|k). \tag{8.1b}$$

Similarly, for each load $i \in \mathbb{N}_{[1,N_\mathrm{d}]}$, the maximum of all scenarios is

$$\overline{w}_{\mathrm{d},i}(k+j|k) = \max_{l \in \mathbb{I}} \hat{w}^l_{\mathrm{d},i}(k+j|k) \tag{8.1c}$$

and the minumum at the same prediction time instant is

$$\underline{w}_{\mathrm{d},i}(k+j|k) = \min_{l \in \mathbb{I}} \hat{w}^l_{\mathrm{d},i}(k+j|k). \tag{8.1d}$$

Combining (8.1a) and (8.1c), the vector of upper bounds can be derived as

$$\begin{aligned}\overline{w}(k+j|k) = \big[&\overline{w}_{\mathrm{r},1}(k+j|k),\ \dots,\ \overline{w}_{\mathrm{r},N_\mathrm{r}}(k+j|k),\\ &\overline{w}_{\mathrm{d},1}(k+j|k),\ \dots,\ \overline{w}_{\mathrm{d},N_\mathrm{d}}(k+j|k)\big]^\top.\end{aligned} \tag{8.2a}$$

Similarly, the vector of lower bounds can be derived as

$$\begin{aligned}\underline{w}(k+j|k) = \big[&\underline{w}_{\mathrm{r},1}(k+j|k),\ \dots,\ \underline{w}_{\mathrm{r},N_\mathrm{r}}(k+j|k),\\ &\underline{w}_{\mathrm{d},1}(k+j|k),\ \dots,\ \underline{w}_{\mathrm{d},N_\mathrm{d}}(k+j|k)\big]^\top\end{aligned} \tag{8.2b}$$

by combining (8.1b) and (8.1d). With (8.2), we can formulate a robust interval for the uncertain input, $[\underline{w}(k+j|k), \overline{w}(k+j|k)]$. In minimax MPC, it is assumed that the uncertain input $\hat{w}(k+j|k)$ can take any value in this interval, i.e.,

$$\hat{w}(k+j|k) \in [\underline{w}(k+j|k), \overline{w}(k+j|k)]. \tag{8.3}$$

Remark 8.1.1. As an alternative to (8.3), one could also consider a confidence region that captures the dependency of some uncertain variables. This way, correlation between the available renewable infeed of wind turbines or PV power plants that are geographically close to each other could be employed to reduce the complexity of the associated minimax MPC approaches and potentially decrease the conservativeness of resulting control actions. However, for simplicity and generality this alternative was *not* considered in this thesis.

8.1.2 Minmax MPC problem formulation

We can easily formulate a minimax MPC problem that considers a bounded uncertain input within the intervals from (8.3).

Therefore, we define $\hat{\boldsymbol{w}} = [\hat{w}(k+j|k)]_{j=0}^{J-1}$, $\underline{\boldsymbol{w}} = [\underline{w}(k+j|k)]_{j=0}^{J-1}$, and $\overline{\boldsymbol{w}} = [\overline{w}(k+j|k)]_{j=0}^{J-1}$. Using these vectors, the minimax MPC problem can be stated as follows.

Recall from Section 5.3 that $\gamma \in (0,1]$ is a discount factor that is used emphasize decisions in the near future. Further recall that the decision variables are $\boldsymbol{v} = [v(k+j|k)]_{j=0}^{J-1}$, $\boldsymbol{x} = [x(k+j|k)]_{j=1}^{J}$ and $\boldsymbol{z} = [z(k+j|k)]_{j=1}^{J}$.

Problem 4 (Minimax MPC of islanded MGs)**.** Solve the optimization problem

$$\min_{\boldsymbol{v},\boldsymbol{x},\boldsymbol{z}} \max_{\hat{\boldsymbol{w}} \in [\underline{\boldsymbol{w}},\overline{\boldsymbol{w}}]} \sum_{j=0}^{J-1} \ell\big(v(k+j-1|k), v(k+j|k), \\ z(k+j+1|k), x(k+j+1|k)\big)\gamma^{j+1}$$

subject to

$$\begin{aligned} x(k+j+1|k) &= Ax(k+j|k) + \tilde{B}z(k+j+1|k), \\ h_1 &\leq H_1\, x(k+j+1|k), \\ h_2 &\leq H_2 \left[v(k+j|k)^\top \quad z(k+j+1|k)^\top \quad \hat{w}(k+j+1|k)^\top\right]^\top, \\ g &= G \left[v(k+j|k)^\top \quad z(k+j+1|k)^\top \quad \hat{w}(k+j+1|k)^\top\right]^\top, \end{aligned}$$

$\forall \hat{w}(k+j|k) \in [\underline{w}(k+j|k), \overline{w}(k+j|k)]$ and $\forall j = 0, \ldots, J-1$, with given initial conditions $x(k|k) = x_k$ and $v(k-1) = v_{k-1}$.

Problem 4 is hard to solve because of two reasons: (i) The constraints in Problem 4 need to hold for any uncertain input $\hat{w}(k+j|k)$ in the interval $[\underline{w}(k+j|k), \overline{w}(k+j|k)]$. (ii) The worst-case cost over all possible disturbance realizations is minimized in Problem 4. In order to identify this worst-case cost, all combinations of minimum and maximum stage costs over the prediction horizon need to be enumerated. Consequently, the number of worst-case cost candidates grows exponentially in the prediction horizon, which can make it hard to solve Problem 4 for longer horizons.

In the next sections, we will see how to formulate an alternative minimax MPC problem that is easier to solve than Problem 4. Therefore, in Section 8.2 the constraints of Problem 4 will be equivalently posed using only combinations extreme values from the interval $[\underline{w}(k+j|k), \overline{w}(k+j|k)]$. Then, in Section 8.3 an alternative cost function that avoids an excessive enumeration of all candidates will be posed. Finally, in Section 8.4 the alternative MPC problem will be posed.

8.2 Model variables

In what follows, the model variables and constraints of the alternative MPC problem are introduced. First, constraints related to the power and energy of the units are provided. Then, power flow over the lines in the context of minimax MPC is discussed.

8.2.1 Power of units

We consider a minimax approach that approximately follows the model with additive disturbance in [138]. Thus, we assume a bounded uncertain input of the form (8.3) and a single control input trajectory $v(k|k), \dots, v(k+J|k)$. In the formulation, we do not consider feedback in the predicted control inputs, i.e., for every step $j \in \mathbb{N}_{[0,J-1]}$ only one control input is assumed [72, 283]. Formulations that disregard feedback in the prediction are often referred to as open-loop schemes [138, 204].[2] In contrast, formulations that consider feedback in the problem formulation are often referred to as closed-loop schemes. Unfortunately, closed-loop formulations that consider state feedback can lead to nonlinear optimization problems or problems that grow exponentially in the length of the prediction horizon [90, 139, 236].[3] Therefore, only an open-loop minimax scheme, which can be formulated as an MIQCP, is considered in this thesis.

[2] Even though these formulations are referred to as open-loop schemes, they are used in a closed-loop control setting (see Figure 8.6). The term "open-loop" only refers to the fact that no feedback is considered in the MPC formulation.

[3] There exist so-called "approximate closed-loop" schemes [90, 139] that consider disturbance feedback in the problem formulation and can be solved more easily than "real" closed-loop schemes. However, for simplicity they were not considered in this thesis.

As only a single input trajectory $v(k|k), \dots, v(k+J|k)$ is considered, the control variables $\delta_\mathrm{t}(k+j|k)$ and $u(k+j|k)$ for $j = 0, \dots, J-1$ are not directly affected by the uncertain input. In contrast, the variables in $z(k+j+1|k)$, i.e., $p(k+j+1|k)$, $\delta_\mathrm{r}(k+j+1|k)$ and $\mu(k+j+1|k)$, are influenced by $\hat{w}(k+j+1|k)$.

Load $w_\mathrm{d}(k+j+1|k)$ and renewable infeed $p_\mathrm{r}(k+j+1|k)$ are both monotonically increasing in $\hat{w}(k+j+1|k)$ because of (4.2) and (4.12). Furthermore, $\mu(k+j+1|k)$ is a function of the uncertain input. This can be seen using (4.28b), i.e.,

In the context of this chapter, (4.12) has the form

$$p_\mathrm{r}(k+j+1|k) = \min(u_\mathrm{r}(k+j|k), \hat{w}_\mathrm{r}(k+j+1|k)).$$

$$0 = 1_{N_\mathrm{t}}^\top p_\mathrm{t}(k+j+1|k) + 1_{N_\mathrm{s}}^\top p_\mathrm{s}(k+j+1|k) + 1_{N_\mathrm{r}}^\top p_\mathrm{r}(k+j+1|k) + 1_{N_\mathrm{d}}^\top w_\mathrm{d}(k+j+1|k). \quad (8.4\mathrm{a})$$

With (4.37), this can be rewritten as

$$0 = \mu(k+j+1|k)\big(1_{N_t}^\top K_t^{-1}\delta_t(k+j|k) + 1_{N_s}^\top K_s^{-1} 1_{N_s}\big) + 1_{N_t}^\top u_t(k+j+1|k) + 1_{N_s}^\top u_s(k+j+1|k) + 1_{N_r}^\top p_r(k+j+1|k) + 1_{N_d}^\top w_d(k+j+1|k). \quad (8.4b)$$

In the context of this chapter, (4.37) becomes

$$K_s(p_s(k+j+1|k) - u_s(k+j|k)) = \mu(k+j+1|k)1_{N_s},$$

and

$$K_t(p_t(k+j+1|k) - u_t(k+j|k)) = \mu(k+j+1|k)\delta_t(k+j|k).$$

Recall that K_t and K_s are diagonal matrices with positive diagonal entries. Therefore, $\mu(k+j+1|k)$ must be monotonically decreasing in $\hat{w}(k+j+1|k)$ to ensure that (8.4b) holds. Because of (4.37), the power vectors of conventional and storage units, $p_t(k+j+1|k)$ and $p_s(k+j+1|k)$, are both monotonically increasing in $\mu(k+j+1|k)$. Consequently, $p_t(k+j+1|k)$ and $p_s(k+j+1|k)$ are monotonically decreasing in $\hat{w}(k+j+1|k)$.

In conclusion, all elements of $z(k+j+1|k)$ are either monotonically increasing or decreasing in $\hat{w}(k+j+1|k)$. Therefore, the extreme values of the auxiliary vector can be deduced by considering the minimum and maximum disturbance. Replacing $z(k+j+1|k)$ by $\overline{z}(k+j+1|k) \in \mathbb{R}^{N_z}$ and $\underline{z}(k+j+1|k) \in \mathbb{R}^{N_z}$ the extreme values can be indirectly obtained via the constraints

$$h_2 \leq H_2 \left[v(k+j|k)^\top \quad \overline{z}(k+j+1|k)^\top \quad \overline{w}(k+j+1|k)^\top\right]^\top, \quad (8.5a)$$

$$g = G \left[v(k+j|k)^\top \quad \overline{z}(k+j+1|k)^\top \quad \overline{w}(k+j+1|k)^\top\right]^\top, \quad (8.5b)$$

and

$$h_2 \leq H_2 \left[v(k+j|k)^\top \quad \underline{z}(k+j+1|k)^\top \quad \underline{w}(k+j+1|k)^\top\right]^\top, \quad (8.5c)$$

$$g = G \left[v(k+j|k)^\top \quad \underline{z}(k+j+1|k)^\top \quad \underline{w}(k+j+1|k)^\top\right]^\top, \quad (8.5d)$$

which are both based on (5.1c) and (5.1d). Note that the vector $\underline{z}(k+j+1|k)$ contains the extreme values associated with $\underline{w}(k+j+1|k)$. Thus, some entries of $\underline{z}(k+j+1|k)$ are at their minimum and others are at their maximum. For example, $\underline{z}(k+j+1|k)$ comprises the minimum value of $p_r(k+j+1|k)$ and the maximum value of $p_s(k+j+1|k)$. The same holds for $\overline{z}(k+j+1|k)$.

If $\overline{z}(k+j+1|k)$ and $\underline{z}(k+j+1|k)$ satisfy unit power and power sharing constraints of the form (5.1c) and (5.1d), then the intermediate power values between these extremes also satisfy these constraints because of their monotonicity in $\hat{w}(k+j+1|k)$. Thus, if (8.5) holds, then the power-related constraints, except for the line power, are satisfied for all $\hat{w}(k+j+1|k)$ in $[\overline{w}(k+j+1|k), \underline{w}(k+j+1|k)]$.

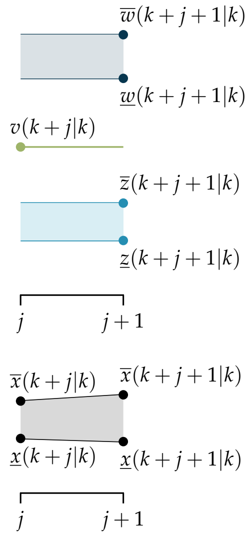

Figure 8.2: Temporal relation variables in minimax MPC.

In Figure 8.2, the relation of the different variables is illustrated. Here, the forecast of the uncertain input performed at time instant k for the prediction interval between j and $j+1$ is represented by the bounds $\underline{w}(k+j+1|k)$, $\overline{w}(k+j+1|k)$ and the area in between. As pointed out in Section 5.1, the control input during this prediction interval is $v(k+j|k)$.

Example 8.2.1 (Relation of uncertain input, control input and power)**.** Consider the MG topology from Figure 4.1. For the time period from $j = 0$ to $j = 1$, the uncertain input, is known to be between $\underline{w}(k+1|k) = [\underline{w}_{\mathrm{r}}(k+1|k)\ \underline{w}_{\mathrm{d}}(k+1|k)]^\top$ and $\overline{w}(k+1|k) = [\overline{w}_{\mathrm{r}}(k+1|k)\ \overline{w}_{\mathrm{d}}(k+1|k)]^\top$. For the same time period, an optimal control decision $v(k|k)$ needs to be made without knowing which $w(k+1|k)$ from the interval $[\underline{w}(k+1|k), \overline{w}(k+1|k)]$ occurs. Thus, the control input $v(k|k) = [u_{\mathrm{t}}(k|k)\ u_{\mathrm{s}}(k|k)\ u_{\mathrm{r}}(k|k)\ \delta_{\mathrm{t}}(k|k)]^\top$ must be feasible for all possible uncertain inputs from this interval. The bounded uncertain input affects the power of the units. Therefore, the unit power is also given in the form of an interval with a lower and an upper bound.

In what follows, three combinations of uncertain input, control input and unit power will be discussed. In these examples, only stage 0 to 1 will be considered.

1. Let us start with the uncertain inputs and power setpoints in Figure 8.3. Here, the bounds of available renewable power, $\underline{w}_{\mathrm{r}}(k+1|k)$ and $\overline{w}_{\mathrm{r}}(k+1|k)$, are both *above* the power setpoint $u_{\mathrm{r}}(k|k)$. Consequently, following (4.12), the power bounds of the wind turbine become

$$\overline{p}_{\mathrm{r}}(k+1|k) = \min(u_{\mathrm{r}}(k|k), \overline{w}_{\mathrm{r}}(k+1|k)) = u_{\mathrm{r}}(k|k), \quad (8.6a)$$
$$\underline{p}_{\mathrm{r}}(k+1|k) = \min(u_{\mathrm{r}}(k|k), \underline{w}_{\mathrm{r}}(k+1|k)) = u_{\mathrm{r}}(k|k). \quad (8.6b)$$

Power and power setpoint of the conventional unit are forced to zero by $\delta_{\mathrm{t}}(k|k) = 0$ via (4.7), i.e., $u_{\mathrm{t}}(k|k) = 0$ and

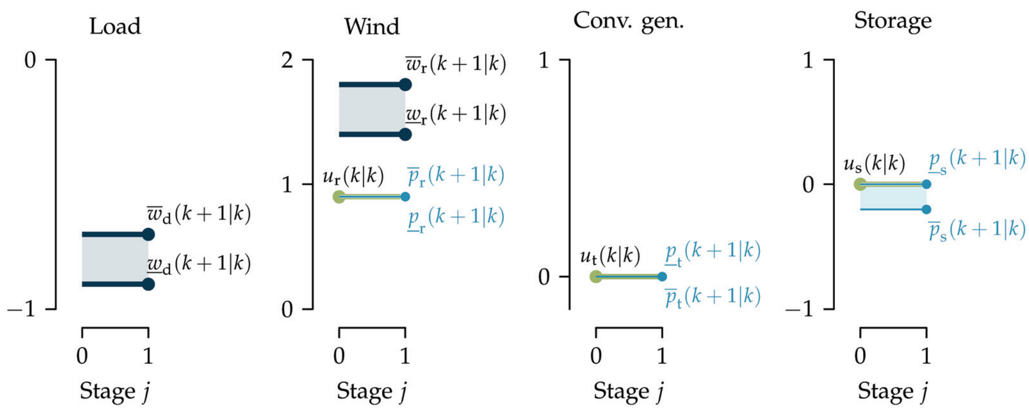

Figure 8.3: Unit power in minimax MPC with high available renewable infeed and disabled conventional generator.

$\underline{p}_{\mathrm{t}}(k+1|k) = \overline{p}_{\mathrm{t}}(k+1|k) = 0$. Therefore, the storage unit must cover all fluctuations of the load and the renewable unit. This is reflected by the power balance equation (4.28b) which with $\underline{p}_{\mathrm{t}}(k+1|k) = \overline{p}_{\mathrm{t}}(k+1|k) = 0$ becomes

$$\begin{aligned}\overline{p}_{\mathrm{s}}(k+1|k) &= -\overline{p}_{\mathrm{r}}(k+1|k) - \overline{w}_{\mathrm{d}}(k+1|k),\\ &= -u_{\mathrm{r}}(k|k) - \overline{w}_{\mathrm{d}}(k+1|k), \qquad (8.6c)\\ \underline{p}_{\mathrm{s}}(k+1|k) &= -\underline{p}_{\mathrm{r}}(k+1|k) - \underline{w}_{\mathrm{d}}(k+1|k),\\ &= -u_{\mathrm{r}}(k|k) - \underline{w}_{\mathrm{d}}(k+1|k). \qquad (8.6d)\end{aligned}$$

In Figure 8.3, this is illustrated by a storage power which changes depending on the uncertain input. If the load power is at the lower bound $\underline{w}_{\mathrm{d}}(k+1|k)$, then the storage power $\underline{p}_{\mathrm{s}}(k+1|k)$ is zero. If the load power is at the upper bound $\overline{w}_{\mathrm{d}}(k+1|k)$, then the storage unit is slightly charged with $\overline{p}_{\mathrm{s}}(k+1|k) < 0$. For intermediate values of load power, the storage power is between these bounds.

2. Let us now consider the uncertain inputs and power setpoints in Figure 8.4. Here, the bounds of the available renewable infeed $\underline{w}_{\mathrm{r}}(k+1|k)$ and $\overline{w}_{\mathrm{r}}(k+1|k)$ are both *below* the maximum allowed renewable infeed $u_{\mathrm{r}}(k|k)$. Consequently, in this case renewable infeed is not curtailed.[4] Following (4.12), the power of the renewable units therefore is within the bounds

$$\overline{p}_{\mathrm{r}}(k+1|k) = \min(u_{\mathrm{r}}(k|k), \overline{w}_{\mathrm{r}}(k+1|k)) = \overline{w}_{\mathrm{r}}(k+1|k), \qquad (8.7a)$$

[4] An operation with uncurtailed RES can also be found in grids with a low share of RES where a limitation renewable infeed is not required.

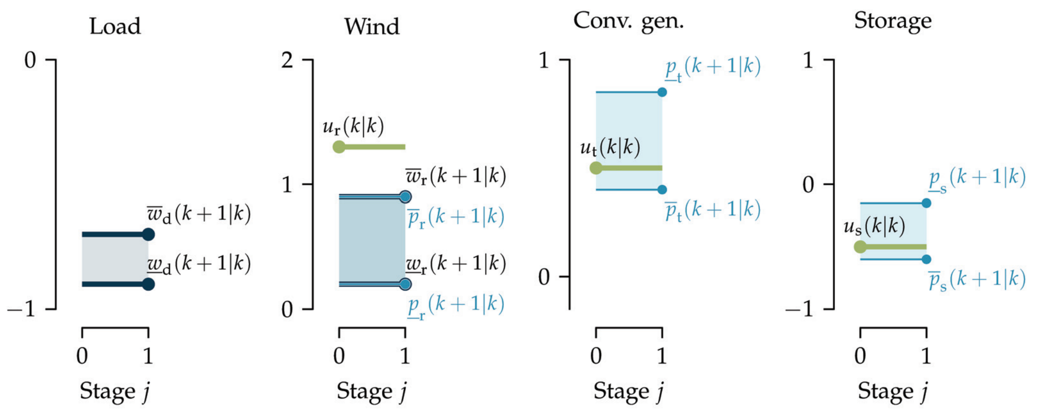

Figure 8.4: Unit power in minimax MPC with low available renewable infeed and enabled conventional generator.

$$\underline{p}_{\mathrm{r}}(k+1|k) = \min(u_{\mathrm{r}}(k|k), \underline{w}_{\mathrm{r}}(k+1|k)) = \underline{w}_{\mathrm{r}}(k+1|k). \tag{8.7b}$$

The power of conventional and storage unit are determined through power sharing (4.35), which for $\chi_{\mathrm{s}} = \chi_{\mathrm{t}} = 1$ reads

$$u_{\mathrm{s}}(k|k) - \overline{p}_{\mathrm{s}}(k+1|k) = u_{\mathrm{t}}(k|k) - \overline{p}_{\mathrm{t}}(k+1|k), \tag{8.7c}$$
$$u_{\mathrm{s}}(k|k) - \underline{p}_{\mathrm{s}}(k+1|k) = u_{\mathrm{t}}(k|k) - \underline{p}_{\mathrm{t}}(k+1|k). \tag{8.7d}$$

Together with the power balance equations (4.28b), i.e.,

$$0 = \overline{p}_{\mathrm{t}}(k+1|k) + \overline{p}_{\mathrm{s}}(k+1|k) + \overline{p}_{\mathrm{r}}(k+1|k) + \overline{w}_{\mathrm{d}}(k+1|k), \tag{8.7e}$$

$$0 = \underline{p}_{\mathrm{t}}(k+1|k) + \underline{p}_{\mathrm{s}}(k+1|k) + \underline{p}_{\mathrm{r}}(k+1|k) + \underline{w}_{\mathrm{d}}(k+1|k), \tag{8.7f}$$

this can be transformed into[5]

$$\overline{p}_{\mathrm{t}}(k+1|k) = \frac{u_{\mathrm{t}}(k|k) - u_{\mathrm{s}}(k|k) - \overline{p}_{\mathrm{r}}(k+1|k) - \overline{w}_{\mathrm{d}}(k+1|k)}{2}, \tag{8.7g}$$

$$\underline{p}_{\mathrm{t}}(k+1|k) = \frac{u_{\mathrm{t}}(k|k) - u_{\mathrm{s}}(k|k) - \underline{p}_{\mathrm{r}}(k+1|k) - \underline{w}_{\mathrm{d}}(k+1|k)}{2}. \tag{8.7h}$$

The storage unit's bounds can be similarly deduced as

$$\overline{p}_{\mathrm{s}}(k+1|k) = \frac{u_{\mathrm{s}}(k|k) - u_{\mathrm{t}}(k|k) - \overline{p}_{\mathrm{r}}(k+1|k) - \overline{w}_{\mathrm{d}}(k+1|k)}{2}, \tag{8.7i}$$

[5] See, e.g., Example 4.8.2 for a detailed derivation of equations (8.7g)–(8.7j).

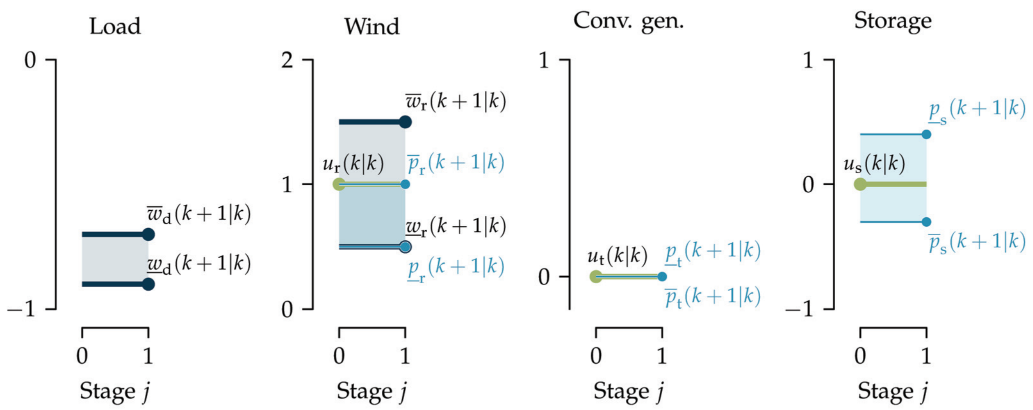

Figure 8.5: Unit power in minimax MPC with medium available renewable infeed and disabled conventional generator.

$$\underline{p}_{\mathrm{s}}(k+1|k) = \frac{u_{\mathrm{s}}(k|k) - u_{\mathrm{t}}(k|k) - \underline{p}_{\mathrm{r}}(k+1|k) - \underline{w}_{\mathrm{d}}(k+1|k)}{2}. \tag{8.7j}$$

In Figure 8.4, it can be seen that the power bounds of the storage and the conventional unit change with the uncertain input. For $\underline{p}_{\mathrm{r}}(k+1|k) = \underline{w}_{\mathrm{r}}(k+1|k)$ and $\underline{w}_{\mathrm{d}}(k+1|k)$ where the absolute value of the load is high and infeed from the wind turbine is low, the storage unit is charged less aggressively with $\underline{p}_{\mathrm{s}}(k+1|k)$ and the conventional unit provides more power $\underline{p}_{\mathrm{t}}(k+1|k)$. For $\overline{p}_{\mathrm{r}}(k+1|k) = \overline{w}_{\mathrm{r}}(k+1|k)$ and $\overline{w}_{\mathrm{d}}(k+1|k)$, where the absolute value of the load is small and infeed from the wind turbine is high, the storage unit is charged more aggressively with $\overline{p}_{\mathrm{s}}(k+1|k)$ and the conventional unit provides less power $\overline{p}_{\mathrm{t}}(k+1|k)$. For intermediate load and renewable power values, the power of the storage and conventional unit lies between the bounds given by (8.7g)–(8.7j).

Note that for $\chi_{\mathrm{s}} = \chi_{\mathrm{t}} = 1$, the distance between power and setpoints is equal for the storage and the conventional unit. Using this relation, one can modify the power of the units by increasing or decreasing the individual setpoints.

3. In this last example, the wind turbine's setpoint $u_{\mathrm{r}}(k|k)$ is between the bounds $\underline{w}_{\mathrm{r}}(k+1|k)$ and $\overline{w}_{\mathrm{r}}(k+1|k)$ (see Figure 8.5). Following (4.12), the power of the renewable

units therefore in the interval $[\underline{p}_\mathrm{r}(k+1|k), \overline{p}_\mathrm{r}(k+1|k)]$ with

$$\overline{p}_\mathrm{r}(k+1|k) = \min(u_\mathrm{r}(k|k), \overline{w}_\mathrm{r}(k+1|k)) = u_\mathrm{r}(k|k), \quad (8.8a)$$
$$\underline{p}_\mathrm{r}(k+1|k) = \min(u_\mathrm{r}(k|k), \underline{w}_\mathrm{r}(k+1|k)) = \underline{w}_\mathrm{r}(k+1|k). \quad (8.8b)$$

Power and setpoint of the conventional unit are forced to zero by $\delta_\mathrm{t}(k|k) = 0$ via (4.7), i.e., $u_\mathrm{t}(k|k) = 0$ and $\underline{p}_\mathrm{t}(k+1|k) = \overline{p}_\mathrm{t}(k+1|k) = 0$. The bounds of the storage unit's power are determined by the power balance equation (4.28b) which with $\underline{p}_\mathrm{t}(k+1|k) = \overline{p}_\mathrm{t}(k+1|k) = 0$ reads

$$\begin{aligned}\overline{p}_\mathrm{s}(k+1|k) &= -\overline{p}_\mathrm{r}(k+1|k) - \overline{w}_\mathrm{d}(k+1|k), \\ &= -\overline{w}_\mathrm{r}(k+1|k) - \overline{w}_\mathrm{d}(k+1|k), \quad (8.8c)\\ \underline{p}_\mathrm{s}(k+1|k) &= -\underline{p}_\mathrm{r}(k+1|k) - \underline{w}_\mathrm{d}(k+1|k), \\ &= -u_\mathrm{r}(k|k) - \underline{w}_\mathrm{d}(k+1|k). \quad (8.8d)\end{aligned}$$

In Figure 8.5, it can be seen that the power of the storage unit changes with the uncertain input. If renewable infeed is low, $\underline{p}_\mathrm{r}(k+1|k) = \underline{w}_\mathrm{r}(k+1|k)$, and the absolute value of the load is large, $\underline{w}_\mathrm{d}(k+1|k)$, then the storage unit is discharged with $\underline{p}_\mathrm{s}(k+1|k)$. For $\overline{p}_\mathrm{r}(k+1|k) = u_\mathrm{r}(k|k)$ and $\overline{w}_\mathrm{d}(k+1|k)$, where the absolute value of the load is small and renewable infeed is large, the storage unit is charged with $\overline{p}_\mathrm{s}(k+1|k)$. For intermediate values, of load and renewable infeed, the storage power is between these bounds.

Note that the inequalities

$$\begin{aligned}\overline{p}_\mathrm{r}(k+1|k) &\le u_\mathrm{r}(k|k),\\ \overline{p}_\mathrm{r}(k+1|k) &\le \overline{w}_\mathrm{r}(k+1|k),\\ \underline{p}_\mathrm{r}(k+1|k) &\le u_\mathrm{r}(k|k),\\ \underline{p}_\mathrm{r}(k+1|k) &\le \underline{w}_\mathrm{r}(k+1|k),\end{aligned}$$

do not model to the same behavior as (8.8a) and (8.8b). Using the above inequalities would, among other undesired effects, allow for power values that are below the forecast of the uncertain input without the need to reduce the power setpoint. In the closed loop, this could result in large power setpoints (and therefore in large power values for the plant) even though, lower power values were considered in the MPC. In conclusion, only the min operator can ensure that a limitation of available renewable power is modeled correctly in the minimax MPC formulations.

One last important thing to note in this example is that the power of the storage unit is independent from the power setpoint and only depends on the power of the renewable unit and the load. The reason for this is that we are in islanded operation where a local power equilibrium needs to be maintained at all times. Because the storage is the only enabled[6] grid-forming unit, it has to cover all fluctuations, independent of its power setpoint. The same naturally hods for the first example (see Figure 8.3).

[6] Recall that the grid forming conventional generator is disabled in this last example.

8.2.2 *Energy of units*

The bounds of the predicted state can be derived from the bounds of the storage power. As the state depends linearly on the storage power, the bounds can be derived from (5.1a) as

$$\overline{x}(k+j+1|k) = A\overline{x}(k+j|k) + \tilde{B}\overline{z}(k+j|k), \tag{8.9a}$$
$$\underline{x}(k+j+1|k) = A\underline{x}(k+j|k) + \tilde{B}\underline{z}(k+j|k), \tag{8.9b}$$

with initial values $\overline{x}(k|k) = \underline{x}(k|k) = x_k$. The evolution of the states is illustrated in Figure 8.2. Here, the gray area represents the robust interval with bounds given by (8.9). For both bounds, constraint (5.1b) must hold, i.e.,

$$h_1 \leq H_1\, \overline{x}(k+j+1|k), \tag{8.10a}$$
$$h_1 \leq H_1\, \underline{x}(k+j+1|k). \tag{8.10b}$$

8.2.3 *Power flow*

The maximum line power cannot always be deduced from one of the extreme cases $\overline{w}(k+j+1|k)$ or $\underline{w}(k+j+1|k)$. This is illustrated in the following section.

Based on (4.28a), the power flow constraints can be formulated as

$$p_{\mathrm{e}}^{\min} \leq p_{\mathrm{e}}(k+j+1|k) \leq p_{\mathrm{e}}^{\max}, \tag{8.11a}$$

where the predicted power of the lines is given by (4.27), i.e.,

$$p_{\mathrm{e}}(k+j+1|k) = \underbrace{\begin{bmatrix} \tilde{f}_{\mathrm{t},1} & \tilde{f}_{\mathrm{s},1} & \tilde{f}_{\mathrm{r},1} & \tilde{f}_{\mathrm{d},1} \\ \vdots & \vdots & \vdots & \vdots \\ \tilde{f}_{\mathrm{t},N_{\mathrm{e}}} & \tilde{f}_{\mathrm{s},N_{\mathrm{e}}} & \tilde{f}_{\mathrm{r},N_{\mathrm{e}}} & \tilde{f}_{\mathrm{d},N_{\mathrm{e}}} \end{bmatrix}}_{\tilde{F}U} \begin{bmatrix} p_{\mathrm{t}}(k+j+1|k) \\ p_{\mathrm{s}}(k+j+1|k) \\ p_{\mathrm{r}}(k+j+1|k) \\ w_{\mathrm{d}}(k+j+1|k) \end{bmatrix} \tag{8.11b}$$

with the row vectors $\tilde{f}_{\mathrm{t},i} \in \mathbb{R}^{1\times N_{\mathrm{t}}}$, $\tilde{f}_{\mathrm{s},i} \in \mathbb{R}^{1\times N_{\mathrm{s}}}$, $\tilde{f}_{\mathrm{r},i} \in \mathbb{R}^{1\times N_{\mathrm{r}}}$, and $\tilde{f}_{\mathrm{d},i} \in \mathbb{R}^{1\times N_{\mathrm{d}}}$ for $i \in \mathbb{N}_{[1,N_{\mathrm{e}}]}$. Using these vectors, the predicted power of transmission line i is

$$\begin{aligned} p_{\mathrm{e},i}(k+j+1|k) = \tilde{f}_{\mathrm{t},i}p_{\mathrm{t}}(k+j+1|k) + \tilde{f}_{\mathrm{s},i}p_{\mathrm{s}}(k+j+1|k) + \\ \tilde{f}_{\mathrm{r},i}p_{\mathrm{r}}(k+j+1|k) + \tilde{f}_{\mathrm{d},i}w_{\mathrm{d}}(k+j+1|k). \end{aligned} \tag{8.12a}$$

With (4.37), this can be rewritten as

$$\begin{aligned}
&p_{\mathrm{e},i}(k+j+1|k) = \\
&\quad \tilde{f}_{\mathrm{t},i}\big(K_{\mathrm{t}}^{-1}\mu(k+j+1|k)\delta_{\mathrm{t}}(k+j|k) + u_{\mathrm{t}}(k+j|k)\big) + \\
&\qquad \tilde{f}_{\mathrm{s},i}\big(K_{\mathrm{s}}^{-1}\mu(k+j+1|k)1_{N_{\mathrm{s}}} + u_{\mathrm{s}}(k+j|k)\big) + \\
&\qquad\quad \tilde{f}_{\mathrm{r},i}p_{\mathrm{r}}(k+j+1|k) + \tilde{f}_{\mathrm{d},i}w_{\mathrm{d}}(k+j+1|k)
\end{aligned} \tag{8.12b}$$

$$\begin{aligned}
\iff &p_{\mathrm{e},i}(k+j+1|k) = \\
&\quad \mu(k+j+1|k)\big(\tilde{f}_{\mathrm{t},i}K_{\mathrm{t}}^{-1}\delta_{\mathrm{t}}(k+j|k) + \tilde{f}_{\mathrm{s},i}K_{\mathrm{s}}^{-1}1_{N_{\mathrm{s}}}\big) + \\
&\qquad \tilde{f}_{\mathrm{t},i}u_{\mathrm{t}}(k+j|k) + \tilde{f}_{\mathrm{s},i}u_{\mathrm{s}}(k+j|k) + \\
&\qquad\quad \tilde{f}_{\mathrm{r},i}p_{\mathrm{r}}(k+j+1|k) + \tilde{f}_{\mathrm{d},i}w_{\mathrm{d}}(k+j+1|k).
\end{aligned} \tag{8.12c}$$

The right hand side of (8.12c) represents a linear combination of values that depend on the uncertain input. For (8.11a) to hold for all $\hat{w}(k+j+1|k) \in [\underline{w}(k+j+1|k), \overline{w}(k+j+1|k)]$, it is required to show that the maximum and minimum values of $p_{\mathrm{e},i}(k+j+1|k)$ are within the limit. Due to positive and negative coefficients in $\tilde{F}U$, the extreme values of the line power are not necessarily given for the extreme values $\underline{w}(k+j+1|k)$ or $\overline{w}(k+j+1|k)$.[7] However, we know that the minimum and maximum are given for combinations of minimum and maximum disturbance values.

In what follows, $\mathbb{W}(k+j+1|k)$ denotes the set of all vectors of combinations of minimum and maximum values except for $\hat{w}(k+j+1|k) = \underline{w}(k+j+1|k)$ and $\hat{w}(k+j+1|k) = \overline{w}(k+j+1|k)$ which are already considered in (8.5). Thus, $\mathbb{W}(k+j+1|k)$ includes $N_{\tilde{\mu}} = (2^{(N_{\mathrm{r}}+N_{\mathrm{d}})} - 2)$ vectors in $\mathbb{R}^{(N_{\mathrm{r}}+N_{\mathrm{d}})}$.[8]

Each combination of minimum and maximum values, i.e., each vector $w^{(l)}(k+j+1|k) \in \mathbb{W}(k+j+1|k)$, $l \in \mathbb{N}_{[1,N_{\tilde{\mu}}]}$ can result in a different $\mu^{(l)}(k+j+1|k) \in \mathbb{R}$ because of (8.4b). The values of $\mu^{(l)}(k+j+1|k)$ are collected in $\tilde{\mu}(k+j+1|k) = [\mu^{(l)}(k+j+1|k)]_{l=1}^{N_{\tilde{\mu}}}$. Moreover, for given $v(k+j|k)$, each combination $w^{(l)}(k+j+1|k)$ can result in a different vector of renewable infeed $p_{\mathrm{r}}^{(l)}(k+j+1|k)$. The elements of $p_{\mathrm{r}}^{(l)}(k+j+1|k)$ are either elements of $\overline{z}(k+j+1|k)$ or of $\underline{z}(k+j+1|k)$. Therefore, no additional decision variables need to be introduced to obtain $p_{\mathrm{r}}^{(l)}(k+j+1|k)$. Thus, the constraints for every combination $l \in \mathbb{N}_{[1,N_{\tilde{\mu}}]}$ of disturbances

[7] For given $\delta_{\mathrm{t}}(k+j|k)$, the extreme combinations of disturbances that lead the maximum an minimum line power could be easily identified offline. However, as $\delta_{\mathrm{t}}(k+j|k)$ is an unknown decision variable this is not possible.

[8] Note that the number of scenarios $N_{\tilde{\mu}}$ can be reduced by exploiting the structure of $\tilde{F}U$. This can be done, for example, by searching for rows in $\tilde{F}U$ that exhibit the same combinations of negative, positive and zero entries.

$w^{(l)}(k+j+1|k) = [w_{\mathrm{r}}^{(l)}(k+j+1|k)^\top \; w_{\mathrm{d}}^{(l)}(k+j+1|k)^\top]^\top$, $w^{(l)}(k+j+1|k) \in \mathbb{W}(k+j+1|k)$ are

$$p_{\mathrm{e}}^{\min} \leq \tilde{F}U \begin{bmatrix} K_{\mathrm{t}}^{-1}\mu^{(l)}(k+j+1|k)\delta_{\mathrm{t}}(k+j|k) + u_{\mathrm{t}}(k+j|k) \\ K_{\mathrm{s}}^{-1}\mu^{(l)}(k+j+1|k)1_{N_{\mathrm{s}}} + u_{\mathrm{s}}(k+j|k) \\ p_{\mathrm{r}}^{(l)}(k+j+1|k) \\ w_{\mathrm{d}}^{(l)}(k+j+1|k) \end{bmatrix} \leq p_{\mathrm{e}}^{\max} \tag{8.13a}$$

and

$$\begin{aligned} 0 = \mu^{(l)}(k+j+1|k)\big(1_{N_{\mathrm{t}}}^\top K_{\mathrm{t}}^{-1}\delta_{\mathrm{t}}(k+j|k) + 1_{N_{\mathrm{s}}}^\top K_{\mathrm{s}}^{-1}1_{N_{\mathrm{s}}}\big) + \\ 1_{N_{\mathrm{t}}}^\top u_{\mathrm{t}}(k+j|k) + 1_{N_{\mathrm{s}}}^\top u_{\mathrm{s}}(k+j|k) + \\ 1_{N_{\mathrm{r}}}^\top p_{\mathrm{r}}^{(l)}(k+j+1|k) + 1_{N_{\mathrm{d}}}^\top w_{\mathrm{d}}^{(l)}(k+j+1|k). \end{aligned} \tag{8.13b}$$

In order to formulate a problem that can be solved by an MIQCP solver, we need to remove the multiplication of the decision variables $\mu^{(l)}(k+j+1|k)$ and $\delta_{\mathrm{t}}(k+j|k)$. This is done by introducing the additional decision variable $\zeta^{(l)}(k+j+1|k) \in \mathbb{R}^{N_{\mathrm{t}}}$ which is a column of the matrix $\zeta(k+j+1|k) = [\zeta^{(l)}(k+j+1|k) \quad \cdots \quad \zeta^{(N_{\tilde{\mu}})}(k+j+1|k)]$ and using the constraint

$$\zeta^{(l)}(k+j+1|k) = \mu^{(l)}(k+j+1|k)\delta_{\mathrm{t}}(k+j|k). \tag{8.14}$$

In a similar fashion as (4.39), this can be reformulated as

$$\zeta^{(l)}(k+j+1|k) \leq \mathrm{M}_{\mathrm{t}}\delta_{\mathrm{t}}(k+j|k), \tag{8.15a}$$

$$\zeta^{(l)}(k+j+1|k) \geq \mathrm{m}_{\mathrm{t}}\delta_{\mathrm{t}}(k+j|k), \tag{8.15b}$$

$$\zeta^{(l)}(k+j+1|k) \leq 1_{N_{\mathrm{t}}}\mu^{(l)}(k+j+1|k) - \mathrm{m}_{\mathrm{t}}(1_{N_{\mathrm{t}}} - \delta_{\mathrm{t}}(k+j|k)), \tag{8.15c}$$

$$\zeta^{(l)}(k+j+1|k) \geq 1_{N_{\mathrm{t}}}\mu^{(l)}(k+j+1|k) - \mathrm{M}_{\mathrm{t}}(1_{N_{\mathrm{t}}} - \delta_{\mathrm{t}}(k+j|k)). \tag{8.15d}$$

Using $\zeta^{(l)}(k+j+1|k)$, we can further reformulate (8.13) into the affine constraints

$$p_{\mathrm{e}}^{\min} \leq \tilde{F}U \begin{bmatrix} K_{\mathrm{t}}^{-1}\zeta^{(l)}(k+j+1|k) + u_{\mathrm{t}}(k+j|k) \\ K_{\mathrm{s}}^{-1}\mu^{(l)}(k+j+1|k)1_{N_{\mathrm{s}}} + u_{\mathrm{s}}(k+j|k) \\ p_{\mathrm{r}}^{(l)}(k+j+1|k) \\ w_{\mathrm{d}}^{(l)}(k+j+1|k) \end{bmatrix} \leq p_{\mathrm{e}}^{\max} \tag{8.15e}$$

and

$$0 = 1_{N_t}^{\top} K_t^{-1} \zeta^{(l)}(k+j+1|k) + 1_{N_s}^{\top} K_s^{-1} \mu^{(l)}(k+j+1|k) 1_{N_s} + \\ 1_{N_t}^{\top} u_t(k+j|k) + 1_{N_s}^{\top} u_s(k+j|k) + \\ 1_{N_r}^{\top} p_r^{(l)}(k+j+1|k) + 1_{N_d}^{\top} w_d^{(l)}(k+j+1|k). \quad (8.15f)$$

Example 8.2.2. For the running example in Figure 4.1, and the set $\mathbb{W}(k+j+1|k)$ is

$$\mathbb{W}(k+j+1|k) = \left\{ \begin{bmatrix} \underline{w}_r(k+j+1|k) \\ \overline{w}_d(k+j+1|k) \end{bmatrix}, \begin{bmatrix} \overline{w}_r(k+j+1|k) \\ \underline{w}_d(k+j+1|k) \end{bmatrix} \right\}.$$

8.3 Cost function

The goal of the presented minimax MPC approach is to minimize the worst-case cost over prediction horizon J for $\hat{w}(k+j|k) \in [\underline{w}(k+j|k), \overline{w}(k+j|k)]$. As the stage cost (5.2) is convex with respect to the disturbance, the worst-case stage cost is the maximum of

$$\overline{\ell}(k+j+1|k) = \ell\big(v(k+j-1|k), v(k+j|k), \\ \overline{z}(k+j+1|k), \overline{x}(k+j+1|k)\big) \quad (8.16a)$$

and

$$\underline{\ell}(k+j+1|k) = \ell\big(v(k+j-1|k), v(k+j|k), \\ \underline{z}(k+j+1|k), \underline{x}(k+j+1|k)\big). \quad (8.16b)$$

Using the epigraph reformulation from Lemma 3.3.2, the maximum stage cost can be described as

$$\max(\underline{\ell}(k+j+1|k), \overline{\ell}(k+j+1|k)) = \min_{\substack{\overline{\ell}(k+j+1|k) \leq t(k+j+1|k) \\ \underline{\ell}(k+j+1|k) \leq t(k+j+1|k)}} t(k+j+1|k), \quad (8.17)$$

with the additional free variable $t(k+j+1|k) \in \mathbb{R}$.

In minimax MPC, the worst-case cost over all possible realizations of uncertain inputs shall be minimized. This includes the case where the uncertain input is always at the maximum and the case where it is always at the minimum. Unfortunately it also includes cases where the maximum cost is obtained by considering the maximum uncertain input at some stages and the minimum at others. Thus, to identify the overall worst-case cost, all combinations of (8.16a) and (8.16b) need to be enumerated over the prediction horizon.[9] Consequently, the number of worst-case cost candidates grows exponentially in the prediction horizon. It is therefore desirable to find an alternative cost function and avoid an enumeration of all candidates. One such alternative which provides a bound to the worst-case costs can be found by combining the stage-wise maximum cost. This can be formulated by a cost $\sum_{j=0}^{J-1} t(k+j+1|k)\gamma^{j+1}$ and the constraints

$$t(k+j+1|k) \geq \overline{\ell}(k+j+1|k), \tag{8.18a}$$
$$t(k+j+1|k) \geq \underline{\ell}(k+j+1|k) \tag{8.18b}$$

for all $j \in \mathbb{N}_{[0,J-1]}$. With this cost and constraints from the previous sections, we can now formulate a minimax MPC problem.

[9] Examples of such combinations are

$$\overline{\ell}(k+1|k)\gamma^1 + \underline{\ell}(k+2|k)\gamma^2 + \dots,$$
$$\overline{\ell}(k+1|k)\gamma^1 + \overline{\ell}(k+2|k)\gamma^2 + \dots$$

and

$$\underline{\ell}(k+1|k)\gamma^1 + \underline{\ell}(k+2|k)\gamma^2 + \dots.$$

8.4 MPC problem formulation

The MPC problem combines the overall cost with the constraints that model an islanded MG. In the problem formulation, the forecast intervals $[\underline{w}(k+j+1|k), \overline{w}(k+j+1|k)]$ from Section 8.2 are used. Hence, the minimax MPC problem with decision variables $\boldsymbol{z} = [\overline{z}(k+j|k) \quad \underline{z}(k+j|k)]_{j=1}^{J}$, $\boldsymbol{x} = [\overline{x}(k+j|k) \quad \underline{x}(k+j|k)]_{j=1}^{J}$, $\boldsymbol{v} = [v(k+j|k)]_{j=0}^{J-1}$, $\tilde{\boldsymbol{\mu}} = [\tilde{\mu}(k+j|k)]_{j=1}^{J}$, $\boldsymbol{\zeta} = [\zeta(k+j|k)]_{j=1}^{J}$ and $\boldsymbol{t} = [t(k+j|k)]_{j=1}^{J}$ reads as follows.

Problem 5 (Alternative minimax MPC of islanded MGs). Solve the optimization problem

$$\min_{\boldsymbol{v},\boldsymbol{x},\boldsymbol{z},\tilde{\boldsymbol{\mu}},\boldsymbol{\zeta},\boldsymbol{t}} \sum_{j=0}^{J-1} t(k+j+1|k)\gamma^{j+1}$$

subject to

constraints (8.5), (8.9), (8.10), (8.18)
as well as (8.15) $\quad \forall \hat{w}(k+j|k) \in \mathbb{W}(k+j|k)$,
$\forall j = 0, \dots, J-1$,
with given initial conditions $\underline{x}(k|k) = \overline{x}(k|k) = x_k$
and $v(k-1|k) = v_{k-1}$.

Recall from Section 5.3 that $\gamma \in (0, 1]$ is a discount factor that is used emphasize decisions in the near future.

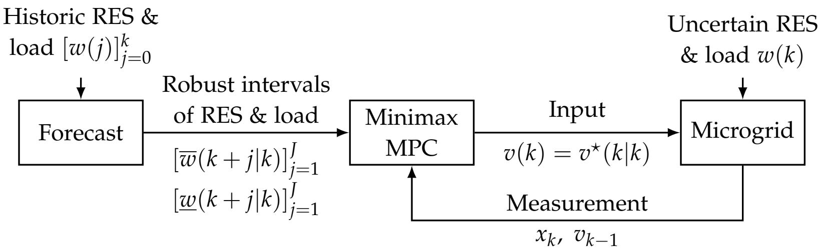

Figure 8.6: Minimax MPC scheme for operation of islanded MG at time instant k.

8.4.1 MPC scheme

For the operation of an islanded MGs, Problem 5 is embedded into the control scheme in Figure 8.6. Before solving the minimax MPC problem, robust forecast intervals of load and available renewable infeed are obtained as described in Section 8.1.1. Together with the measurements of the current state x_k and the control input v_{k-1} that was applied in the most recent time instant, they are used as an input to the minimax MPC. For these inputs, Problem 5 is solved. From the resulting optimal input trajectory the value associated with the first prediction instant $v^{\star}(k|k)$ is applied to the MG. At the next sampling time instant the robust intervals and the measurements are updated and Problem 5 is solved repeatedly in a receding horizon fashion (see, e.g., [18, 23, 204] and Section 3.2).

8.5 Example

In Figure 8.7 on page 116, the forecasts of the uncertain input, power, setpoints and stored energy are shown. They were derived by solving Problem 5 with initial conditions $x_k = 0.5\,\mathrm{pu\,h}$ and $\delta_{\mathrm{t}(k-1|k)} = 0$. In the problem, the running example in Figure 4.1 was considered.[10] As uncertain input, the forecast intervals from Figure 8.1 were scaled for a rated wind turbine power of 2 pu.

[10] The unit parameters and the weights of the cost function can be found in Tables 12.1 and 12.2.

As described in Section 8.2, only one setpoint is considered for each unit and each time instant. Power and energy are given in the form of time-varying intervals.

The results in Figure 8.7 illustrate that the solution of Problem 5 leads to power setpoints where the worst-case, i.e., low available wind power and high load are considered. In direct

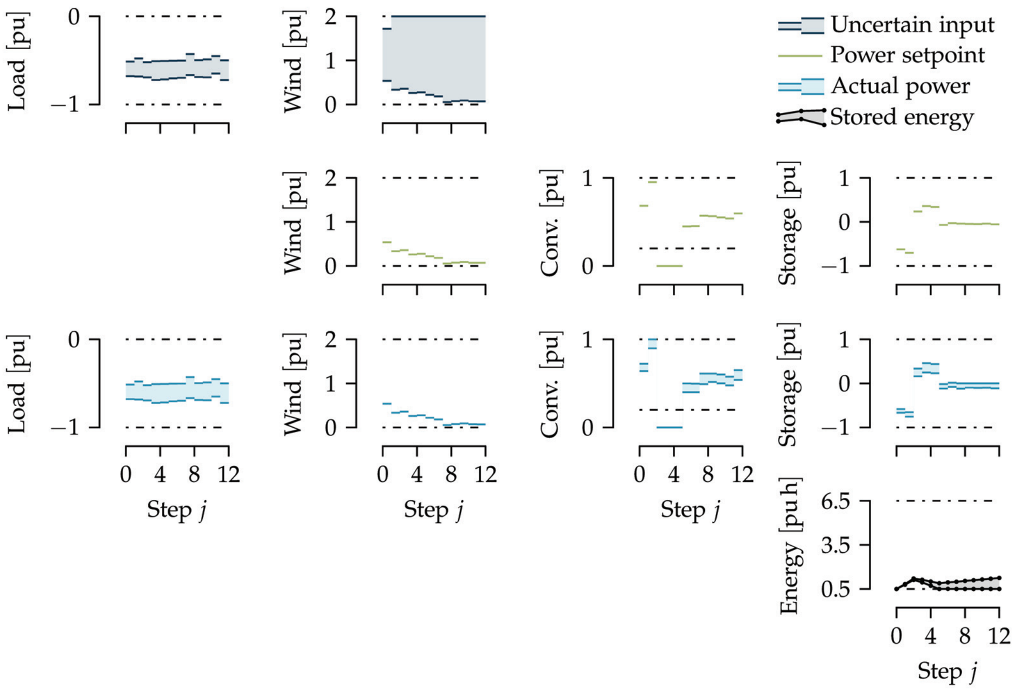

Figure 8.7: Open-loop trajectories of minimax MPC.

comparison with the results of the certainty equivalence approach from Section 7.3, it can be noted in Table 8.1 that the power setpoint for the wind turbine is much smaller for the minimax MPC. Furthermore, the conventional generator is enabled many times in Figure 8.7, whereas in the certainty equivalence approach it was not enabled at all. This also indicates that the increased security associated with robust forecast intervals comes at the price of very conservative power setpoints in the minimax approach.

Table 8.1: Power setpoints of certainty equivalence and minimax MPC.

	Cert. equiv.	Mini-max
$u_t(k)$	0	0.68
$u_s(k)$	−0.81	−0.62
$u_r(k)$	1.38	0.54

8.6 Summary

In this chapter a minimax MPC approach for islanded MGs was derived. The approach is based on the assumption that the prediction of the uncertain input is given in the form of time-varying lower and upper bounds. Compared to the certainty equivalence MPC in Chapter 7, it provides the robustness required in Sections 2.3.6 and 2.3.7. As no probabilistic information is considered, the worst-case cost with respect to the given forecast interval is minimized in the approach.

The use of robust forecast intervals leads to a safe operation in the sense that no constraint violations occur in closed-loop simulations in Chapter 12. However, considering only a robust interval with no probabilistic information can lead to overly conservative control actions and high costs in the closed loop as the worst-case is very unlikely to occur. Additionally, using only a single control input trajectory for all possible values of the uncertain input can further increase the conservativeness of the controller.

To cope with these drawbacks, in Chapters 10 and 11 a risk-neutral stochastic and a risk-averse MPC approach are derived. Both approaches consider multiple forecast scenarios, where each scenario is associated with a certain probability. Furthermore, they model feedback within the MPC, i.e., depending on the forecast of the uncertain input and the resulting state, different control actions are considered in the optimal control problems. Both approaches consider probability distributions in the form of scenario trees which are introduced in the next chapter.

9 Scenario trees

In the previous chapters, a certainty equivalence and a minimax MPC formulation were presented. The certainty equivalence approach, however, was found to lack robustness and the minimax MPC came with overly conservative control actions. Both drawbacks can be addressed at the same time by using scenario-based MPC. Here, a large number of independent forecast scenarios of load and available renewable infeed is desired to resemble the underlying probability distribution sufficiently accurate. Unfortunately, this leads to a large number of decision variables which increases the computational complexity of associated MPC problems. The use of scenario trees, which can be interpreted as a discrete approximation of probability distributions, can lead to a good compromise in the form of manageable computational complexity and sufficiently accurate forecast probability distributions.

This chapter aims to provide some basics on scenario trees. It is based on [91, 93, 96, 169] and structured as follows. First, a formal description of scenario trees is given in Section 9.1. Then, the relation of model variables is discussed in Section 9.2. Finally, one possible method to derive a scenario tree from a collection of independent forecast scenarios is sketched in Section 9.3.

9.1 Formal description of scenario trees

In what follows, first the relation of the different nodes in the tree is outlined. Then, the probabilities of the nodes and probability distributions on scenario trees are discussed.

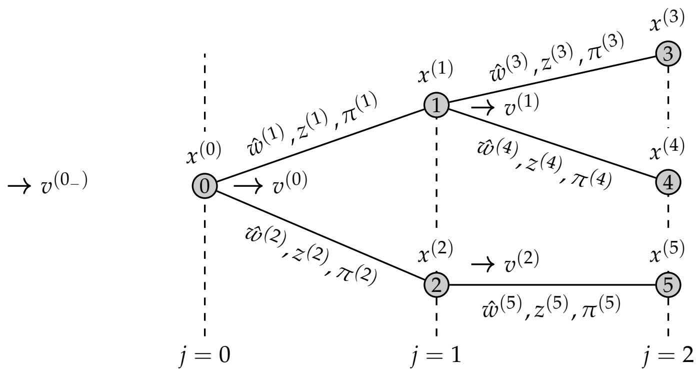

Figure 9.1: Example of a scenario tree with states $x^{(i)}$, control inputs $v^{(i)}$, uncertain inputs $\hat{w}^{(i)}$, auxiliary vectors $z^{(i)}$, and probabilities $\pi^{(i)}$. Source: [93].

9.1.1 *Relation of nodes*

The following relation of nodes in a scenario tree employs a notation that is very similar to the one in [51, 241]. Related notations can also be found in [25, 186, 192, 212, 219, 222].

A scenario tree is a collection of $N_\mathrm{n} \in \mathbb{N}$ nodes. Each node is associated with a unique index $i = 0, \ldots, N_\mathrm{n} - 1$. The nodes can be partitioned according to their prediction time instant, i.e., the stages $j = 0, \ldots, J$, with prediction horizon $J \in \mathbb{N}$. For the example in Figure 9.1, $N_\mathrm{n} = 6$ and $J = 2$. The subset that includes exactly the elements of stage j is denoted by $\mathrm{nodes}(j) \subseteq \mathbb{N}_{[0,N_\mathrm{n}-1]}$. The stage of a node can be accessed via $\mathrm{stage}(i) \in \mathbb{N}_{[0,J]}$. In Figure 9.1, the stage-wise partitions are $\mathrm{nodes}(0) = \{0\}$, $\mathrm{nodes}(1) = \{1, 2\}$ and $\mathrm{nodes}(2) = \{3, 4, 5\}$. Furthermore, $\mathrm{stage}(0) = 0$, $\mathrm{stage}(1) = \mathrm{stage}(2) = 1$ and $\mathrm{stage}(3) = \mathrm{stage}(4) = \mathrm{stage}(5) = 2$ (see also Table 9.1).

The nodes at stage J are called leaf nodes and the unique node $i = 0$ at stage $j = 0$ is called root node. In Figure 9.1, the set of leaf nodes is $\{3, 4, 5\}$. All non-leaf nodes, i.e., the elements of $\mathbb{N}_{[1,N_\mathrm{n}]} \setminus \mathrm{nodes}(J)$ are connected to child nodes. The set that includes all child nodes of $i \in \mathrm{nodes}(j)$ is $\mathrm{child}(i) \subseteq \mathrm{nodes}(j+1)$. Similarly, all non-root nodes $i \in \mathrm{nodes}(j)$, $j \in \mathbb{N}_{[1,J]}$ are connected to a single ancestor node at stage $j - 1$. This ancestor can be accessed via $\mathrm{anc}(i) \in \mathrm{nodes}(\mathrm{stage}(i) - 1)$. In Figure 9.1, $\mathrm{child}(0) = \{1, 2\}$, $\mathrm{child}(1) = \{3, 4\}$ and $\mathrm{child}(2) = \{5\}$. The ancestors are $\mathrm{anc}(1) = \mathrm{anc}(2) = 0$, $\mathrm{anc}(3) = \mathrm{anc}(4) = 1$ and $\mathrm{anc}(5) = 2$.

A sequence of nodes $(s_0, \ldots, s_J)$ with $s_J \in \mathrm{nodes}(J)$, $s_0 = 0$ and $\mathrm{anc}(s_j) = s_{j-1}$ for all $j = 1, \ldots, J$ is called a scenario. Each

Node	i	0	1	2	3	4	5
Stage	$\mathrm{stage}(i)$	0	1	1	2	2	2
Set of children	$\mathrm{child}(i)$	$\{1,2\}$	$\{3,4\}$	$\{5\}$	$\emptyset$	$\emptyset$	$\emptyset$
Ancestor	$\mathrm{anc}(i)$	n/a	0	0	1	1	2
Probability	$\pi^{(i)}$	1	$\pi^{(1)}$	$\pi^{(2)}$	$\pi^{(3)}$	$\pi^{(4)}$	$\pi^{(5)}$
			$\sum = 1$		$\sum = \pi^{(1)}$		$= \pi^{(2)}$
State	$x^{(i)}$	$x^{(0)}$	$x^{(1)}$	$x^{(2)}$	$x^{(3)}$	$z^{(4)}$	$x^{(5)}$
Control input	$v^{(i)}$	$v^{(0)}$	$v^{(1)}$	$v^{(2)}$	n/a	n/a	n/a
Uncertain input	$\hat{w}^{(i)}$	n/a	$\hat{w}^{(1)}$	$\hat{w}^{(2)}$	$\hat{w}^{(3)}$	$\hat{w}^{(4)}$	$\hat{w}^{(5)}$
Auxiliary vector	$z^{(i)}$	n/a	$z^{(1)}$	$z^{(2)}$	$z^{(3)}$	$z^{(4)}$	$z^{(5)}$

Table 9.1: Operators, probabilities and model variables of scenario tree in Figure 9.1. Note that fields where corresponding variables were not required are marked n/a.

scenario ends with a unique leaf node. Therefore, the number of scenarios equals the number of leaf nodes and every scenario can be uniquely identified by its leaf node. The set of all nodes that form the scenario that ends with s_J is denoted by $\mathrm{scen}(s_J)$. The scenarios in Figure 9.1 are $(0,1,3)$, $(0,1,4)$ and $(0,2,5)$ with $\mathrm{scen}(3) = \{0,1,3\}$, $\mathrm{scen}(4) = \{0,1,4\}$ and $\mathrm{scen}(5) = \{0,2,5\}$.

9.1.2 *Probabilities*

This section follows the notation introduced in [93, 222].[1] Each node i is associated with a probability $\pi^{(i)} \in (0,1]$. For the probabilities of all nodes of stage j it holds that

$$\textstyle\sum_{i \in \mathrm{nodes}(j)} \pi^{(i)} = 1. \tag{9.1}$$

Furthermore, for every non-leaf node

$$\pi^{(i)} = \textstyle\sum_{i_+ \in \mathrm{child}(i)} \pi^{(i_+)} \tag{9.2}$$

holds. For Figure 9.1, this means that $\pi^{(0)} = 1$, $\pi^{(1)} + \pi^{(2)} = 1$ and $\pi^{(3)} + \pi^{(4)} + \pi^{(5)} = 1$ as well as $\pi^{(3)} + \pi^{(4)} = \pi^{(1)}$ and $\pi^{(5)} = \pi^{(2)}$.

[1] If required the notation could be easily transformed into, for example, the one in [241].

9.1.3 *Probability distributions*

Let us assume a time-varying discrete probability distribution in the form of a scenario tree. For every stage $j \in \mathbb{N}_{[1,J]}$, the sample space of this distribution is $\mathrm{nodes}(j)$.[2] Each element $i \in \mathrm{nodes}(j)$ is associated with a probability $\pi^{(i)} > 0$. As

[2] Note that $\mathrm{nodes}(j)$ originates from a common probability space for the entire scenario tree using the concept of filtration [241].

described in Section 9.1.2, it holds that $\sum_{i\in\text{nodes}(j)} \pi^{(i)} = 1$. Let us denote the vector of all probabilities associated with stage j by $\pi_j = [\pi^{(i)}]_{i\in\text{nodes}(j)}$. For the example in Figure 9.1, the sample spaces are $\text{nodes}(1) = \{1, 2\}$ and $\text{nodes}(2) = \{3, 4, 5\}$ with $\pi_1 = [\pi^{(1)}\ \pi^{(2)}]^\top$ and $\pi_2 = [\pi^{(3)}\ \pi^{(4)}\ \pi^{(5)}]^\top$. At all stages $j = 0, \dots, J$, the probability vectors π_j are elements of

$$\mathbb{D}_j = \left\{ \pi' \in \mathbb{R}^{|\text{nodes}(j)|}_{\geq 0} \,\middle|\, \sum_{i=1}^{|\text{nodes}(j)|} \pi'_i = 1 \right\}. \tag{9.3}$$

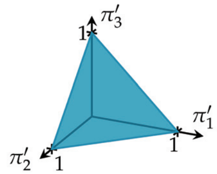

Figure 9.2: Probability simplex of probability space with $|\text{nodes}(j)| = 3$. Source: [93].

This set is called probability simplex. The probability simplex of a sample space with three elements is illustrated in Figure 9.2.

In the context of scenario-based optimization, a random variable on $\text{nodes}(j)$ is a function $\tilde{\ell}_j : \text{nodes}(j) \to \mathbb{R}$ with $\tilde{\ell}_j(i) = \ell^{(i)}$. In our case, $\ell^{(i)}$ represents the operating cost[3] from Section 5.2 that is associated with node i. The values of $\tilde{\ell}_j$ are collected in $\ell_j = [\ell^{(i)}]_{i\in\text{nodes}(j)}$. Thus, for the scenario tree in Figure 9.3, the vectors $\ell_1 = [\ell^{(1)}\ \ell^{(2)}]^\top$ and $\ell_2 = [\ell^{(3)}\ \ell^{(4)}\ \ell^{(5)}]^\top$ can be formed. Using the sample space $\text{nodes}(j)$, the events collected in ℓ_j and the probabilities collected in π_j, a probability space of dimension $\text{nodes}(j)$ can be formed.

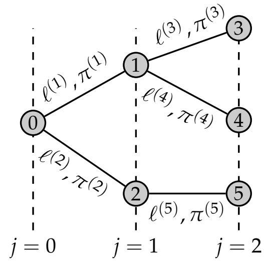

Figure 9.3: Example of scenario tree with costs $\ell^{(i)}$ and probabilities $\pi^{(i)}$.

[3] More details on the cost $\ell^{(i)}$ can be found in Section 9.2.

Conditional probability distributions on scenario trees. We can define conditional probability distributions on the space $\text{nodes}(j+1)$, given that at stage j node $i \in \text{nodes}(j)$ is visited [241]. Therefore, we partition the set of nodes at stage $j+1$ according to their ancestors at stage j. The resulting partitions are disjoint sets $\text{child}(i) \subseteq \text{nodes}(j+1)$ for all $i \in \text{nodes}(j)$ with

$$\text{nodes}(j+1) = \bigcup_{i\in\text{nodes}(j)} \text{child}(i). \tag{9.4}$$

In this context, conditional probability means that given we are at non-leaf node $i \in \mathbb{N}_{[0,N_\text{n}-1]} \setminus \text{nodes}(J)$, the probability of node $i_+ \in \text{child}(i)$ is $\pi^{(i_+)}/\pi^{(i)}$ [25, 241]. This allows to form a probability space on $\text{child}(i)$ using the conditional probabilities of the child nodes of i,

$$\pi^{[i]} = \frac{1}{\pi^{(i)}} \left[\pi^{(i_+)}\right]_{i_+\in\text{child}(i)}, \tag{9.5a}$$

and random variables with vectors

$$\ell^{[i]} = \left[\ell^{(i_+)}\right]_{i_+ \in \mathrm{child}(i)}. \tag{9.5b}$$

Note that due to (9.2), the sum over all elements in $\pi^{[i]}$ is 1.

In Figure 9.3 the probability space nodes(2) can be partitioned into child(1) and child(2). These spaces then have probability vectors $\pi^{[1]} = 1/\pi^{(1)}[\pi^{(3)}\ \pi^{(4)}]^\top$, $\pi^{[2]} = 1/\pi^{(2)}[\pi^{(5)}]$ and random variables with values $\ell^{[1]} = [\ell^{(3)}\ \ell^{(4)}]^\top$ and $\ell^{[2]} = [\ell^{(5)}]$.

9.2 *Model variables*

Each node in a scenario tree is associated with decision variables and forecasts of load and available renewable infeed. In what follows, the relation of these variables on a scenario tree is discussed.

All non-leaf nodes $i \in \mathbb{N}_{[0,N_\mathrm{n}-1]} \setminus \mathrm{nodes}(J)$ are associated with a vector of control inputs $v^{(i)}$. For $v^{(i)}$, the uncertain input, i.e., load and available renewable infeed, can take different values. More precisely, all uncertain inputs $\hat{w}^{(i_+)}$ with $i_+ \in \mathrm{child}(i)$ can occur. Hence, the control input $v^{(i)}$ has to be suitable for all possible values of $\hat{w}^{(i_+)}$. The auxiliary vector $z^{(i_+)}$ changes with the control input $v^{(i)}$ and the predicted uncertain input $\hat{w}^{(i_+)}$. To indicate that $v^{(i)}$ is considered for the same prediction time instant as all $\hat{w}^{(i_+)}$, the control input $v^{(i)}$ is positioned between the edges of the children of node i in Figure 9.1. For node 0 of Figure 9.1, the relation of variables is illustrated in Figure 9.4. Here, $z^{(1)}$ depends on $(v^{(0)}, \hat{w}^{(1)})$ and $z^{(2)}$ depends on $(v^{(0)}, \hat{w}^{(2)})$.

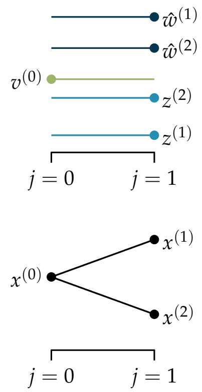

Figure 9.4: Temporal relation of variables on scenario tree. Source: [93].

Each node i is associated with state $x^{(i)}$ where $x^{(0)}$ corresponds to an initially measured state. State $x^{(i_+)}$ is a function of the auxiliary vector $z^{(i_+)}$ and the state of its ancestor, i.e.,

$$x^{(i_+)} = f_x(x^{(i)}, z^{(i_+)}), \tag{9.6}$$

with $i = \mathrm{anc}(i_+)$. Note that via (9.6), the state $x^{(i_+)}$ of each node is associated with the auxiliary vector $z^{(i_+)}$ and thereby also with the uncertain input $\hat{w}^{(i_+)}$.

Remark 9.2.1 (Nonanticipativity)**.** In multistage stochastic optimization problems, the decisions taken at each stage should be made without knowledge about the exact outcome of the uncertain input. Thus, the decisions taken at stage $k+j$ should only depend on the knowledge available up to that stage. This concept is typically referred to as nonanticipativity [55, 214, 241]. In the context of this thesis, the relation of variables on the scenario trees is designed such that nonanticipativity is automatically encoded into each scenario-based problem. In detail, the control decision $v^{(i)}$ needs to take all uncertain inputs, i.e., all elements of the set $\{\hat{w}^{(i_+)}\}_{i_+ \in \mathrm{child}(i)}$, into consideration without knowing which one will occur.

A prominent alternative to this strategy is to initially ignore nonanticipativity in the design of the scenario tree, i.e., in the relation of variables, and enforce it later using equality constraints. This leads to optimization problems with a larger number of decision variables than the ones presented in this thesis which, in the end, model the same system behavior. Such a strategy is, for example, employed in [55].

Example 9.2.2 (Relation of uncertain input, control input and power)**.** Consider the MG topology from Figure 4.1 and the scenario tree in Figure 9.1. For the time period from $j=0$ to $j=1$, two realizations of uncertain inputs, $w^{(1)} = [w_\mathrm{r}^{(1)}\ w_\mathrm{d}^{(1)}]^\top$ and $w^{(2)} = [w_\mathrm{r}^{(2)}\ w_\mathrm{d}^{(2)}]^\top$, are considered (see Figure 9.5). For the same time period, an optimal control decision $v^{(0)}$ needs to be made without knowing whether $w^{(1)}$ or $w^{(2)}$ will occur. Thus, the control input $v^{(0)} = [u_\mathrm{t}^{(0)}\ u_\mathrm{s}^{(0)}\ u_\mathrm{r}^{(0)}\ \delta_\mathrm{t}^{(0)}]^\top$ needs to lead to a feasible solution for both possible uncertain inputs $w^{(1)}$ and $w^{(2)}$. This includes feasible power values which depend on the uncertain input and the control input. Therefore, in scenario-based MPC, for each realization of the uncertain input, a vector of power values is considered.

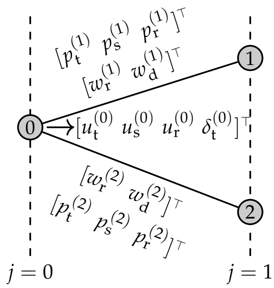

Figure 9.5: Scenario tree with power-related variables.

In what follows, three examples with different uncertain input, control input and unit power will be discussed. The focus of these examples lies on stages 0 and 1 of the scenario tree in Figure 9.1. However, the example works similarly for any node with two child nodes, e.g., node 1 in Figure 9.1.

1. Let us first consider the uncertain inputs and power setpoints in Figure 9.6. Here, both forecasts of available renewable power, $w_\mathrm{r}^{(1)}$ and $w_\mathrm{r}^{(2)}$, are *above* the power setpoint $u_\mathrm{r}^{(0)}$. Consequently, following (4.12), the power of the re-

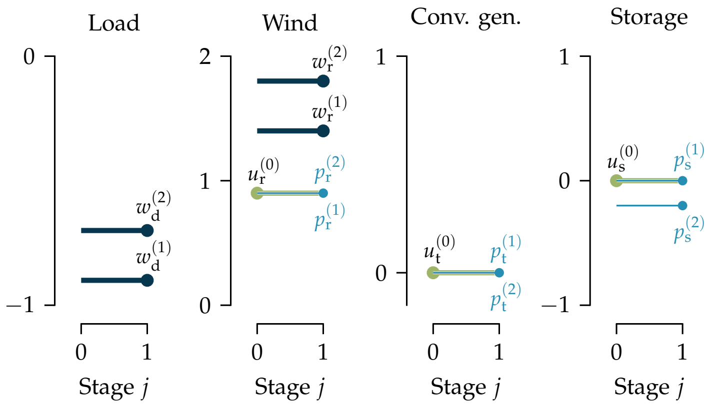

Figure 9.6: Unit power on scenario tree with high available renewable infeed and disabled conventional generator.

newable units becomes

$$p_\mathrm{r}^{(1)} = \min(u_\mathrm{r}^{(0)}, w_\mathrm{r}^{(1)}) = u_\mathrm{r}^{(0)}, \tag{9.7a}$$
$$p_\mathrm{r}^{(2)} = \min(u_\mathrm{r}^{(0)}, w_\mathrm{r}^{(2)}) = u_\mathrm{r}^{(0)}. \tag{9.7b}$$

The power and the power setpoint of the conventional unit are forced to zero by $\delta_\mathrm{t}^{(0)} = 0$ via (4.7), i.e., $u_\mathrm{t}^{(0)} = 0$ and $p_\mathrm{t}^{(1)} = p_\mathrm{t}^{(2)} = 0$. Hence, the storage unit needs to cover all fluctuations of the load and the renewable generator. This is reflected by the power balance equation (4.28b) which with $p_\mathrm{t}^{(1)} = p_\mathrm{t}^{(2)} = 0$ becomes

$$p_\mathrm{s}^{(1)} = -p_\mathrm{r}^{(1)} - w_\mathrm{d}^{(1)} = -u_\mathrm{r}^{(0)} - w_\mathrm{d}^{(1)}, \tag{9.7c}$$
$$p_\mathrm{s}^{(2)} = -p_\mathrm{r}^{(2)} - w_\mathrm{d}^{(2)} = -u_\mathrm{r}^{(0)} - w_\mathrm{d}^{(2)}. \tag{9.7d}$$

In Figure 9.6, it is shown how the storage power changes with the uncertain input. For a large absolute load power $w_\mathrm{d}^{(1)}$, the storage power $p_\mathrm{s}^{(1)}$ is zero. For a lower absolute load power $w_\mathrm{d}^{(2)}$, the storage is slightly charged with $p_\mathrm{s}^{(2)}$.

2. Let us now consider the uncertain inputs and power setpoints in Figure 9.7. Here, both forecasts of available renewable power, $w_\mathrm{r}^{(1)}$ and $w_\mathrm{r}^{(2)}$, are *below* the maximum allowed renewable infeed $u_\mathrm{r}^{(0)}$. Consequently, in this case, renewable infeed is not curtailed.[4] Following (4.12), the

[4] An operation with uncurtailed RES can also be found in grids with a low share of RES where a limitation renewable infeed is not required.

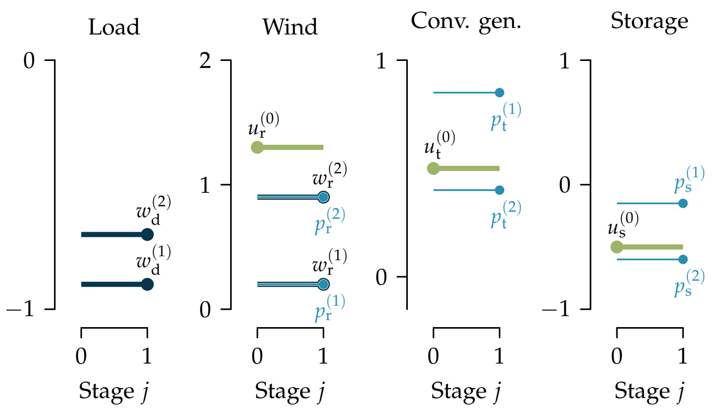

Figure 9.7: Unit power on scenario tree with low available renewable infeed and enabled conventional generator.

power of the renewable units therefore becomes

$$p_r^{(1)} = \min(u_r^{(0)}, w_r^{(1)}) = w_r^{(1)}, \tag{9.8a}$$

$$p_r^{(2)} = \min(u_r^{(0)}, w_r^{(2)}) = w_r^{(2)}. \tag{9.8b}$$

The power of the conventional and the storage unit are determined by power sharing (4.35). For $\chi_s = \chi_t = 1$, the equations in this example read

$$u_s^{(0)} - p_s^{(1)} = u_t^{(0)} - p_t^{(1)}, \tag{9.8c}$$

$$u_s^{(0)} - p_s^{(2)} = u_t^{(0)} - p_t^{(2)}. \tag{9.8d}$$

Together with the power balance equation (4.28b), i.e.,

$$0 = p_t^{(1)} + p_s^{(1)} + p_r^{(1)} + w_d^{(1)}, \tag{9.8e}$$

$$0 = p_t^{(2)} + p_s^{(2)} + p_r^{(2)} + w_d^{(2)}, \tag{9.8f}$$

this can be transformed into[5]

$$p_t^{(1)} = \frac{u_t^{(0)} - u_s^{(0)} - p_r^{(1)} - w_d^{(1)}}{2}, \tag{9.8g}$$

$$p_t^{(2)} = \frac{u_t^{(0)} - u_s^{(0)} - p_r^{(2)} - w_d^{(2)}}{2}. \tag{9.8h}$$

The power of the storage unit can be similarly deduced as

$$p_s^{(1)} = \frac{u_s^{(0)} - u_t^{(0)} - p_r^{(1)} - w_d^{(1)}}{2}, \tag{9.8i}$$

$$p_s^{(2)} = \frac{u_s^{(0)} - u_t^{(0)} - p_r^{(2)} - w_d^{(2)}}{2}. \tag{9.8j}$$

[5] See, e.g., Example 4.8.2 for a detailed derivation of equations (9.8g)–(9.8j).

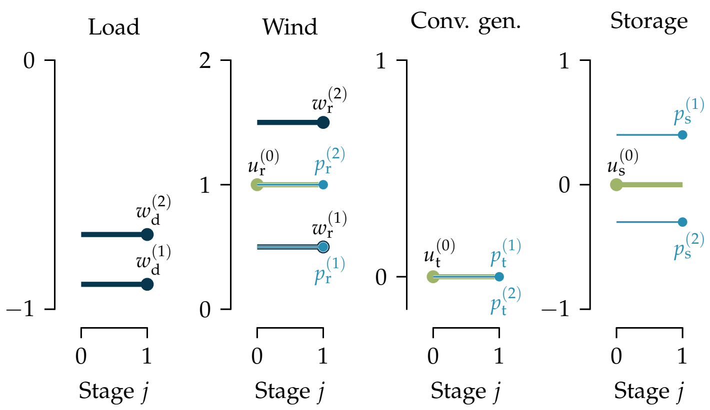

Figure 9.8: Unit power on scenario tree with medium available renewable infeed and disabled conventional generator.

In Figure 9.7, it can be seen that the power of the storage and the conventional unit changes depending on the uncertain input. For $p_r^{(1)} = w_r^{(1)}$ and $w_d^{(1)}$, where the absolute value of the load is large and infeed from the wind turbine is low, the storage unit is charged less aggressively with $p_s^{(1)}$ and the conventional unit provides more power $p_t^{(1)}$. A similar behavior can be observed for $p_r^{(2)} = w_r^{(2)}$ and $w_d^{(2)}$, where the absolute value of the load is small and infeed from the wind turbine is high. Here, the storage unit is charged more aggressively with $p_s^{(2)}$ and the conventional unit provides less power $p_t^{(2)}$.

Note that for $\chi_s = \chi_t = 1$, the distance between power and power setpoints is equal for the storage and the conventional unit. With this relation, one can modify the power of the units by increasing or decreasing the power setpoints.

3. In the last example in Figure 9.8, the wind turbine's power setpoint $u_r^{(0)}$ is between $w_r^{(1)}$ and $w_r^{(2)}$. Following (4.12), the power of the renewable generator therefore becomes

$$p_r^{(1)} = \min(u_r^{(0)}, w_r^{(1)}) = w_r^{(1)}, \tag{9.9a}$$
$$p_r^{(2)} = \min(u_r^{(0)}, w_r^{(2)}) = u_r^{(0)}. \tag{9.9b}$$

Power and power setpoint of the conventional unit are forced to zero, i.e., $u_t^{(0)} = p_t^{(1)} = p_t^{(2)} = 0$, by $\delta_t^{(0)} = 0$ via (4.7). The power of the storage unit is determined by

Note that the inequalities

$$p_r^{(1)} \le u_r^{(0)},$$
$$p_r^{(1)} \le w_r^{(1)},$$
$$p_r^{(2)} \le u_r^{(0)},$$
$$p_r^{(2)} \le w_r^{(2)},$$

do not model to the same behavior as (9.9a) and (9.9b). Using the above inequalities would, among other undesired effects, allow for power values that are below the forecast of the uncertain input without the need to reduce the power setpoint. In the closed loop, this could result in large power setpoints (and therefore also large power values for the plant) even though, lower power values were considered in the MPC. In conclusion, only the min operator can ensure that a limitation of available renewable power is modeled correctly in the scenario-based MPC formulations.

(4.28b) which with $p_{\mathrm{t}}^{(1)} = p_{\mathrm{t}}^{(2)} = 0$ can be transformed into

$$p_{\mathrm{s}}^{(1)} = -p_{\mathrm{r}}^{(1)} - w_{\mathrm{d}}^{(1)} = -u_{\mathrm{r}}^{(0)} - w_{\mathrm{d}}^{(1)}, \tag{9.9c}$$

$$p_{\mathrm{s}}^{(2)} = -p_{\mathrm{r}}^{(2)} - w_{\mathrm{d}}^{(2)} = -w_{\mathrm{r}}^{(2)} - w_{\mathrm{d}}^{(2)}. \tag{9.9d}$$

In Figure 9.8, it can be seen how the power of the storage unit changes with the uncertain input. In case of $p_{\mathrm{r}}^{(1)} = w_{\mathrm{r}}^{(1)}$ and $w_{\mathrm{d}}^{(1)}$, where the absolute value of the load is high and infeed from the wind turbine is low, the storage unit is discharged with $p_{\mathrm{s}}^{(1)}$. For $p_{\mathrm{r}}^{(2)} = u_{\mathrm{r}}^{(0)}$ and $w_{\mathrm{d}}^{(2)}$, where the absolute value of the load is low and renewable infeed is high, the storage unit is charged with $p_{\mathrm{s}}^{(2)}$.

One last important thing to note in this example is that the power of the storage unit is independent of its setpoint and only depends on the power of the renewable unit and the load. The reason for this is that we are in islanded operation where a local power equilibrium needs to be maintained at all times. Because the storage is the one grid-forming unit, it has to cover all fluctuations, independent of its setpoint. The same naturally hods for the first example in Figure 9.6.

Compact MG model for scenario-based MPC. Using the relation of model variables discussed earlier, the constraints (5.1) can be formulated for a scenario tree. For every non-root node $i_+ \in \mathbb{N}_{[1,N_{\mathrm{n}}-1]}$ with $i = \mathrm{anc}(i_+)$, they are

$$x^{(i_+)} = Ax^{(i)} + \tilde{B}z^{(i_+)}, \tag{9.10a}$$

$$h_1 \leq H_1\, x^{(i_+)}, \tag{9.10b}$$

$$h_2 \leq H_2 \begin{bmatrix} v^{(i)\top} & z^{(i_+)\top} & \hat{w}^{(i_+)\top} \end{bmatrix}^\top, \tag{9.10c}$$

$$g = G \begin{bmatrix} v^{(i)\top} & z^{(i_+)\top} & \hat{w}^{(i_+)\top} \end{bmatrix}^\top, \tag{9.10d}$$

with given initial state $x^{(0)} = x_k$.

The costs at every non-root node $i_+ \in \mathbb{N}_{[1,N_{\mathrm{n}}-1]}$ with $i = \mathrm{anc}(i_+)$ and $i_- = \mathrm{anc}(i)$ is

Recall from Section 5.3 that $\gamma \in (0,1]$ is a discount factor that is used emphasize decisions in the near future.

$$\ell^{(i_+)} = \ell(v^{(i_-)}, v^{(i)}, z^{(i_+)}, x^{(i_+)})\gamma^{\mathrm{stage}(i_+)}, \tag{9.11a}$$

with given current input $v^{(0_-)} = v_{k-1}$. Even though the cost is associated with node i_+, it mostly depends on the decision

$v^{(i)}$ as $z^{(i_+)}$ and $x^{(i_+)}$ change with $v^{(i)}$. Moreover, it depends on the on/off switch of the conventional unit at ancestor node i_-. Hence, the decision at the root node $v^{(0)}$ also depends on the current value of $\delta_{\mathrm{t}}^{(0_-)}$ which is part of $v^{(0_-)}$.

Using (9.11a), the vector of costs for every stage $j \in \mathbb{N}_{[1,J]}$ is

$$\ell_j = [\ell^{(i_+)}]_{i_+ \in \mathrm{nodes}(j)}. \tag{9.11b}$$

Thus, the multi-stage cost of the entire tree can be described by the sequence of vectors $(\ell_1, \ldots, \ell_J)$.

Remark 9.2.3 (Decision variables on tree)**.** Note that (9.10) and (9.11) do not include the control inputs at stage J, i.e., $[v^{(i)}]_{i \in \mathrm{nodes}(J)}$. The reason for this is that states $[x^{(i)}]_{i \in \mathrm{nodes}(J)}$ and auxiliary vectors $[z^{(i)}]_{i \in \mathrm{nodes}(J)}$ at stage J are functions of the inputs $[v^{(i)}]_{i \in \mathrm{nodes}(J-1)}$. Thus, the decision variables at the leaf nodes, $[v^{(i)}]_{i \in \mathrm{nodes}(J)}$, do not affect the constraints or the cost function in the scenario-based MPC problems in Chapters 10 and 11. Therefore, the vector of decision variables in these problems is $\boldsymbol{v} = [v^{(i)}]_{i \in \mathbb{N}_{[0,N_{\mathrm{n}}-1]} \setminus \mathrm{nodes}(J)}$.

Remark 9.2.4 (Robustness to uncertain load and renewable generation)**.** The state and the auxiliary variables are either monotonically increasing or decreasing in the uncertain input (see Section 8.2). Thus, if the units' power and energy constraints hold for the minimum and maximum uncertain input, then they also hold for uncertain values that lie in between. Unfortunately, this is not the case for the line power limits which are therefore not automatically guaranteed to be satisfied (see Section 8.2.3). For scenario trees that exhibits a sufficiently large number of scenarios, the line power limits are approximately accounted for via samples that implicitly numerate extreme values of line power. To explicitly implement robust line power constraints, scenario-based MPC problems could be robustified in a similar fashion as in Section 8.2.3. The closed-loop simulations in Chapter 12, however, showed no violation of line limits when only using the samples in the scenario tree. Therefore, in what follows the power flow limits are only checked at the discrete values $\hat{w}^{(i)}$, $i \in \mathbb{N}_{[1,N_{\mathrm{n}}]}$ and are consequently only approximately accounted for.

Example 9.2.5. In Figure 9.1, the dynamics (9.10a) are

$$x^{(0)} = x_k, \tag{9.12a}$$
$$x^{(1)} = Ax^{(0)} + \tilde{B}z^{(1)}, \tag{9.12b}$$
$$x^{(2)} = Ax^{(0)} + \tilde{B}z^{(2)}, \tag{9.12c}$$
$$x^{(3)} = Ax^{(1)} + \tilde{B}z^{(3)}, \tag{9.12d}$$
$$x^{(4)} = Ax^{(1)} + \tilde{B}z^{(4)}, \tag{9.12e}$$
$$x^{(5)} = Ax^{(2)} + \tilde{B}z^{(5)}, \tag{9.12f}$$

with state limits (9.10b)

$$h_1 \leq H_1 x^{(1)}, \tag{9.12g}$$
$$h_1 \leq H_1 x^{(2)}, \tag{9.12h}$$
$$h_1 \leq H_1 x^{(3)}, \tag{9.12i}$$
$$h_1 \leq H_1 x^{(4)}, \tag{9.12j}$$
$$h_1 \leq H_1 x^{(5)}. \tag{9.12k}$$

Moreover, the inequality constraints (9.10c) are

$$h_2 \leq H_2 \left[(v^{(0)\top} \quad z^{(1)\top} \quad \hat{w}^{(1)\top} \right]^\top, \tag{9.12l}$$
$$h_2 \leq H_2 \left[(v^{(0)\top} \quad z^{(2)\top} \quad \hat{w}^{(2)\top} \right]^\top, \tag{9.12m}$$
$$h_2 \leq H_2 \left[(v^{(1)\top} \quad z^{(3)\top} \quad \hat{w}^{(3)\top} \right]^\top, \tag{9.12n}$$
$$h_2 \leq H_2 \left[(v^{(1)\top} \quad z^{(4)\top} \quad \hat{w}^{(4)\top} \right]^\top, \tag{9.12o}$$
$$h_2 \leq H_2 \left[(v^{(2)\top} \quad z^{(5)\top} \quad \hat{w}^{(5)\top} \right]^\top, \tag{9.12p}$$

and the equality constraints (9.10d) are

$$g = G \left[(v^{(0)\top} \quad z^{(1)\top} \quad \hat{w}^{(1)\top} \right]^\top, \tag{9.12q}$$
$$g = G \left[(v^{(0)\top} \quad z^{(2)\top} \quad \hat{w}^{(2)\top} \right]^\top, \tag{9.12r}$$
$$g = G \left[(v^{(1)\top} \quad z^{(3)\top} \quad \hat{w}^{(3)\top} \right]^\top, \tag{9.12s}$$
$$g = G \left[(v^{(1)\top} \quad z^{(4)\top} \quad \hat{w}^{(4)\top} \right]^\top, \tag{9.12t}$$
$$g = G \left[(v^{(2)\top} \quad z^{(5)\top} \quad \hat{w}^{(5)\top} \right]^\top. \tag{9.12u}$$

The cost associated with the nodes in Figure 9.1 is based on (9.11) and given by

$$\ell^{(1)} = \ell(v^{(0-)}, v^{(0)}, z^{(1)}, x^{(1)})\gamma^1, \tag{9.13a}$$
$$\ell^{(2)} = \ell(v^{(0-)}, v^{(0)}, z^{(2)}, x^{(2)})\gamma^1, \tag{9.13b}$$
$$\ell^{(3)} = \ell(v^{(0)}, v^{(1)}, z^{(3)}, x^{(3)})\gamma^2, \tag{9.13c}$$
$$\ell^{(4)} = \ell(v^{(0)}, v^{(1)}, z^{(4)}, x^{(4)})\gamma^2, \tag{9.13d}$$
$$\ell^{(5)} = \ell(v^{(0)}, v^{(2)}, z^{(5)}, x^{(5)})\gamma^2. \tag{9.13e}$$

Using these costs, the vectors of costs for stages 1 and 2 are

$$\ell_1 = \begin{bmatrix} \ell^{(1)} & \ell^{(2)} \end{bmatrix}^\top, \tag{9.13f}$$
$$\ell_2 = \begin{bmatrix} \ell^{(3)} & \ell^{(4)} & \ell^{(5)} \end{bmatrix}^\top. \tag{9.13g}$$

Using these vectors, the multi-stage cost of the tree can be described by the sequence (ℓ_1, ℓ_2).

9.3 *Generation of scenario trees from forecast scenarios*

There exist many approaches to generate scenario trees from collections of independent forecast scenarios [21, 46, 57, 66, 84, 105, 136, 189, 193, 238]. In this thesis, especially for the simulations in Chapter 12, a variant of forward tree construction that is close to the approaches in [58, 78, 96, 98, 99] was chosen as an example.

The following section is based on [169] and structured as follows. First, a general introduction is provided. Then, the forward selection algorithm is introduced and employed to generate scenario trees.

9.3.1 *Introduction*

Consider collections of N_Ω independent forecast scenarios (see Section 6.1.4) for each renewable unit and each load. These collections are combined such that for each scenario $i \in \mathbb{I} = \mathbb{N}_{[1,N_\Omega]}$ and each forecast time instant j the vector

$$\begin{aligned} \hat{w}^i(k+j|k) = \big[&\hat{w}^i_{\mathrm{r},1}(k+j|k),\ \ldots,\ \hat{w}^i_{\mathrm{r},N_\mathrm{r}}(k+j|k), \\ &\hat{w}^i_{\mathrm{d},1}(k+j|k),\ \ldots,\ \hat{w}^i_{\mathrm{d},N_\mathrm{d}}(k+j|k)\big]^\top \end{aligned} \tag{9.14}$$

is formed. Thus $\hat{w}^i(k+j|k)$ is composed of forecast scenarios of load and weather-dependent available renewable infeed.

Consider a sample space $\Omega = \{\Omega^1, \ldots, \Omega^{N_\Omega}\}$, where each element Ω^i, $i \in \mathbb{I}$ has probability $\pi^i = 1/N_\Omega$ and $\sum_{i=1}^{N_\Omega} \pi^i = 1$. Random variables on Ω are functions $\tilde{w} : \Omega \to \mathbb{R}^{(N_\mathrm{r}+N_\mathrm{d})}$ with $\tilde{w}(\Omega^i) = \hat{w}^i(k+j|k)$, i.e., each element Ω^i is associated with a vector of forecast scenarios $\hat{w}^i(k+j|k)$.

The goal of scenario reduction is to find a subset of scenarios $\mathbb{L} \subset \mathbb{I}$ that can be removed from the original set of scenarios $\mathbb{I}$ such that the quantization error, represented by the Wasserstein-Kantorovitch L_r-metric (see, e.g., [76, Introduction] or [192, Chapter 2]), which can be formulated as in (9.15a), is minimized. If $\mathbb{L}$ is known, then the goal of the reduction is to assign all elements of $\mathbb{L}$ to the scenarios $\overline{\mathbb{L}} = \mathbb{I} \setminus \mathbb{L}$ that are kept. Let us assume that the difference between two vectors of forecast scenarios can be described by the Euclidean distance. Then, a redistribution that minimizes the quantization error for a given set of reduced scenarios $\mathbb{L}$ has the optimal value [58, Theorem 2]

$$D_{\mathbb{L}} = \sum_{l \in \mathbb{L}} \pi^l \min_{i \in \overline{\mathbb{L}}} \|\hat{w}^i(k+j|k) - \hat{w}^l(k+j|k)\|_2. \tag{9.15a}$$

Thus, the quantization error is minimized by assigning each reduced scenario $l \in \mathbb{L}$ to the kept scenario $i \in \overline{\mathbb{L}}$ that has the smallest Euclidean distance to it. Let us define the set of scenarios that are assigned to scenario $i^\star \in \overline{\mathbb{L}}$ as

$$\widetilde{\mathbb{L}}(i^\star) = \left\{ l \in \mathbb{L} \mid i^\star \in \arg\min_{i \in \overline{\mathbb{L}}} \|\hat{w}^i(k+j|k) - \hat{w}^l(k+j|k)\|_2 \right\}. \tag{9.15b}$$

The probabilities of the removed scenarios are added to the probability of the kept scenario that has the smallest distance to them. Scenario $i \in \overline{\mathbb{L}}$ then has has probability

$$\tilde{\pi}^i = \pi^i + \sum_{l \in \widetilde{\mathbb{L}}(i)} \pi^l. \tag{9.15c}$$

Thus, given a set $\mathbb{L}$ of removed scenarios, a reduced probability distribution with values $\hat{w}^i(k+j|k)$ and probabilities $\tilde{\pi}^i$ for $i \in \overline{\mathbb{L}}$ can be formed. Note that in what follows, (9.15) is referred to as “optimal redistribution” as it optimally assigns the reduced scenarios in $\mathbb{L}$ to kept scenarios in $\overline{\mathbb{L}}$.

For optimal redistribution to be applied, the index set of reduced scenario $\mathbb{L}$ needs to be identified. If the number of kept scenarios $b_j^d \in \mathbb{N}$ is known, then finding a suitable set of removed scenarios $\mathbb{L}$ can be formulated as the set covering problem [96, 98]

$$\min_{\substack{\mathbb{L}\subset\mathbb{I}\\ |\mathbb{L}|=N_\Omega-b_j^d}} D_{\mathbb{L}}. \tag{9.16}$$

This optimization problem can be formulated as an integer program [167] which is known to be NP-hard. Therefore, instead of solving the original combinatorial optimization problem, fast heuristics such as "simultaneous backward reduction" (see, e.g., [96, Algorithm 2.2]) or "fast forward selection" [96, Algorithm 2.4] can be used. If the number of scenarios that are kept, b_j^d, is much smaller than the number of initial scenarios, N_Ω, then the computational complexity of forward selection is lower [96]. As we aim to reduce a large number of forecast scenarios to a small number of scenarios in the tree, forward selection appears beneficial in our case.

9.3.2 *Forward selection*

In what follows, basics on forward selection are introduced. Note that this introduction is heavily based on [96, 169].

If only one a priori unknown scenario $n \in \mathbb{I}$ is kept, i.e., $|\mathbb{L}| = N_\Omega - 1$, then (9.16) becomes

$$\min_{\substack{n\in\mathbb{I}\\ \mathbb{L}=\mathbb{I}\setminus\{n\}}} D_{\mathbb{L}}. \tag{9.17}$$

With $\mathbb{L} = \mathbb{I} \setminus \{n\}$, $\overline{\mathbb{L}} = \{n\}$ and (9.15a), this becomes

$$\min_{n\in\mathbb{I}} \sum_{l\in\mathbb{L}} \pi^l \min_{i\in\{n\}} \|\hat{w}^i(k+j|k) - \hat{w}^l(k+j|k)\|_2 \tag{9.18a}$$

$$\iff \min_{n\in\mathbb{I}} \sum_{l\in\mathbb{I}\setminus\{n\}} \pi^l \|\hat{w}^n(k+j|k) - \hat{w}^l(k+j|k)\|_2. \tag{9.18b}$$

Thus, the scenario $n^\star \in \mathbb{I}$ that is kept is

$$n^\star \in \arg\min_{n\in\mathbb{I}} \sum_{l\in\mathbb{I}\setminus\{n\}} \pi^l \|\hat{w}^n(k+j|k) - \hat{w}^l(k+j|k)\|_2. \tag{9.19}$$

In forward selection, this strategy is repetitively applied by successively adding scenarios to the set of kept ones $\overline{\mathbb{L}}$. This principle is sketched in Algorithm 2.

In Algorithm 2, first the set of all scenarios, $\mathbb{I}$ is initialized. Furthermore, the set of initially removed scenarios, $\mathbb{L}^0$, is

1: $\mathbb{I} \leftarrow \mathbb{N}_{[1,N_\Omega]}$
2: $\mathbb{L}^0 \leftarrow \mathbb{I}$
3: **for** $i = 1, \ldots, b_j^d$ **do**
4: $\quad \overline{\mathbb{L}}^{i-1} \leftarrow \mathbb{I} \setminus \mathbb{L}^{i-1}$
5: $\quad n_i \in \arg\min_{n \in \mathbb{L}^{i-1}} D_{\mathbb{L}^{i-1} \setminus \{n\}}$
6: $\quad \mathbb{L}^i \leftarrow \mathbb{L}^{i-1} \setminus \{n_i\}$
7: Apply optimal redistribution (9.15) to $\mathbb{L}^{b_j^d}$

Algorithm 2: Forward selection according to [169, Algorithm 4].

set to contain all scenarios. Then, in line 4 the set of kept scenarios $\overline{\mathbb{L}}^{i-1}$ is updated. For $i = 1$, this is $\overline{\mathbb{L}}^0 = \emptyset$, for $i = 2$, this is $\overline{\mathbb{L}}^1 = \{n_1\}$, $n_1 \in \mathbb{I}$, for $i = 3$, this is $\overline{\mathbb{L}}^2 = \{n_1, n_2\}$, $n_2 \in \mathbb{I}$, and so on. Then, in line 5 an additional scenario $n_i \in \mathbb{I}$ that leads to a minimum quantization error is identified. With (9.15a), line 5 has the form

$$n_i \in \arg\min_{n \in \mathbb{L}^{i-1}} \sum_{l \in \mathbb{L}^{i-1} \setminus \{n\}} \pi^l \min_{\tilde{n} \in \overline{\mathbb{L}}^{i-1} \cup \{n\}} \| w^{\tilde{n}}(k+j|k) - w^l(k+j|k) \|_2. \tag{9.20}$$

Then, in line 6 the current set of reduced scenarios $\mathbb{L}^i$ is determined by excluding n_i from $\mathbb{L}^{i-1}$.

Note that in Chapter 12, fast forward selection as described in [96, Algorithm 2.4] and [78, Algorithm 2] was used. Fast forward selection is an implementation of Algorithm 2 that has lower computational complexity but is a solution of the forward selection principle (see [96, Theorem 2.5]).

In Figure 9.9, Algorithm 2 is illustrated. Here, the number of initial scenarios is $N_\Omega = 11$ and the number of kept scenarios is $b_j^d = 4$. The identified scenarios are $n_1 = 7$, $n_2 = 10$, $n_3 = 11$, $n_4 = 1$ as indicated in Figure 9.9(b) by the red color. After the scenarios are identified, optimal redistribution (9.15) is applied to $\mathbb{L}^{b_j^d} = \{1, \ldots, 11\} \setminus \{1, 7, 10, 11\}$. Using (9.15b), the sets of optimally assigned scenarios are determined as $\widetilde{\mathbb{L}}(1) = \{5, 6, 9\}$, $\widetilde{\mathbb{L}}(7) = \{2, 3, 4, 8, 12\}$, $\widetilde{\mathbb{L}}(10) = \emptyset$ and $\widetilde{\mathbb{L}}(11) = \emptyset$. In Figure 9.9(c), this assignment is indicated by arrows. With (9.15c), the probabilities of the selected scenarios are then determined as $\tilde{\pi}^1 = 4/12$, $\tilde{\pi}^7 = 6/12$, $\tilde{\pi}^{10} = 1/12$ and $\tilde{\pi}^{11} = 1/12$. In Figure 9.9(d), the updated probabilities are illustrated by different dot sizes.

9.3.3 *Forward tree construction*

The forward selection strategy described in the last section can now be used to construct scenario trees from collections of independent forecast scenarios. More precisely, it can be used to construct scenario trees from multi-stage scenarios

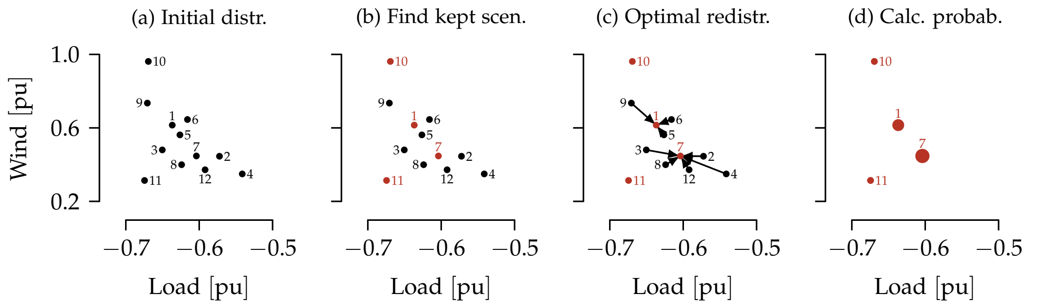

Figure 9.9: Forward selection following [169, Algorithm 4] for $b_j^d = 4$. The kept scenarios are $\overline{\mathbb{L}}^4 = \{1, 7, 10, 11\}$. Figure motivated by [183].

$\hat{w}^i(k+j|k)$ for $i \in \mathbb{N}_{[1,N_\Omega]}$ and $j = 1, \ldots, J$. The algorithm presented here is closely related to [97, Algorithm 4], [98, Algorithm 4.5] and [99, Algorithm 3.2]. However, these algorithms determine the number of scenarios using a fixed tolerance between the original probability distribution and the one of the tree. Opposed to this, we use a fixed number of branches b_j^d at prediction instant j to explicitly shape the scenario tree's structure.

1: $\mathbb{I}_1^1 \leftarrow \{1, \ldots, N_\Omega\}$, $\mathcal{I}_1 \leftarrow \{\mathbb{I}_1^1\}$
2: **for** $j = 1, \ldots, J$ **do**
3:     $\mathcal{I}_{j+1} \leftarrow \emptyset$, $i \leftarrow 0$
4:     **for** $l = 1, \ldots, |\mathcal{I}_j|$ **do**   ▷ Note that $\mathcal{I}_j = \{\mathbb{I}_j^1, \ldots, \mathbb{I}_j^{|\mathcal{I}_j|}\}$
5:         $\overline{\mathbb{L}}_j^l \leftarrow$ scenario reduction for $\mathbb{I} = \mathbb{I}_j^l$ and $|\overline{\mathbb{L}}_j^l| = b_j^d$
6:         **for** $n \in \overline{\mathbb{L}}_j^l$ **do**
7:             $i \leftarrow i + 1$
8:             $\mathbb{I}_{j+1}^i \leftarrow \{n\} \cup \widetilde{\mathbb{L}}_j^l(n)$
9:             $\mathcal{I}_{j+1} \leftarrow \mathcal{I}_{j+1} \cup \{\mathbb{I}_{j+1}^i\}$

Algorithm 3: Forward tree construction following [169, Algorithm 5].

The idea behind forward tree construction, as sketched in Algorithm 3, is to repeatedly apply scenario reduction to nodes with a common ancestor. In the algorithm, $\mathbb{I}_j^l$ is the set of nodes that are part of cluster $l \in \mathbb{N}$ at prediction step $j \in \mathbb{N}_{[1,J]}$, i.e., nodes that share the same ancestor at $j-1$. Moreover, the set of all clusters at prediction step j is $\mathcal{I}_j = \{\mathbb{I}_j^1, \ldots, \mathbb{I}_j^{|\mathcal{I}_j|}\}$. Note that the scenario reduction in line 5 only leads to $|\overline{\mathbb{L}}_j^l| = b_j^d$ if $\mathbb{I}_j^l$ includes a sufficient number of elements. If that is not the case, then $\overline{\mathbb{L}}_j^l = \mathbb{I}_j^l$.

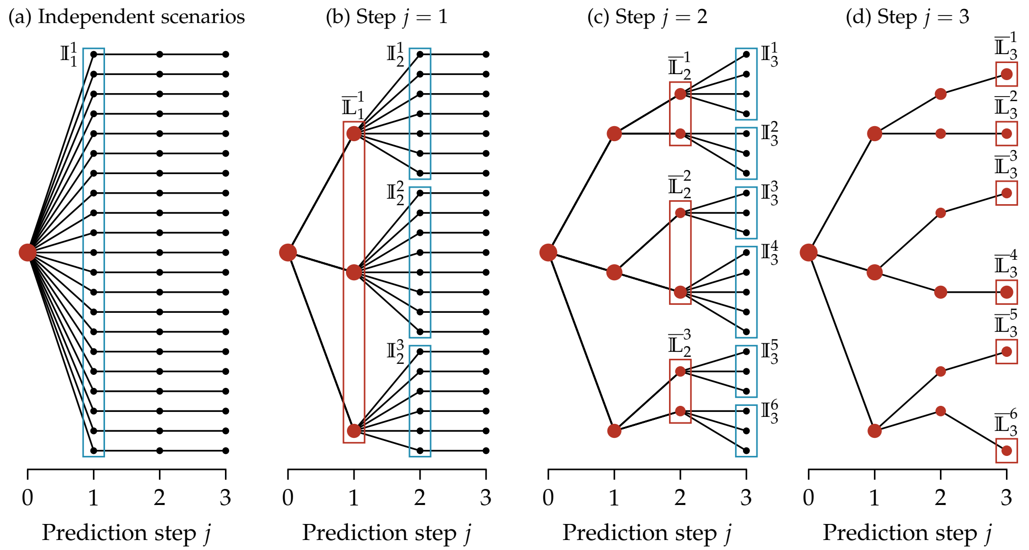

Figure 9.10: Forward tree construction following [169, Algorithm 5]. The scenario tree was determined for branching factors $[b_1^d, b_2^d, b_3^d]^\top = [3, 2, 1]^\top$. Figure motivated by [183].

In what follows, Algorithm 3 is discussed for the scenarios and the resulting tree in Figure 9.10. First, the set $\mathcal{I}_1$ is initialized with the cluster $\mathbb{I}_1^1$ as illustrated in Figure 9.10(a). Then, in line 3 $\mathcal{I}_2$ is initialized as an empty set and the iterator i is set to 0. Afterwards, scenario reduction is applied to $\mathbb{I}_1^l$ for scenarios in the set $\{\hat{w}^i(k+1|k)\}_{i\in\mathbb{I}_1^1}$ and a branching factor $b_1^d = 3$ using, e.g., forward selection (see Algorithm 2). This results in the set of reduced and kept scenarios, $\mathbb{L}_1^1$ and $\overline{\mathbb{L}}_1^1$ as illustrated in Figure 9.10(b). Based on these sets, the clusters for $j = 2$ can be determined by iterating through all kept nodes in $\overline{\mathbb{L}}_1^1$ and successively assigning nodes with the smallest distance to the kept node to the sets $\mathbb{I}_2^i$ in line 8. These are identified using a modified version of (9.15b) that reads

$$\widetilde{\mathbb{L}}_j^l(n^\star) = \left\{ m \in \mathbb{L}_j^l \mid n^\star \in \arg\min_{n\in\overline{\mathbb{L}}_j^l} \|\hat{w}^n(k+j|k) - \hat{w}^m(k+j|k)\|_2 \right\}. \tag{9.21}$$

In Figure 9.10(b) this is illustrated for the sets $\mathbb{I}_2^1$, $\mathbb{I}_2^2$, $\mathbb{I}_2^3$. Finally, the resulting sets are used to form $\mathcal{I}_2 = \{\mathbb{I}_2^1, \mathbb{I}_2^2, \mathbb{I}_2^3\}$.

Then, the same procedure is applied for $j = 2$. First, $\mathcal{I}_3$ is initialized as an empty set and the iterator i is set to 0. Then, scenario reduction is applied for all clusters in $\mathcal{I}_2$ in line 5 of Algorithm 3. For each cluster $l = 1, \ldots, |\mathcal{I}_2|$, the

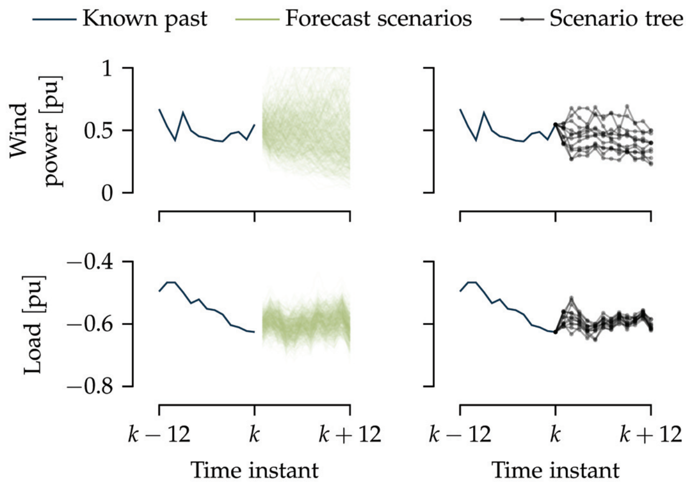

Figure 9.11: Independent forecast scenarios of wind turbine, PV power plant and load as well as resulting scenarios tree. The tree was generated from 500 forecast scenarios, a prediction horizon of $J = 12$ and branching factors $[b_j^d]_{j=1}^{12} = [6, 2, 1, 1, \ldots, 1]^\top$.

resulting sets of kept nodes $\overline{\mathbb{L}}_2^l$ are then used to form clusters $\mathbb{I}_3^i$ which become elements of the set $\mathcal{I}_3$. This is illustrated in Figure 9.10(c) for a branching factor $b_2^d = 2$ and resulting set of clusters $\mathcal{I}_3 = \{\mathbb{I}_3^1, \ldots, \mathbb{I}_3^6\}$.

This procedure is then repeated for the remaining time instants until the leaf nodes at prediction time instant J are determined. In Figure 9.10(d) this is shown for $J = 3$ and a branching factor $b_3^d = 1$.

Note that for $j = J$, the calculation of clusters for prediction time instant $J + 1$ in lines 6–9 is not required and was only kept for readability in Algorithm 3.

The resulting tree can now be transformed into a scenario tree that follows the notation in Section 9.1. Therefore, the sets $\overline{\mathbb{L}}_j^l$ and $\mathbb{I}_j^l$ for $j = 1, \ldots, J$ and $l = 1, \ldots, |\mathcal{I}_j|$ can be used to number the nodes and formulate the functions $\mathrm{anc}(\cdot)$ and $\mathrm{child}(\cdot)$ for every node. The $\mathrm{stage}(\cdot)$ function can be formulated using the fact that all sets are indexed by stage j. Furthermore, together with the number of scenarios, N_Ω and the sets $\overline{\mathbb{L}}_j^l$, $\mathbb{I}_j^l$, the probabilities $\pi^{(\cdot)}$ of the nodes can be calculated. The values the nodes $\hat{w}^{(\cdot)}$ can be determined from the known $\hat{w}^i(j + k|k)$ for all kept nodes.

Example 9.3.1 (Forward tree generation)**.** In Figure 9.11, Algorithm 3 was used to construct a scenario tree for the independent forecast scenarios from Figures 6.5 and 6.9. For easier understanding, the forecast scenarios from these figures are shown in the left plots. In the right plots, the values of the scenario trees are shown. Note that the disturbance at node 0 was set to $\hat{w}^{(0)} = [w_{\mathrm{r},1}(k)\ w_{\mathrm{d},1}(k)]^\top$ to illustrate that all nodes have a common root node. However, the values of the root node are not used in the scenario-based MPC formulations as discussed in Section 9.2.

9.4 *Summary*

In this chapter, scenario trees were introduced. The relation of the nodes and the associated probabilities as well as the relation of decision variables and costs were discussed. Furthermore, the generation of scenario trees from independent forecast scenarios was sketched.

With the introduction given in this chapter, different scenario-based MPC approaches can be deduced: In Chapter 10, a risk-neutral stochastic MPC scheme that minimizes the expected cost is presented. Furthermore, a risk-averse approach that allows to continuously interpolate between worst-case and risk-neutral stochastic MPC is derived in Chapter 11.

10 Risk-neutral stochastic MPC

In Chapter 8, a minimax approach that assumes forecasts of the uncertain available renewable infeed and load in the form of robust intervals was presented. This approach minimizes the worst-case cost considering bounded uncertain forecast intervals. One drawback of the approach is that it tends to be overly conservative as the worst-case disturbance might only occur very rarely. This conservativeness can be overcome by considering more complex forecast probability distributions, e.g., the scenario trees introduced in Chapter 9.

The main contributions of this chapter are as follows. Motivated by [22, 103, 158, 178], a scenario-based risk-neutral stochastic MPC formulation for the operation of islanded MG is derived. Based on the model from Chapter 4, the MPC problem is formulated as an MIQP that can be solved by available numerical solvers. In the MPC, the expected cost from Chapter 5 is minimized assuming forecast probability distributions of load and available renewable infeed in the form of scenario trees as introduced in Chapter 9. The presented scenario-based approach is fundamentally different from the controllers derived in the previous chapters. As opposed to the certainty equivalence MPC from Chapter 7, the approach provides robustness to uncertain load and available renewable infeed by considering multiple forecast scenarios. Moreover, compared to the minimax MPC from Chapter 8 and the certainty equivalence MPC, a more complex[1] forecast probability distribution in the form of scenarios is considered. Furthermore, as opposed to both approaches, feedback is taken into account in the MPC formulation by considering

An overview of risk-neutral stochastic approaches in MG operation control can be found in Section 1.3.3.

[1] Recall that only the mean value of the forecasts was considered in the certainty equivalence MPC in Chapter 7. Further recall that in the minimax MPC in Chapter 8, forecast intervals without any probabilistic information were employed.

different control input trajectories. We will see that these differences will lead to less conservative control actions that are robust to uncertain load and renewable infeed.

In what follows, a scenario-based risk-neutral stochastic MPC formulation that can be used for the operation of islanded MGs is derived. First, an introduction of the expectation operator and expectation mappings in the context of scenario trees is given in Section 10.1. Then, a risk-neutral stochastic MPC problem is formulated in Section 10.2. This formulation employs conditional expectation mappings on scenario trees and thereby allows to minimize the expected multi-stage cost. Finally the risk-neutral stochastic MPC is used in a small simulation example in Section 10.3.

Please note that Section 10.1.2 is based on the author's work [93, Section VI]. Further, note that the MPC formulation in Section 10.2 was published in the author's work [91].

10.1 Expectation

In the risk-neutral stochastic MPC formulation presented in this chapter, the expected cost over all scenarios is minimized. To formulate this cost, stage-wise expectation and conditional expectation on scenario trees need to be introduced.

10.1.1 Stage-wise expectation

Consider a scenario tree with stage-wise discrete probability distributions as introduced in Section 9.1.3. The probability distribution at stage $j \in \mathbb{N}_{[0,J]}$, has sample space nodes(j), a random variable with corresponding vector $\ell_j = [\ell^{(i)}]_{i \in \mathrm{nodes}(j)}$ and probabilities $\pi_j = [\pi^{(i)}]_{i \in \mathrm{nodes}(j)}$. Then, the stage-wise expected cost is [25]

Recall from Section 9.2 that $\ell^{(i)}$ represents the cost at node $i \in \mathbb{N}_{[1,N_\mathrm{n}]}$.

$$\mathbf{E}_{\pi_j}(\ell_j) = \sum_{i \in \mathrm{nodes}(j)} \pi^{(i)} \ell^{(i)} = \pi_j^\top \ell_j. \tag{10.1}$$

10.1.2 Conditional expectation on scenario trees

Using the expected cost for sample space nodes(j) in (10.1), we can deduce conditional expectation mappings on scenario trees. These mappings allow to model how the expected cost at stage $j \in \mathbb{N}_{[0,J-1]}$ of a scenario tree depends on the expected cost at stage $j+1$ using conditional expectation [240, 241]. In detail, they allow to model the fact that the decision at every non-leaf node $i \in \operatorname{nodes}(j)$, also depends on the decisions taken at the children of i.

Recall that at each stage $j \in \mathbb{N}_{[0,J-1]}$, a probability space can be formed. This probability space is composed of the sample space $\operatorname{nodes}(j)$, random variables with values collected in ℓ_j and corresponding probabilities collected in π_j. Naturally, the same can be done with the sample space $\operatorname{nodes}(j+1)$, costs ℓ_{j+1} and probabilities π_{j+1}. Conditional expectation mappings are used to link the probability space at stage $j+1$ to the probability space at stage j. Such a mapping at stage j has the general form

$$\mathbf{E}_j : \mathbb{R}^{|\operatorname{nodes}(j+1)|} \to \mathbb{R}^{|\operatorname{nodes}(j)|}. \tag{10.2}$$

As described in Section 9.1.3, we can partition the probability space associated with stage $j+1$ into disjoint probability spaces $\operatorname{child}(i)$, $i \in \operatorname{nodes}(j)$ with corresponding vectors of costs and probabilities of the child nodes, $\ell^{[i]}$ and $\pi^{[i]}$. For every subspace we can compute the expectation $\mathbf{E}_{\pi^{[i]}}(\ell^{[i]})$. Combining $\mathbf{E}_{\pi^{[i]}}(\ell^{[i]})$ for all subspaces, i.e., for all $i \in \operatorname{nodes}(j)$, we can define the conditional expectation conditioned at stage $j \in \mathbb{N}_{[0,J-1]}$ as

Recall from (9.5) that
$\pi^{[i]} = \frac{1}{\pi^{(i)}}\left[\pi^{(i_+)}\right]_{i_+ \in \operatorname{child}(i)}$,
$\ell^{[i]} = \left[\ell^{(i_+)}\right]_{i_+ \in \operatorname{child}(i)}$.

$$\mathbf{E}_j(\ell_{j+1}) = \left[\, \mathbf{E}_{\pi^{[i]}}(\ell^{[i]})\right]_{i \in \operatorname{nodes}(j)}. \tag{10.3}$$

Roughly speaking, based on the probability distribution associated with ℓ_{j+1}, the mapping (10.3) provides a vector where the ith entry represents the expected cost of the child nodes given that node $i \in \operatorname{nodes}(j)$ is visited. In the following example, this is discussed for the tree in Figure 10.1.

Example 10.1.1. Consider the simple scenario tree in Figure 10.1. Here the vector associated with the probability space at stage $j = 2$ is $\ell_2 = [\ell^{(3)} \ \cdots \ \ell^{(7)}]^\top$. Following the tree structure, $\operatorname{nodes}(2)$ is partitioned into $\operatorname{child}(1) = \{3,4,5\}$ and $\operatorname{child}(2) = \{6,7\}$. Consequently, we can from two probability subspaces with vectors $\ell^{[1]} = [\ell^{(3)} \ \ell^{(4)} \ \ell^{(5)}]^\top$ and $\pi^{[1]} = 1/\pi^{(1)}[\pi^{(3)} \ \pi^{(4)} \ \pi^{(5)}]^\top$ as well as $\ell^{[2]} = [\ell^{(6)} \ \ell^{(7)}]^\top$ and $\pi^{[2]} = 1/\pi^{(2)}[\pi^{(6)} \ \pi^{(7)}]^\top$. Using the expectation operator, we can determine the expected cost of the child nodes given that

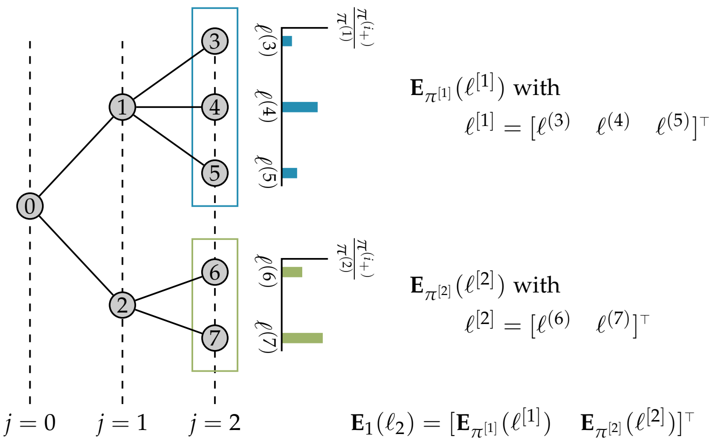

Figure 10.1: Example of scenario tree with conditional probability mapping conditioned at stage 1. Motivated by [93].

node 1 is visited as

$$\mathbf{E}_{\pi^{[1]}}(\ell^{[1]}) = \mathbf{E}_{\pi^{[1]}}([\ell^{(3)} \quad \ell^{(4)} \quad \ell^{(5)}]^\top) \tag{10.4a}$$

and the expected cost of the child nodes given that node 2 is visited as

$$\mathbf{E}_{\pi^{[2]}}(\ell^{[2]}) = \mathbf{E}_{\pi^{[1]}}([\ell^{(6)} \quad \ell^{(7)}]^\top). \tag{10.4b}$$

Combining (10.4a) and (10.4b), the conditional expectation conditioned at stage 1 can be derived as

$$\mathbf{E}_1(\ell_2) = \mathbf{E}_1([\ell^{(3)} \quad \cdots \quad \ell^{(7)}]^\top) = \begin{bmatrix} \mathbf{E}_{\pi^{[1]}}([\ell^{(3)} \quad \ell^{(4)} \quad \ell^{(5)}]^\top) \\ \mathbf{E}_{\pi^{[2]}}([\ell^{(6)} \quad \ell^{(7)}]^\top) \end{bmatrix}. \tag{10.4c}$$

10.2 *MPC problem formulation*

Broadly speaking, the expected cost at each node $i \in \text{nodes}(j)$ of stage $j \in \mathbb{N}_{[1,J-1]}$ is composed of the expected cost of the node itself and the expected cost of the nodes that follow this node, i.e., the child nodes, their children, and so on. For the sequence of random variables with associated cost vectors $(\ell_1, \dots, \ell_J)$ from (9.11), this is captured in the nested multi-stage expectation [241], which is defined as

$$\widetilde{\mathbf{E}}_J(\ell_1, \dots, \ell_J) = \mathbf{E}_0\left(\ell_1 + \mathbf{E}_1\left(\ell_2 + \dots + \mathbf{E}_{J-1}(\ell_J)\right) \dots\right). \tag{10.5}$$

Note that this equation makes extensive use of conditional expectation mappings of the form (10.3).

Example 10.2.1. For the simple scenario tree in Figure 10.1, the nested multi-stage expectation (10.5) is

$$\widetilde{\mathbf{E}}_2(\ell_1, \ell_2) = \mathbf{E}_0(\ell_1 + \mathbf{E}_1(\ell_2)) \tag{10.6a}$$

with

$$\mathbf{E}_1(\ell_2) = \begin{bmatrix} \mathbf{E}_{\pi^{[1]}}([\ell^{(3)} \quad \ell^{(4)} \quad \ell^{(5)}]^\top) \\ \mathbf{E}_{\pi^{[2]}}([\ell^{(6)} \quad \ell^{(7)}]^\top) \end{bmatrix}. \tag{10.6b}$$

From (10.3) it follows that $\mathbf{E}_0(\ell_1) = \left[\mathbf{E}_{\pi^{[i]}}(\ell^{[i]})\right]_{i \in \mathrm{nodes}(0)}$, i.e., $\mathbf{E}_0(\ell_1) = \mathbf{E}_{\pi^{[0]}}(\ell^{[0]})$ with $\pi^{[0]} = {}^1\!/_{\pi^{(0)}}[\pi^{(1)} \ \pi^{(2)}]$ and $\ell^{[0]} = [\ell^{(1)} \ \ell^{(2)}]^\top$. Thus, (10.6a) can be transformed into

$$\widetilde{\mathbf{E}}_2(\ell_1, \ell_2) = \mathbf{E}_{\pi^{[0]}}\left(\begin{bmatrix} \ell^{(1)} + \mathbf{E}_{\pi^{[1]}}([\ell^{(3)} \quad \ell^{(4)} \quad \ell^{(5)}]^\top) \\ \ell^{(2)} + \mathbf{E}_{\pi^{[2]}}([\ell^{(6)} \quad \ell^{(7)}]^\top) \end{bmatrix}\right). \tag{10.6c}$$

Using (10.1) and $\pi^{(0)} = 1$, this becomes

$$\begin{aligned} \widetilde{\mathbf{E}}_2(\ell_1, \ell_2) &= \frac{[\pi^{(1)} \quad \pi^{(2)}]}{\pi^{(0)}} \begin{bmatrix} \ell^{(1)} + \frac{\pi^{(3)}\ell^{(3)} + \pi^{(4)}\ell^{(4)} + \pi^{(5)}\ell^{(5)}}{\pi^{(1)}} \\ \ell^{(2)} + \frac{\pi^{(3)}\ell^{(6)} + \pi^{(7)}\ell^{(7)}}{\pi^{(2)}} \end{bmatrix} \\ &= \sum_{i=1}^{7} \pi^{(i)}\ell^{(i)} = \mathbf{E}_{\pi_1}(\ell_1) + \mathbf{E}_{\pi_2}(\ell_2). \end{aligned} \tag{10.6d}$$

This motivates the formulation of the following proposition.

Proposition 10.2.2. The nested multi-stage expectation (10.5) can be equally expressed as

$$\widetilde{\mathbf{E}}_J(\ell_1, \ldots, \ell_J) = \sum_{j=1}^{J} \mathbf{E}_{\pi_j}(\ell_j). \tag{10.7}$$

Proof. As the expectation operator is linear [25], we can equally state (10.5) as

$$\widetilde{\mathbf{E}}_J(\ell_1, \ldots, \ell_J) = \mathbf{E}_0(\ell_1) + \mathbf{E}_0\left(\mathbf{E}_1\left(\ell_2 + \ldots + \mathbf{E}_{J-1}(\ell_J)\right) \ldots\right) \tag{10.8a}$$

$$\begin{aligned} &\vdots \\ &= \mathbf{E}_0(\ell_1) + \mathbf{E}_0(\mathbf{E}_1(\ell_2)) + \\ &\qquad \ldots + \mathbf{E}_0(\mathbf{E}_1(\ldots \mathbf{E}_{J-2}(\mathbf{E}_{J-1}(\ell_J)) \ldots)). \end{aligned} \tag{10.8b}$$

Moreover, because of the way the conditional expectation mapping (10.3) is defined, we have that

$$\mathbf{E}_{\pi_j}(\ell_j) = \mathbf{E}_0(\mathbf{E}_1(\ldots \mathbf{E}_{j-2}(\mathbf{E}_{j-1}(\ell_j)) \ldots))$$

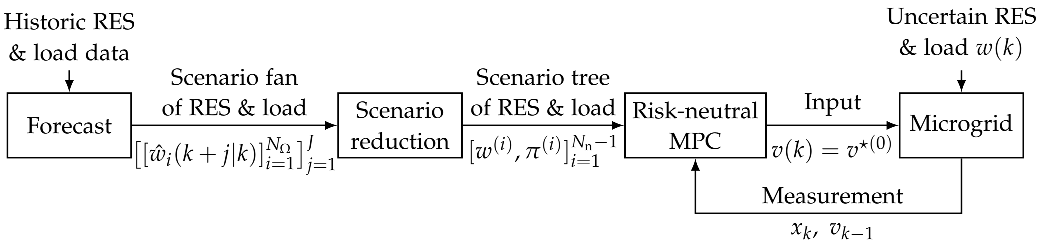

Figure 10.2: Risk-neutral stochastic MPC scheme for operation of islanded MGs at time instant k.

which is known as the tower property of conditional expectation [192, 241]. Therefore, (10.8b) can be equally stated as

$$\widetilde{\mathbf{E}}_J(\ell_1, \ldots, \ell_J) = \mathbf{E}_{\pi_1}(\ell_1) + \mathbf{E}_{\pi_2}(\ell_2) + \ldots + \mathbf{E}_{\pi_J}(\ell_J). \qquad (10.9)$$

which is equivalent to (10.7) completing the proof. □

With (10.7), we can formulate a risk-neutral MPC problem for the operation of islanded MG. Therefore, we consider a forecast of load and available renewable infeed in the form of a scenario tree. Thus, the constraints that model the islanded MG are given by (9.10) and the decision variables are the control inputs $\boldsymbol{v} = [v^{(i)}]_{i \in \mathbb{N}_{[0,N_n-1]} \setminus \text{nodes}(J)}$ as well as the states $\boldsymbol{x} = [x^{(i)}]_{i \in \mathbb{N}_{[1,N_n-1]}}$ and the auxiliary variables $\boldsymbol{z} = [z^{(i)}]_{i \in \mathbb{N}_{[1,N_n-1]}}$. This results in the following risk-neutral stochastic MPC problem.

As discussed in Remark 9.2.3, the control input $[v^{(i)}]_{i \in \text{nodes}(J)}$ is not part of the MPC problem.

Problem 6 (Risk-neutral stochastic MPC of islanded MGs). Solve the optimization problem

$$\min_{\boldsymbol{v},\boldsymbol{x},\boldsymbol{z}} \sum_{j=1}^{J} \mathbf{E}_{\pi_j}(\ell_j)$$

subject to

constraints (9.10),
$\forall i_+ \in \mathbb{N}_{[1,N_n-1]}$ and $i = \text{anc}(i_+)$,
with given initial conditions $x^{(0)} = x_k$ and $v^{(0_-)} = v_{k-1}$.

10.2.1 *MPC scheme*

For the operation of an islanded MG, Problem 6 is embedded into the control scheme in Figure 10.2. Before solving the risk-neutral stochastic MPC problem, a new collection of forecast scenarios of load and available renewable infeed is obtained (see Chapter 6). These scenarios are then transformed into a scenario tree using scenario reduction (see Chapter 9). Together with the measurements of the current state x_k and the control input v_{k-1} that was applied in the most recent time instant, the scenario tree is used as an input to the MPC. For these inputs, the risk-neutral stochastic MPC formulation in Problem 6 is then solved. From the resulting optimal input trajectory, the value associated with the first prediction instant $v^{\star(0)}$ is applied to the MG plant. At the next sampling instant, the scenario tree and the measurements are updated and Problem 6 is solved repeatedly in a receding horizon fashion (see, e.g., [18, 23, 204] and Section 3.2). An example of optimal trajectories obtained via Problem 6 is discussed in the next section.

10.3 *Example*

In Figure 10.3 on page 146, the forecast of the uncertain input, power, power setpoints and stored energy are shown. They were derived by solving Problem 6 with initial conditions $\delta_{\mathrm{t}}^{(0_-)} = 0$ and $x^{(0)} = 0.5\,\mathrm{pu\,h}$ for the running example[2] in Figure 4.1. The scenario tree was generated from the collections of independent forecast scenarios in Figure 9.11. Before deducing the scenario tree, the independent forecast scenarios of available renewable power were scaled for a rated wind turbine power of 2 pu.

[2] The unit parameters and the weights of the cost function can be found in Tables 12.1 and 12.2.

It can be observed in Figure 10.3 that, as discussed in Section 9.2, there only exists one power setpoint for each unit between $j = 0$ and $j = 1$. Furthermore, it can be observed that between $j = 0$ and $j = 1$ multiple forecasts of the uncertain input as well as multiple power values exist. Moreover, different state trajectories result from these power values.

Comparing the optimal trajectories of this example with the ones from the minimax MPC in Section 8.5, it can be noted that the power setpoints of the risk-neutral stochastic approach lead to scenarios with a higher share of renewable infeed. For the risk-neutral stochastic MPC, there is not a single scenario where the conventional generator needs to be

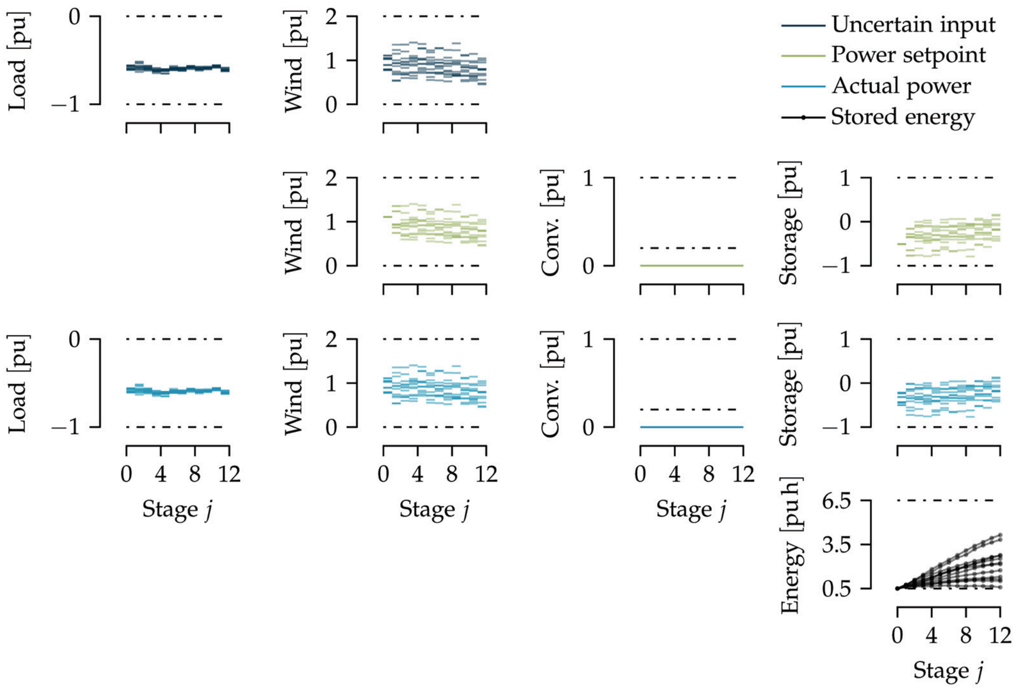

Figure 10.3: Open-loop trajectories of risk-neutral stochastic MPC.

enabled, whereas for the minimax MPC it is enabled in the first time instant right away.

Considering the worst case in the minimax MPC also results in lower limits for the renewable unit. As shown in Table 10.1, the power setpoint $u_{\mathrm{r}}(k)$ of the renewable unit increases significantly when using the risk-neutral stochastic approach instead.

Table 10.1: Power setpoints of minimax and risk-neutral stochastic MPC.

	Minimax	Risk-n. stoch.
$u_{\mathrm{t}}(k)$	0.68	0
$u_{\mathrm{s}}(k)$	-0.62	-0.51
$u_{\mathrm{r}}(k)$	0.54	1.11

10.4 *Summary*

In this chapter a scenario-based risk-neutral stochastic MPC problem was formulated. This problem minimizes the expected multi-stage cost assuming a known probability distribution provided in the form of a scenario tree.

To derive the MPC problem, first the expected value of a probability distribution was introduced and conditional expectation mappings were discussed. These mappings allow to model how the expected cost is linked between the stages of a scenario trees. Using them, a scenario-based risk-neutral stochastic MPC problem was posed as an MIQP that can be solved by off-the-shelf software.

The presented approach satisfies the desired robustness to uncertain renewable generation in load that was requested in Section 2.3.6. However, it relies on an accurate forecast probability distribution of the scenario tree. In practical applications such as the operation of MG, these may not always be present (see Section 2.3.7). Therefore, a risk-averse MPC approach that allows to consider ambiguity in forecast probability distributions is derived in the next chapter.

11
Risk-averse MPC

In the previous chapter, a risk-neutral stochastic approach that employs scenario trees was presented. In the approach, the probability distribution of the scenario tree is fully trusted and the expected cost is minimized. For real-world applications it is desirable to use controllers that provide a certain robustness to misestimated probability distribution. Such approaches are often referred to as risk-averse.

In this chapter, a scenario-based risk-averse MPC approach is deduced. The presented controller makes use of the MG model from Chapter 4, the cost function from Chapter 5, and the scenario trees from Chapter 9. The main contributions of this chapter are twofold.

An overview of risk-averse approaches in power systems can be found in Section 1.3.4.

1. Motivated by [48, 118], a risk-averse MPC scheme that allows to consider uncertain probability values in scenario trees is derived. In this scheme, one can explicitly tune the trust in the probability distribution of the scenario trees by seamlessly interpolating between risk-neutral stochastic [91] where the probability distribution of the tree is fully trusted and worst-case [89] MPC where no probabilistic information is used. Additionally, risk-averse approaches come with the following benefits. (i) They render MPC suitable for applications where the probability distribution changes over time or is not exactly known. (ii) The provide robustness against poor forecast models and high-effect low-probability events. (iii) Scenario trees with fewer nodes can be used as the MPC considers uncertainty in the underlying probability distribution.

2. Following [247], an epigraph relaxation is used to formulate a risk-averse MPC approach in a computationally tractable way. The resulting MPC problem is posed as an MIQCP which can be solved online by existing software. This allows for sufficiently fast computing times such that the controller can be used for real-time operation control of islanded MG. Compared to other risk-averse approaches [32, 148, 160, 282], the presented formulation considers a multi-stage MPC problem that models how the risk of the different prediction steps is linked.

In what follows, a risk-averse MPC scheme for the operation of islanded MGs is derived. First, risk measures are introduced in Section 11.1. This includes a discussion on coherent risk measures such as AVaR. Then, a risk-averse MPC problem is posed in Section 11.2. Here, conditional risk mappings are employed to formulate a risk-averse MPC problem with nested risk mappings which is then posed as an MIQCP. Finally, in Section 11.3, the risk-averse MPC scheme is used in a small example assuming different rates of uncertainties in the probability distribution. Note that the results of this Chapter were published in the author's work [93].

11.1 Measuring risk

In this section we introduce the notion of risk measures and provide a few examples thereof. Furthermore, we will discuss one specific risk measure: the average value-at-risk (AVaR). Finally, conditional risk mappings are introduced.

11.1.1 Introduction

Roughly speaking, a risk measure can quantify the importance of extreme scenarios that have a low probability. More precisely, considering a discrete probability distribution formed from the nodes at stage j of a scenario tree (see Section 9.1.3), it is a mapping $\rho : \mathbb{R}^{|\operatorname{nodes}(j)|} \to \mathbb{R}$. Two widely known risk measures are the expectation operator and the maximum operator.

Recall from (10.1) that the expectation operator has the form

$$\mathbf{E}_{\pi_j}(\ell_j) = \sum_{i \in \text{nodes}(j)} \pi^{(i)} \ell^{(i)} = \pi_j^\top \ell_j. \tag{11.1}$$

The expectation operator is a risk-neutral risk measure [241] in the sense that no uncertainty regarding the probabilities π_j, i.e., no ambiguity[1], is assumed.

[1] In what follows, uncertainty regarding the probabilities π_j will be referred to as ambiguity.

The maximum operator is another risk measure. It provides the worst case of all possible values in ℓ_j, i.e.,

$$\max(\ell_j) = \max_{i \in \text{nodes}(j)} \ell^{(i)}. \tag{11.2}$$

The maximum operator considers maximum uncertainty regarding the probabilities π_j, i.e., maximum ambiguity.

With the probability simplex $\mathbb{D}_j$ from (9.3) and the expectation operator (11.1), the maximum operator can also be formulated as

$$\max(\ell_j) = \max_{\pi' \in \mathbb{D}_j} \mathbf{E}_{\pi'}(\ell_j). \tag{11.3}$$

Here, the maximum expectation over all probability vectors $\pi' \in \mathbb{D}_j$ is provided, i.e., (11.3) returns the highest cost of all possible probability distributions. Using a similar notation as in (11.3), we can express the expectation operator by

$$\mathbf{E}_{\pi_j}(\ell_j) = \max_{\pi' \in \{\pi_j\}} \mathbf{E}_{\pi'}(\ell_j). \tag{11.4}$$

Coherent risk measures. In this work we focus on coherent risk measures. Following [10, 218, 241], a risk measure is called coherent if it satisfies the following axioms.

Definition 11.1.1 (Coherent risk measure)**.** Consider two random variables on $\text{nodes}(j)$ with corresponding vectors ℓ_j and ℓ_j'. A risk measure $\rho : \mathbb{R}^{|\text{nodes}(j)|} \to \mathbb{R}$ is said to be coherent if it satisfies the following conditions [241, Definition 6.4.].

1. Convexity: $\rho(\lambda \ell_j + (1-\lambda)\ell_j') \leq \lambda \rho(\ell_j) + (1-\lambda)\rho(\ell_j')$ for all $\lambda \in [0,1]$.

2. Monotonicity: If $\ell_j \leq \ell_j'$, then $\rho(\ell_j) \leq \rho(\ell_j')$.

3. Translation equivariance: $\rho(a + \ell_j) = a + \rho(\ell_j)$ for all $a \in \mathbb{R}$.

4. Positive Homogeneity: $\rho(a\ell_j) = a\rho(\ell_j)$ for all $a \in \mathbb{R}_{\geq 0}$.

As stated in [241, Theorem 6.5], all coherent risk measures can be posed in a way that resembles (11.3) and (11.4) as

$$\rho(\ell_j) = \max_{\pi' \in \mathbb{A}_j} \mathbf{E}_{\pi'}(\ell_j). \tag{11.5}$$

Here, the set $\mathbb{A}_j \subseteq \mathbb{D}_j$ is called ambiguity set of ρ. If $\mathbb{A}_j$ is a closed and convex set that contains π_j, then and only then (11.5) is coherent [241, Theorem 6.7]. Equation (11.5) provides the maximum expectation with respect to the uncertain probability vector $\pi' \in \mathbb{A}_j$. Thus, we obtain the worst-case expectation of ℓ_j over all probabilities π' in $\mathbb{A}_j$ [262].

The maximum operator (11.2) can be obtained from (11.5) by assuming maximum ambiguity, i.e., the largest possible ambiguity set $\mathbb{A}_j = \mathbb{D}_j$ (see Figure 11.1(a)). The expectation operator can be obtained from (11.5) by assuming no ambiguity, i.e., the smallest possible ambiguity set with $\mathbb{A}_j = \{\pi_j\}$ (see Figure 11.1(c)). Thus, the maximum and the expectation operator represent two extreme cases of coherent risk measures, one where the ambiguity set has maximum size, $\mathbb{A}_j = \mathbb{D}_j$, and one where it has minimum size, $\mathbb{A}_j = \{\pi_j\}$. It is further possible to construct ambiguity sets of intermediate size to account for a certain ambiguity in the probability distribution, i.e., to consider distributions with probabilities that are within a certain range around π_j. The AVaR is a risk measure that includes such ambiguity sets of intermediate size as will be discussed in the next section.

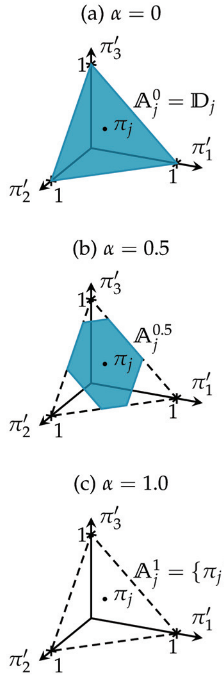

Figure 11.1: Ambiguity sets $\mathbb{A}_j^\alpha$ on three dimensional probability space with $\pi_j = [0.3\ 0.3\ 0.4]^\top$. Note that for $\alpha = 0$, the ambiguity set covers the entire probability simplex. For $\alpha = 1$, the ambiguity set only covers the point $\{\pi_j\}$. Source: [93].

11.1.2 *Average value-at-risk*

The average value-at-risk [191, 213, 241] is a widely adopted coherent risk measure. It is given in a form reminiscent of (11.5) as

$$\rho(\ell_j) = \mathrm{AV@R}_\alpha(\ell_j) = \max_{\pi' \in \mathbb{A}_j^\alpha} \mathbf{E}_{\pi'}(\ell_j). \tag{11.6a}$$

Other coherent risk measures are, for example, the entropic value-at-risk [1] and the mean-upper-semideviation of order p [241].

Here, for $\alpha \in [0, 1] \subset \mathbb{R}$, the ambiguity set is defined as

$$\mathbb{A}_j^\alpha = \begin{cases} \{\pi' \in \mathbb{D}_j \mid \pi' \leq \frac{1}{\alpha}\pi_j\}, & \text{if } \alpha \in (0, 1], \\ \mathbb{D}_j, & \text{if } \alpha = 0. \end{cases} \tag{11.6b}$$

In Figure 11.1, ambiguity sets of a three dimensional probability space for different values of α are shown. For $\alpha = 0$, the ambiguity set $\mathbb{A}_j^0$ covers the entire probability simplex, i.e., $\mathbb{A}_j^0 = \mathbb{D}_j$ and $\text{AV@R}_0(\ell_j) = \max_{\pi' \in \mathbb{D}_j} \mathbf{E}_{\pi'}(\ell_j) = \max(\ell_j)$ (see (11.3)). For $\alpha = 1$, the ambiguity set $\mathbb{A}_j^1$ only includes the point $\{\pi_j\}$ and $\text{AV@R}_1(\ell_j) = \max_{\pi' \in \{\pi_j\}} \mathbf{E}_{\pi'}(\ell_j) = \mathbf{E}_{\pi_j}(\ell_j)$ (see (11.4)). For $\alpha = 0.5$, the ambiguity set covers some parts of the probability simplex. As can be seen in Figure 11.1, for $\alpha_1 \geq \alpha_2$ it holds that $\mathbb{A}_j^{\alpha_1} \subseteq \mathbb{A}_j^{\alpha_2}$. As illustrated in [241, Example 6.19], with the additional free variable $t \in \mathbb{R}$ and convex duality arguments, (11.6) can be transformed into

$$\text{AV@R}_\alpha(\ell_j) = \begin{cases} \min\left(t + \mathbf{E}_{\pi_j}\left(\max(\frac{\ell_j - t}{\alpha}, 0)\right)\right), & \text{if } \alpha \in (0,1], \\ \max(\ell_j), & \text{if } \alpha = 0. \end{cases} \tag{11.7}$$

To facilitate the solution of the risk-averse optimal control problem in Section 11.2.2, another equivalent representation is now introduced. Note that the following proposition was published as part of the author's work [93, Proposition V.1].

Proposition 11.1.2. The AVaR at level $\alpha \in [0,1]$ is given by

$$\text{AV@R}_\alpha(\ell_j) = \min_{\substack{\xi \geq 0 \\ \alpha\xi \geq \ell_j - t}} (t + \mathbf{E}_{\pi_j}(\xi)). \tag{11.8}$$

Proof. Let $\alpha \in (0,1]$. Using the epigraph reformulation of $\max(\cdot, 0)$ from Lemma 3.3.2, we have that

$$\max(y, 0) = \min_{\substack{\xi \geq 0 \\ \xi \geq y}} \xi, \tag{11.9}$$

for all $y \in \mathbb{R}^K$ and slack variable $\xi \in \mathbb{R}^K$. Therefore,

$$\text{AV@R}_\alpha(\ell_j) = \min\left(t + \mathbf{E}_{\pi_j}\left(\max(\frac{\ell_j - t}{\alpha}, 0)\right)\right) \tag{11.10a}$$

$$= \min\left(t + \mathbf{E}_{\pi_j}\left(\min_{\substack{\xi \geq 0 \\ \xi \geq \frac{\ell_j - t}{\alpha}}} \xi\right)\right) \tag{11.10b}$$

$$= \min\left(t + \mathbf{E}_{\pi_j}\left(\min_{\substack{\xi \geq 0 \\ \alpha\xi \geq \ell_j - t}} \xi\right)\right), \tag{11.10c}$$

where (11.10b) is derived via (11.9). Using [241, Proposition 6.60], we interchange the expectation $\mathbf{E}_\pi$ and the minimum operator to arrive at (11.8).

The right-hand side of (11.8) is well defined for $\alpha = 0$ as

$$\begin{aligned} \mathrm{AV@R}_0(\ell_j) &= \min_{\substack{\xi \geq 0 \\ t \geq \ell_j}} (t + \mathbf{E}_\pi(\xi)) && (11.11a) \\ &= \min_{t \geq \ell_j} t + \min_{\xi \geq 0} \mathbf{E}_\pi(\xi) && (11.11b) \\ &= \min_{t \geq \ell_j} t + 0 && (11.11c) \\ &= \max(\ell_j). && (11.11d) \end{aligned}$$

Consequently, (11.8) holds for all $\alpha \in [0, 1]$. □

11.1.3 Conditional risk on scenario trees

In the last section, risk measures were defined separately for each stage j of a scenario tree, i.e., for each sample space nodes(j). In what follows, we will see how risk at stage $j \in \mathbb{N}_{[0,J-1]}$ of a scenario tree depends on risk at stage $j+1$ using conditional risk mappings. These mappings generalize conditional expectation [217, 241] from Section 10.1.2 and model the fact that the decision at every non-leaf node $i \in$ nodes(j), depends on the knowledge of the probability distribution at its child nodes.

For more information on conditional risk mappings, the reader is kindly referred to [191, 192, 241].

Recall that the set nodes(j) at stage $j \in \mathbb{N}_{[0,J-1]}$ is associated with a probability space with costs ℓ_j and probabilities π_j. Similarly, the set nodes$(j+1)$ is associated with a probability space with costs ℓ_{j+1} and probabilities π_{j+1}. Conditional risk mappings link the probability space at stage $j+1$ to the probability space at stage j. Generally speaking, the mapping at stage j has the form

$$\rho_j : \mathbb{R}^{|\,\mathrm{nodes}(j+1)|} \to \mathbb{R}^{|\,\mathrm{nodes}(j)|} \qquad (11.12)$$

and is composed as follows.

As described in Section 9.1.3, the probability space associated with stage $j+1$ can be partitioned into disjoint subspaces child(i) with vectors $\ell^{[i]}$ and $\pi^{[i]}$. For every subspace, we compute the risk $\rho(\ell^{[i]})$ using a coherent risk measure $\rho : \mathbb{R}^{|\,\mathrm{child}(i)|} \to \mathbb{R}$. Combining the risk of all subspaces, we define the conditional risk mapping conditioned at stage $j \in \mathbb{N}_{[0,J-1]}$ as

Recall from (9.5) that
$$\pi^{[i]} = \tfrac{1}{\pi^{(i)}} \left[\pi^{(i_+)}\right]_{i_+ \in \mathrm{child}(i)}, \quad \ell^{[i]} = \left[\ell^{(i_+)}\right]_{i_+ \in \mathrm{child}(i)}.$$

$$\rho_j(\ell_{j+1}) = \left[\rho(\ell^{[i]})\right]_{i \in \mathrm{nodes}(j)}. \qquad (11.13)$$

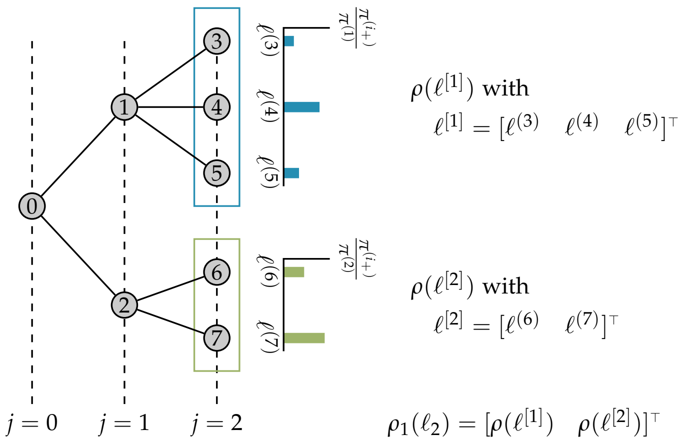

Figure 11.2: Example of scenario tree with conditional risk mapping conditioned at stage 1. Source: [93].

Thus, based on the probability distribution associated with ℓ_{j+1}, (11.13) provides a vector where the entry associated with node $i \in \text{nodes}(j)$ represents the risk of the child nodes given that i is visited.

Example 11.1.3. Consider the simple scenario tree in Figure 11.2. Here the vector associated with the probability space at stage $j = 2$ is $\ell_2 = [\ell^{(3)} \ \cdots \ \ell^{(7)}]^\top$. Following the tree structure, $\text{nodes}(2)$ is partitioned into $\text{child}(1) = \{3, 4, 5\}$ and $\text{child}(2) = \{6, 7\}$. Consequently, we can form two probability subspaces with corresponding vectors $\ell^{[1]} = [\ell^{(3)} \ \ell^{(4)} \ \ell^{(5)}]^\top$ and $\pi^{[1]} = {}^1\!/\!_{\pi^{(1)}}[\pi^{(3)} \ \pi^{(4)} \ \pi^{(5)}]^\top$ as well as $\ell^{[2]} = [\ell^{(6)} \ \ell^{(7)}]^\top$ and $\pi^{[2]} = {}^1\!/\!_{\pi^{(2)}}[\pi^{(6)} \ \pi^{(7)}]^\top$. Using any coherent risk measure ρ (see Definition 11.1.1), we can determine the risk of the child nodes given that node 1 is visited as $\rho(\ell^{[1]}) = \rho([\ell^{(3)} \ \ell^{(4)} \ \ell^{(5)}]^\top)$ and the risk of the child nodes given that node 2 is visited as $\rho(\ell^{[2]}) = \rho([\ell^{(6)} \ \ell^{(7)}]^\top)$. Combining them, the conditional risk mapping (11.12) conditioned at stage $j = 1$ is

$$\rho_1(\ell_2) = \rho_1([\ell^{(3)} \ \cdots \ \ell^{(7)}]^\top) = \begin{bmatrix} \rho([\ell^{(3)} \ \ell^{(4)} \ \ell^{(5)}]^\top) \\ \rho([\ell^{(6)} \ \ell^{(7)}]^\top) \end{bmatrix}.$$

Remark 11.1.4. One coherent risk measure that can be used in conditional risk mappings is AV@R_α (see Section 11.1.2). Using AV@R_α from (11.8), the risk associated with $\ell^{[i]}$ for

$i \in \text{nodes}(j)$ and $j \in \mathbb{N}_{[0,J-1]}$ is

$$\rho(\ell^{[i]}) = \min_{\substack{\xi^{[i]} \geq 0 \\ \alpha\xi^{[i]} \geq \ell^{[i]} - t^{(i)}}} \left(t^{(i)} + \mathbf{E}_{\pi^{[i]}}(\xi^{[i]})\right). \tag{11.14a}$$

Here, $t^{(i)} \in \mathbb{R}$ and $\xi^{[i]} = [\xi^{(i_+)}]_{i_+ \in \text{child}(i)}$ with $\xi^{(i_+)} \in \mathbb{R}$ for all $i_+ \in \text{child}(i)$. As posed in (9.5a), the probabilities associated with the subspace $\text{child}(i)$, i.e., the probabilities of the child nodes given that node i is visited, are collected in $\pi^{[i]} = [\pi^{(i_+)}/\pi^{(i)}]_{i_+ \in \text{child}(i)}$. Therefore, (11.14a) is equivalent to

$$\rho(\ell^{[i]}) = \min_{\substack{\xi^{[i]} \geq 0 \\ \alpha\xi^{[i]} \geq \ell^{[i]} - t^{(i)}}} \left(t^{(i)} + \sum_{i_+ \in \text{child}(i)} \frac{\pi^{(i_+)}}{\pi^{(i)}} \xi^{(i_+)}\right). \tag{11.14b}$$

Using conditional risk mappings, we can now compose multi-stage risk measures. These provide a risk-measure that considers random variables with vectors $\ell_1, \ldots, \ell_J$ at all stages.

11.2 *MPC problem formulation*

In this section we formulate a tractable risk-averse MPC problem. Therefore, an MPC problem with nested conditional risk mappings is posed. This problem is then reformulated as an MIQCP that can be solved by available software.

11.2.1 *Risk-averse optimal control*

Broadly speaking, the risk at every node $i \in \text{nodes}(j)$ of stage $j \in \mathbb{N}_{[1,J-1]}$ is composed of the risk of the node itself and the risk of the nodes that follow, i.e., the risk of the child nodes, their children, and so on. For a sequence of random variables with associated cost vectors $\ell_1, \ldots, \ell_J$ from (9.11), this relation is captured by the nested multi-stage risk measure [48, 217, 241, 247] which is defined analogously to (10.5) as

$$\varrho_J(\ell_1, \ldots, \ell_J) = \rho_0\left(\ell_1 + \rho_1\left(\ell_2 + \ldots + \rho_{J-1}(\ell_J)\right)\ldots\right) \tag{11.15}$$

by making extensive use of conditional risk mappings.

Example 11.2.1. For the simple scenario tree in Figure 11.2, the nested multi-stage risk measure is

$$\varrho_2(\ell_1, \ell_2) = \rho_0(\ell_1 + \rho_1(\ell_2)) \tag{11.16}$$

with

$$\rho_1(\ell_2) = \begin{bmatrix} \rho([\ell^{(3)} \quad \ell^{(4)} \quad \ell^{(5)}]^\top) \\ \rho([\ell^{(6)} \quad \ell^{(7)}]^\top) \end{bmatrix}. \tag{11.17}$$

From (11.13) follows that $\rho_0(\ell_1) = \left[\rho(\ell^{[i]})\right]_{i\in\mathrm{nodes}(0)} = \rho(\ell^{[0]})$ with $\ell^{[0]} = [\ell^{(1)}\ \ell^{(2)}]^\top$. Hence, (11.16) can be transformed into

$$\varrho_2(\ell_1, \ell_2) = \rho\left(\begin{bmatrix} \ell^{(1)} + \rho([\ell^{(3)} \quad \ell^{(4)} \quad \ell^{(5)}]^\top) \\ \ell^{(2)} + \rho([\ell^{(6)} \quad \ell^{(7)}]^\top) \end{bmatrix}\right). \tag{11.18}$$

The nested structure of multi-stage risk measures of the form (11.15) can be hard to handle. Still, multi-stage risk measures enjoy desirable properties that render them very suitable for MPC formulations. These are, as stated in [93]:

1. They measure how risk propagates over time and are suitable for multi-stage formulations.
2. They are coherent risk measures over the space $\mathbb{R}^{|\,\mathrm{nodes}(1)|} \times \cdots \times \mathbb{R}^{|\,\mathrm{nodes}(N)|}$ [241, Section 6.8].
3. The give rise to optimal control problems which are amenable to dynamic programming formulations [239].
4. They allow for MPC formulations with closed-loop stability guarantees [48, 247].

Using (11.15), we can formulate a risk-averse MPC problem. Using the decision variables from Chapter 10, the optimal control problem reads as follows.

Problem 7 (Risk-averse MPC of islanded MGs with nested conditional risk mappings)**.** Solve the optimization problem

$$\min_{\boldsymbol{v},\boldsymbol{x},\boldsymbol{z}} \ \varrho_J(\ell_1, \dots, \ell_J)$$

subject to

constraints (9.10),

$\forall i_+ \in \mathbb{N}_{[1,N_\mathrm{n}-1]}$ and $i = \mathrm{anc}(i_+)$,

with given initial conditions $x^{(0)} = x_k$ and $v^{(0_-)} = v_{k-1}$.

Recall the decision variables from Chapter 10:

$$\boldsymbol{v} = [v^{(i)}]_{i\in\mathbb{N}_{[0,N_\mathrm{n}-1]}\setminus\mathrm{nodes}(J)},$$
$$\boldsymbol{x} = [x^{(i)}]_{i\in\mathbb{N}_{[1,N_\mathrm{n}-1]}},$$
$$\boldsymbol{z} = [z^{(i)}]_{i\in\mathbb{N}_{[1,N_\mathrm{n}-1]}}.$$

One big drawback this formulation is that $\varrho_J(\ell_1, \dots, \ell_J)$ is a composition of typically nonsmooth mappings. Problems of this kind are often solved using cutting plane methods

[11, 50]. However, these only allow to solve problems with linear stage costs and short prediction horizons. Another way to solve such problems is multiparametric piecewise quadratic programming [185] which is unfortunately only applicable to systems with a short prediction horizon and a small number of states [184]. To model systems with a larger number of states, longer prediction horizons and quadratic cost functions, we use the approach presented in [247] and extended in [248], which will enable us to pose Problem 7 as an MIQCP.

11.2.2 *Reformulation as MIQCP*

In what follows, we will reformulate Problem 7 as an MIQCP for the case where ρ_i is AVaR. This reformulation will allow us to solve the risk-averse optimal control problem using off-the-shelf numerical solvers, such as, Gurobi [85] or CPLEX [107]. Before posing the reformulation, some new variables are introduced.

Define the objective in the conditional risk mapping with AVaR in (11.14a) as

$$\Psi^{(i)} = t^{(i)} + \mathbf{E}_{\pi^{[i]}}(\xi^{[i]}) \tag{11.19}$$

Here, $t^{(i)} \in \mathbb{R}$ for all non-leaf nodes $i \in \mathbb{N}_{[0,N_\mathrm{n}]} \setminus \mathrm{nodes}(J)$ and $\xi^{[i]} = [\xi^{(i_+)}]_{i_+ \in \mathrm{child}(i)}$ with $\xi^{(i_+)} \in \mathbb{R}$ for all $i_+ \in \mathrm{child}(i)$. Using (11.19), the conditional risk mapping (11.14b) of AVaR reads

$$\rho(\ell^{[i]}) = \min_{\substack{\xi^{[i]} \geq 0 \\ \alpha \xi^{[i]} \geq \ell^{[i]} - t^{(i)}}} \Psi^{(i)}. \tag{11.20}$$

Let us form the vectors $\boldsymbol{t} = [t^{(i)}]_{i \in \mathbb{N}_{[0,N_\mathrm{n}-1]} \setminus \mathrm{nodes}(J)}$ as well as $\boldsymbol{\xi} = [\xi^{(i)}]_{i \in \mathbb{N}_{[1,N_\mathrm{n}-1]}}$. These allow us to pose the following theorem. Please note that this theorem was published in author's work [93, Theorem VI.2].

Theorem 11.2.2. Suppose that Problem 7 is feasible and has at least one minimizer. If the underlying risk measure is AVaR with $\alpha \in [0, 1]$, then Problem 7 is equivalent to the following problem, in the sense that both result in equal optimal values.

Problem 8 (Risk-averse MPC of islanded MGs)**.** Solve the optimization problem

$$\min_{v,x,z,t,\xi} \Psi^{(0)}$$

subject to

$$\xi^{[i]} \geq 0,$$

$$\alpha\xi^{[i]} \geq \begin{cases} \ell^{[i]} + \Psi^{[i]} - t^{(i)}, & \text{if stage}(i) < J-1, \\ \ell^{[i]} - t^{(i)}, & \text{if stage}(i) = J-1, \end{cases}$$

and constraints (9.10),

$\forall i_+ \in \mathbb{N}_{[1,N_\mathrm{n}-1]}$ and $i = \mathrm{anc}(i_+)$,

with given initial conditions $x^{(0)} = x_k$ and $v^{(0-)} = v_{k-1}$,

where $\Psi^{[i]} = [\Psi^{(i_+)}]_{i_+\in\mathrm{child}(i)}$ with $\Psi^{(i_+)} = t^{(i_+)} + \mathbf{E}_{\pi^{[i_+]}}(\xi^{[i_+]})$ for all $i_+ \in \bigcup_{j=1}^{J-1} \mathrm{nodes}(j)$.

Proof. We want to show that Problem 7 is equivalent to Problem 8 in the sense that both result in equal optimal values. Therefore, let us first associate every non-leaf node $i \in \mathbb{N}_{[0,N_\mathrm{n}-1]} \setminus \mathrm{nodes}(J)$ with a value $\Phi^{(i)} \in \mathbb{R}$. All of these values are collected in $\Phi \in \mathbb{R}^{N_\mathrm{n}-|\,\mathrm{nodes}(J)|}$. Analogously to ℓ_j, we segment this vector stage-wise into $\Phi_j = [\Phi^{(i)}]_{i\in\mathrm{nodes}(j)}$.

At stage $J-1$ we define Φ_{J-1} to be equal to the conditional risk mapping conditioned at stage $J-1$, i.e.,

$$\Phi_{J-1} = \rho_{J-1}(\ell_J). \tag{11.21a}$$

Following (11.13), Φ_{J-1} is composed of elements $\rho(\ell^{[i]})$ for all $i \in \mathrm{nodes}(J-1)$ and with $\ell^{[i]} = [\ell^{(i_+)}]_{i_+\in\mathrm{child}(i)}$. Using (11.20), for AVaR the elements of Φ_{J-1} are

$$\Phi^{(i)} = \rho(\ell^{[i]}) = \min_{\substack{\xi^{[i]}\geq 0 \\ \alpha\xi^{[i]}\geq \ell^{[i]}-t^{(i)}}} \Psi^{(i)}, \tag{11.21b}$$

$i \in \mathrm{nodes}(J-1)$. We can now replace $\rho_{J-1}(\ell_J)$ by Φ_{J-1} in (11.15), i.e.,

$$\varrho_J(\ell_1,\ldots,\ell_J) = \rho_0(\ell_1 + \rho_1(\ell_2 + \ldots + \rho_{J-2}(\ell_{J-1} + \Phi_{J-1}))\ldots). \tag{11.22}$$

At stage $0,\ldots,J-2$, the risk at every node is composed of the risk of the cost associated with the node and the risk of its child nodes (see Section 11.2.1). We can include this by using ℓ_{j+1} and the risk of the child nodes, Φ_{j+1}, as inputs to the conditional risk mapping conditioned at stage $j \in \mathbb{N}_{[0,J-2]}$ by recursively defining

$$\Phi_j = \rho_j(\ell_{j+1} + \Phi_{j+1}). \tag{11.23a}$$

Following (11.13), Φ_j is composed of elements $\rho(\ell^{[i]} + \Phi^{[i]})$ with $\ell^{[i]} = [\ell^{(i_+)}]_{i_+ \in \mathrm{child}(i)}$ and $\Phi^{[i]} = [\Phi^{(i_+)}]_{i_+ \in \mathrm{child}(i)}$ for $i \in \mathrm{nodes}(j)$. Using (11.20), for AVaR the elements of Φ_j are

Note the difference to (11.21b) in the second constraint below the minimization.

$$\Phi^{(i)} = \rho(\ell^{[i]} + \Phi^{[i]}) = \min_{\substack{\xi^{[i]} \geq 0 \\ \alpha\xi^{[i]} \geq \ell^{[i]} + \Phi^{[i]} - t^{(i)}}} \Psi^{(i)}, \tag{11.23b}$$

$i \in \bigcup_{j=0}^{J-2} \mathrm{nodes}(j)$.

Using (11.23a), we can now equally express (11.22) as

$$\begin{aligned}
\varrho_J(\ell_1, \ldots, \ell_J) &= \rho_0(\ell_1 + \rho_1(\ell_2 + \ldots + \underbrace{\rho_{J-2}(\ell_{J-1} + \Phi_{J-1})}_{\Phi_{J-2}}) \ldots) \\
&\vdots \\
&= \rho_0(\ell_1 + \rho_1(\ell_2 + \Phi_2)) \\
&= \rho_0(\ell_1 + \Phi_1) \\
&= \Phi_0.
\end{aligned} \tag{11.24}$$

Let us assume, without loss of generality[2], that $J > 1$. Then, we can reformulate the minimization of Problem 7 as

$$\min\ \varrho_J(\ell_1, \ldots, \ell_J) = \min \Phi_0 = \min \min_{\substack{\xi^{[0]} \geq 0 \\ \alpha\xi^{[0]} \geq \ell^{[0]} + \Phi^{[0]} - t^{(0)}}} \Psi^{(0)} \tag{11.25a}$$

$$= \min_{\substack{\xi^{[0]} \geq 0 \\ \alpha\xi^{[0]} \geq \ell^{[0]} + \Phi^{[0]} - t^{(0)}}} \Psi^{(0)}. \tag{11.25b}$$

[2] If $J = 1$, then

$$\begin{aligned}
\min \varrho_1(\ell_1) &= \min \Phi_0 \\
&= \min_{\substack{\xi^{[0]} \geq 0 \\ \alpha\xi^{[0]} \geq \ell^{[0]} - t^{(0)}}} \Psi^{(0)}.
\end{aligned}$$

This is equivalent to (11.29) for $J = 1$, i.e., (11.25)–(11.28) can be skipped in this case.

Let us now assume, without loss of generality[3], that $\mathrm{stage}(0) < J - 2$. For any node $i \in \bigcup_{j=0}^{J-3} \mathrm{nodes}(j)$, we can use (11.23b) to transform $\alpha\xi^{[i]} \geq \ell^{[i]} + \Phi^{[i]} - t^{(i)}$ into

$$\alpha\xi^{[i]} \geq \ell^{[i]} - t^{(i)} + \left[\min_{\substack{\xi^{[i_+]} \geq 0 \\ \alpha\xi^{[i_+]} \geq \ell^{[i_+]} + \Phi^{[i_+]} - t^{(i_+)}}} \Psi^{(i_+)} \right]_{i_+ \in \mathrm{child}(i)}.$$

[3] If $\mathrm{stage}(0) < J - 2$, i.e., if $J = 2$, then (11.26)–(11.28) can be skipped.

Lemma 3.3.1 allows to equivalently state this as

$$\begin{aligned}
\alpha\xi^{[i]} &\geq \ell^{[i]} + \Psi^{[i]} - t^{(i)}, \\
\xi^{[i_+]} &\geq 0, \\
\alpha\xi^{[i_+]} &\geq \ell^{[i_+]} + \Phi^{[i_+]} - t^{(i_+)}, \\
&\forall i_+ \in \mathrm{child}(i).
\end{aligned}$$

Consequently, with (11.23b) and Lemma 3.3.1, we can equivalently state (11.25b) as

$$\min \varrho_J(\ell_1,\ldots,\ell_J) = \min_{\substack{\xi^{[0]}\geq 0 \\ \alpha\xi^{[0]}\geq \ell^{[0]}+\Psi^{[0]}-t^{(0)} \\ \xi^{[i_+]}\geq 0 \\ \alpha\xi^{[i_+]}\geq \ell^{[i_+]}+\Phi^{[i_+]}-t^{(i_+)} \\ \forall i_+\in\mathrm{child}(0)}} \Psi^{(0)}. \tag{11.26}$$

In the above equation, $\mathrm{child}(0) = \mathrm{nodes}(1)$, i.e., the constraints in (11.26) must hold for all nodes $i_+ \in \mathrm{nodes}(1)$.

Let us now assume, without loss of generality[4], that $\mathrm{stage}(1) < J-2$. Then, we can apply the same transformation as before on (11.26) which yields

$$\min \varrho_J(\ell_1,\ldots,\ell_J) = \min_{\substack{\xi^{[i]}\geq 0 \\ \alpha\xi^{[i]}\geq \ell^{[i]}+\Psi^{[i]}-t^{(i)} \\ \forall i\in\bigcup_{j=0}^{1}\mathrm{nodes}(j) \\ \xi^{[i_+]}\geq 0 \\ \alpha\xi^{[i_+]}\geq \ell^{[i_+]}+\Phi^{[i_+]}-t^{(i_+)} \\ \forall i_+\in\mathrm{nodes}(2)}} \Psi^{(0)}. \tag{11.27}$$

Note that $\bigcup_{i\in\mathrm{nodes}(j)}\mathrm{child}(i) = \mathrm{nodes}(j+1)$ for all stages $j = 0,\ldots,J-1$. Therefore, $\bigcup_{i\in\mathrm{nodes}(1)}\mathrm{child}(i) = \mathrm{nodes}(2)$ and we can formulate the constraints in terms of stages instead of child nodes.

We can now apply the equivalence transformation from before recursively until we reach

$$\min \varrho_J(\ell_1,\ldots,\ell_J) = \min_{\substack{\xi^{[i]}\geq 0 \\ \alpha\xi^{[i]}\geq \ell^{[i]}+\Psi^{[i]}-t^{(i)} \\ \forall i\in\bigcup_{j=0}^{J-3}\mathrm{nodes}(j) \\ \xi^{[i_+]}\geq 0 \\ \alpha\xi^{[i_+]}\geq \ell^{[i_+]}+\Phi^{[i_+]}-t^{(i_+)} \\ \forall i_+\in\mathrm{nodes}(J-2)}} \Psi^{(0)}. \tag{11.28}$$

Note that the elements of $\Phi^{[i_+]}$ for $i_+ \in \mathrm{nodes}(J-2)$ are given by (11.21b). Therefore, we can equivalently state (11.28) with Lemma 3.3.1 as[5]

$$\min \varrho_J(\ell_1,\ldots,\ell_J) = \min_{\substack{\xi^{[i]}\geq 0 \\ \alpha\xi^{[i]}\geq \ell^{[i]}+\Psi^{[i]}-t^{(i)} \\ \forall i\in\bigcup_{j=0}^{J-2}\mathrm{nodes}(j) \\ \xi^{[i_+]}\geq 0 \\ \alpha\xi^{[i_+]}\geq \ell^{[i_+]}-t^{(i_+)} \\ \forall i_+\in\mathrm{nodes}(J-1)}} \Psi^{(0)}. \tag{11.29}$$

[4] If $\mathrm{stage}(1) < J-2$, i.e., if $J = 3$, then (11.27) and (11.28) can be skipped.

[5] For node $i \in \mathrm{nodes}(J-2)$, we can use (11.21b) to reformulate $\alpha\xi^{[i]} \geq \ell^{[i]} + \Phi^{[i]} - t^{(i)}$ as

$$\alpha\xi^{[i]} \geq \ell^{[i]} - t^{(i)} + \left[\min_{\substack{\xi^{[i_+]}\geq 0 \\ \alpha\xi^{[i_+]}\geq \ell^{[i_+]}-t^{(i_+)}}} \Psi^{(i_+)}\right]_{i_+\in\mathrm{child}(i)}.$$

Lemma 3.3.1 allows to equivalently state this as

$$\begin{aligned} \alpha\xi^{[i]} &\geq \ell^{[i]} + \Psi^{[i]} - t^{(i)}, \\ \xi^{[i_+]} &\geq 0, \\ \alpha\xi^{[i_+]} &\geq \ell^{[i_+]} - t^{(i_+)}, \\ &\forall i_+ \in \mathrm{child}(i). \end{aligned}$$

Adding the constraints below the minimization in (11.29) and the new decision variables $\boldsymbol{\xi}$, $\boldsymbol{t}$ to Problem 7 and replacing $\varrho_J(\ell_1, \dots, \ell_J)$ by $\Psi^{(0)}$ makes Problem 7 an equivalent representation of Problem 8. This completes the proof. □

Note that the quadratic cost $\ell^{[i]}$ from Section 5.2 is part of the constraints in Problem 8. This and the fact that the problem includes real-valued and Boolean variables makes Problem 8 into an MIQCP. In Chapter 12, it will be demonstrated that this formulation can be solved sufficiently fast by off-the-shelf numerical solvers.

Remark 11.2.3 (Risk-averse MPC for $\alpha = 1$)**.** As discussed in Section 11.1.2, for $\alpha = 1$, $\text{AV@R}_1(\cdot)$ provides the expected value of the function argument. In this case, the nested multi-stage risk measure (11.15) is equal to the nested multi-stage expectation (10.5). Consequently, for $\alpha = 1$ the risk-averse MPC in Problem 8 is identical to the risk-neutral stochastic MPC in Problem 6 in the sense that both provide the same optimal cost.

Remark 11.2.4 (Risk-averse MPC for $\alpha = 0$)**.** As discussed in Section 11.1.2, for $\alpha = 0$, $\text{AV@R}_0(\cdot)$ provides the maximum of the function argument. In this case, the conditional risk mapping (11.13) becomes

$$\rho_j(\ell_{j+1}) = \left[\max(\ell^{[i]})\right]_{i \in \text{nodes}(j)}, \tag{11.30a}$$

i.e., $\rho_j(\ell_{j+1})$ provides the maximum cost of the child nodes of $i \in \text{nodes}(j)$ for $j = 0, \dots, J-1$. In this case, the conditional risk mapping (11.15) is composed of nested maximum operators. Due to the nested structure, where the mapping at every stage provides the maximum cost of the children of each node, Problem 8 then minimizes the maximum cost of all scenarios $\text{scen}(i)$, $i \in \text{nodes}(J)$ of the tree for $\alpha = 0$.

For the example in Figure 11.2, the maximum operator leads to the multi-stage risk

$$\varrho_2(\ell_1, \ell_2) = \max([\ell^{(1)} + \max(\ell^{[1]}) \quad \ell^{(2)} + \max(\ell^{[2]})]^\top) \tag{11.30b}$$

$$= \max\left(\begin{bmatrix} \ell^{(1)} + \max([\ell^{(3)} \quad \ell^{(4)} \quad \ell^{(5)}]^\top) \\ \ell^{(2)} + \max([\ell^{(6)} \quad \ell^{(7)}]^\top) \end{bmatrix}\right). \tag{11.30c}$$

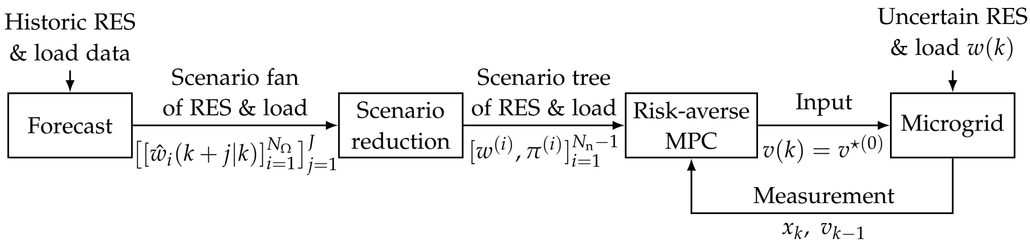

Figure 11.3: Control scheme with risk-averse MPC at time instant k.

This can be transformed into

$$\varrho_2(\ell_1, \ell_2) = \max([\ell^{(1)} + \ell^{(3)} \quad \ell^{(1)} + \ell^{(4)} \quad \ell^{(1)} + \ell^{(5)} \quad \ell^{(2)} + \ell^{(6)} \quad \ell^{(2)} + \ell^{(7)}]^\top) \quad (11.30d)$$

which corresponds to the maximum cost, i.e., the worst-case, of all scenarios in the tree.

11.2.3 MPC scheme

For the operation of islanded MGs, Problem 8 is embedded into the control scheme in Figure 11.3. Before solving the MPC problem, a new collection of forecast scenarios of load and available renewable infeed is obtained (see Chapter 6). These scenarios are then transformed into a scenario tree using scenario reduction (see Chapter 9). Together with the measurement of the current state x_k and the control input v_{k-1} that was applied in the last time instant, the scenario tree is provided to the MPC. For these inputs, Problem 8 is solved. From the resulting optimal input trajectory, the value associated with the first prediction instant, $v^{\star(0)}$, is applied to the MG plant. At the next sampling time instant, the scenario tree and the measurements are updated and Problem 8 is solved repeatedly in a receding horizon fashion (see, e.g., [18, 23, 204] and Section 3.2). Some trajectories obtained by solving Problem 8 for different values of α are discussed next.

11.3 Example

In Figures 11.4 to 11.6, the forecasts of the uncertain input, power, setpoints and stored energy are shown. The trajectories were derived by solving Problem 8 for different values of

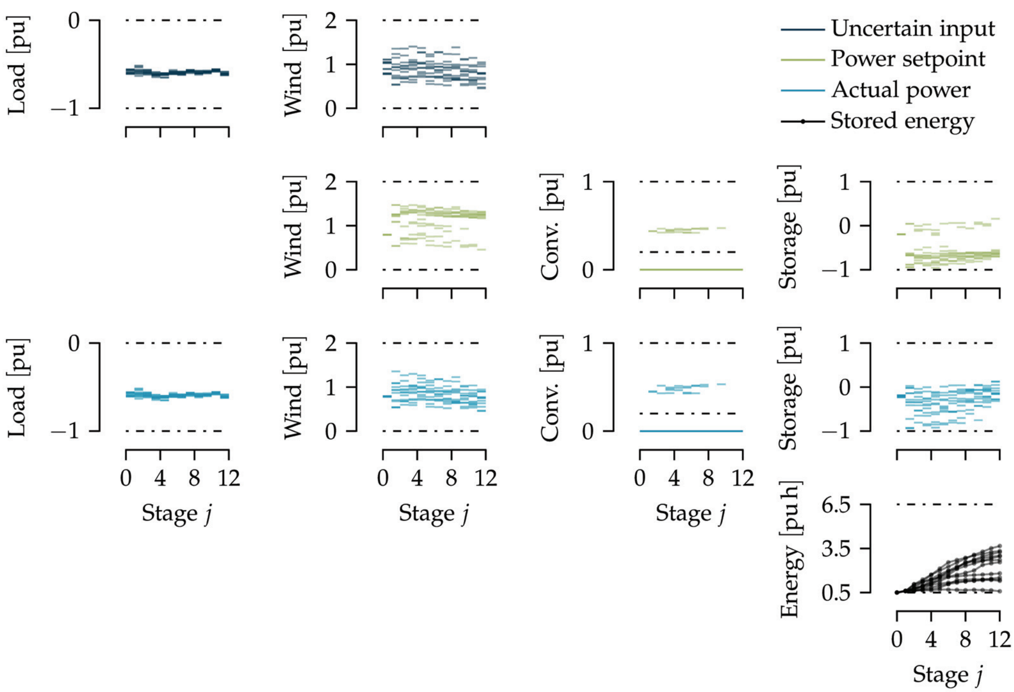

Figure 11.4: Open-loop trajectories of risk-averse MPC ($\alpha = 0$).

α with initial conditions $x^{(0)} = 0.5\,\mathrm{pu\,h}$ as well as $\delta_t^{(0-)} = 0$ for the running example in Figure 4.1.[6] The scenario tree was generated from the collections of independent forecast scenarios in Figure 9.11. Before deducing the scenario tree, the independent forecast scenarios of available power were scaled for a rated wind turbine power of 2 pu.

[6] The unit parameters and the weights of the cost function can be found in Tables 12.1 and 12.2.

Comparing Figures 11.4 to 11.6, it can be noted that with increasing α, the power setpoints become less conservative, as less ambiguity in the probability distribution is considered. For the risk-averse MPC with $\alpha = 1.0$, where the probability distribution is fully trusted, there is not a single scenario where the conventional unit is enabled. With decreasing α, the number of nodes with enabled conventional generator increases. In Figures 11.4 and 11.5 this can be noted by a larger number of nonzero setpoints of this unit.

Considering uncertainty in the probability distribution by choosing smaller values of α also affects renewable infeed. As shown in Table 11.1, the power setpoints $u_r(k)$ applied to the renewable unit increase with α. A similar effect can

Table 11.1: Power setpoints of risk-averse MPC for different values of α.

	$\alpha =$		
	0.0	0.5	1.0
$u_s(k)$	−0.2	−0.43	−0.51
$u_r(k)$	0.79	1.03	1.11

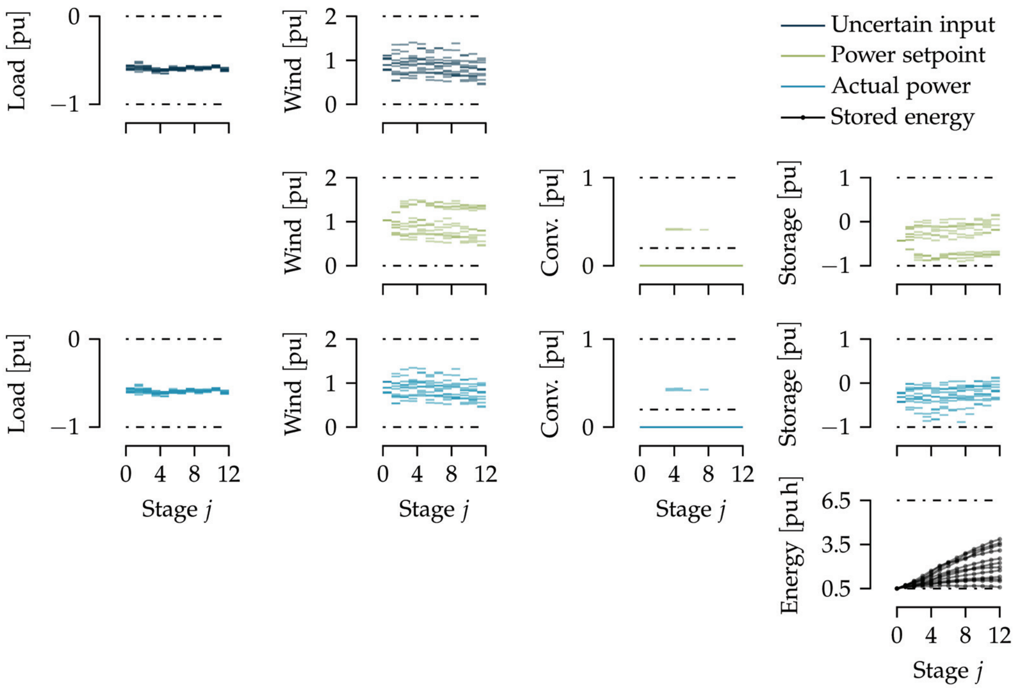

Figure 11.5: Open-loop trajectories of risk-averse MPC ($\alpha = 0.5$).

be observed for the storage unit which is charged less for smaller α (see Table 11.1). Furthermore, the forecast scenarios of stored energy are closer to each other for smaller α. This illustrates how the considered ambiguity affects the optimal control decisions.

11.4 Summary

In this chapter a risk-averse MPC problem was formulated. It allows to model ambiguity in the forecast probability distributions of load and available renewable infeed and satisfies all requirements formulated in Section 2.3.

To derive a tractable MPC problem formulation, first the notion of risk measures was introduced. Furthermore, coherent risk measures were discussed and some examples thereof were given. Among these examples was the AVaR that allows to include ambiguity in probability distributions. To formulate a multi-stage risk-averse MPC problem, conditional risk mappings in the context of scenario trees were introduced.

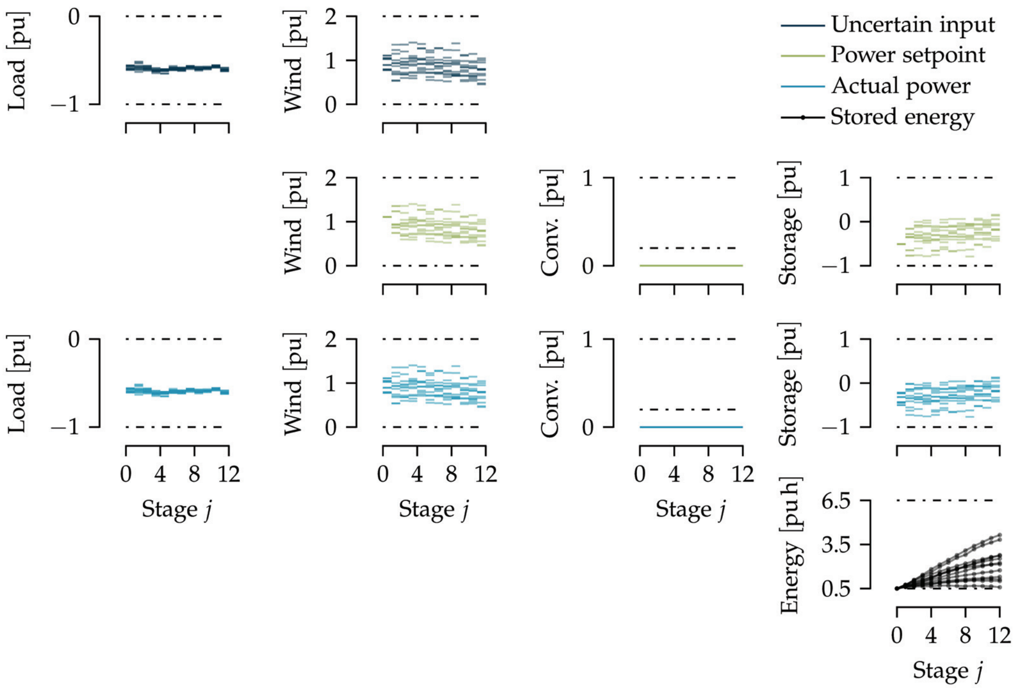

Figure 11.6: Open-loop trajectories of risk-averse MPC ($\alpha = 1$).

These mappings allow to model how risk propagates, i.e., how the risk of the different prediction steps is interlinked. Employing conditional risk mappings, a nested formulation of the risk-averse MPC problem was posed and reformulated as an MIQCP that can be solved by off-the-shelf software.

The MPC formulation derived in this chapter is now used to control different islanded MGs in Chapter 12. Here, risk-averse controllers with different values of α are compared to each other and to the controllers derived in Chapters 7, 8 and 10.[7]

[7] Note that for $\alpha = 1$, the controller derived in this chapter is identical to the risk-neutral stochastic controller from Chapter 10 (see Remark 11.2.3).

12

Case study

In the past chapters, different MPC schemes for the operation of islanded MGs were introduced. In this chapter, their properties are compared to each other in closed-loop simulations.

The contributions of this chapter are as follows. A numerical case study is conducted where different islanded MGs are operated using (i) the prescient MPC from Chapter 5, (ii) the certainty equivalence MPC from Chapter 7, (iii) the minimax MPC from Chapter 8, (iv) the scenario-based risk-neutral stochastic MPC from Chapter 10 and (v) the scenario-based risk-averse MPC from Chapter 11. In the closed-loop simulations, the forecast models identified in Chapter 6 are used to simulate real-world setups with no prior knowledge about the future infeed and load.[1] Two MGs are operated for one week with each controller. The MGs considered have a large amount of installed renewable power such that, in some cases, a renewable share of more than 90 % is achieved. In addition to nominal simulations, a sensitivity analysis is conducted. This analysis investigates the robustness of the approaches to misestimated forecast probability distributions.

[1] Except for the prescient MPC that has full information about future load and renewable infeed.

The remainder of this chapter is partly based on [89–91, 93] and structured as follows. First, the simulation setup is discussed in Section 12.1. Then, a simulation case study that employs the running example will be presented in Section 12.2. This includes nominal simulations in Section 12.2.2 and a sensitivity analysis in Section 12.2.3. Moreover, the results of a single simulation run with a more complex MG will be discussed in Section 12.3.

12.1 Simulation setup

For the simulation, the control schemes from Figures 5.5, 7.2, 8.6, 10.2 and 11.3 were implemented in MATLAB 2015a. Basic components of the simulations are ARIMA forecasts, scenario reduction, model predictive controllers and microgrid models. These components will be discussed in more detail after outlining the hardware used to run the simulations.

Hardware. The simulations—except for the sensitivity analysis in Section 12.2.3—were preformed on a small server with an Intel® Xeon® E5-1620 v2 processor @3.70 GHz with 4 CPU cores and 32 GB RAM. To emulate real-world setups where one dedicated controller is used to operate a single MG, only one simulation was performed at the time.

12.1.1 Forecast

The forecasts of load demand, wind speed and irradiance, which include the nominal forecasts and the collections of 500 independent forecast scenarios, were derived using the MATLAB Econometrics toolbox. Here, the models that were identified in Chapter 6 were employed. For all forecasts, a sampling time $T_s = 1/2\,\mathrm{h}$ and a prediction horizon of $J = 12$ were chosen to cover a possible full charge of discharge of the storage unit with the largest capacity. The forecasts of weather-dependent available power of the wind turbines was derived from wind speed using (6.14). Likewise, the forecasts of available power of the PV plant were deduced from irradiance using (6.15). For the certainty equivalence MPC, the nominal forecast was used. For the minimax MPC, the robust forecast intervals were identified from the collections 500 of independent forecast scenarios using the stage wise minimum and maximum, i.e., the 100 % interval. For the scenario-based approaches, a new scenario tree was derived at every simulation step via scenario reduction.

Recall that the following models were derived in Chapter 6:

- $\mathrm{ARIMA}(10, 0, 8)(7, 1, 7)_{48}$ for load,
- $\mathrm{ARIMA}(16, 0, 6)$ for wind speed, and
- $\mathrm{ARIMA}(6, 1, 2)(1, 1, 1)_{48}$ for irradiance.

12.1.2 Scenario reduction

The scenario trees were deduced using a variant of forward tree construction (see Algorithm 3) with branching factors

$[b_j^d]_{j=1}^{12} = [6, 2, 1, 1, \dots, 1]^\top$. To increase robustness, scenarios where the first prediction step represents an extreme combination of load and available renewable infeed were artificially added to the tree. Namely, these are maximum available renewable infeed and minimum load as well as maximum load and minimum available renewable infeed. The resulting scenarios have a very low probability as they combine extreme cases for demand and renewable infeed. Therefore, they have minor influence on the cost of the risk-averse MPC for $\alpha = 1$ and only come to bear for smaller values of α (see Sections 12.2.2 and 12.3.2).[2]

[2] Note that, even for $\alpha = 1$, these scenarios increase the robustness regarding the units' power and energy constraints (see Remark 9.2.4).

Remark 12.1.1 (Probabilities of additional scenarios)**.** In the simulations, the probabilities of the additional scenarios were assumed to be $1/500^2$, i.e., $4 \cdot 10^{-6}$. Lower probabilities were tested as well. Unfortunately, they led to numerical problems of the solver which are probably caused by coefficients in the cost function that are orders of magnitude away from each other. These emerge as follows. On one end there are probabilities of the original tree with values up to 0.5 and on the other end there are the very small probabilities of the additional scenarios. Both are multiplied with the weights of the cost function that range from 10^0 to 10^{-3}. This leads to effective coefficients in the cost function that are orders of magnitude away from each other. Therefore, $4 \cdot 10^{-6}$ was chosen as a compromise between an accurate reproduction of the actual probabilities and a solvable problem formulation.

Remark 12.1.2 (Structure of scenario tree)**.** The structure of the scenario tree has an impact on the quantization error between the initial probability distribution in the form of independent forecast scenarios and the reduced probability distribution in the form of a scenario tree. In the context of this thesis, the structure of the scenario trees was implicitly decided by heuristically choosing the branching factors $[b_j^d]_{j=1}^{12}$ with the following considerations in mind.

There is a trade-off between solve times (which typically increase with the number of scenarios) and the approximation accuracy with respect to the underlying probability distribution (which typically becomes worse as the number of scenarios decreases). Another important point to consider is that only the first control input is applied to the plant. Therefore, it is desirable to use a large number of scenarios right in the beginning to include as much probabilistic information as possible when searching for optimal control inputs for the first prediction step. Finally, it is important to keep in mind is that a smaller number of scenarios can be acceptable in risk-averse approaches which can provide robustness to inaccurate forecast probability distributions.

12.1.3 Model predictive controllers

The MPC problems were formulated in MATLAB using YALMIP [140] (Release R20180817) and solved numerically with Gurobi 7.5.2 [85]. The problems were formulated using a forgetting factor of $\gamma = 0.95$.

Remark 12.1.3 (Warm-start of optimization solver)**.** To reduce the solve time, the results from the previous executions of the controllers were used in the closed-loop simulations with the scenario-based and minimax MPC to warm-start the numerical solver. In detail, for each node i and each prediction step j, the initial value was chosen to be identical to the result from the previous execution of the controller. Naturally, this was only possible if the scenario trees had an identical structure and if a result from the previous execution was present.

Remark 12.1.4 (Simplification of scenario-based controllers)**.** The computational complexity of the scenario-based approaches, i.e., the risk-neutral stochastic and the risk-averse MPC, was reduced by relaxing the switch variable of the conventional generators for stages greater than or equal to 4, i.e., $\delta_{\mathrm{t}}^{(i)} \in [0,1]^{N_{\mathrm{t}}} \subset \mathbb{R}^{N_{\mathrm{t}}}$ for all nodes $i \in \mathrm{nodes}(j)$ with $j \geq 4$. The same relaxation was performed on $\delta_{\mathrm{r}}^{(i)}$, i.e., $\delta_{\mathrm{r}}^{(i)} \in [0,1]^{N_{\mathrm{r}}} \subset \mathbb{R}^{N_{\mathrm{r}}}$, for all nodes i that are singletons.

Remark 12.1.5 (Solve times)**.** For the sampling time of 30 min considered in this case study, the solve times were found to be sufficiently small (see Sections 12.2.1 and 12.3.1). If identified to cause problems, they could be further reduced by employing servers with more RAM and CPU cores. Moreover, the relaxation of Boolean decision variables (see Remark 12.1.4) could be further exploited.

12.1.4 Microgrid simulation model

The optimal control inputs from the MPC approaches were used to control MG models that were implemented in MATLAB. The MG models, i.e., the plant models, that were used in the closed-loop simulations strictly follow the model described in Section 4.9. This concerns the dynamics as well the relations of power, control input and uncertain input. Wind and irradiance data from [12] was used to calculate the available renewable power under weather conditions based on (6.14) and (6.15). The load power data was based on a real power measurements from an islanded MG.[3] Note that the uncertain input $w(k)$ that is applied to the plant at time k is different from the forecasts. The load, wind and irradiance data used to deduce $w(k)$ is, however, used to forecast the future uncertain input for time instants $k+1$ to $k+J$.

[3] Gaussian noise with zero mean and a small standard deviation was added to obfuscate the source of the data.

The closed-loop simulations were numerically assessed using the following metrics. The average economically motivated cost over simulation horizon $K \in \mathbb{N}$ is given by

Please note that the temporal relation of variables in the case study is identical to the one described in Section 4.9.

$$\bar{\ell}_{\mathrm{o}} = \frac{1}{K} \sum_{k=1}^{K} \ell_{\mathrm{o}}(v(k-1), v(k), z(k)). \tag{12.1}$$

The average cost associated with the state of charge over the same simulation horizon is

$$\bar{\ell}_x = \frac{1}{K} \sum_{k=1}^{K} \ell_x(x(k)). \tag{12.2}$$

The average infeed from the conventional generators is

$$\bar{p}_{\mathrm{t}} = \frac{1}{K} \sum_{k=1}^{K} \sum_{i=1}^{N_{\mathrm{t}}} p_{\mathrm{t},i}(k) \tag{12.3}$$

and the average infeed from renewable sources is

$$\bar{p}_{\mathrm{r}} = \frac{1}{K} \sum_{k=1}^{K} \sum_{i=1}^{N_{\mathrm{r}}} p_{\mathrm{r},i}(k). \tag{12.4}$$

Finally, the average share of the RES can be determined as

$$\frac{\bar{p}_{\mathrm{r}}}{\bar{p}_{\mathrm{t}} + \bar{p}_{\mathrm{r}}} \cdot 100\,\%. \tag{12.5}$$

Remark 12.1.6 (Model uncertainties)**.** This work focuses on the effects associated with the uncertain load and renewable infeed. Therefore, a plant model that strictly follows the MG model in Chapter 4 was considered. This allows to analyze the effects of the uncertain input on the different MPC approaches without having to worry about plant-model mismatch. Moreover, neglecting model uncertainties directly follows Assumptions 4.2.7 and 4.2.8 which state that the error introduced by uncertain load and renewable infeed is much larger than the error introduced by model uncertainties.

In the author's work [93], a more complex plant that includes storage efficiencies and a nonlinear power flow model was considered. The conclusions drawn from the simulations are very similar to those presented in this thesis which further justifies the use of a simple plant model.

12.2 *Closed-loop simulations with simple MG*

In what follows, simulations performed with the MG in Figure 12.1 are discussed. The main goal of this section is to highlight properties of the different MPC approaches. Therefore, the running example[4] from Chapter 4 was considered.

[4] Recall that the running example only represents a very small fraction of topologies in the class of islanded MG.

In what follows, first, the parameters of the MG and the weights of the cost function are posed. Then, the results of a single simulation run will be discussed. Finally, the robustness of the different approaches will be assessed in a sensitivity analysis.

12.2.1 *Grid setup*

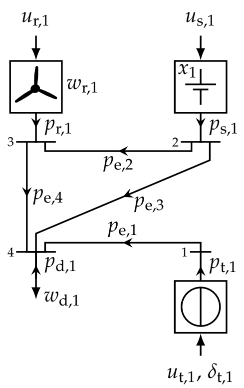

Figure 12.1: Setup of simple MG from Chapter 4.

For the simulations, the running example form Chapter 4 is considered (see Figure 12.1). The grid contains one unit of each kind, i.e., one conventional, one storage and one renewable unit and a load. The rated power of the transmission lines that connect the units and the load is assumed to be such that each line can transmit power between $-1.3\,\mathrm{pu}$ and $1.3\,\mathrm{pu}$. Moreover, $\tilde{F}$ and U from (4.33) and (4.34) are considered, i.e., all lines are assumed to have the same admittance. Hence, the relation between the power of the transmission lines and the power of the units and the load is

$$\begin{bmatrix} p_{e,1} \\ p_{e,2} \\ p_{e,3} \\ p_{e,4} \end{bmatrix} = \underbrace{\begin{bmatrix} 1 & 0 & 0 & 0 \\ 0 & 1/3 & -1/3 & 0 \\ 0 & 2/3 & 1/3 & 0 \\ 0 & 1/3 & 2/3 & 0 \end{bmatrix}}_{\tilde{F}U} \begin{bmatrix} p_{t,1} \\ p_{s,1} \\ p_{r,1} \\ w_{d,1} \end{bmatrix}.$$

The parameters of the units can be found in Table 12.1. Note that the storage unit has a relatively high capacity of $x^{\max} = 7\,\mathrm{pu\,h}$ at a rated power of $p_s^{\max} = 1\,\mathrm{pu}$. Also note that the power sharing factors are chosen such that all fluctuations are covered equally by both grid-forming units. The rated power of the conventional generator is such that it can fully serve the load at all times. The rated power of the wind turbine is such that the load can be served and the storage unit can be charged in times of high wind speed.

The weights of the cost function (5.2) are shown in Table 12.2. Here, the fuel cost is based on unit 16 in [265].

Table 12.1: Unit parameters of simple MG.

Parameter	Value
$p_t^{\min}$	0.4 pu
$p_t^{\max}$	1 pu
$p_s^{\min}$	−1 pu
$p_s^{\max}$	1 pu
$p_r^{\min}$	0 pu
$p_r^{\max}$	2 pu
$x_1^{\min}$	0 pu h
$x_1^{\max}$	7 pu h
$\tilde{x}_1^{\min}$	0.5 pu h
$\tilde{x}_1^{\max}$	6.5 pu h
x_0	3 pu h
K_t	1
K_s	1

Table 12.2: Weights in cost function of simple MG.

Weight	Value
c_t	0.1178 k$
c'_t	0.751 k$/pu
c''_t	0.0048 k$/pu^2
c_t^{sw}	0.1 k$
c''_s	0.05 k$/pu^2
c'_r	$1 \cdot 10^{-3}$ k$/pu
c''_r	1 k$/pu^2
c_x	$1 \cdot 10^{3}$ k$/pu h

Remark 12.2.1 (Penalty on renewable power setpoint)**.** Note that the weight associated with the cost of a large power setpoint of the RES c'_r was initially chosen much smaller. Unfortunately, this led to numerical problems of the optimization solver for scenarios with low probabilities. These numerical problems were probably caused by coefficients being orders of magnitude away from each other: On end there are relatively small probabilities of the additional scenarios in the range of $4 \cdot 10^{-6}$ (see Remark 12.1.1) that are multiplied by small values of c'_r which can lead to effective weights in the range of 10^{-9}. On the other end there are probabilities in the scenario tree of up to 0.5 that are multiplied by, for example, c'_r, which leads to effective weights in the range of 10^{-1}. To prevent these problems, a small value that does not cause numerical issues was heuristically chosen for c'_r. The same hold for the weights in the cost function of the larger grid in Section 12.3.

12.2.2 *Results of single simulation run*

Simulations with different controllers were executed for the time-series shown in Figure 12.2 with a sampling time of $T_s = 30\,\mathrm{min}$ and a simulation horizon of 7 d, i.e., 336 data points.

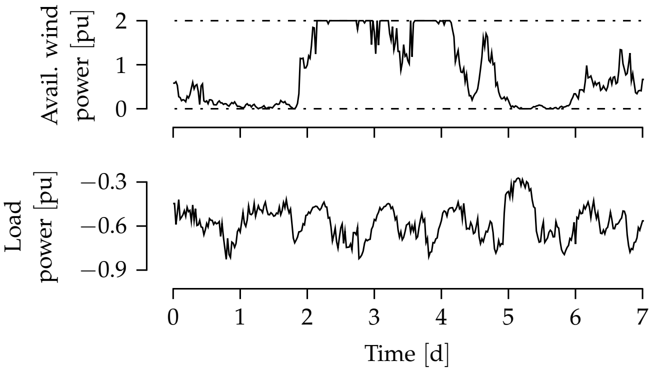

Figure 12.2: Time-series of available infeed of wind turbine and demand for simulation with simple MG.

The simulation scenario was generated using wind speed measurements from [12] which exhibit very high available wind power on days three to five. The demand time-series was based on measurements where Gaussian noise with zero mean and a small standard deviation was added to obfuscate the source of the data. Here, a daily pattern with high load in the evening and low load at night can be easily identified.

The simulations were executed for the MPC approaches presented earlier, i.e., for the

1. prescient MPC from Chapter 5,
2. certainty equivalence MPC from Chapter 7,
3. minimax MPC from Chapter 8,
4. risk-averse MPC from Chapter 11 for $\alpha = 0.0$,
5. risk-neutral stochastic MPC from Chapter 10 which is equivalent to the risk-averse MPC from Chapter 11 for $\alpha = 1.0$, and
6. risk-averse MPC from Chapter 11 for $\alpha = 0.5$.

The accumulated results of the simulations are summarized in Table 12.3. Here, it can be observed that the average time required to solve the optimization problems is in the range of seconds for all approaches. It can be further noted that the solve times increase when using more complex models of the uncertain input. The maximum solve time of all approaches is below 30 s. Considering a sampling time of 30 min, this seems adequately fast.

	Prescient	Cert. equiv.	Minimax	Risk-averse, $\alpha =$ 0.0	0.5	1.0
Mean econ. motiv. cost $\overline{\ell}_o$ [k$]	2.7	2.78	3.2	3.18	2.79	2.72
Mean energy-related cost $\overline{\ell}_x$ [k$]	0	3.19	0.13	0.01	0.29	0.47
Share of RES [%]	75.86	73.21	55.36	56.14	71.93	74.14
Switching actions	6	8	17	19	8	14
Power constraint violations	0	5	0	0	0	0
Mean solve time [s]	0.03	0.03	0.27	0.84	1.04	1.93
Maximum solve time [s]	0.06	0.06	1.08	3.4	6.23	26.12

Table 12.3: Results of simulations performed with the simple MG.

In what follows, the results of the simulations will be discussed. Therefore, we move column-wise from left to right in Table 12.3, i.e., from prescient to risk-averse MPC.

Prescient MPC. This approach serves as a reference. It assumes a hypothetical case there the future time-series of load and available power of the wind turbine are perfectly known over the entire prediction horizon. As we do not consider any modeling errors (see Remark 12.1.6), the prescient controller represents the best result that could be achieved with a predictive controller with prediction horizon $J = 12$, given a perfect forecast. The formal description of the MPC scheme is given by Problem 2.

The closed-loop simulation results are show in Figure 12.3 on page 176. It can be noted that initially, the storage unit is discharged due to low available power from the wind turbine. When the battery is empty, the conventional generator is enabled to provide power to the load. In the end of the period where power is provided by the conventional generator, its power is increased in order to charge the battery and disable the conventional generator for some time. After a short period with more available wind power, the conventional generator is enabled again to provide power to the load. As soon as the available power of the wind turbine is sufficient to serve the load, the conventional generator is disabled and the storage unit is charged. When the stored energy reaches the upper end of the range of desired states of charge, the setpoint of the wind turbine is selected such that the wind power only covers the load. Thus, the stored energy approx-

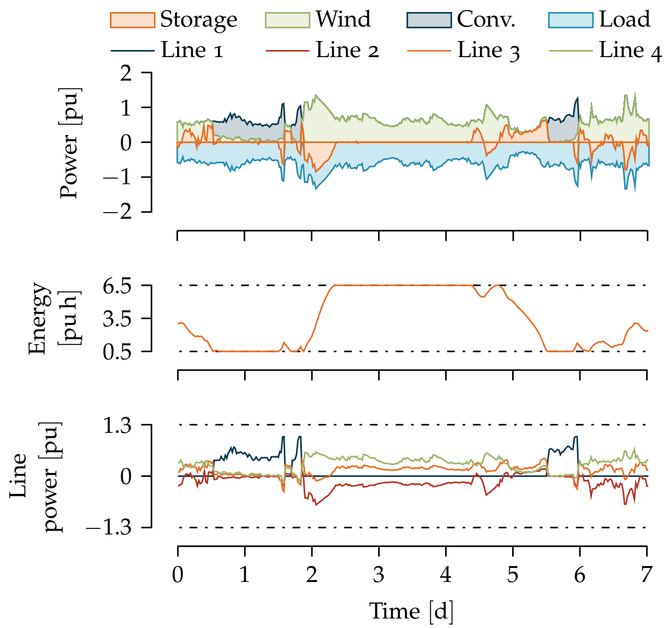

Figure 12.3: Power of units and load as well as stored energy and line power of simple MG in closed-loop simulation with prescient MPC approach.

imately remains at $\tilde{x}_1^{\max} = 6.5\,\mathrm{pu\,h}$. At some point, the available wind power cannot cover the entire load and the storage is discharged. The conventional generator is enabled again to provide power to the load soon as the stored energy reaches $\tilde{x}_1^{\min} = 0.5\,\mathrm{pu\,h}$. In the end of the simulation, the available renewable power increases again and the storage unit can be charged by the wind turbine. Note that the line power in the lower plot is within the given bounds of $\pm 1.3\,\mathrm{pu}$ at all times.

As indicated in Table 12.3, the overall renewable share of the prescient case is slightly above 75 %. The number of constraint violations is zero, i.e., no power limit of any unit was violated in the closed-loop simulations. The number of switching actions is 6, i.e., the conventional generator was enabled and disabled 3 times.

In real-world settings we never have perfect knowledge about the uncertain future. Therefore, these simulation represent a reference that shows what would be possible with a hypothetical perfect forecast. In what follows, closed-loop simulations with "real" MPC schemes will be discussed. These use real forecasts of the uncertain input and do not rely on perfect knowledge about the future.

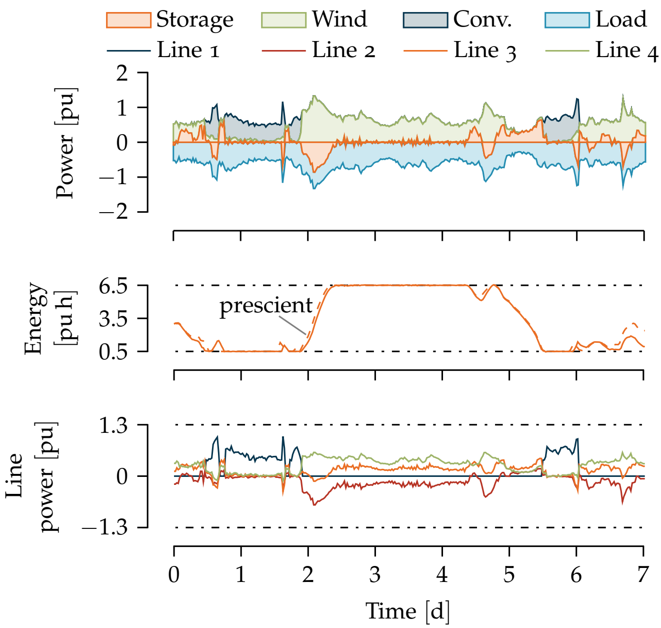

Figure 12.4: Power of units and load as well as stored energy and line power of simple MG in closed-loop simulation with certainty equivalence MPC approach.

Certainty equivalence MPC. This approach can be understood as the state of the art for the operation of islanded MGs. It is based on the assumption that future load and and available renewable infeed perfectly follow the nominal forecast. In comparison to the prescient MPC, it employs the nominal forecasts that were obtained from historic data. These were deduced as described in Section 12.1.1 and provided to the MPC formulation given by Problem 3.

The closed-loop simulation results are show in Figure 12.4. It can be observed that the power and energy trajectories slightly deviate from the prescient case. Notably, the storage unit is not charged as fast as with the prescient MPC. Still, the stored energy approximately follows the trajectory from the prescient controller. Moreover, it can be noted that wind and storage power are not as smooth as they were with the prescient controller.

Comparing the prescient and the certainty equivalence MPC in Table 12.3 shows that the mean economically motivated cost is a little less than 3 % higher. The cost associated with the state of charge increased to the highest value of all control approaches, indicating a lack of robustness to uncertain renewable infeed. In total, 5 power constraint violations could be observed. These are solely caused by the conventional generator with a maximum of 0.023 pu outside the given bounds. Considering that the conventional generator is enabled for 88 time instants one can find that these violations occur in 5.6 % of the time where the unit is operated. For the transmission lines, no power constraint violation could be observed. The number of switching actions, which is an indicator for thermal stress of conventional generators, is slightly higher than with prescient MPC.

The power constraint violations could in practice be resolved by artificially choosing tighter constraints. However, this can only be done heuristically and does not guarantee constraint satisfaction. Additionally, the cost associated with the state of charge is much higher than in any other approach. These drawbacks render the certainty equivalence MPC unsuitable for the operation of MGs with high renewable share.

Minimax MPC. This approach can be seen as a logical next step from the certainty equivalence MPC. It is based on the assumption that load and available renewable infeed are within bounded intervals. As indicated in Section 12.1.1, these intervals were obtained using the stage-wise minima and maxima from collections of 500 independent forecast scenarios. The resulting time-varying bounds were then used in the MPC formulation given by Problem 5.

The closed-loop simulation results are show in Figure 12.5. Here, it can be seen that the infeed from the wind turbine is much lower than with the prescient MPC. Furthermore, the conventional generator is enabled more often and the storage unit is charged slower and discharged faster than with the prescient MPC. The reason for this behavior is, in parts, that the worst-case cost is minimized in minimax MPC. In many time instant, this worst-case is identical to low available renewable infeed and high load. Considering such a scenario, the conventional generator is enabled because low renewable infeed is expected. This leads to an increased conservativeness of the approach in the closed loop.

This conservativeness can also be noted in Table 12.3. Here, the mean economically motivated cost is almost 19 % higher than with the prescient controller. Furthermore, the renewable

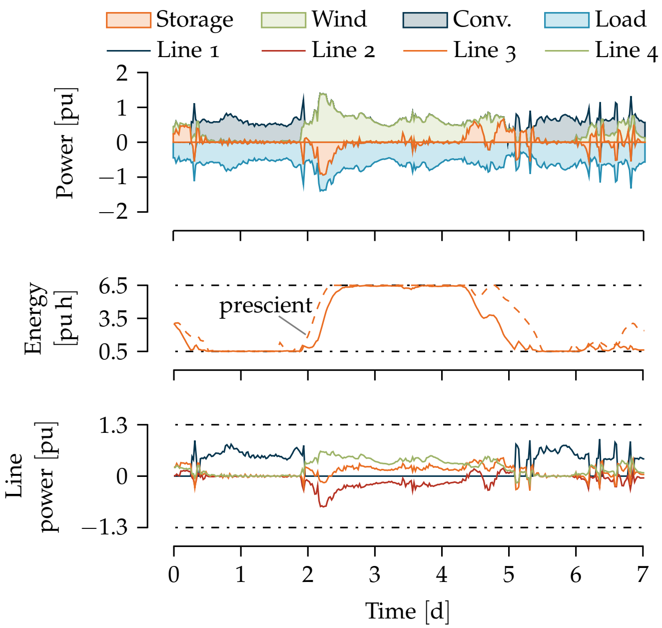

Figure 12.5: Power of units and load as well as stored energy and line power of simple MG in closed-loop simulation with minimax MPC approach.

share is significantly reduced by around 20 %. Compared to the certainty equivalence approach, the cost associated with the state of charge is lower, which indicates an increased robustness to uncertain renewable infeed and load. Moreover, the number of constraint violations could be reduced to 0, i.e., no unit or line power constraint was violated.

The major drawback of the minimax MPC is its increased conservativeness which translates into increased costs and decreased renewable share. One reason for this conservativeness is that Problem 5 represents an open-loop approach, i.e., feedback of the controller is *not* modeled in the problem formulation. The simulation results when considering feedback in the prediction is discussed next.

Risk-averse MPC ($\alpha = 0$). For $\alpha = 0$, the risk-averse MPC becomes a scenario-based worst-case MPC (see Remark 11.2.4). One big difference compared to minimax MPC is that the formulation allows to model possible feedback actions in the controller. This typically leads to less conservative control actions than with minimax MPC.

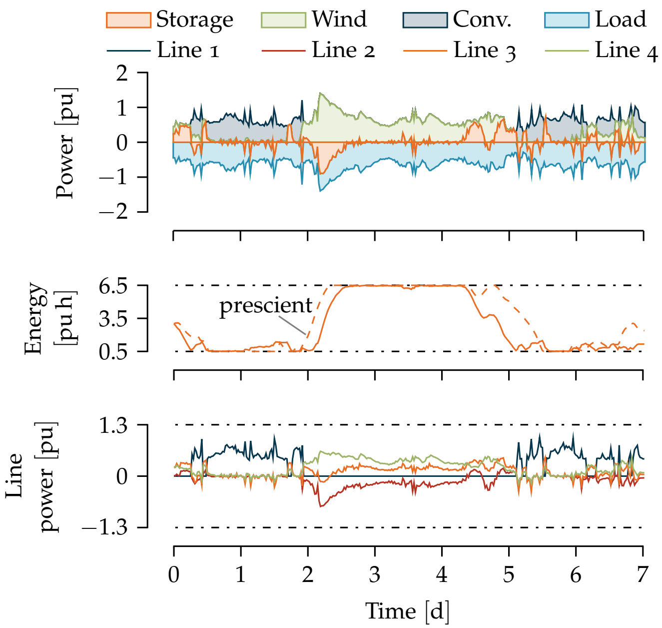

Figure 12.6: Power of units and load as well as stored energy and line power of simple MG in closed-loop simulation with risk-averse MPC approach for $\alpha = 0$.

The closed-loop simulation results are show in Figure 12.6. It can be seen that considering feedback in the MPC formulation leads to slightly less conservative control actions than with the minimax approach. Another reason for less conservative control actions is that the underlying tree only includes the worst-case at the first stage (see Section 12.1.2). This leads to less extreme worst-case scenarios that require less conservative control actions.

The reduced conservativeness compared to the minimax MPC can also be noted in Table 12.3. Here, the mean costs are lower than with the minimax MPC. Still, the economically motivated cost is more than 17 % higher and the renewable share almost 20 % below the prescient case. The number of switching actions is a little bit higher than with the minimax approach. Note that the approach did not lead to any unit or line power constraint violations.

One disadvantage of the approach is its conservativeness which translates into increased cost and decreased renewable share. The main reason for this is that the worst-case cost is minimized. A different way to find suitable power setpoints is to minimize the expected value of the cost, as discussed next.

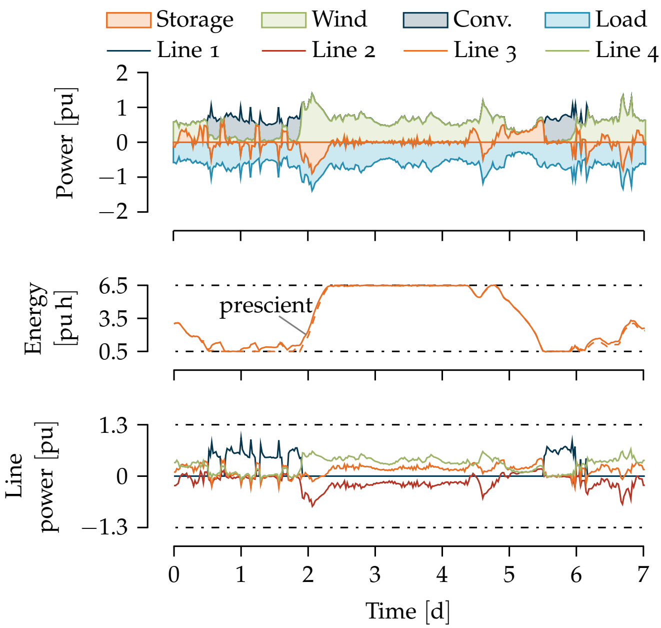

Figure 12.7: Power of units and load as well as stored energy and line power of simple MG in closed-loop simulation with risk-averse MPC approach for $\alpha = 1$ which is equivalent to the risk-neutral stochastic MPC.

Risk-neutral stochastic / risk-averse MPC ($\alpha = 1$). Similar to the worst-case approach from the previous paragraph, this controller considers a forecast in the form of a scenario tree. As discussed in Remark 11.2.3, the risk-neutral stochastic MPC is identical to the risk-averse MPC for $\alpha = 1$. Therefore, the results of this paragraph cover both approaches.

The closed-loop simulation results are show in Figure 12.7. It can be noted that the operation setpoints lead to a much less conservative operation that with risk-averse MPC for $\alpha = 0$. This can be seen in the significantly increased renewable infeed. Moreover, the number of time instants where the conventional generator is enabled is smaller than for $\alpha = 0$. The stored energy closely follows the trajectory of the prescient controller.

The good performance is also reflected in Table 12.3: The average economically motivated cost has the lowest value of all approaches that consider a real forecaster and is only 0.74 % higher than the cost from the simulation with the prescient controller. Unfortunately, the energy-related cost is higher than with the other risk-averse and the minimax approaches such that the overall cost $\overline{\ell}_o + \overline{\ell}_x$ is identical to the

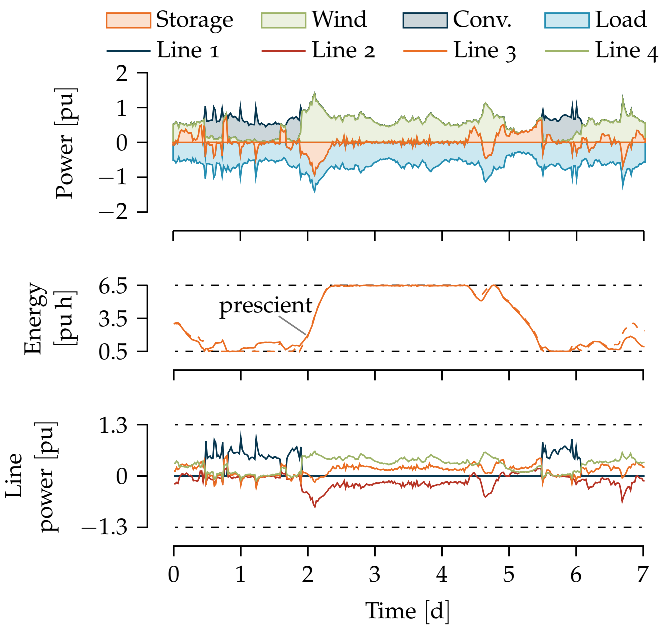

Figure 12.8: Power of units and load as well as stored energy and line power of simple MG in closed-loop simulation with risk-averse MPC approach for $\alpha = 0.5$.

one from of the risk-averse MPC with $\alpha = 0$. The number of switching actions is more than twice as high as in the prescient simulation. However, no unit or line power constraint is violated in the closed-loop simulations with this controller.

Even though this controller performs well in terms of economically motivated costs and renewable share, it can lead to a higher energy-related cost, especially in presence of high-effect low-probability events. To compensate for this drawback, a risk-averse controller that considers some ambiguity in the forecast probability distribution is used to operate the MG in the next paragraph.

Risk-averse MPC ($\alpha = 0.5$). Similar to other risk-averse approaches, the controller considered in this paragraph also requires a forecast scenario tree. As discussed in Chapter 11, for $\alpha \in (0, 1)$ the risk-averse MPC approach interpolates between worst-case MPC ($\alpha = 0$) and risk-neutral stochastic MPC ($\alpha = 1$). In this example, we assume some ambiguity in the forecast probability distribution by selecting $\alpha = 0.5$.

The closed-loop simulation results are show in Figure 12.8. It can be noted, e.g., by the charging rate of the battery, that the approach is more conservative than the risk-averse MPC with $\alpha = 1$ but less conservative than the risk-averse MPC with $\alpha = 0$. Another indicator of the increased conservativeness in comparison to the risk-averse approach with $\alpha = 1$ is the larger number of time instants where the conventional generator is enabled.[5]

The average economically motivated costs $\bar{\ell}_o$ for $\alpha = 0.5$ lie between those for $\alpha = 0$ and $\alpha = 1$ (see Table 12.3). However, the lowest overall cost $\bar{\ell}_o + \bar{\ell}_x$ of all approaches with real forecasts could be achieved using the risk-averse MPC with $\alpha = 0.5$. This indicates that the risk-averse approach for $\alpha \in (0, 1)$ can provide a good trade-off between worst-case and risk-neutral stochastic MPC. The number of switching action is slightly above the prescient controller. During the simulation, no unit or line power constraints were violated.

Note that in this example, $\alpha = 0.5$ was chosen to show an operation regime between risk-neutral and worst-case. Depending on the setup and the accuracy of the forecast probability distribution, tuning α will most likely lead to a better performance than the one obtained for $\alpha = 0.5$.

[5] Note that despite the decreased number of switching actions, the conventional generator is operated more often for $\alpha = 0.5$ than for $\alpha = 1$.

12.2.3 *Sensitivity analysis*

The following analysis aims to illustrate the operation with different control schemes in presence of misestimated forecast probability distributions. First, the data considered in the sensitivity analysis is introduced. Then, the simulation results are discussed.

Data. For the sensitivity analysis, 1 000 closed-loop simulations with simulation horizon $K = 144$ and initial state $x_0 = 0.5\,\text{pu}\,\text{h}$ were performed. For each closed-loop simulation, a different scenario of load and available renewable power was considered as uncertain input to the plant model, while using the same forecasts for all scenarios.[6] Thereby, a misestimated forecast probability distribution was emulated.

[6] Naturally, the forecast was adapted at each simulation step $k \in \mathbb{N}_{[1,K]}$ by using the nominal past values of load and wind speed.

	Mean	Std. dev.
Load	$-0.085\,\text{pu}$	$0.028\,\text{pu}$
Wind speed	$-1.883\,\text{m/s}$	$0.628\,\text{m/s}$

Table 12.4: Mean and standard deviation of normally distributed errors in sensitivity analysis.

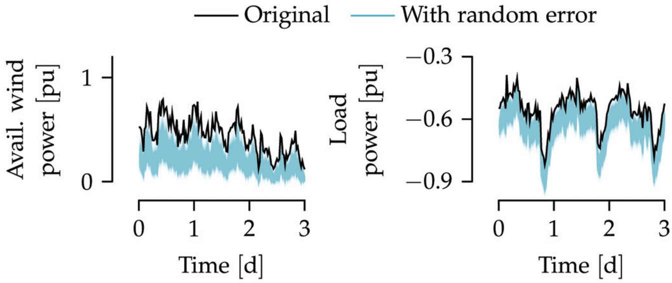

Figure 12.9: 1 000 scenarios of wind and load data used in sensitivity analysis with constant offset of 3 times the standard deviation.

All 1 000 scenarios considered as uncertain input of the plant model together with the original data used to obtain the nominal forecasts are shown in Figure 12.9. The original data of load and wind speed directly succeeds the data considered in the nominal simulations in Figure 12.2. To emulate misestimated forecast probability distributions, the data used as uncertain input to the plant model was modified by adding Gaussian noise. Therefore, the mean and the standard deviation in Table 12.4 were considered. This way, the number of high-effect low-probability (HELP) events, i.e., events that rarely occur but have a high effect on the operation cost, was artificially increased. Note that the error of the wind turbine was added to wind speed before the available renewable power was calculated using (6.14).

Analysis. With each controller, 1 000 closed-loop simulations were performed. For each simulation and each controller the economically motivated cost $\overline{\ell}_0$ and the cost associated with the state of charge $\overline{\ell}_x$ were deduced. The probability distributions resulting from these simulations are shown in Figure 12.10.

A brief introduction to box plots can be found in Section 3.1.

For the prescient MPC from Chapter 5 which represents a hypothetical best case the forecast data was given in form of the noisy input to the plant model from Figure 12.9. It can be seen in Figure 12.10 that the economically motivated cost $\overline{\ell}_0$ of the prescient MPC has the lowest median of all controllers. Moreover, the energy-related cost $\overline{\ell}_x$ with a mean of less than $0.1 \cdot 10^{-12}$ is practically zero. The reason for the low cost is that the uncertain input of the plant in this case is a priori known to the MPC. Therefore, the prescient controller can easily minimize the cost for everything that will happen.

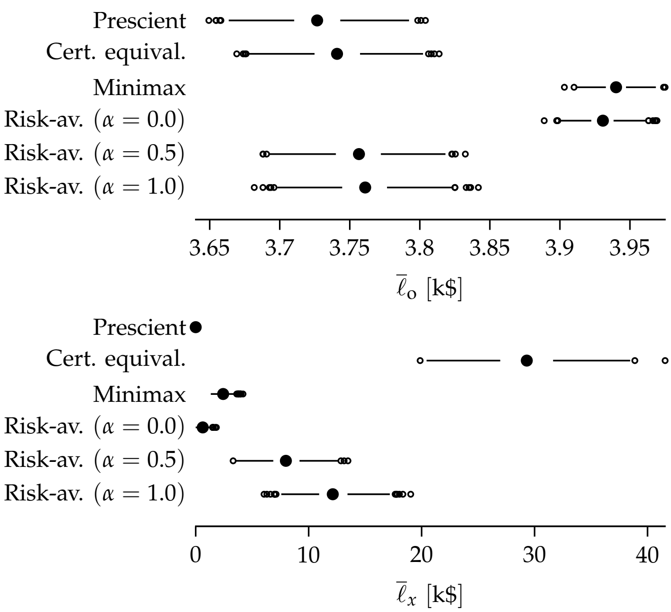

Figure 12.10: Probability distributions of costs in sensitivity analysis. The costs were obtained from closed-loop simulations with different controllers where an error with nonzero mean was added to the uncertain input of the plant model.

The probability distribution of the economically motivated cost $\overline{\ell}_o$ derived with the certainty equivalence MPC from Chapter 7 has an almost identical standard deviation and a slightly higher median than the distribution obtained with the prescient controller. The energy-related cost $\overline{\ell}_x$ has the highest median and standard deviation of all controllers. This clearly illustrates a lack of robustness to uncertain probability distributions and HELP events and underlines that the approach is not suitable for islanded MGs with high renewable share.

The highest median as well as the lowest standard deviation of all distributions of $\overline{\ell}_o$ can be observed for the minimax MPC from Chapter 8. Median and standard deviation of $\overline{\ell}_x$ are significantly lower than with the certainty equivalence controller. This indicates a major increase in robustness which results in a decreased sensitivity of $\overline{\ell}_x$ to uncertain probability distributions and HELP events. This robustness, however, comes at the price of higher values of $\overline{\ell}_o$.

A slightly lower economically motivated cost than with the minimax MPC can be achieved with the risk-averse approach for $\alpha = 0$. Here, the cost associated with the state of charge $\overline{\ell}_x$ has the lowest median and standard deviation of all approaches with real forecasts. This indicates a small increase in performance compared to the minimax MPC. Even though the economically motivated cost slightly decreases compared to the minimax approach, the increased robustness still comes at the price of a high median of $\overline{\ell}_o$.

The risk-averse controller with $\alpha = 1$ leads to a significantly lower median in the distribution of $\overline{\ell}_o$ than the controller with $\alpha = 0$. The standard deviation of this cost is more than two times as high as for $\alpha = 0$. This shows that the lower cost comes at the price of an increased sensitivity to misestimated forecast probability distributions. Furthermore, mean and standard deviation of $\overline{\ell}_x$ are higher than for $\alpha = 0$. This indicates a decreased robustness to misestimated probability distributions compared to $\alpha = 0$.

Median and standard deviation the distribution associated with $\overline{\ell}_o$ decrease for $\alpha = 0.5$ compared to $\alpha = 1$. The same holds for cost associated with the state of charge $\overline{\ell}_x$. This indicates an increased robustness of the controller to misestimated forecast probability distributions and HELP events. The results also reflect that choosing $\alpha \in (0, 1)$ allows to interpolate between worst-case and risk-neutral stochastic MPC to tune the robustness of the controller.

In conclusion, if the number of misestimated forecasts is expected to be very large, it is beneficial to chose α close to zero. This can be seen in the mean value of the overall cost $\overline{\ell}_o + \overline{\ell}_x$ which is minimal for $\alpha = 0$. The sensitivity analysis considers an extreme case that aims to illustrate how robustness to misestimated forecasts changes with α. In setups, where the forecast is not expected to exhibit a systematic error, it is usually beneficial to choose $\alpha > 0$.

12.3 *Closed-loop simulations with extended MG*

In this section, the results of simulations performed with the MG in Figure 12.11 are presented. First, the parameters of the MG and the weights of the cost function are introduced. Then, the results of a single simulation run are discussed.

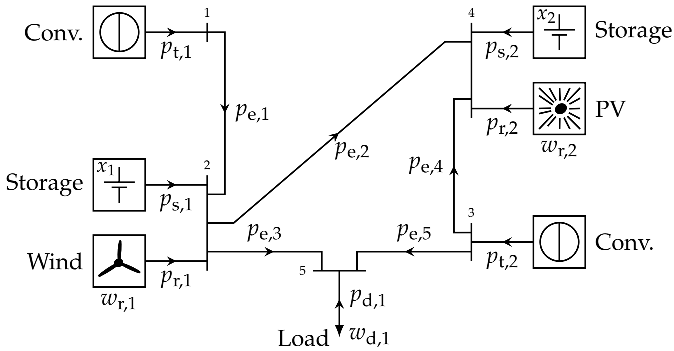

Figure 12.11: Setup of extended MG, motivated by [123]. The grid includes two conventional, two storage and two renewable units, i.e., a photovoltaic (PV) power plant and a wind turbine. These units and the load are connected by transmission lines.

12.3.1 Grid setup

The extended MG considered in this section is shown in Figure 12.11. It is composed of two conventional, two storage units, a wind turbine and a PV power plant. The units are connected to each other and the load by transmission lines with impedances

$$\begin{bmatrix} y_1 & y_2 & y_3 & y_4 & y_5 \end{bmatrix} = \begin{bmatrix} y & y & y/2 & y & y/2 \end{bmatrix},$$

where $y \in \mathbb{R}_{>0}$, i.e., all lines except for those that connect the load have the same impedance. With these values and the grid structure shown in Figure 12.11, the power of the lines can be calculated from the power of the units and the load via

$$\begin{bmatrix} p_{e,1} \\ p_{e,2} \\ p_{e,3} \\ p_{e,4} \\ p_{e,5} \end{bmatrix} = \underbrace{\begin{bmatrix} 1 & 0 & 0 & 0 & 0 & 0 & 0 \\ 1/3 & -1/3 & 1/3 & -1/2 & 1/3 & -1/2 & 0 \\ 2/3 & 1/3 & 2/3 & 1/2 & 2/3 & 1/2 & 0 \\ -1/3 & 1/3 & -1/3 & -1/2 & -1/3 & -1/2 & 0 \\ 1/3 & 2/3 & 1/3 & 1/2 & 1/3 & 1/2 & 0 \end{bmatrix}}_{\tilde{F}U} \begin{bmatrix} p_{t,1} \\ p_{t,2} \\ p_{s,1} \\ p_{s,2} \\ p_{r,1} \\ p_{r,2} \\ w_{d,1} \end{bmatrix}.$$

The rated power of the lines is assumed to be such that each line allows to transmit power between -1.3 pu and 1.3 pu.

The unit parameters can be found in Table 12.5. Note that the rated power of the storage units is such that the MG can run without requiring a conventional generator for a certain duration. Storage unit 1 at bus 2 has a larger storage capacity (7 pu h) than storage unit 2 at bus 4 (4 pu h). Furthermore, storage 1 is assumed to cover less fluctuations as $\chi_{s,1} = 4$ is

Table 12.5: Transmission line and unit parameters of extended MG.

Parameter	Value
$p_t^{\min}$	$\begin{bmatrix} 0.6 \\ 0.4 \end{bmatrix}$ pu
$p_t^{\max}$	$\begin{bmatrix} 1 \\ 1 \end{bmatrix}$ pu
$p_s^{\min}$	$\begin{bmatrix} -1 \\ -1 \end{bmatrix}$ pu
$p_s^{\max}$	$\begin{bmatrix} 1 \\ 1 \end{bmatrix}$ pu
$p_r^{\min}$	$\begin{bmatrix} 0 \\ 0 \end{bmatrix}$ pu
$p_r^{\max}$	$\begin{bmatrix} 2 \\ 2 \end{bmatrix}$ pu
$x^{\min}$	$\begin{bmatrix} 0 \\ 0 \end{bmatrix}$ pu h
$x^{\min}$	$\begin{bmatrix} 7 \\ 4 \end{bmatrix}$ pu h
$\tilde{x}^{\min}$	$\begin{bmatrix} 0.5 \\ 0.5 \end{bmatrix}$ pu h
$\tilde{x}^{\max}$	$\begin{bmatrix} 6.5 \\ 3.5 \end{bmatrix}$ pu h
x_0	$\begin{bmatrix} 3 \\ 2 \end{bmatrix}$ pu h
K_t	$\begin{bmatrix} 1 & 0 \\ 0 & 1/2 \end{bmatrix}$
K_s	$\begin{bmatrix} 1/4 & 0 \\ 0 & 1/8 \end{bmatrix}$

smaller than $\chi_{s,2} = 8$.[7] The minimum power of the conventional generators was chosen such that unit 1 at bus 1 has a larger minimum power than conventional unit 2 at bus 3. The unit at bus 1 is further assumed to cover less fluctuations as $\chi_{t,1} = 1$ is smaller than $\chi_{t,2} = 2$. Moreover, both units are assumed to cover less fluctuations than the storage units. The maximum power of the conventional generators is such that the load can always be covered if both generators are running. The rated power of the wind turbine and the PV power plant, is such that in times of high renewable infeed the load can be served and the storage units can be charged.

[7] For the MG considered here, we have $K_s = \mathrm{diag}([1/\chi_{s,1} \quad 1/\chi_{s,2}]^\top)$, $K_t = \mathrm{diag}([1/\chi_{t,1} \quad 1/\chi_{t,2}]^\top)$.

The weights of the cost function can be found in Table 12.6. Here, the fuel costs are based on the costs of units 16 and 19 in [265]. For the storage units, it is assumed that the costs for unit 1, i.e., the unit with a larger capacity, are higher than for the other unit. The weight for the renewable power was chosen to emphasize infeed from the PV power plant as it was assumed to cause less operation and maintenance costs than the wind turbine. For a brief discussion on c_r', the reader is kindly referred to Remark 12.2.1. Finally, the weights of the energy-related cost were chosen to be equal for both units. Here the same value as for the small MG from Section 12.2 was selected.

Table 12.6: Weights in cost function of extended MG.

Weight	Value
c_t	$\begin{bmatrix} 0.1178 \\ 0.1188 \end{bmatrix}$ k\$
c_t'	$\begin{bmatrix} 0.751 \\ 0.7578 \end{bmatrix}$ k\$/pu
c_t''	$\begin{bmatrix} 0.0048 \\ 0.0057 \end{bmatrix}$ k\$/pu^2
c_t^{sw}	$\begin{bmatrix} 0.1 \\ 0.11 \end{bmatrix}$ k\$
c_s''	$\begin{bmatrix} 0.05 \\ 0.03 \end{bmatrix}$ k\$/pu^2
c_r'	$\begin{bmatrix} 0.001 \\ 0.0012 \end{bmatrix}$ k\$/pu
c_r''	$\begin{bmatrix} 1.0 \\ 1.2 \end{bmatrix}$ k\$/pu^2
c_x	$\begin{bmatrix} 10^3 \\ 10^3 \end{bmatrix}$ k\$/pu h

12.3.2 *Results of single simulation run*

Simulations with different controllers were executed for the simulation time-series shown in Figure 12.12. Using a sampling time of $T_s = 30$ min and a simulation horizon of 7 d, the simulation time-series consists of 336 data points. The data was generated using the wind speed and irradiance measurements from [12]. The load time-series originates from the same source as the one from Section 12.2 and was scaled by a factor of 1.5. As indicated in Section 12.1.4, Gaussian noise with zero mean and a small standard deviation was added to obfuscate the source of the load data.

The simulations were executed for the MPC approaches presented earlier, i.e., for the

1. prescient MPC from Chapter 5,

2. certainty equivalence MPC from Chapter 7,

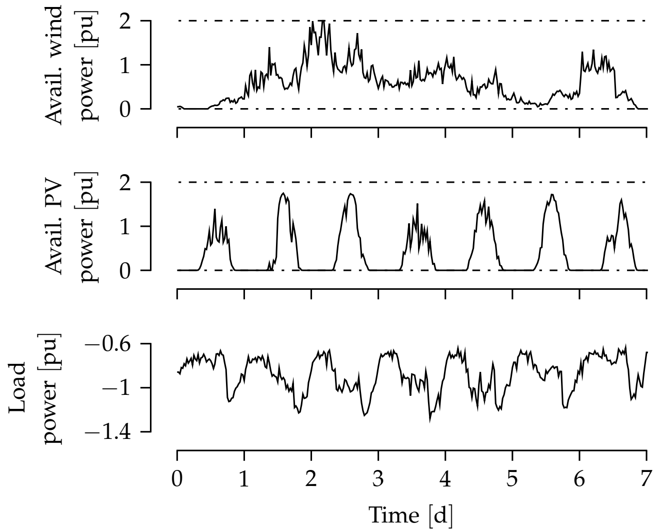

Figure 12.12: Time-series of available infeed of wind turbine and photovoltaic (PV) plant as well as demand for simulation with extended MG.

3. minimax MPC from Chapter 8,
4. risk-averse MPC from Chapter 11 for $\alpha = 0.0$,
5. risk-neutral stochastic MPC from Chapter 10 which is equivalent to the risk-averse MPC from Chapter 11 for $\alpha = 1.0$, and
6. risk-averse MPC from Chapter 11 for $\alpha = 0.5$.

The accumulated results of the simulations are summarized in Table 12.7 on page 190. It can be observed, that the maximum time required to solve the problems is below 4 min for all approaches. Considering a sampling time of 30 min, this seems adequately fast.

In the following paragraphs the results of the simulations are discussed in more details. Therefore, we move columnwise from left to right in Table 12.7, i.e., from prescient to risk-averse MPC. For compactness, only the plots of the simulation with the prescient and the risk-averse ($\alpha = 0.5$) controller are shown here. The remaining plots can be found in Appendix A.

Prescient MPC. As for the simulations with the simple grid in Section 12.2, the prescient controller is used as a reference.

	Prescient	Cert. equiv.	Minimax	Risk-averse, $\alpha =$ 0.0	0.5	1.0
Mean econ. motiv. cost $\overline{\ell}_o$ [k$]	5.99	6.08	7.64	7.42	6.09	6.01
Mean energy-related cost $\overline{\ell}_x$ [k$]	0	1.64	0.02	0.03	0.59	1.06
Share of RES [%]	95.45	92.05	49.41	56.47	93.02	93.26
Switching actions	8	10	33	59	14	12
Power constraint violations	0	3	0	0	0	0
Mean solve time [s]	0.03	0.04	4.16	3.44	2.87	4.27
Maximum solve time [s]	0.08	0.29	26.07	93.08	40.28	206.32

Table 12.7: Results of all simulations performed with the extended MG.

It assumes a hypothetical perfect forecast, i.e., the future load and available renewable power are perfectly known over the prediction horizon. As we do not consider any modeling errors (see Remark 12.1.6), the prescient controller represents a hypothetical best-case. The formal description of the controller is given by Problem 2.

The results of the closed-loop simulation are show in Figure 12.13. Here, it can be seen that initially both storage units are discharged due to low available renewable power. When both batteries are almost empty, conventional generator 1, i.e., the generator with lower fuel cost, less participation in power sharing and higher minimum power is enabled. At some point, the available renewable power increases, such that the conventional generator can be disabled and the batteries are charged by the renewable units. After a period where first conventional generator 1 and then conventional generator 2 is enabled, the available power of the wind turbine and the PV power plant increases and the storage units can be charged using renewable infeed. If power from both renewable units is available, a mix is chosen that puts an emphasis on infeed from the PV power plant due to the choice of weights in the cost function. By the time the storage units are fully charged, renewable infeed is limited. Due to the seasonal pattern of load and PV power plant, small charging cycles of the storage units can be observed. This cycles are dominantly covered by the smaller storage unit 2 which has a lower power-related cost. At the end of day five, the storage units start a full discharge that is caused by low available renewable infeed. After a short period in which conventional generator 1 is enabled,

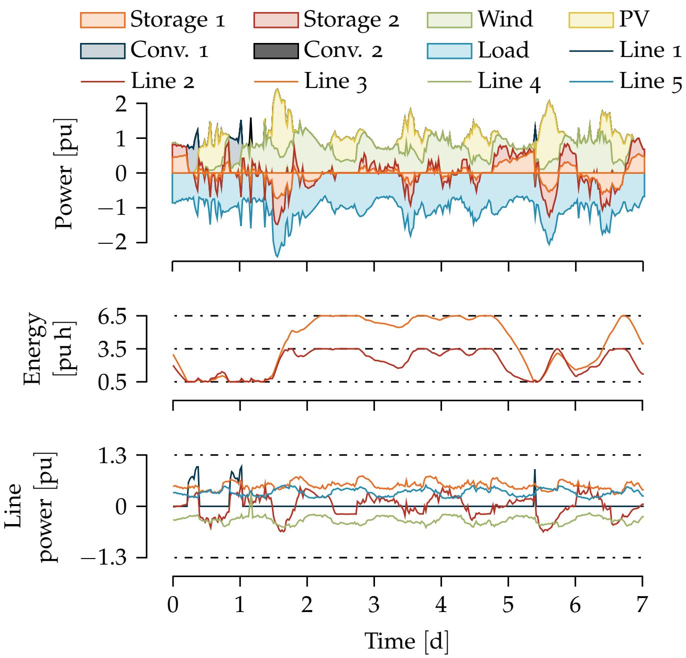

Figure 12.13: Power of units and load as well as stored energy and line power of extended MG in closed-loop simulation with prescient MPC approach.

the available power from the PV power plant increases such that the storage units can be charged again. Like before, the small cycles are dominantly covered by storage unit 2.

As indicated in Table 12.7, the overall renewable share of the prescient case is above 95 %. This is significantly higher that the share of RES in the small grid which is only around 75 %. The reason for this increase, despite the higher storage capacity and larger number of installed RES, is the temporal dissimilarity of available infeed from the PV power plant and the wind turbine. In many time instants, low available infeed from one source is compensated by higher infeed from the other. The number of constraint violations is zero, i.e., no unit or line power limit of the plant model is violated in the closed-loop simulations. The number of switching actions is 8, i.e., conventional generators are enabled 4 times and disabled 4 times.

In the next paragraph, the certainty equivalence MPC is used. For this controller, the perfect forecast is replaced by a nominal forecast obtained with the ARIMA models from Chapter 6.

Certainty equivalence MPC. This approach represents the state-of-the-art for the operation of MGs. It is based on the assumption that future load and available renewable infeed follow their nominal forecasts. These forecasts were obtained as described in Section 12.1.1 and used in the MPC formulation given by Problem 3.

In comparison to the prescient controller (see Table 12.7), the mean economically motivated cost is around 1.5 % higher and the renewable share 3 % lower. Furthermore, high energy-related costs can be observed. In total, there are 3 power constraint violations, all for violating the lower limits of the conventional generators with a maximum violation of $5.6 \cdot 10^{-3}$ pu. For the transmission lines, no constraint violations could be observed. The number of switching actions is above the prescient controller, but still small.

Similar to the results for the simple MG in Section 12.2.2, the violation of power constraints and the high energy-related costs render this approach unsuitable for use in a practical setup with a high share renewable infeed. To find power setpoints that are robust to uncertain renewable infeed, a minimax approach is used next.

Minimax MPC. This approach is based on the assumption that load and available power of the wind turbine and the PV power plant are within bounded intervals. These intervals were obtained, as indicated in Section 12.1.1, based on real forecasts without prior knowledge about the future. The optimal setpoints for the MG were deduced using the MPC formulation given by Problem 5.

The controller leads to much more conservative control actions than the other approaches. This can be noted by an increase in mean economically motivated costs of 27.5 % compared to the prescient controller (see Table 12.7). The average costs associated with the state of charge are almost zero. The overall cost, $\overline{\ell}_0 + \overline{\ell}_x$, is slightly lower than for the certainty equivalence approach. Furthermore, the renewable share is significantly reduced by more than 45 % and the number of switching actions more than four times as high as with the prescient controller. Using the minimax controller, no power or energy constraints were violated.

The major drawback of the minimax approach is the significant increase in conservativeness which translates into increased economically motivated cost and decreased renewable share. One reason for this is that the minimax MPC does not consider feedback over the prediction horizon in the problem formulation. The simulation results when considering feedback are discussed in the next paragraph.

Risk-averse MPC ($\alpha = 0$). This approach can be understood as an extension of the minimax MPC as it considers feedback over the prediction horizon in the MPC formulation and thereby allows to reduce the conservativeness of the controller. As posed in Remark 11.2.4, the risk-averse MPC for $\alpha = 0$ is equal to a scenario-based worst-case MPC. For the approach, collections of independent forecast scenarios are derived (see Section 12.1.1) and used to construct scenario trees (see Section 12.1.2).

The reduced conservativeness of the approach in comparison to the minimax MPC can be noted in Table 12.7. Here, the mean economically motivated cost is lower than with the minimax MPC. Still, it remains around 24 % higher than the one of the prescient MPC. The overall cost, $\overline{\ell}_o + \overline{\ell}_x$, is lower than for the minimax approach. The number of switching actions has the largest value of all controllers. No unit or transmission line power constraints were violated with this approach.

One big disadvantage of this approach is that it is much more conservative than the prescient MPC. This especially shows in the increased cost and the decreased renewable share. One major reason for this conservativeness is that the worst-case cost is minimized. An alternative way to find suitable power setpoints is to minimize the expected value of the cost, as discussed next.

Risk-neutral stochastic / risk-averse MPC ($\alpha = 1$). Similar to the worst-case MPC from the previous paragraph, this controller considers a forecast scenario tree. As indicated in Remark 11.2.3, the scenario-based risk-neutral stochastic MPC is identical to the risk-averse MPC with $\alpha = 1$. Therefore, the results of this paragraph cover the schemes that employ Problems 6 and 8.

The numerical comparison with other controllers in Table 12.7 shows that the approach performs well in terms of economically motivated costs and renewable share. The average cost $\overline{\ell}_o$ is only 0.3 % above the prescient controller, which is the lowest value of all schemes that consider real forecasters. The overall costs, $\overline{\ell}_o + \overline{\ell}_x$, are lower than for the approach with $\alpha = 0$. The number of switching actions is higher than with the prescient controller but still in a similar range. During the closed-loop simulation, no unit or line power constraints of the plant were violated with this approach.

Even though, the controller performs well in terms of economically motivated costs, it can lead to higher energy-related costs, especially if the probability distribution of the scenario tree cannot be fully trusted. To compensate for this drawback, a risk-averse approach that considers ambiguity in the forecast probability distribution is used in the next paragraph.

Risk-averse MPC ($\alpha = 0.5$). The risk-averse controller for $\alpha \in (0, 1)$ assumes some ambiguity in the forecast probability distribution as described in Chapter 11. This can help to reduce the impact of HELP events and misestimated forecast probability distributions.

The results of the closed-loop simulation are show in Figure 12.14. It can be noted, e.g., by the lower charging rates of the batteries, that the approach is more conservative than the prescient MPC. Moreover, the storage units are not always fully charged.

The average economically motivated cost for $\alpha = 0.5$ lies between the cost for $\alpha = 0$ and $\alpha = 1$ (see Table 12.3). It is about 1.7 % higher than with the prescient MPC and about 1.3 % higher than with the risk-averse controller with $\alpha = 1.0$. The overall cost, $\overline{\ell}_o + \overline{\ell}_x$, has the lowest value of all approaches with real forecasters. The renewable share is about 2.4 % lower than with the prescient controller. The number of switching actions is above the prescient MPC but still in a similar region as with the certainty equivalence and the risk-neutral stochastic MPC. During the closed-loop simulations, no unit or line power limit of the plant model was violated using the risk-averse controller with $\alpha = 0.5$.

The results indicate that the risk-averse approach for values of α between 0 and 1 allows for a good trade-off between

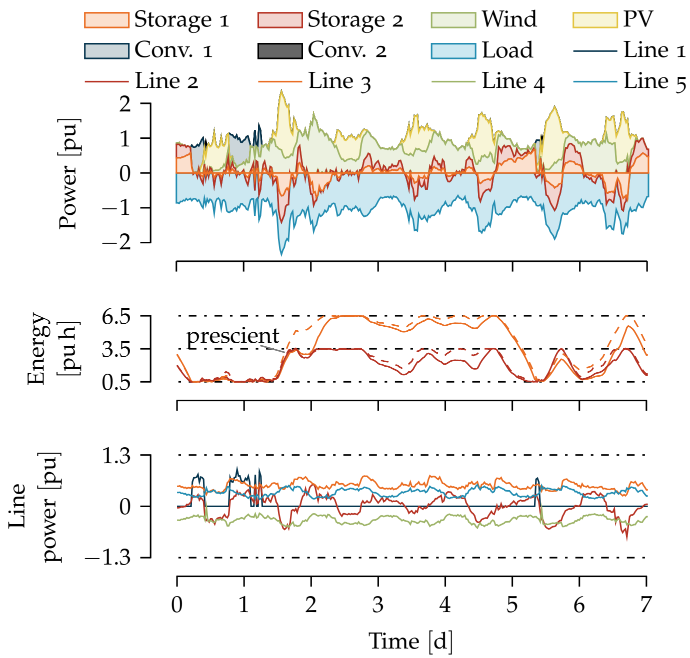

Figure 12.14: Power of units and load as well as stored energy and line power of extended MG in closed-loop simulation with risk-averse MPC approach for $\alpha = 0.5$.

worst-case and risk-neutral stochastic MPC. In this example, $\alpha = 0.5$ was chosen to show the interpolation between the two other extreme cases. Depending on the setup and the accuracy of the forecast probability distribution, tuning α can help to further increase the performance.

12.4 Summary

In this chapter, the use of the forecast and the controllers derived in the previous chapters has been illustrated on two different islanded MGs. The computing time of the numerical solver was assessed indicating that all controllers are sufficiently fast considering a sampling time of 30 min for both MG setups. Furthermore, a sensitivity analysis that included a high number of simulation runs was conducted to assess the robustness of the approaches to uncertainties in the forecast probability distribution.

The properties of the different controllers were analyzed leading to the conclusion that the risk-averse controller for $\alpha \in (0, 1)$ provides a good trade-off between performance in terms of cost and robustness to ambiguity in forecast probability distributions. The sensitivity analysis further indicated that the operation costs can be reduced by assuming certain ambiguity in the forecast probability distribution. In addition, it could be shown that the standard deviation of costs decreases for approaches that are more averse to misestimated forecast probability distributions. This translates into less uncertainty about the operation cost which renders the risk-averse MPC especially suitable for real-world applications.

For the two grid setups considered, it could be shown that with the risk-averse approach, an economically beneficial operation of islanded MG with high share of renewable sources can be achieved. Moreover, the importance of the operation management could be illustrated: depending on the controller chosen for this layer, the costs, the renewable share and the number of constraint violations significantly vary. In conclusion, the choice of a suitable control scheme was shown to be crucial for a safe and meaningful operation of MGs with high share of renewable sources.

13 Conclusion

In this thesis, MPC approaches for the operation of islanded MGs were deduced in computationally tractable ways and compared to each other. These approaches can be distinguished by the way they model uncertain load and available renewable infeed. In summary, the main findings of this thesis are as follows.

- Suitable optimization models that account for the behavior of the lower control layers enable the design of appropriate operation control schemes for islanded MGs with high renewable share.
- The forecast probability distributions of renewable infeed and load need to be explicitly considered in operation control approaches for islanded MGs with high renewable share.
- Risk-averse MPC allows for a safe and economically meaningful MG operation that is robust to misestimated forecast probability distributions and high-effect low-probability events.

In what follows, first, a detailed summary is provided in Section 13.1. Then, future research directions are highlighted in Section 13.2.

13.1 Summary

In Chapter 2, a general introduction to MGs and hierarchical control thereof was provided. Based on this introduction, requirements for the operation control layer were formulated.

These can be divided into requirements that concern the MG model and requirements that concern the uncertain load and available renewable infeed. The former include the modeling of power flow over the transmission lines, power sharing between grid-forming units, and curtailment of renewable infeed in the control scheme. The latter demand the MPC schemes to be robust to uncertain available renewable infeed and load as well as misestimated forecasts. The identified requirements provide a basis for the formulation and evaluation of different operation control strategies.

In Chapter 3, basic notation and reformulations from optimization theory were introduced. Moreover, a general introduction on power flow over transmission lines was provided.

In Chapter 4, the mathematical model of an islanded MG was derived. This model provides the basis for various operation control schemes designed for island MGs with an arbitrary finite number of units, loads and transmission lines. The model includes (i) renewable energy sources, where the power infeed can be limited, e.g., if storage units are fully charged; (ii) grid-forming storage units; and (iii) conventional generators that can be disabled, e.g., in times of high available renewable infeed. Furthermore, it considers power flow over the transmission lines as well as power sharing of grid-forming units. Opposed to existing approaches, the model is especially tailored for MGs with high share of RES. This, for example, shows in the way the effects of uncertain renewable infeed and load on the grid-forming storage and conventional units are included or the fact that an operation mode without conventional units is considered.

Using the mathematical model of an islanded MG, in Chapter 5 a generic MPC problem was formulated. Therefore, a cost function was derived that includes costs incurred by fuel consumption of conventional generators and by curtailment of renewable infeed. Additionally, it comprises costs related to storage losses and to the state of charge. The generic MPC problem formulation serves as a reference for the real-world controllers derived in the succeeding chapters.

Before designing real-world MPC schemes, in Chapter 6 different ARIMA forecast models for load and available renewable power of wind turbines and PV power plants were identified by performing an exhaustive search that included more than 6 000 model structures. The identified ARIMA models are required to generate forecasts of the uncertain input for the different MPC formulations.

Based on the generic MPC formulation and the nominal forecasts of load and available renewable infeed, a certainty equivalence operation control scheme was obtained in Chapter 7. This scheme assumes that the nominal forecasts are certain. However, this assumption was identified to be unsuitable for the control of an islanded MG with high share of RES: In closed-loop simulations, the certainty equivalence scheme led to violations of power limits and high costs incurred by states of charge outside the desired intervals.

To counteract the drawbacks of the certainty equivalence MPC, a robust minimax operation control scheme was derived in Chapter 8. This scheme considers a forecast in the form of time-varying intervals that do not exhibit any probabilistic information and minimizes the worst-case cost over all possible disturbance values in these intervals. In the closed loop, limit violations and high costs incurred by states of charge outside the desired operating range could be avoided at the expense of higher economically motivated costs.

The conservativeness of the minimax scheme can be reduced employing forecast probability distributions of loads and renewable infeed. Scenario trees can be seen as a compact representation of these probability distributions. In Chapter 9, they were introduced by illustrating how constraints and costs can be formulated on a scenario tree. Furthermore, the derivation of scenario trees from collections of independent forecast scenarios was highlighted.

Employing scenario trees, a risk-neutral stochastic MPC scheme for the operation of islanded MGs was derived in Chapter 10. In this scheme, different scenarios of load and available renewable infeed are considered in the constraints and the cost function. The expected cost over all forecast scenarios was minimized, assuming that the predicted probability distribution in the form of a scenario tree is certain. For accurate forecast probability distributions, this approach led to much less conservative control actions while avoiding constraint violations in the closed loop.

One drawback of the risk-neutral stochastic MPC approach is that it relies on the forecast probability distributions to be certain. With the risk-averse MPC approach presented in Chapter 11, this drawback could be addressed by considering ambiguity in the probabilities of the forecast scenario tree. The presented risk-averse approach allows to tune the controller by continuously interpolating between risk-neutral stochastic MPC where the forecast probability distribution is fully trusted and worst-case MPC where the distribution is not trusted at all. By appropriately tuning the controller, robustness to misestimated forecast probability distributions and high-effect low-probability events could be provided.

To underline the properties of the different controllers, extensive closed-loop simulations with two MG topologies were performed in Chapter 12. These include a sensitivity analysis that illustrates the robustness of the risk-averse approach to misestimated forecast probability distributions. The case study showed that choosing the right operation strategy is crucial for a safe and reliable operation of islanded MGs. Furthermore, it highlighted the importance of operation control on the real-world performance of islanded MGs: The share of renewable infeed could be significantly increased without adding more RES by choosing a proper operation control strategy.

13.2 *Future research directions*

This work opens perspectives for various future research directions. In what follows, five of them are highlighted: (i) extension of the microgrid model, (ii) modifications related to uncertainties, (iii) augmentation of the MPC problem formulation, (iv) derivation of distributed MPC approaches, and (v) real-world application of the control schemes.

Microgrid model. The generic model of an islanded MG with high share of RES deduced in this thesis provides a basis for more complex control-oriented MG models. In this context, the storage model could be extended to improve the predictions of stored energy by including conversion losses and self-discharge. This could be done, for example, using charging and discharging efficiencies as proposed in [38, 180].

Alternatively, power dependent conversion losses could be approximated by piecewise affine functions (see, e.g., [233]).

Another extension concern the power flow. Here, the linearized DC power flow model for AC grids could be replaced by a model that includes the losses of the lines using, for example, techniques from optimal power flow [144–146].

Moreover, the model could be extended to include a minimum time that a unit needs to remain on (or off) once it is enabled (or disabled) as proposed in [180]. Furthermore, the optimal moment for maintenance of the units could be determined based on future predictions of available renewable infeed and load using MPC. Related tasks, such as, the calibration of batteries that requires a full charge could also be optimally scheduled using MPC.

The generic model deduced in this thesis would also allow to add more unit types to the MG. Motivated by [142], electric vehicles could be included. Furthermore, the model could be modified to consider so-called "prosumer" nodes that can provide and consume energy [251]. The model could further be extended to represent multimodal grids that combine thermal and electric power and energy. Such multimodal MGs could, for example, comprise combined heat and power plants as proposed in [16, 154] or thermal storage units as proposed in [9].

Uncertainties. Another future research direction concern the uncertain load and available renewable infeed. In this context, the ARIMA model could be extended by employing different historic time-series, e.g., load and temperature to forecast load as in [47].

Moreover, the presented models could be extended to include uncertain parameters, such as, an uncertain wind speed to power curve as proposed in [199] or uncertain storage dynamics. Furthermore, uncertain availability of power lines, i.e., transmission line failures, could be included into the model in a similar fashion as in [250]. Additionally, robustness to failures of communication channels could be investigated, e.g., in a similar way as in [143].[1]

[1] Note that [143] builds upon the MG model presented in this thesis.

MPC problem. A future research direction that would also build upon the results of this thesis is the inclusion of chance constraints (see, e.g., [170]) in the operation control formulations. Using them can help to decrease the conservativeness of the approaches, for example, by ensuring only a certain desired security of supply.

Moreover, the conservativeness of the minimax MPC could be further reduced. One interesting path towards this goal could be along the lines of tube-based MPC approaches (see, e.g., [137, 157]).

Additionally, in the context of risk-averse MPC, the choice of α should to be further investigated. Here, one could, for example, adapt the ambiguity considered in risk-averse MPC depending on past observations in a similar way as in [234].

Distributed MPC formulations. Based on the central MPC problems presented in this thesis, distributed control schemes could be developed. Simple distributed certainty equivalent control schemes for interconnected MGs were already investigated in the author's work [92]. One major challenge in this context lies in approaches that consider more complex forecasts, e.g., robust intervals or scenario trees. Another open topic in this field is how to employ risk-measures in distributed MPC schemes.

Real-world application. The schemes developed in this thesis allow for generic MG topologies which enables their application to control real-word or lab-scale MGs such as the ones presented in [86, 180]. In this context, modeling assumptions could be verified and systematic modeling errors identified and addressed. Considering more complex MG setups that include a higher number of units and loads would further allow to investigate how the control approaches scale. In this context, the application of GPUs to solve complex MPC problems, as proposed in [221] for water networks, is another open future research topic.

In conclusion, this work opens perspectives for many engineering and research questions related to the operation control of MGs. To many of them, the generic model of an islanded MG with high share of RES provides a wide foundation upon which extensions of the MG and new control approaches can be developed. The different MPC schemes presented in this thesis additionally provide a broad basis for the development and refinement of operation control strategies for grids with high share of uncertain renewable infeed.

A
Simulation results with extended MG

This chapter contains plots from the simulations with the extended grid. For compactness, only the plots of the prescient and the risk-averse controller for $\alpha = 0.5$ were presented in Section 12.3. In what follows, the simulation results that led to the accumulated values (see Table 12.7) for the other cases, i.e., the

1. certainty equivalence MPC from Chapter 7,
2. minimax MPC from Chapter 8,
3. risk-averse MPC from Chapter 11 for $\alpha = 0.0$, and
4. risk-neutral stochastic MPC from Chapter 10 which is equivalent to the risk-averse MPC from Chapter 11 for $\alpha = 1.0$

are presented.

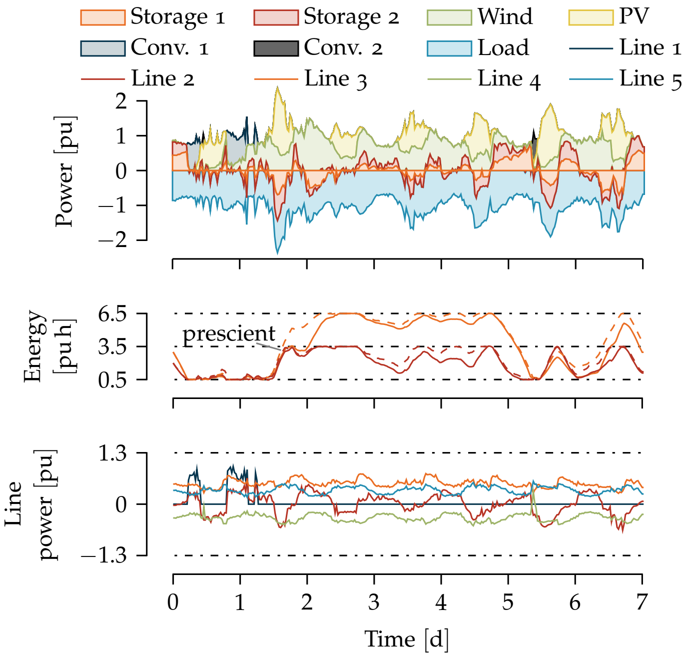

Figure A.1: Power of units and load as well as stored energy and line power of extended MG in closed-loop simulation with certainty equivalence MPC approach.

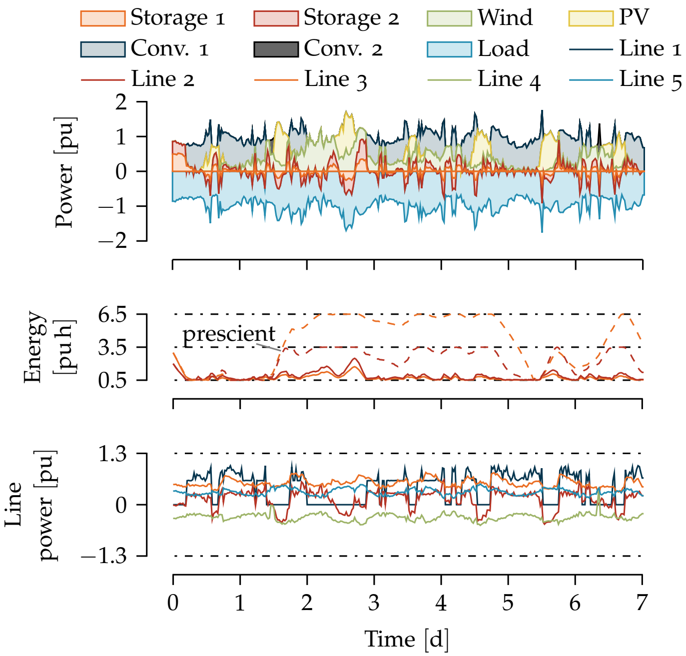

Figure A.2: Power of units and load as well as stored energy and line power of extended MG in closed-loop simulation with minimax MPC approach.

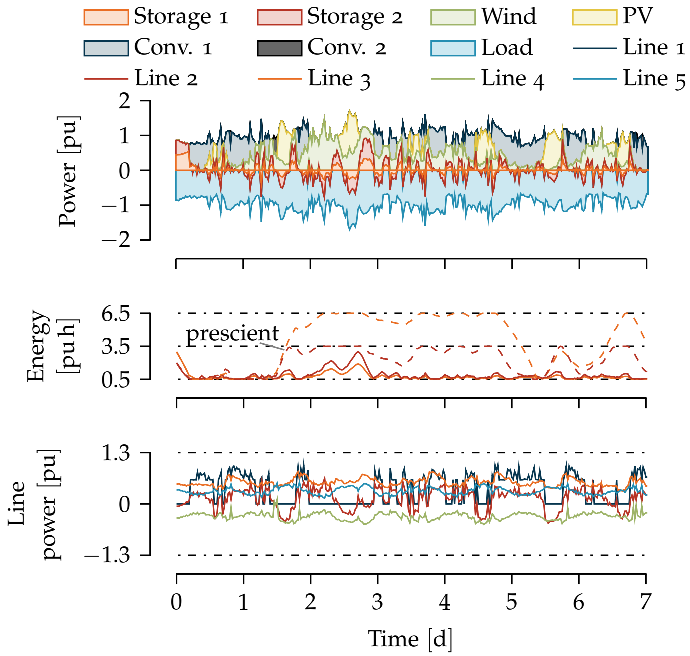

Figure A.3: Power of units and load as well as stored energy and line power of extended MG in closed-loop simulation with risk-averse MPC approach for $\alpha = 0$.

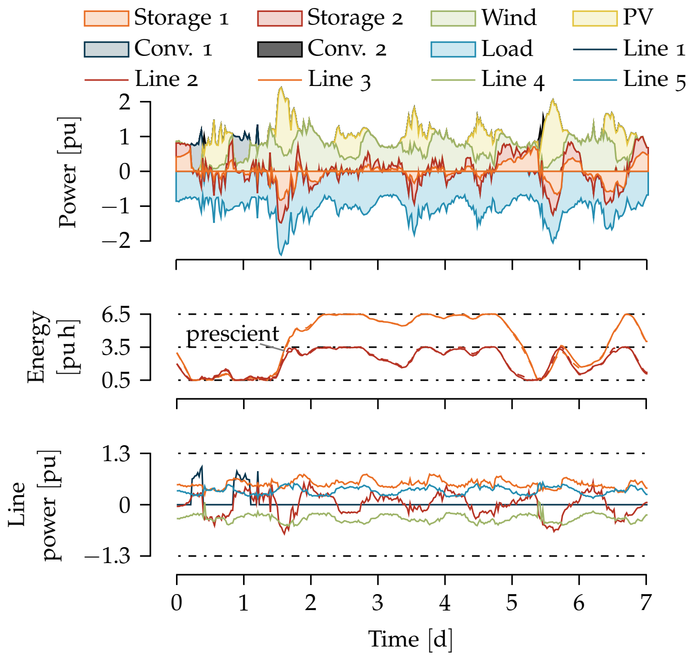

Figure A.4: Power of units and load as well as stored energy and line power of extended MG in closed-loop simulation with risk-averse MPC approach for $\alpha = 1$ which is equivalent to the risk-neutral stochastic MPC.

Bibliography

[1] A. Ahmadi-Javid. Entropic value-at-risk: A new coherent risk measure. *Journal of Optimization Theory and Applications*, 155(3):1105–1123, 2012.

[2] A. Ahsan, Q. Zhao, A. M. Khambadkone, and M. H. Chia. Dynamic battery operational cost modeling for energy dispatch. In *IEEE Energy Conversion Congress and Exposition*. IEEE, 2016.

[3] F. Allgöwer, T. A. Badgwell, J. S. Qin, J. B. Rawlings, and S. J. Wright. Nonlinear predictive control and moving horizon estimation–an introductory overview. In *Advances in control*, pages 391–449. Springer, 1999.

[4] P. M. Anderson and A. A. Fouad. *Power system control and stability*. John Wiley & Sons, 2003.

[5] G. Andersson. Modelling and analysis of electric power systems, 2008. Lecture 227-0526-00, Information Technology and Electrical Engineering, ETH Zürich.

[6] R. J. Andres, D. J. Fielding, G. Marland, T. A. Boden, N. Kumar, and A. T. Kearney. Carbon dioxide emissions from fossil-fuel use, 1751–1950. *Tellus B: Chemical and Physical Meteorology*, 51(4):759–765, 1999.

[7] R. R. Appino, J. Á. G. Ordiano, R. Mikut, T. Faulwasser, and V. Hagenmeyer. On the use of probabilistic forecasts in scheduling of renewable energy sources coupled to storages. *Applied energy*, 210:1207–1218, 2018.

[8] M. Arnold and G. Andersson. Model predictive control of energy storage including uncertain forecasts. In *17th Power Systems Computation Conference*, volume 23, pages 24–29, 2011.

[9] M. Arnold, R. R. Negenborn, G. Andersson, and B. De Schutter. Model-based predictive control applied to multi-carrier energy systems. In *IEEE Power and Energy Society General Meeting*, 2009.

[10] P. Artzner, F. Delbaen, J.-M. Eber, and D. Heath. Coherent measures of risk. *Mathematical finance*, 9(3):203–228, 1999.

[11] T. Asamov and A. Ruszczyński. Time-consistent approximations of risk-averse multistage stochastic optimization problems. *Mathematical Programming*, 153(2): 459–493, 2015.

[12] Atmospheric Radiation Measurement (ARM) Climate Research Facility. Surface Meteorology System (MET) and Sky radiation (SKYRAD) collection of radiometers. June 2009–January 2010, 39° 5′ 28" N, 28° 1′ 45" W: Eastern North Atlantic Facility, windspeed and irradiance. ARM Data Archive: Oak Ridge, TN, USA, 1994, updated daily. Data set accessed 14 July 2011 at `http://dx.doi.org/10.5439/1021460`.

[13] X. Bai, L. Qu, and W. Qiao. Robust AC optimal power flow for power networks with wind power generation. *IEEE Transactions on Power Systems*, 31(5):4163–4164, 2016.

[14] E. Balas. Disjunctive programming. In *Annals of Discrete Mathematics*, volume 5, pages 3–51. Elsevier, 1979.

[15] M. E. Baran and F. F. Wu. Optimal sizing of capacitors placed on a radial distribution system. *IEEE Transactions on power Delivery*, 4(1):735–743, 1989.

[16] E. Barklund, N. Pogaku, M. Prodanovic, C. Hernandez-Aramburo, and T. C. Green. Energy management in autonomous microgrid using stability-constrained droop control of inverters. *IEEE Transactions on Power Electronics*, 23(5):2346–2352, 2008.

[17] S. Barsali, M. Ceraolo, P. Pelacchi, and D. Poli. Control techniques of dispersed generators to improve the continuity of electricity supply. In *IEEE Power Engineering Society Winter Meeting*, volume 2, pages 789–794, 2002.

[18] A. Bemporad and M. Morari. Control of systems integrating logic, dynamics, and constraints. *Automatica*, 35 (3):407–427, 1999.

[19] A. Bemporad and M. Morari. Robust model predictive control: A survey. In *Robustness in identification and control*, pages 207–226. Springer, 1999.

[20] A. Bemporad, F. Borrelli, and M. Morari. Min-max control of constrained uncertain discrete-time linear systems. *IEEE Transactions on Automatic Control*, 48(9): 1600–1606, 2003.

[21] P. Beraldi, F. D. Simone, and A. Violi. Generating scenario trees: A parallel integrated simulation-optimization approach. *Journal of Computational and Applied Mathematics*, 233(9):2322–2331, 2010.

[22] D. Bernardini and A. Bemporad. Scenario-based model predictive control of stochastic constrained linear systems. In *48th IEEE Conference on Decision and Control & 28th Chinese Control Conference*, pages 6333–6338, 2009.

[23] D. P. Bertsekas. *Dynamic programming and optimal control*, volume 1. Athena Scientific Belmont, 2005.

[24] D. P. Bertsekas. Dynamic programming and suboptimal control: A survey from adp to mpc. *European Journal of Control*, 11(4-5):310–334, 2005.

[25] D. P. Bertsekas and J. N. Tsitsiklis. *Introduction to probability*. Athena Scientific, 2002.

[26] D. P. Bertsekas, A. Nedic, and A. E. Ozdaglar. *Convex Analysis and Optimization*. Athena Scientific, 2003.

[27] A. Bidram and A. Davoudi. Hierarchical structure of microgrids control system. *IEEE Transactions on Smart Grid*, 3(4):1963–1976, 2012.

[28] A. Bidram, F. L. Lewis, and A. Davoudi. Distributed control systems for small-scale power networks: Using multiagent cooperative control theory. *IEEE Control Systems Magazine*, 34(6):56–77, 2014.

[29] N. Biggs. *Algebraic graph theory*. Cambridge University Press, 2nd edition, 1993.

[30] R. Billinton and R. N. Allan. *Reliability evaluation of power systems*, volume 2. Plenum press New York, 1984.

[31] F. Borrelli, A. Bemporad, and M. Morari. *Predictive control for linear and hybrid systems*. Cambridge University Press, 2012.

[32] A. Botterud, Z. Zhou, J. Wang, R. J. Bessa, H. Keko, J. Sumaili, and V. Miranda. Wind power trading under uncertainty in lmp markets. *IEEE Transactions on Power Systems*, 27(2):894–903, 2012.

[33] G. E. Box, G. M. Jenkins, and G. C. Reinsel. *Time series analysis: forecasting and control*. John Wiley & Sons, 2013.

[34] S. Boyd and L. Vandenberghe. *Convex optimization*. Cambridge University Press, 2004.

[35] P. Braun, L. Grüne, C. M. Kellett, S. R. Weller, and K. Worthmann. A distributed optimization algorithm for the predictive control of smart grids. *IEEE Transactions on Automatic Control*, pages 3898–3911, 2016.

[36] P. Braun, T. Faulwasser, L. Grüne, C. M. Kellett, S. R. Weller, and K. Worthmann. Hierarchical distributed ADMM for predictive control with applications in power networks. *IFAC Journal of Systems and Control*, 3:10–22, 2018.

[37] P. Braun, P. Sauerteig, and K. Worthmann. Distributed optimization based control on the example of microgrids. In *Computational Intelligence and Optimization Methods for Control Engineering*, volume 150, pages 173–200. Springer, 2019.

[38] T. K. A. Brekken, A. Yokochi, A. von Jouanne, Z. Z. Yen, H. M. Hapke, and D. A. Halamay. Optimal energy storage sizing and control for wind power applications. *IEEE Transactions on Sustainable Energy*, 2(1):69–77, 2011.

[39] M. Broussely, P. Biensan, F. Bonhomme, P. Blanchard, S. Herreyre, K. Nechev, and R. Staniewicz. Main aging mechanisms in li ion batteries. *Journal of power sources*, 146(1-2):90–96, 2005.

[40] M. Carrión and J. M. Arroyo. A computationally efficient mixed-integer linear formulation for the thermal unit commitment problem. *IEEE Transactions on power systems*, 21(3):1371–1378, 2006.

[41] T. M. Cavalier, P. M. Pardalos, and A. L. Soyster. Modeling and integer programming techniques applied to propositional calculus. *Computers & operations research*, 17(6):561–570, 1990.

[42] S. Ceria and J. Soares. Convex programming for disjunctive convex optimization. *Mathematical Programming*, 86(3):595–614, 1999.

[43] K. M. Chandy, S. H. Low, U. Topcu, and H. Xu. A simple optimal power flow model with energy storage. In *49th IEEE Conference on Decision and Control*, pages 1051–1057, 2010.

[44] A. Chaouachi, R. M. Kamel, R. Andoulsi, and K. Nagasaka. Multiobjective intelligent energy management for a microgrid. *IEEE Transactions on Industrial Electronics*, 60(4):1688–1699, 2012.

[45] C. Chen, S. Duan, T. Cai, B. Liu, and G. Hu. Smart energy management system for optimal microgrid economic operation. *IET renewable power generation*, 5(3): 258–267, 2011.

[46] Z. Chen and D. Xu. Knowledge-based scenario tree generation methods and application in multiperiod portfolio selection problem. *Applied Stochastic Models in Business and Industry*, 30(3):240–257, 2014.

[47] M. Y. Cho, J. C. Hwang, and C. S. Chen. Customer short term load forecasting by using arima transfer function model. In *International Conference on Energy Management and Power Delivery*, volume 1, pages 317–322, 1995.

[48] Y.-L. Chow and M. Pavone. A framework for time-consistent, risk-averse model predictive control: Theory and algorithms. In *American Control Conference*, pages 4204–4211, 2014.

[49] C. Coffrin and P. Van Hentenryck. A linear-programming approximation of ac power flows. *INFORMS Journal on Computing*, 26(4):718–734, 2014.

[50] R. A. Collado, D. Papp, and A. Ruszczyński. Scenario decomposition of risk-averse multistage stochastic programming problems. *Annals of Operations Research*, 200:147–170, 2012.

[51] M. Diehl. Formulation of closed-loop min–max MPC as a quadratically constrained quadratic program. *IEEE Transactions on Automatic Control*, 52(2):339–343, 2007.

[52] M. Diehl and J. Bjornberg. Robust dynamic programming for min-max model predictive control of constrained uncertain systems. *IEEE Transactions on Automatic Control*, 49(12):2253–2257, 2004.

[53] R. Diestel. *Graph Theory*, volume 173 of *Graduate Texts in Mathematics*. Springer, 5th edition, 2017.

[54] A. L. Dimeas and N. D. Hatziargyriou. Operation of a multiagent system for microgrid control. *IEEE Transactions on Power Systems*, 20(3):1447–1455, 2005.

[55] T. Ding, Y. Hu, and Z. Bie. Multi-stage stochastic programming with nonanticipativity constraints for expansion of combined power and natural gas systems. *IEEE Transactions on Power Systems*, 33(1):317–328, 2018.

[56] J. Driesen and F. Katiraei. Design for distributed energy resources. *IEEE Power and Energy Magazine*, 6(3):30–40, 2008.

[57] J. Dupačová, G. Consigli, and S. W. Wallace. Scenarios for multistage stochastic programs. *Annals of operations research*, 100(1-4):25–53, 2000.

[58] J. Dupačová, N. Gröwe-Kuska, and W. Römisch. Scenario reduction in stochastic programming. *Mathematical programming*, 95(3):493–511, 2003.

[59] W. Enders. *Applied econometric time series*. John Wiley & Sons, 4th edition, 2014.

[60] ENERCON. ENERCON product overview. Technical report, ENERCON GmbH, 2015. File accessed 10 October 2017 at `https://www.enercon.de/fileadmin/Redakteur/Medien-Portal/broschueren/pdf/en/ENERCON_Produkt_en_06_2015.pdf`.

[61] H. Farhangi. The path of the smart grid. *IEEE Power and Energy Magazine*, 8(1):18–28, 2010.

[62] M. Farrokhabadi, C. A. Cañizares, J. W. Simpson-Porco, E. Nasr, L. Fan, P. A. Mendoza-Araya, R. Tonkoski, U. Tamrakar, N. Hatziargyriou, D. Lagos, R. W. Wies, M. Paolone, M. Liserre, L. Meegahapola, M. Kabalan, A. H. Hajimiragha, D. Peralta, M. A. Elizondo, K. P. Schneider, F. K. Tuffner, and J. Reilly. Microgrid stability definitions, analysis, and examples. *IEEE Transactions on Power Systems*, 35(1):13–29, 2020.

[63] T. Faulwasser, A. Engelmann, T. Mühlpfordt, and V. Hagenmeyer. Optimal power flow: an introduction to predictive, distributed and stochastic control challenges. *at-Automatisierungstechnik*, 66(7):573–589, 2018.

[64] S. Frank, I. Steponavice, and S. Rebennack. Optimal power flow: a bibliographic survey I. *Energy Systems*, 3 (3):221–258, 2012.

[65] S. Frank, I. Steponavice, and S. Rebennack. Optimal power flow: a bibliographic survey II. *Energy Systems*, 3 (3):259–289, 2012.

[66] K. Frauendorfer. Barycentric scenario trees in convex multistage stochastic programming. *Mathematical Programming*, 75(2):277–293, 1996.

[67] L. Gao, S. Liu, and R. A. Dougal. Dynamic lithium-ion battery model for system simulation. *IEEE transactions on components and packaging technologies*, 25(3):495–505, 2002.

[68] C. E. Garcia, D. M. Prett, and M. Morari. Model predictive control: theory and practice—a survey. *Automatica*, 25(3):335–348, 1989.

[69] J. García-González, E. Parrilla, and A. Mateo. Risk-averse profit-based optimal scheduling of a hydro-chain in the day-ahead electricity market. *European Journal of Operational Research*, 181(3):1354–1369, 2007.

[70] M. Geidl and G. Andersson. Optimal power flow of multiple energy carriers. *IEEE Transactions on Power Systems*, 22(1):145–155, 2007.

[71] M. Geidl, G. Koeppel, P. Favre-Perrod, B. Klockl, G. Andersson, and K. Frohlich. Energy hubs for the future. *IEEE Power and Energy Magazine*, 5(1):24–30, 2007.

[72] H. Genceli and M. Nikolaou. Robust stability analysis of constrained l1-norm model predictive control. *AIChE Journal*, 39(12):1954–1965, 1993.

[73] G. M. Gilbert, D. E. Bouchard, and A. Y. Chikhani. A comparison of load flow analysis using distflow, gauss-seidel, and optimal load flow algorithms. In *IEEE Canadian Conference on Electrical and Computer Engineering*, volume 2, pages 850–853, 1998.

[74] J. D. Glover, M. S. Sarma, and T. Overbye. *Power System Analysis and Design*. Cengage Learning, 2012.

[75] C. Godsil and G. Royle. *Algebraic Graph Theory*. Springer, 2001.

[76] S. Graf and H. Luschgy. *Foundations of quantization for probability distributions*. Springer, 2007.

[77] J. J. Grainger and W. D. Stevenson. *Power system analysis*. McGraw-Hill New York, 1st edition, 1994.

[78] N. Gröwe-Kuska, H. Heitsch, and W. Romisch. Scenario reduction and scenario tree construction for power management problems. In *IEEE Bologna Power Tech*, 2003.

[79] L. Grüne and J. Pannek. *Nonlinear model predictive control*. Springer, 2011.

[80] J. M. Guerrero, J. C. Vásquez, and R. Teodorescu. Hierarchical control of droop-controlled DC and AC microgrids—a general approach towards standardization. In *35th Annual Conference of IEEE Industrial Electronics*, pages 4305–4310, 2009.

[81] J. M. Guerrero, M. Chandorkar, T. Lee, and P. Loh. Advanced control architectures for intelligent microgrids – Part II: Power quality, energy storage, and AC/DC microgrids. *IEEE Transactions on Industrial Electronics*, 60 (4):1263–1270, 2013.

[82] J. M. Guerrero, P. Loh, M. Chandorkar, and T. Lee. Advanced control architectures for intelligent microgrids – Part I: Decentralized and hierarchical control. *IEEE Transactions on Industrial Electronics*, 60(4):1254–1262, 2013.

[83] M. Gulin, J. Matuško, and M. Vašak. Stochastic model predictive control for optimal economic operation of a residential DC microgrid. In *IEEE International Conference on Industrial Technology*, pages 505–510, 2015.

[84] N. Gülpınar, B. Rustem, and R. Settergren. Simulation and optimization approaches to scenario tree generation. *Journal of Economic Dynamics and Control*, 28(7): 1291–1315, 2004.

[85] Gurobi Optimization, LLC. Gurobi optimizer reference manual, 2018. Online available at `https://www.gurobi.com`.

[86] V. Hagenmeyer, H. Kemal Çakmak, C. Düpmeier, T. Faulwasser, J. Isele, H. B. Keller, P. Kohlhepp, U. Kühnapfel, U. Stucky, S. Waczowicz, et al. Information and communication technology in energy lab 2.0: Smart energies system simulation and control center with an open-street-map-based power flow simulation example. *Energy Technology*, 4(1):145–162, 2016.

[87] J. D. Hamilton. *Time series analysis*. Princeton University Press, 1st edition, 1994.

[88] C. A. Hans and E. Klages. Very short term time-series forecasting of solar irradiance without exogenous inputs. In *6th International Conference on Time Series and Forecasting*, pages 1007–1018, 2019.

[89] C. A. Hans, V. Nenchev, J. Raisch, and C. Reincke-Collon. Minimax model predictive operation control of microgrids. In *19th IFAC World Congress*, pages 10287–10292, 2014.

[90] C. A. Hans, V. Nenchev, J. Raisch, and C. Reincke-Collon. Approximate closed-loop minimax model predictive operation control of microgrids. In *European Control Conference*, pages 241–246, 2015.

[91] C. A. Hans, P. Sopasakis, A. Bemporad, J. Raisch, and C. Reincke-Collon. Scenario-based model predictive operation control of islanded microgrids. In *54th IEEE Conference on Decision and Control*, pages 3272–3277, 2015.

[92] C. A. Hans, P. Braun, J. Raisch, L. Grüne, and C. Reincke-Collon. Hierarchical distributed model predictive control of interconnected microgrids. *IEEE Transactions on Sustainable Energy*, 10(1):407–416, 2019.

[93] C. A. Hans, P. Sopasakis, J. Raisch, C. Reincke-Collon, and P. Patrinos. Risk-averse model predictive operation control of islanded microgrids. *IEEE Transactions on Control Systems Technology*, 28(6):2136–2151, 2020.

[94] N. Hatziargyriou. *Microgrids: architectures and control*. John Wiley & Sons, 2014.

[95] N. Hatziargyriou, H. Asano, R. Iravani, and C. Marnay. Microgrids. *IEEE Power and Energy Magazine*, 5(4):78–94, 2007.

[96] H. Heitsch and W. Römisch. Scenario reduction algorithms in stochastic programming. *Computational Optimization and Applications*, 24(2-3):187–206, 2003.

[97] H. Heitsch and W. Romisch. Generation of multivariate scenario trees to model stochasticity in power management. In *IEEE Russia Power Tech*, 2005.

[98] H. Heitsch and W. Römisch. Scenario tree modeling for multistage stochastic programs. *Mathematical Programming*, 118(2):371–406, 2009.

[99] H. Heitsch and W. Römisch. Stability and scenario trees for multistage stochastic programs. In *Stochastic Programming*, volume 150, pages 139–164. Springer, 2010.

[100] B. Heymann, J. F. Bonnans, F. Silva, and G. Jimenez. A stochastic continuous time model for microgrid energy management. In *European Control Conference*, pages 2084–2089, 2016.

[101] B. Heymann, J. F. Bonnans, P. Martinon, F. J. Silva, F. Lanas, and G. Jiménez-Estévez. Continuous optimal control approaches to microgrid energy management. *Energy Systems*, 9(1):59–77, 2018.

[102] S. Hofmann, A. K. Sampathirao, C. A. Hans, J. Raisch, A. Heidt, and E. Bosch. Saturation-aware model predictive energy management for droop-controlled islanded microgrids. *Preprint*, 2019. arXiv:2107.02719v1 [math.OC].

[103] A. Hooshmand, M. H. Poursaeidi, J. Mohammadpour, H. A. Malki, and K. Grigoriads. Stochastic model predictive control method for microgrid management. In *IEEE Power and Energy Society Innovative Smart Grid Technologies Conference*, 2012.

[104] M. Hosseinzadeh and F. R. Salmasi. Robust optimal power management system for a hybrid AC/DC microgrid. *IEEE Transactions on Sustainable Energy*, 6(3):675–687, 2015.

[105] K. Høyland and S. W. Wallace. Generating scenario trees for multistage decision problems. *Management science*, 47(2):295–307, 2001.

[106] R. J. Hyndman and G. Athanasopoulos. *Forecasting: principles and practice*. OTexts, 2014.

[107] IBM ILOG CPLEX. CPLEX user's manual, 2016. Online available at `https://www.ibm.com`.

[108] IEA, IRENA, UNSD, WB, and WHO. Tracking SDG7: The energy progress report. Technical report, IEA and IRENA and UNSD and WB and WHO, 2019.

[109] IEEE Power and Energy Society. IEEE application guide for AC high-voltage circuit breakers > 1000 Vac rated on a symmetrical current basis. (IEEE Std C37.010-2016):1–123, 2017.

[110] Q. Jiang, M. Xue, and G. Geng. Energy management of microgrid in grid-connected and stand-alone modes. *IEEE Transactions on Power Systems*, 28(3):3380–3389, 2013.

[111] M. Kanagawa and T. Nakata. Assessment of access to electricity and the socio-economic impacts in rural areas of developing countries. *Energy policy*, 36(6):2016–2029, 2008.

[112] H. Kanchev, D. Lu, F. Colas, V. Lazarov, and B. Francois. Energy management and operational planning of a microgrid with a PV-based active generator for smart grid applications. *IEEE Transactions on Industrial Electronics*, 58(10):4583–4592, 2011.

[113] F. Katiraei and J. R. Aguero. Solar PV integration challenges. *IEEE Power and Energy Magazine*, 9(3):62–71, 2011.

[114] F. Katiraei and M. R. Iravani. Power management strategies for a microgrid with multiple distributed generation units. *IEEE Transactions on Power Systems*, 21 (4):1821–1831, 2006.

[115] F. Katiraei, M. R. Iravani, and P. W. Lehn. Micro-grid autonomous operation during and subsequent to islanding process. *IEEE Transactions on Power Delivery*, 20 (1):248–257, 2005.

[116] F. Katiraei, R. Iravani, N. Hatziargyriou, and A. Dimeas. Microgrids management. *IEEE Power and Energy Magazine*, 6(3):54–65, 2008.

[117] W. Katzenstein, E. Fertig, and J. Apt. The variability of interconnected wind plants. *Energy policy*, 38(8): 4400–4410, 2010.

[118] R. Khodabakhsh and S. Sirouspour. Optimal control of energy storage in a microgrid by minimizing conditional value-at-risk. *IEEE Transactions on Sustainable Energy*, 7(3):1264–1273, 2016.

[119] P. Kou, F. Gao, and X. Guan. Stochastic predictive control of battery energy storage for wind farm dispatching: Using probabilistic wind power forecasts. *Renewable Energy*, 80:286–300, 2015.

[120] P. Kou, D. Liang, L. Gao, and F. Gao. Stochastic coordination of plug-in electric vehicles and wind turbines in microgrid: A model predictive control approach. *IEEE Transactions on Smart Grid*, 7(3):1537–1551, 2016.

[121] P. Kou, D. Liang, and L. Gao. Stochastic energy scheduling in microgrids considering the uncertainties in both supply and demand. *IEEE Systems Journal*, 12(3):2589–2600, 2018.

[122] T. Kral, C. A. Hans, and P. Merk. System for handling short circuits on an electrical network, 2020. U.S. Patent No. 10,756,536.

[123] A. Krishna, C. A. Hans, J. Schiffer, J. Raisch, and T. Kral. Steady state evaluation of distributed secondary frequency control strategies for microgrids in the presence of clock drifts. In *25th Mediterranean Conference on Control and Automation*, pages 508–515, 2017.

[124] A. Krishna, J. Schiffer, and J. Raisch. A consensus-based control law for accurate frequency restoration and power sharing in microgrids in the presence of clock drifts. In *European Control Conference*, pages 2575–2580, 2018.

[125] A. Krishna, J. Schiffer, N. Monshizadeh, and J. Raisch. A consensus-based voltage control for reactive power sharing and PCC voltage regulation in microgrids with parallel-connected inverters. In *European Control Conference*, pages 542–547, 2019.

[126] A. Krishna, J. Schiffer, and J. Raisch. Distributed secondary frequency control in microgrids: Robustness and steady-state performance in the presence of clock drifts. *European Journal of Control*, 51:135–145, 2020.

[127] P. Kundur, N. J. Balu, and M. G. Lauby. *Power system stability and control*. McGraw-Hill, 1st edition, 1994.

[128] E. Kuznetsova, Y.-F. Li, C. Ruiz, and E. Zio. An integrated framework of agent-based modelling and robust optimization for microgrid energy management. *Applied Energy*, 129:70–88, 2014.

[129] E. Kuznetsova, C. Ruiz, Y.-F. Li, and E. Zio. Analysis of robust optimization for decentralized microgrid energy management under uncertainty. *International Journal of Electrical Power & Energy Systems*, 64:815–832, 2015.

[130] M. Lange. On the uncertainty of wind power predictions—analysis of the forecast accuracy and statistical distribution of errors. *Journal of Solar Energy Engineering*, 127(2):177–184, 2005.

[131] B. Lasseter. Microgrids. In *IEEE Power and Energy Society Winter Meeting*, pages 146–149, 2001.

[132] R. H. Lasseter. MicroGrids. In *IEEE Power and Energy Society Winter Meeting*, pages 305–308, 2002.

[133] R. H. Lasseter. Smart distribution: Coupled microgrids. *Proceedings of the IEEE*, 99(6):1074–1082, 2011.

[134] R. H. Lasseter and P. Paigi. Microgrid: a conceptual solution. In *35th IEEE Annual Power Electronics Specialists Conference*, volume 6, pages 4285–4290, 2004.

[135] R. H. Lasseter, J. H. Eto, B. Schenkman, J. Stevens, H. Vollkommer, D. Klapp, E. Linton, H. Hurtado, and J. Roy. CERTS microgrid laboratory test bed. *IEEE Transactions on Power Delivery*, 26(1):325–332, 2010.

[136] J. M. Latorre, S. Cerisola, and A. Ramos. Clustering algorithms for scenario tree generation: Application to natural hydro inflows. *European Journal of Operational Research*, 181(3):1339–1353, 2007.

[137] D. Limon, I. Alvarado, T. Alamo, and E. Camacho. On the design of robust tube-based mpc for tracking. *IFAC Proceedings Volumes*, 41(2):15333–15338, 2008.

[138] J. Löfberg. *Minimax approaches to robust model predictive control*. PhD thesis, Linköping University, 2003.

[139] J. Löfberg. Approximations of closed-loop minimax MPC. In *42nd IEEE Conference on Decision and Control*, pages 1438–1442, 2003.

[140] J. Löfberg. YALMIP: A toolbox for modeling and optimization in MATLAB. In *IEEE International Symposium on Computer Aided Control System Design*, pages 284–289, 2004.

[141] T. Logenthiran and D. Srinivasan. Short term generation scheduling of a microgrid. In *IEEE Region 10 Conference*, 2009.

[142] J. A. P. Lopes, F. J. Soares, and P. M. R. Almeida. Integration of electric vehicles in the electric power system. *Proceedings of the IEEE*, 99(1):168–183, 2010.

[143] I. Löser, A. K. Sampathirao, S. Hofmann, and J. Raisch. Fallback strategies in operation control of microgrids with communication failures. In *58th IEEE Conference on Decision and Control*, pages 3885–3891, 2019.

[144] S. H. Low. Convex relaxation of optimal power flow: a tutorial. In *IREP Symposium Bulk Power System Dynamics and Control - IX Optimization, Security and Control of the Emerging Power Grid*, 2013.

[145] S. H. Low. Convex relaxation of optimal power flow—part I: Formulations and equivalence. *IEEE Transactions on Control of Network Systems*, 1(1):15–27, 2014.

[146] S. H. Low. Convex relaxation of optimal power flow—part II: Exactness. *IEEE Transactions on Control of Network Systems*, 1(2):177–189, 2014.

[147] M. Lubin, Y. Dvorkin, and S. Backhaus. A robust approach to chance constrained optimal power flow with renewable generation. *IEEE Transactions on Power Systems*, 31(5):3840–3849, 2016.

[148] M. Maceira, L. Marzano, D. Penna, A. Diniz, and T. Justino. Application of CVaR risk aversion approach in the expansion and operation planning and for setting the spot price in the brazilian hydrothermal interconnected system. *International Journal of Electrical Power & Energy Systems*, 72:126–135, 2015.

[149] J. Machowski, J. W. Bialek, and J. R. Bumby. *Power System Dynamics: Stability and Control*. John Wiley & Sons, 2008.

[150] J. M. Maciejowski. *Predictive control: with constraints*. Pearson education, 2002.

[151] J. Marcos, L. Marroyo, E. Lorenzo, and M. García. Smoothing of PV power fluctuations by geographical dispersion. *Progress in Photovoltaics: Research and Applications*, 20(2):226–237, 2012.

[152] M. N. Marwali, Jin-Woo Jung, and A. Keyhani. Control of distributed generation systems - part ii: Load sharing control. *IEEE Transactions on Power Electronics*, 19(6): 1551–1561, 2004.

[153] F. J. Massey Jr. The Kolmogorov-Smirnov test for goodness of fit. *Journal of the American Statistical Association*, 46(253):68–78, 1951.

[154] A. Maulik and D. Das. Optimal operation of droop-controlled islanded microgrids. *IEEE Transactions on Sustainable Energy*, 9(3):1337–1348, 2017.

[155] E. Mayhorn, K. Kalsi, M. Elizondo, W. Zhang, S. Lu, N. Samaan, and K. Butler-Purry. Optimal control of distributed energy resources using model predictive control. In *IEEE Power and Energy Society General Meeting*, 2012.

[156] D. Q. Mayne, J. B. Rawlings, C. V. Rao, and P. O. M. Scokaert. Constrained model predictive control: Stability and optimality. *Automatica*, 36(6):789–814, 2000.

[157] D. Q. Mayne, E. C. Kerrigan, E. Van Wyk, and P. Falugi. Tube-based robust nonlinear model predictive control. *International Journal of Robust and Nonlinear Control*, 21 (11):1341–1353, 2011.

[158] A. Mesbah. Stochastic model predictive control: An overview and perspectives for future research. *IEEE Control Systems Magazine*, 36(6):30–44, 2016.

[159] A. Micallef, M. Apap, C. Spiteri-Staines, and J. M. Guerrero. Secondary control for reactive power sharing in droop-controlled islanded microgrids. In *IEEE International Symposium on Industrial Electronics*, pages 1627–1633, 2012.

[160] I. G. Moghaddam, M. Nick, F. Fallahi, M. Sanei, and S. Mortazavi. Risk-averse profit-based optimal operation strategy of a combined wind farm–cascade hydro system in an electricity market. *Renewable Energy*, 55: 252–259, 2013.

[161] S. Mohammadi, S. Soleymani, and B. Mozafari. Scenario-based stochastic operation management of microgrid including wind, photovoltaic, micro-turbine, fuel cell and energy storage devices. *International Journal of Electrical Power & Energy Systems*, 54:525–535, 2014.

[162] J. M. Morales, A. J. Conejo, and J. Pérez-Ruiz. Short-term trading for a wind power producer. *IEEE Transactions on Power Systems*, 25(1):554–564, 2010.

[163] M. Morari and J. H. Lee. Model predictive control: past, present and future. *Computers & Chemical Engineering*, 23(4-5):667–682, 1999.

[164] M. Mueller-Stoffels, J. VanderMeer, H. Schaede, L. Miranda, D. Light, A. Simmons, and H. Merkel. Diesel generator fuel consumption under dynamic loading. Technical report, Alaska Center for Energy and Power, 2017. Power Systems Integration Program.

[165] T. Mühlpfordt, T. Faulwasser, L. Roald, and V. Hagenmeyer. Solving optimal power flow with non-gaussian uncertainties via polynomial chaos expansion. In *56th IEEE Conference on Decision and Control*, pages 4490–4496, 2017.

[166] A. Narayan and K. Ponnambalam. Risk-averse stochastic programming approach for microgrid planning under uncertainty. *Renewable Energy*, 101:399–408, 2017.

[167] G. L. Nemhauser and L. A. Wolsey. *Integer and Combinatorial Optimization*. Wiley-Interscience, 1999.

[168] V. Nenchev and C. A. Hans. Optimal adaptive predictive control of a combustion engine. In *European Control Conference*, page 1409–1413, 2015.

[169] C. Ocampo-Martinez, V. Puig, G. Cembrano, J. M. Grosso, P. Sopasakis, A. K. Sampathirao, P. Patrinos, D. Bernardini, and G. S. Gnecco. Real-time control algorithms for optimal operational management. Technical report, Efficient Integrated Real-time Monitoring and Control of Drinking Water Networks (EFFINET), 2015.

[170] F. Oldewurtel, C. N. Jones, and M. Morari. A tractable approximation of chance constrained stochastic MPC based on affine disturbance feedback. In *47th IEEE Conference on Decision and Control*, pages 4731–4736, 2008.

[171] D. E. Olivares, C. A. Cañizares, and M. Kazerani. A centralized optimal energy management system for microgrids. In *IEEE Power and Energy Society General Meeting*, 2011.

[172] D. E. Olivares, C. A. Cañizares, and M. Kazerani. A centralized energy management system for isolated microgrids. *IEEE Transactions on Smart Grid*, 5(4):1864–1875, 2014.

[173] D. E. Olivares, A. Mehrizi-Sani, A. H. Etemadi, C. A. Cañizares, R. Iravani, M. Kazerani, A. H. Hajimiragha, O. Gomis-Bellmunt, M. Saeedifard, R. Palma-Behnke, G. A. Jiménez-Estévez, and N. D. Hatziargyriou. Trends in microgrid control. *IEEE Transactions on Smart Grid*, 5 (4):1905–1919, 2014.

[174] N. P. Padhy. Unit commitment-a bibliographical survey. *IEEE Transactions on Power Systems*, 19(2):1196–1205, 2004.

[175] R. Palma-Behnke, C. Benavides, F. Lanas, B. Severino, L. Reyes, J. Llanos, and D. Sáez. A microgrid energy management system based on the rolling horizon strategy. *IEEE Transactions on Smart Grid*, 4(2):996–1006, 2013.

[176] J. Palomares-Salas, J. De la Rosa, J. Ramiro, J. Melgar, A. Aguera, and A. Moreno. ARIMA vs. neural networks for wind speed forecasting. In *International Conference on Computational Intelligence for Measurement Systems and Applications*, pages 129–133, 2009.

[177] A. Parisio and L. Glielmo. Energy efficient microgrid management using model predictive control. In *50th IEEE Conference on Decision and Control*, pages 5449–5454, 2011.

[178] A. Parisio and L. Glielmo. Stochastic model predictive control for economic/environmental operation management of microgrids. In *European Control Conference*, pages 2014–2019, 2013.

[179] A. Parisio, C. Del Vecchio, and A. Vaccaro. A robust optimization approach to energy hub management. *International Journal of Electrical Power & Energy Systems*, 42(1):98–104, 2012.

[180] A. Parisio, E. Rikos, and L. Glielmo. A model predictive control approach to microgrid operation optimization. *IEEE Transactions on Control Systems Technology*, 22(5): 1813–1827, 2014.

[181] A. Parisio, E. Rikos, G. Tzamalis, and L. Glielmo. Use of model predictive control for experimental microgrid optimization. *Applied Energy*, 115:37–46, 2014.

[182] A. Parisio, E. Rikos, and L. Glielmo. Stochastic model predictive control for economic/environmental operation management of microgrids: An experimental case study. *Journal of Process Control*, 43:24–37, 2016.

[183] P. Patrinos. Stochastic model predictive control approaches to energy management. Technical report, E-PRICE, 2012. Deliverable 3.1.

[184] P. Patrinos and H. Sarimveis. An explicit optimal control approach for mean-risk dynamic portfolio allocation. In *European Control Conference*, pages 3364–3370, 2007.

[185] P. Patrinos and H. Sarimveis. Convex parametric piecewise quadratic optimization: theory and algorithms. *Automatica*, 47(8):1770–1777, 2011.

[186] P. Patrinos, S. Trimboli, and A. Bemporad. Stochastic MPC for real-time market-based optimal power dispatch. In *50th IEEE Conference on Decision and Control and European Control Conference*, pages 7111–7116, 2011.

[187] J. A. Peças Lopes, C. L. Moreira, and A. G. Madureira. Defining control strategies for microgrids islanded operation. *IEEE Transactions on Power Systems*, 21(2): 916–924, 2006.

[188] M. Pehnt. Dynamic life cycle assessment (LCA) of renewable energy technologies. *Renewable Energy*, 31(1): 55–71, 2006.

[189] T. Pennanen and M. Koivu. Epi-convergent discretizations of stochastic programs via integration quadratures. *Numerische mathematik*, 100(1):141–163, 2005.

[190] M. Petrollese, L. Valverde, D. Cocco, G. Cau, and J. Guerra. Real-time integration of optimal generation scheduling with MPC for the energy management of a renewable hydrogen-based microgrid. *Applied Energy*, 166:96–106, 2016.

[191] G. Pflug and W. Römisch. *Modeling, Measuring and Managing Risk*. World Scientific, 2007.

[192] G. C. Pflug and A. Pichler. *Multistage stochastic optimization*. Springer, 2014.

[193] G. C. Pflug and A. Pichler. Dynamic generation of scenario trees. *Computational Optimization and Applications*, 62(3):641–668, 2015.

[194] P. Piagi and R. Lasseter. Autonomous control of microgrids. In *IEEE Power and Energy Society General Meeting*, 2006.

[195] P. Pinson. *Estimation of the uncertainty in wind power forecasting*. PhD thesis, École Nationale Supérieure des Mines de Paris, 2006.

[196] P. Pinson, H. Madsen, H. A. Nielsen, G. Papaefthymiou, and B. Klöckl. From probabilistic forecasts to statistical scenarios of short-term wind power production. *Wind Energy*, 12(1):51–62, 2009.

[197] N. Pogaku, M. Prodanovic, and T. C. Green. Modeling, analysis and testing of autonomous operation of an inverter-based microgrid. *IEEE Transactions on Power Electronics*, 22(2):613–625, 2007.

[198] B. Prindle, M. Eldridge, M. Eckhardt, and A. Frederick. The twin pillars of sustainable energy: synergies between energy efficiency and renewable energy technology and policy. Technical Report E074, American Council for an Energy-Efficient Economy, 2007.

[199] I. Prodan and E. Zio. A model predictive control framework for reliable microgrid energy management. *International Journal of Electrical Power & Energy Systems*, 61: 399–409, 2014.

[200] K. Purchala, L. Meeus, D. Van Dommelen, and R. Belmans. Usefulness of DC power flow for active power flow analysis. In *IEEE Power and Energy Society General Meeting*, pages 454–459, 2005.

[201] S. J. Qin and T. A. Badgwell. A survey of industrial model predictive control technology. *Control engineering practice*, 11(7):733–764, 2003.

[202] S. Raimondi Cominesi, M. Farina, L. Giulioni, B. Picasso, and R. Scattolini. A two-layer stochastic model predictive control scheme for microgrids. *IEEE Transactions on Control Systems Technology*, 26(1):1–13, 2018.

[203] J. B. Rawlings. Tutorial overview of model predictive control. *IEEE Control Systems*, 20(3):38–52, 2000.

[204] J. B. Rawlings and D. Q. Mayne. *Model predictive control: Theory and design*. Nob Hill Pub., 2009.

[205] REN21 Secretariat. Renewables 2019 global status report. Technical report, REN21, 2019.

[206] G. Ripaccioli, D. Bernardini, S. Di Cairano, A. Bemporad, and I. Kolmanovsky. A stochastic model predictive control approach for series hybrid electric vehicle power management. In *American Control Conference*, pages 5844–5849, 2010.

[207] L. Roald, F. Oldewurtel, B. Van Parys, and G. Andersson. Security constrained optimal power flow with distributionally robust chance constraints. *Preprint*, 2015. arXiv:1508.06061v1 [math.OC].

[208] L. Roald, M. Vrakopoulou, F. Oldewurtel, and G. Andersson. Risk-based optimal power flow with probabilistic guarantees. *International Journal of Electrical Power & Energy Systems*, 72:66–74, 2015.

[209] J. Rocabert, G. M. S. Azevedo, A. Luna, J. M. Guerrero, J. I. Candela, and P. Rodríguez. Intelligent connection agent for three-phase grid-connected microgrids. *IEEE Transactions on Power Electronics*, 26(10):2993–3005, 2011.

[210] J. Rocabert, A. Luna, F. Blaabjerg, and P. Rodríguez. Control of power converters in AC microgrids. *IEEE Transactions on Power Electronics*, 27(11):4734–4749, 2012.

[211] R. T. Rockafellar. *Convex analysis*. Princeton University Press, 1996.

[212] R. T. Rockafellar. Duality and optimality in multistage stochastic programming. *Annals of Operations Research*, 85, 1999.

[213] R. T. Rockafellar and S. Uryasev. Optimization of conditional value-at-risk. *Journal of Risk*, 2:21–42, 2000.

[214] R. T. Rockafellar and R. J.-B. Wets. Nonanticipativity and $\mathcal{L}^1$-martingales in stochastic optimization problems. In *Stochastic Systems: Modeling, Identification and Optimization, II*, pages 170–187. Springer, 1976.

[215] R. T. Rockafellar and R. J.-B. Wets. *Variational analysis*. Springer, 3rd edition, 2009.

[216] K. Rudion, A. Orths, Z. A. Styczynski, and K. Strunz. Design of benchmark of medium voltage distribution network for investigation of DG integration. In *IEEE Power and Energy Society General Meeting*, 2006.

[217] A. Ruszczyński and A. Shapiro. Conditional risk mappings. *Mathematics of operations research*, 31(3):544–561, 2006.

[218] A. Ruszczyński and A. Shapiro. Optimization of risk measures. In *Probabilistic and randomized methods for design under uncertainty*, pages 119–157. Springer, 2006.

[219] A. K. Sampathirao. *Parallel methods for solving stochastic optimal control problems: control of drinking water networks*. PhD thesis, IMT School for Advanced Studies, 2016.

[220] A. K. Sampathirao, J. M. Grosso, P. Sopasakis, C. Ocampo-Martinez, A. Bemporad, and V. Puig. Water demand forecasting for the optimal operation of large-scale drinking water networks: The barcelona case study. In *19th IFAC World Congress*, pages 10457–10462, 2014.

[221] A. K. Sampathirao, P. Sopasakis, A. Bemporad, and P. Patrinos. Distributed solution of stochastic optimal control problems on GPUs. In *54th IEEE Conference on Decision and Control*, pages 7183–7188, 2015.

[222] A. K. Sampathirao, P. Sopasakis, A. Bemporad, and P. P. Patrinos. GPU-accelerated stochastic predictive control of drinking water networks. *IEEE Transactions on Control Systems Technology*, 26(2):551–562, 2018.

[223] A. K. Sampathirao, S. Hofmann, J. Raisch, and C. A. Hans. Distributed conditional cooperation model predictive control of interconnected microgrids. *Preprint*, 2021. arXiv:1810.03361v2 [cs.SY].

[224] J. Schiffer, D. U. Sauer, H. Bindner, T. Cronin, P. Lundsager, and R. Kaiser. Model prediction for ranking lead-acid batteries according to expected lifetime in renewable energy systems and autonomous power-supply systems. *Journal of Power sources*, 168(1):66–78, 2007.

[225] J. Schiffer, A. Anta, T. Trung, J. Raisch, and T. Sezi. On power sharing and stability in autonomous inverter-based microgrids. In *51st IEEE Conference on Decision and Control*, pages 1105–1110, 2012.

[226] J. Schiffer, D. Goldin, J. Raisch, and T. Sezi. Synchronization of droop-controlled autonomous microgrids with distributed rotational and electronic generation. In *52nd IEEE Conference on Decision and Control*, pages 2334–2339, 2013.

[227] J. Schiffer, R. Ortega, A. Astolfi, J. Raisch, and T. Sezi. Conditions for stability of droop-controlled inverter-based microgrids. *Automatica*, 50(10):2457–2469, 2014.

[228] J. Schiffer, T. Seel, J. Raisch, and T. Sezi. A consensus-based distributed voltage control for reactive power sharing in microgrids. In *European Control Conference*, pages 1299–1305, 2014.

[229] J. Schiffer, R. Ortega, C. A. Hans, and J. Raisch. Droop-controlled inverter-based microgrids are robust to clock drifts. In *American Control Conference*, pages 2341–2346, 2015.

[230] J. Schiffer, T. Seel, J. Raisch, and T. Sezi. Voltage stability and reactive power sharing in inverter-based microgrids with consensus-based distributed voltage control. *IEEE Transactions on Control Systems Technology*, 24(1):96–109, 2015.

[231] J. Schiffer, D. Zonetti, R. Ortega, A. M. Stanković, T. Sezi, and J. Raisch. A survey on modeling of microgrids—from fundamental physics to phasors and voltage sources. *Automatica*, 74:135–150, 2016.

[232] J. Schiffer, C. A. Hans, T. Kral, R. Ortega, and J. Raisch. Modelling, analysis and experimental validation of clock drift effects in low-inertia power systems. *IEEE Transactions on Industrial Electronics*, 64(7):5942–5951, 2017.

[233] M. Schimpe, M. Naumann, N. Truong, H. C. Hesse, S. Santhanagopalan, A. Saxon, and A. Jossen. Energy efficiency evaluation of a stationary lithium-ion battery container storage system via electro-thermal modeling and detailed component analysis. *Applied Energy*, 210: 211–229, 2018.

[234] M. Schuurmans, P. Sopasakis, and P. Patrinos. Safe learning-based control of stochastic jump linear systems: a distributionally robust approach. In *58th IEEE Conference on Decision and Control*, pages 6498–6503, 2019.

[235] A. J. Schwab. *Elektroenergiesysteme: Erzeugung, Transport, Übertragung und Verteilung elektrischer Energie*. Springer, 2006.

[236] P. O. M. Scokaert and D. Q. Mayne. Min-max feedback model predictive control for constrained linear systems. *IEEE Transactions on Automatic control*, 43(8):1136–1142, 1998.

[237] Q. Shafiee, J. M. Guerrero, and J. C. Vasquez. Distributed secondary control for islanded microgrids—a novel approach. *IEEE Transactions on Power Electronics*, 29(2):1018–1031, 2014.

[238] A. Shapiro. Inference of statistical bounds for multistage stochastic programming problems. *Mathematical Methods of Operations Research*, 58(1):57–68, 2003.

[239] A. Shapiro. Minimax and risk averse multistage stochastic programming. *European Journal of Operational Research*, 219(3):719–726, 2012.

[240] A. Shapiro and A. Philpott. A tutorial on stochastic programming, 2007. File accessed 27 August 2021 at `https://stoprog.org/sites/default/files/SPTutorial/TutorialSP.pdf`.

[241] A. Shapiro, D. Dentcheva, and A. Ruszczyński. *Lectures on stochastic programming: modeling and theory*. SIAM, 2nd edition, 2014.

[242] G. B. Sheble and G. N. Fahd. Unit commitment literature synopsis. *IEEE Transactions on Power Systems*, 9(1): 128–135, 1994.

[243] J. W. Simpson-Porco, F. Dörfler, and F. Bullo. Synchronization and power sharing for droop-controlled inverters in islanded microgrids. *Automatica*, 49(9):2603–2611, 2013.

[244] J. W. Simpson-Porco, Q. Shafiee, F. Dörfler, J. C. Vasquez, J. M. Guerrero, and F. Bullo. Secondary frequency and voltage control of islanded microgrids via distributed averaging. *IEEE Transactions on Industrial Electronics*, 62(11):7025–7038, 2015.

[245] Y. Song, Y. Zheng, T. Liu, S. Lei, and D. J. Hill. A new formulation of distribution network reconfiguration for reducing the voltage volatility induced by distributed generation. *IEEE Transactions on Power Systems*, 35(1): 496–507, 2020.

[246] N. Soni, S. Doolla, and M. C. Chandorkar. Improvement of transient response in microgrids using virtual inertia. *IEEE Transactions on Power Delivery*, 28(3):1830–1838, 2013.

[247] P. Sopasakis, D. Herceg, A. Bemporad, and P. Patrinos. Risk-averse model predictive control. *Automatica*, 100: 281–288, 2019.

[248] P. Sopasakis, M. Schuurmans, and P. Patrinos. Risk-averse risk-constrained optimal control. In *European Control Conference*, pages 375–380, 2019.

[249] B. K. Sovacool. The political economy of energy poverty: A review of key challenges. *Energy for Sustainable Development*, 16(3):272–282, 2012.

[250] L. Strenge, H. Kirchhoff, G. L. Ndow, and F. Hellmann. Stability of meshed DC microgrids using probabilistic analysis. In *IEEE Second International Conference on DC Microgrids*, pages 175–180, 2017.

[251] L. Strenge, G. Schafaschek, and J. Raisch. Modeling and control of prosumer-based microgrids: a petri net approach. In *15th IEEE International Conference on Automation Science and Engineering*, pages 209–215, 2019.

[252] W. Su and J. Wang. Energy management systems in microgrid operations. *The Electricity Journal*, 25(8):45–60, 2012.

[253] W. Su, J. Wang, and J. Roh. Stochastic energy scheduling in microgrids with intermittent renewable energy resources. *IEEE Transactions on Smart Grid*, 5(4):1876–1883, 2014.

[254] T. Summers, J. Warrington, M. Morari, and J. Lygeros. Stochastic optimal power flow based on conditional value at risk and distributional robustness. *International Journal of Electrical Power & Energy Systems*, 72:116–125, 2015.

[255] S. B. Taieb, G. Bontempi, A. F. Atiya, and A. Sorjamaa. A review and comparison of strategies for multi-step ahead time series forecasting based on the nn5 forecasting competition. *Expert systems with applications*, 39(8): 7067–7083, 2012.

[256] A. G. Tsikalakis and N. D. Hatziargyriou. Centralized control for optimizing microgrids operation. In *IEEE Power and Energy Society General Meeting*, 2011.

[257] J. W. Tukey. *Exploratory Data Analysis*. Addison-Wesley Publishing Company, 1977.

[258] U. Ugurlu, I. Oksuz, and O. Tas. Electricity price forecasting using recurrent neural networks. *Energies*, 11(5): 1255, 2018.

[259] United Nations Framework Convention on Climate Change. Kyoto Protocol, 1997.

[260] United Nations Framework Convention on Climate Change. Paris Agreement, 2015.

[261] U.S. Energy Information Administration. Levelized cost and levelized avoided cost of new generation resources. *Annual Energy Outlook*, 2019.

[262] B. P. Van Parys, D. Kuhn, P. J. Goulart, and M. Morari. Distributionally robust control of constrained stochastic systems. *IEEE Transactions on Automatic Control*, 61(2): 430–442, 2016.

[263] A. Vecchietti, S. Lee, and I. E. Grossmann. Modeling of discrete/continuous optimization problems: characterization and formulation of disjunctions and their relaxations. *Computers & chemical engineering*, 27(3): 433–448, 2003.

[264] J. Vetter, P. Novák, M. R. Wagner, C. Veit, K.-C. Möller, J. Besenhard, M. Winter, M. Wohlfahrt-Mehrens, C. Vogler, and A. Hammouche. Ageing mechanisms in lithium-ion batteries. *Journal of power sources*, 147 (1–2):269–281, 2005.

[265] C. Wang and S. Shahidehpour. Effects of ramp-rate limits on unit commitment and economic dispatch. *IEEE Transactions on Power Systems*, 8(3):1341–1350, 1993.

[266] S. Wang, S. Shahidehpour, D. S. Kirschen, S. Mokhtari, and G. Irisarri. Short-term generation scheduling with transmission and environmental constraints using an augmented lagrangian relaxation. *IEEE Transactions on Power Systems*, 10(3):1294–1301, 1995.

[267] T. Wang, H. Kamath, and S. Willard. Control and optimization of grid-tied photovoltaic storage systems using model predictive control. *IEEE Transactions on Smart Grid*, 5(2):1010–1017, 2014.

[268] X. Wang, J. M. Guerrero, Z. Chen, and F. Blaabjerg. Distributed energy resources in grid interactive AC microgrids. In *2nd IEEE International Symposium on Power Electronics for Distributed Generation Systems*, pages 806–812, 2010.

[269] Z. Wang, Q. Bian, H. Xin, and D. Gan. A distributionally robust co-ordinated reserve scheduling model considering cvar-based wind power reserve requirements. *IEEE Transactions on Sustainable Energy*, 7(2): 625–636, 2016.

[270] D. Weisser. On the economics of electricity consumption in small island developing states: a role for renewable energy technologies? *Energy Policy*, 32(1):127–140, 2004.

[271] H. P. Williams. Logical problems and integer programming. *Bulletin of the Institute of Mathematics and its Applications*, 13:18–20, 1977.

[272] H. P. Williams. Linear and integer programming applied to the propositional calculus. *Systems Research and Information Science*, 2:81–100, 1987.

[273] K. Worthmann, C. M. Kellett, P. Braun, L. Grüne, and S. R. Weller. Distributed and decentralized control of residential energy systems incorporating battery storage. *IEEE Transactions on Smart Grid*, 6(4):1914–1923, 2015.

[274] P. Xiong, P. Jirutitijaroen, and C. Singh. A distributionally robust optimization model for unit commitment considering uncertain wind power generation. *IEEE Transactions on Power Systems*, 32(1):39–49, 2017.

[275] F. R. Yu, P. Zhang, W. Xiao, and P. Choudhury. Communication systems for grid integration of renewable energy resources. *IEEE Network*, 25(5):22–29, 2011.

[276] A. Zerrahn, W.-P. Schill, and C. Kemfert. On the economics of electrical storage for variable renewable energy sources. *European Economic Review*, 108:259–279, 2018.

[277] Q. Zhai, X. Guan, and J. Yang. Fast unit commitment based on optimal linear approximation to nonlinear fuel cost: Error analysis and applications. *Electric Power Systems Research*, 79(11):1604–1613, 2009.

[278] Y. Zhang and G. B. Giannakis. Robust optimal power flow with wind integration using conditional value-at-risk. In *IEEE International Conference on Smart Grid Communications*, pages 654–659, 2013.

[279] Y. Zhang, N. Gatsis, and G. B. Giannakis. Robust energy management for microgrids with high-penetration renewables. *IEEE Transactions on Sustainable Energy*, 4(4): 944–953, 2013.

[280] Y. Zhang, S. Shen, and J. L. Mathieu. Distributionally robust chance-constrained optimal power flow with uncertain renewables and uncertain reserves provided by loads. *IEEE Transactions on Power Systems*, 32(2): 1378–1388, 2017.

[281] C. Zhao and Y. Guan. Unified stochastic and robust unit commitment. *IEEE Transactions on Power Systems*, 28(3):3353–3361, 2013.

[282] C. Zhao and R. Jiang. Distributionally robust contingency-constrained unit commitment. *IEEE Transactions on Power Systems*, 33(1):94–102, 2018.

[283] Z. Q. Zheng and M. Morari. Robust stability of constrained model predictive control. In *American Control Conference*, pages 379–383. IEEE, 1993.

[284] H. Zhou, C. A. Hans, and W. Zhang. Minimax model predictive operation control of grid-connected microgrids. In *IEEE Conference on Control Applications*, pages 58–63, 2016.

List of Figures

List of Tables

Abbreviations

AC	Alternating current
ARIMA	Autoregressive integrated moving average
AVaR	Average value-at-risk
CPU	Central processing unit
DC	Direct current
GPU	Graphics processing unit
HELP	High-effect low-probability
MG	Microgrid
MIQCP	Mixed-integer quadratically-constrained program
MIQP	Mixed-integer quadratic program
MPC	Model predictive control
n/a	Not applicable
NP-hard	Non-deterministic polynomial-time hard
PCC	Point of common coupling
PRMSE	Prediction root mean squared error
PV	Photovoltaic
RAM	Random access memory
RES	Renewable energy sources

Nomenclature

$\mathbb{B}$	Set of Boolean numbers
$\mathbb{C}$	Set of complex numbers
$\mathbb{N}$	Set of natural numbers
$\mathbb{N}_0$	Set of nonnegative integers
$\mathbb{R}$	Set of real numbers
$\mathbb{R}_{>0}$	Set of positive real numbers
$\mathbb{R}_{\geq 0}$	Set of nonnegative real numbers
$\mathbb{R}_{<0}$	Set of negative real numbers
$\mathbb{R}_{\leq 0}$	Set of nonpositive real numbers
$\Im(x)$	Imaginary part of complex variable x
$\Re(x)$	Real part of complex variable x
$\imath$	Imaginary unit
$\mathbb{A}_j$	Ambiguity set at stage j
$\mathrm{anc}(i)$	Ancestor of node i
$\mathrm{AV@R}_\alpha$	Average value-at-risk
B	Backshift operator
b_j^d	Branching factor in scenario tree generation at stage j
b_{il}	Susceptance between nodes i and l
χ_i	Power sharing factor of unit i
$\mathrm{child}(i)$	Set of children of node i
c_{il}	Current flow from node i to node l
δ_r	Boolean auxiliary variable of renewable units
δ_t	Boolean control input of conventional generators
$\mathbb{D}_j$	Probability simplex at stage j
$\mathbb{E}$	Set of edges
$\mathbf{E}_{\pi_j}$	Expectation operator considering probability vector π_j
F	Edge-node incidence matrix

$\mathcal{G}$	Weighted, undirected, connected graph
γ	Discount factor
g_{il}	Conductance between nodes i and l
$\mathbb{I}$	Set of all forecast scenarios
J	Prediction horizon
j	Discrete prediction time instant
k	Discrete time instant
K_{s}	Inverse power sharing factors of storage units
K_{t}	Inverse power sharing factors of conventional generators
$\mathcal{L}$	Weighted graph Laplacian matrix
ℓ	Overall cost
ℓ_{o}	Economically motivated cost
ℓ_x	Cost associated with state of charge
$\bar{\ell}_{\mathrm{o}}$	Average economically motivated cost
$\bar{\ell}_x$	Average cost associated with state of charge
$\mathbb{L}$	Set of removed forecast scenarios
$\overline{\mathbb{L}}$	Set of kept forecast scenarios
μ	Real-valued auxiliary variable
N_{b}	Number of nodes, i.e., buses, in transmission network
N_{d}	Number of loads
N_{e}	Number of edges in transmission network, i.e., number of transmission lines
N_{n}	Number of nodes in scenario tree
N_{Ω}	Number of scenarios in collection of forecasts
N_{r}	Number of renewable units
N_{s}	Number of storage units
N_{t}	Number of conventional generators
N_{u}	Number of units
N_{v}	Number of elements in vector of control inputs
N_{w}	Number of elements in vector of uncertain inputs
N_{z}	Number of elements in vector of auxiliary variables
p	Power of units
p_{e}	Power of transmission lines
p_{g}	Active power of nodes in transmission network
p_{l}	Load power
p_{r}	Power of renewable units
p_{s}	Power of storage units

p_{t}	Power of conventional generators
$\overline{p}_{\mathrm{r}}$	Average infeed from renewable units
$\overline{p}_{\mathrm{t}}$	Average infeed from conventional generators
Φ	Vector of minimum cost in conditional risk mapping
$\pi^{(i)}$	Probability of node i
π_j	Probabilities of stage j
p_{il}	Active power flow from node i to node l
Ψ	Vector of cost in conditional risk mapping
q_{g}	Reactive power of nodes in transmission network
q_{il}	Reactive power flow from node i to node l
ρ	Risk measure
s_{il}	Apparent power flow from node i to node l
$\mathrm{stage}(i)$	Stage of node i
t	Auxiliary variable in reformulation of AVaR
θ_i	Phase angle at node i
θ_{il}	Phase angle difference between nodes i and l $(\theta_i - \theta_l)$
U	Matrix to connect units and loads to buses of transmission network
u	Power setpoints of units
u_{r}	Power setpoints, i.e., maximum power, of renewable units
u_{s}	Power setpoints of storage units
u_{t}	Power setpoints of conventional generators
$\mathbb{V}$	Set of nodes, i.e., buses, in transmission network
v	Control input vector
$v^{(i)}$	Control input vector at node i
$\hat{v}_i$	Voltage amplitude at node i
w	Uncertain input
$\overline{w}$	Upper bound of forecast of uncertain input
$\underline{w}$	Lower bound of forecast of uncertain input
w_{d}	Load power
$\hat{w}_i$	Forecast of uncertain input i
$\hat{w}^{(i)}$	Forecast of uncertain input at node i
w_{r}	Available renewable infeed
x	State vector
$x^{(i)}$	State vector at node i
$\overline{x}$	Upper bound of state vector
$\underline{x}$	Lower bound of state vector

ξ	Auxiliary variable in reformulation of AVaR
y_{il}	Admittance between nodes i and l
y_n	Admittance of transmission line n
z	Vector of auxiliary variables
$\overline{z}$	Vector of auxiliary variables associated with $\overline{w}$
$\underline{z}$	Vector of auxiliary variables associated with $\underline{w}$
$z^{(i)}$	Vector of auxiliary variables at node i

Index